

Assessment of a Global Contrail Modeling Method and Operational Strategies for Contrail Mitigation

by

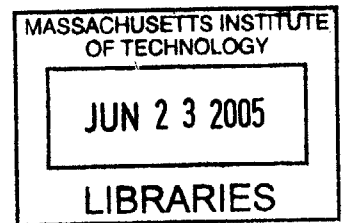
Kelly Klima

B.S. Mechanical Engineering
California Institute of Technology, 2003

SUBMITTED TO THE DEPARTMENT OF AERONAUTICS AND ASTRONAUTICS
IN PARTIAL FULFILLMENT OF THE REQUIREMENTS FOR THE DEGREE OF

MASTER OF SCIENCE IN AERONAUTICS AND ASTRONAUTICS
AT THE
MASSACHUSETTS INSTITUTE OF TECHNOLOGY

MAY 2005 *[June 2005]*



© 2005 Massachusetts Institute of Technology. All rights reserved.

The author hereby grants to MIT permission to reproduce
and to distribute publicly paper and electronic
copies of this thesis document in whole or in part.

Signature of Author.....

[Signature]
Department of Aeronautics and Astronautics
May 2005

Certified by.....

[Signature]
Professor and Deputy Head
Aeronautics and Astronautics
Thesis Supervisor

Accepted by.....

[Signature]
Professor of Aeronautics and Astronautics
Chairman, Committee for Graduate Students

AERO

Assessment of a Global Contrail Modeling Method and Operational Strategies for Contrail Mitigation

by
Kelly Klima

Submitted to the Department of Aeronautics and Astronautics
on May 20, 2005 in Partial Fulfillment of the
Requirements for the Degree of Master of Science in
At the Massachusetts Institute of Technology in
Aeronautics and Astronautics

ABSTRACT

Recent updates to the IPCC estimates of radiative forcing contributions from aircraft have raised concerns about the impacts of contrails and aviation-induced cirrus on climate. Increasing demand for aviation will further increase contrail formation. This thesis provides a model to assess operational options for reducing contrail coverage. This model couples realistic flight performance and best-available global meteorological data assimilations.

Comparisons were made between satellite-identified contrails and contrail persistence estimates from flight data for 53,844 U.S. continental flights performed during the week of November 11/12-18, 2001. The satellite data were processed by NASA Langley Research Center using methods for identifying contrails as described by Mannstein [28]. Given detailed knowledge of the aircraft types and radar-based trajectory data, simulated contrails did not match contrails observed in the satellite images. First, striated cirrus cloud formations were misidentified as contrail pixels. This resulted in the “contrails” typically aligning N-S, while most aircraft routes are aligned E-W. Perhaps 40-50% of the contrail pixels were misidentified. Second, a total of 60-90% of the contrail pixels (all demonstrated to be either contrails or clouds) occurred in areas where the assimilated meteorological fields showed RHi < 100%. This demonstrates that the RHi fields, although representative, do not accurately portray the true RHi fields on a given day in 2001. Finally, the typical length of the estimated contrails (several degrees) was longer than the typical length of the observed contrails (one degree). This may reflect a limitation of the satellite sensing of the contrails, but it also implies that the chord lengths used within aviation system model need to be shortened so that they are consistent with length-scales observed in the RHi data.

Despite the inability to replicate satellite data, the model was used to develop preliminary estimates of the costs and benefits of operational strategies for contrail and aviation-induced cirrus mitigation. Custom reroutes which minimized fuel burn were created reflecting different options for flying above, below, and around regions of high relative humidity. These options were all consistent with standard reroute procedures employed by the airlines and the Federal Aviation Administration. Using these custom reroutes, analyses were completed for 581 continental flights between 14 city pairs, and 628 international flights over the North Atlantic between 15 city pairs. Given perfect knowledge of meteorological data and no air traffic controls, if aircraft were individually rerouted, it was possible to mitigate 65%-80% of

persistent contrails and simultaneously achieve an average decrease of 5%-7% of the total operating cost for the week in November 2001 for which this analysis was carried out. These reductions are relative to the actual routes flown by the aircraft during this week, reflecting the impact of non-optimal routing not only on contrail formation, but also on fuel burn and operating costs in general. Significant contrail reduction may also be achieved if aircraft are rerouted in weekly increments. For the time period that was analyzed it was possible to mitigate 40%-75% of persistent contrails for a change of -10% to +5% of the total operating cost. An assessment was also made of the cost for mitigating contrails compared to the custom reroute that minimized fuel burn. In this case, 55%-85% of the contrails could be mitigated, for roughly a 0.5-1% increase in time and 2.5-3.5% increase in fuel burn (or 1-2% increase in total operating cost). In general, contrail persistence can be mitigated by altering latitude/longitude trajectory, flying at an altitude much lower or much higher than the tropopause, flying a route that minimizes fuel burn, and choosing more northerly routes over the Atlantic Ocean.

Key areas of uncertainty that may impact these results include the validity of the contrail identification methods, the validity/range/resolution of the RHi estimates obtained from the assimilated meteorological data, the advection of contrails over time, the chord lengths in the aviation system model, the value of RHi assumed as the contrail persistence threshold, the validity of the engine modeling methods, the database of flights examined, and the construction of the custom reroutes. Further, contrail formation is a strong function of latitude and time of year. Therefore, the results cannot be generalized beyond the global regions and times of year that were analyzed.

Thesis Supervisor:
Title:

Ian Waitz
Professor and Deputy Head
Aeronautics and Astronautics

ACKNOWLEDGEMENTS

The mind is its own place, and in itself, can make a Heaven of Hell, a Hell of Heaven.
~ John Milton

I am truly grateful for all those who contributed to make a Heaven of Hell.

Foremost, I thank Professor Ian Waitz for refining my skills, developing my cognitive abilities, and teaching me how to formulate problems and solutions. He also always bolstered my spirits, and was willing to step in whenever I needed help.

Next I would like to thank the Volpe National Transportation Systems Center. Gregg Fleming, Dr. Brian Kim, Sathya Balasubramanian, and Andrew Malwitz were instrumental to my success, and I greatly appreciate their willingness to further my research. I know they put in long hours to help me complete this work. Additionally, I especially thank Matt Maki, who volunteered his own free time to allow me access to the rerouting software.

Dr. Patrick Minnis, Dr. David Duda, and Rabi Palikonda at the NASA Langley Research Center were extremely helpful in providing all of the satellite images, contrail masks, and meteorological data. I especially appreciate last minute phone calls and data reconstructions nearing the end of my thesis. Dr. Peter Spichtinger's input on atmospheric processes was also a huge help in allowing me to understand contrail processes.

I would also like to thank Dr. Brian Hoskins and Dr. Peter Clark at the Joint Centre for Mesoscale Meteorology in providing the set of global meteorological data, as well as Paul Gerbi for helping me translate the Fortran encoding into a .txt format. I would also like to thank the ARM database for providing archived data swiftly and efficiently.

I also would like to thank all those who contributed ideas and/or data to this work. Special thanks go out to Dr. Steve Baughcum (Boeing), Dr. Bob Liebeck (Boeing), Dr. Rick Miake-Lye (Aerodyne), Dr. Ilan Kroo (Stanford), and Dr. Yifang Gong (MIT) for their expert advice.

Finally I would like to thank all the members of the GTL who made my time a memorable one. Thanks Lori, Dave, Chris, Yuto, Steve, Joe... I shall always remember you guys.

CONTENTS

ABSTRACT

ACKNOWLEDGEMENTS

CONTENTS

LIST OF FIGURES

LIST OF TABLES

NOMENCLATURE

GLOSSARY

CHAPTER 1: INTRODUCTION.....	19
CHAPTER 2: ANALYSIS PROCEDURE AND DATA	22
2.1. CONTRAIL MODEL	22
2.1.1. <i>Schmidt-Appleman procedure</i>	22
2.1.2. <i>Schumann Hypothesis</i>	24
2.1.3. <i>Application</i>	25
2.2. AVIATION SYSTEM MODEL.....	26
2.2.1. <i>Model Background</i>	26
2.2.1.1. <i>Purpose</i>	26
2.2.1.2. <i>Model Structure</i>	26
2.2.1.3. <i>Example Output</i>	27
2.2.1.4. <i>Uncertainty in SAGE Model</i>	29
2.2.2. <i>Improvements to the Aerodynamic Model: Compressibility Effects</i>	30
2.2.3. <i>Cruise Velocity Filter</i>	31
2.2.4. <i>Engine Equation</i>	32
2.2.5. <i>Additional Factors</i>	36
2.3. METEOROLOGICAL DATA	36
2.3.1. <i>Rapid Update Cycle (RUC) Data</i>	37
2.3.2. <i>Unified Forecast / Climate Model (UM) Data</i>	40
2.3.3. <i>Processing Meteorological Information for SAGE Use</i>	41
2.3.4. <i>Implementation</i>	42
2.3.5. <i>Filtering of ETMS Flight Bearings (Latitude & Longitude)</i>	42
2.3.6. <i>Summary of SAGE Changes</i>	44
2.4. COST-BENEFIT ASSESSMENT METHODS	44
2.4.1. <i>Background</i>	44
2.4.2. <i>Cost Data</i>	47
2.4.2.1. <i>Fuel Costs</i>	47
2.4.2.2. <i>Time Costs</i>	47
2.4.3. <i>Application</i>	49

CHAPTER 3: ASSESSMENT OF CONTRAIL ESTIMATION PROCEDURE AGAINST SATELLITE DATA	50
3.1. CONTRAIL MASKS	50
3.1.1. <i>Description</i>	50
3.1.2. <i>Caveats</i>	53
3.1.2.1. Misidentification as Contrail.....	55
3.1.2.2. Accuracy of RHi data.....	55
3.2. COMPARISON OF ESTIMATED CONTRAILS AND CONTRAIL MASK	58
3.2.1. <i>Advection of Estimated Contrails</i>	58
3.2.2. <i>Sample Day</i>	58
3.2.3. <i>Alignment of Estimated Contrail Data With Contrail Mask</i>	58
3.2.4. <i>Extended Results</i>	59
3.3. SENSITIVITY OF RESULTS TO AVIATION SYSTEM MODEL	72
3.3.1. <i>Percent of RHi Saturation at Which Contrails Persist</i>	72
3.3.2. <i>Aviation System Model</i>	74
3.3.3. <i>Meteorological Data</i>	76
3.4. CONCLUSIONS AND RECOMMENDATIONS FOR FUTURE WORK	77
CHAPTER 4: ASSESSMENT OF OPERATIONAL STRATEGIES FOR CONTRAIL MITIGATION.....	79
4.1. CURRENT PRACTICE.....	79
4.2. REROUTE CONSTRUCTION.....	87
4.2.1. <i>Background</i>	87
4.2.2. <i>Choosing Latitude/Longitude Trajectories</i>	87
4.2.3. <i>Choosing Altitude/Mach Number Trajectory</i>	91
4.2.3.1. Constant Altitude, Constant Mach Number.....	93
4.2.3.2. Constant Altitude, Mach Number Corresponding to Minimum Drag	93
4.2.3.3. Constant Velocity, Altitude Corresponding to Minimum Drag.....	94
4.2.3.4. Step Climb	94
4.2.4. <i>Time Period</i>	94
4.3. RESULTS	94
4.3.1. <i>Assessment of Custom Reroutes' Ability to Mimic Current Practice</i>	94
4.3.2. <i>Rerouting, One Flight at a Time</i>	98
4.3.3. <i>Rerouting, One Week at a Time</i>	101
4.3.4. <i>Comparison of Custom Reroutes</i>	105
4.3.5. <i>Schemes to Reduce Contrail Persistence Levels</i>	106
4.3.5.1. Raising Altitude One Flight Level.....	106
4.3.5.2. Using a Step Climb Trajectory Instead of Constant Altitude/ Constant Mach Number	106
4.3.5.3. More Northern Routes Over the Transatlantic.....	107
CHAPTER 5: SUMMARY AND RECOMMENDATIONS.....	108
5.1. SUMMARY	108
5.2. RECOMMENDATIONS FOR FUTURE WORK	109
APPENDIX A: CONTRAILS AND AVIATION INDUCED CIRRUS CLOUDINESS. 111	

A.1. CONTRAIL PHYSICS	111
<i>A.1.1. Small Scale</i>	112
<i>A.1.2. Large Scale</i>	113
A.1.2.1. Schmidt-Appleman procedure	113
A.1.2.2. Schumann Hypothesis.....	115
A.1.2.3. Role of Other Volatile Particles	116
A.2. OTHER CONSIDERATIONS	116
<i>A.2.1. Addition of Exhaust Water Vapor Increasing Humidity</i>	116
<i>A.2.2. Ideal vs. Empirical Saturation Curves</i>	118
<i>A.2.3. Changing Specific Heat in Contrail Formation Equation</i>	120
<i>A.2.4. Modeling of Emission Plume: Do Engines Affect Each Other?</i>	121
A.3. EXAMPLE OUTPUT	122
A.4. CONTRAILS IN CLOUDS.....	123
APPENDIX B: CHANGES FROM SAGE V1.1 TO V1.5	124
APPENDIX C: AERODYNAMIC MODEL	125
C.1. IDENTIFICATION OF THE PROBLEM.....	125
C.2. DEFINITION OF TRANSONIC DRAG RISE (COMPRESSIBILITY EFFECTS)....	125
C.3. KROO METHOD.....	127
C.4. ADAPTATION OF KROO METHOD TO SAGE.....	128
C.5. WEATHER EFFECTS	128
C.6. TYPE OF FLIGHT: ETMS OR OAG.....	130
C.7. FINAL IMPLEMENTATION.....	130
APPENDIX D: ENGINE EQUATION	131
D.1. JETS	131
D.2. TURBOPROPS	136
D.3. PISTONS.....	136
APPENDIX E: CALCULATION OF GREAT CIRCLE DISTANCE.....	137
APPENDIX F: SATELLITE AND CONTRAIL MASK IMAGES	138
APPENDIX G: ETMS METRICS FOR REROUTE ANALYSIS	163

REFERENCES

LIST OF FIGURES

FIGURE 1.1 - CONTRAIL EVOLUTION IN ALBUQUERQUE, NM [6].....	19
FIGURE 1.2 - RADIATIVE IMBALANCE AT TROPOPAUSE [7].....	20
FIGURE 2.1 - ILLUSTRATION OF THE SCHMIDT-APPLEMAN PROCEDURE	23
FIGURE 2.2 - ILLUSTRATION OF THREE POSSIBLE SCENARIOS OF AMBIENT CONDITIONS AND ENGINE EXIT CONDITIONS.....	23
FIGURE 2.3 - ILLUSTRATION OF THE SCHUMANN HYPOTHESIS.....	24
FIGURE 2.4 - PICTORIAL MODEL OF SAGE [11]	27
FIGURE 2.5 - SAGE GLOBAL 2000 FUEL BURN PLOT (1° BY 1° , ALL ALTITUDES AGGREGATED) [11].....	28
FIGURE 2.6 - HISTOGRAM RESULTS OF SAGE FUEL BURN COMPARISONS TO AIRLINE-REPORTED DATA [11]	28
FIGURE 2.7 – CHANGES IN SAGE EMISSIONS DUE TO 1% INCREASE IN KEY INPUT VARIABLES (CRUISE AT 35,000 FT, M0.8, ALL AIRCRAFT TYPES IN SAGE) [11].....	29
FIGURE 2.8 - SFC VERSUS ALTITUDE AT VARYING MACH NUMBERS, B767-200.....	33
FIGURE 2.9 – PERCENT CHANGE IN SFC WITH RESPECT TO ALTITUDE, B767-200.....	33
FIGURE 2.10 - SFC VERSUS ALTITUDE AT VARYING MACH NUMBERS, B767-300.....	34
FIGURE 2.11 – PERCENT CHANGE IN FUEL FLOW WITH RESPECT TO ALTITUDE, B767-300.....	34
FIGURE 2.12 - SFC VERSUS ALTITUDE AT VARYING MACH NUMBER, B757-300.....	35
FIGURE 2.13 - RUC DATA COVERAGE, MAP ADAPTED [16]	38
FIGURE 2.14 - RELATIVE HUMIDITY WITH RESPECT TO ICE. 2/5/2002, HOUR 13, ALTITUDE 10972.8, FROM RUC DATA	39
FIGURE 2.15 - RELATIVE HUMIDITY WITH RESPECT TO ICE. 11/12/2003, HOUR 18, ALTITUDE 10972.8, FROM UM DATA.....	40
FIGURE 2.16 - CONTRAILS AND HUMIDITY OVER NORTHEASTERN USA, 18 NOVEMBER 2001. (A) TERRA MODIS T11-T12 IMAGE, 1624 UTC. (B) 225-hPa RH _i (%) FROM RUC REANALYSIS, 1600 UTC [21].....	41
FIGURE 2.17 - RELATIVE HUMIDITY WITH RESPECT TO ICE. 11/18/2001, HOUR 16, ALTITUDE 10972.8, FROM RUC DATA	41
FIGURE 2.18 - THE TRADEOFF BETWEEN FUEL AND TIME COST, ADAPTED FROM [22].....	45
FIGURE 2.19 - THE TRADEOFF BETWEEN FUEL, TIME, AND (RANDOMLY ASSIGNED) CONTRAIL COST	45
FIGURE 2.20 – BUREAU OF TRANSPORTATION STATISTICS AIRLINE FUEL COST (1977-2005), AS OF MARCH 29, 2005 [23]. NOTE THAT THESE DATA DO NOT ACCOUNT FOR INFLATION.....	46
FIGURE 2.21 – FIGURE 2.20, CONVERTED IN 2005 U.S. DOLLARS [24]	46
FIGURE 3.1 - THREE SETS OF SATELLITE DATA AND MATCHING HUMIDITY DATA [28].....	51
FIGURE 3.2 - TERRA TRACKS FOR NOAA-16 SATELLITE, NOVEMBER 18, 2001 [26].	52
FIGURE 3.3 - NOAA-16 SATELLITE IMAGE AND MATCHING CONTRAIL MASK (WHITE PIXEL INDICATES CONTRAIL FORMATION), NOVEMBER 18, 2001 1888 UTC. NOTE THAT THE SATELLITE IMAGE IS REVERSED FROM EAST TO WEST. THIS OCCURS DUE TO THE DIRECTION THE SATELLITE PASSES OVERHEAD.....	52
FIGURE 3.4 - PORTION OF DIFFERENCE IMAGE AND MATCHING CONTRAIL MASK FOR 11/18/2001, 1888 UTC (MIDDLE OF FIGURE 3.3). IN THIS CASE, CONTRAILS APPEAR TO BE CORRECTLY IDENTIFIED IN MANY CASES.....	53

FIGURE 3.5 - PORTION OF DIFFERENCE IMAGE AND MATCHING CONTRAIL MASK FOR 11/18/2001, 1888 UTC (UPPER RIGHT OF FIGURE 3.3). IN THIS CASE, STRIATED CIRRUS CLOUD FORMATION IS MISIDENTIFIED AS CONTRAILS..... 54

FIGURE 3.6 - PORTION OF DIFFERENCE IMAGE AND MATCHING CONTRAIL MASK FOR 11/12/2001, 1827 UTC (MIDDLE LEFT OF FIGURE F.1). IN THIS CASE, STRIATED CIRRUS CLOUD FORMATION IS MISIDENTIFIED AS CONTRAILS..... 54

FIGURE 3.7 - PORTION OF DIFFERENCE IMAGE AND MATCHING CONTRAIL MASK FOR 11/15/2001, 1827 UTC (MIDDLE RIGHT OF FIGURE F.11). IN THIS CASE, STRIATED CIRRUS CLOUD FORMATION IS MISIDENTIFIED AS CONTRAILS..... 55

FIGURE 3.8 - ALL POINTS OF THE SATELLITE IMAGE (11/12/2001 HR 1996). RHi (HOUR 19 FIELD). 56

FIGURE 3.9 - THE HIGH CONFIDENCE REGIONS OF THE SATELLITE IMAGE (11/12/2001 HR 1996). RHi (HOUR 19 FIELD). NOTE THAT CROSSES INDICATE THE AREA OF NONEXISTENT OR UNCERTAIN SATELLITE PIXELS. 56

FIGURE 3.10 - FRACTION OF CONTRAIL PIXELS WHICH OCCUR IN THEORETICALLY CORRECT PLACES (I.E. WHERE RHi > 100%). THE "AT ANY ALTITUDE" CATEGORY ENCOMPASSES ALL CONTRAIL PIXELS WHICH COULD HAVE OCCURRED AT ANY OF THE FLIGHT LEVELS EXAMINED..... 57

FIGURE 3.11 - CONTINENTAL US FLIGHTS ON 11/12/2001 WHICH TEMPORALLY OVERLAP WITH DATA IN FIGURE 3.9. 60

FIGURE 3.12 – SAGE ESTIMATED CONTRAILS, FILTERED BY CONTRAIL MASK FILTER. (11/12/2001 HR 1996). RHi (HOUR 19 FIELD). 60

FIGURE 3.13 - 11/12/2001 HR 1827, RHi HOUR 16 FIELD. A) FILTERED CONTRAIL MASK. CONTRAILS (45N 75W) CAUSED PARTIALLY BY THREADING. B) FLIGHTS EXAMINED, C) FILTERED CONTRAIL ESTIMATION. LACK OF CONTRAILS CAUSED PARTIALLY BY INSUFFICIENT FLIGHT DATA..... 61

FIGURE 3.14 - 11/12/2001 HR 1996, RHi HOUR 19 FIELD. A) FILTERED CONTRAIL MASK. CONTRAILS (47N 100W) CAUSED BY INCORRECT RHi FIELD (TEMPORALLY CHANGING). CONTRAILS (32N 110W) CAUSED BY THREADING. B) FLIGHTS EXAMINED, C) FILTERED CONTRAIL ESTIMATION. 62

FIGURE 3.15 - 11/12/2001 HR 2167, RHi HOUR 20 FIELD. A) FILTERED CONTRAIL MASK. B) FLIGHTS EXAMINED, C) FILTERED CONTRAIL ESTIMATION. CONTRAILS (32N, 120W) CAUSED BY INCORRECT RHi FIELD (BAD IN GENERAL). LACK OF CONTRAILS s (32N 112W) CAUSED BY INSUFFICIENT FLIGHT DATA..... 63

FIGURE 3.16 - 11/15/2001 HR 1942, RHi HOUR 18 FIELD. A) FILTERED CONTRAIL MASK. B) FLIGHTS EXAMINED, C) FILTERED CONTRAIL ESTIMATION. CONTRAILS (35N 96W, 35N 90W) CAUSED BY INCORRECT CONTRAIL ADVECTION. LACK OF CONTRAILS (45N 95W) CAUSED BY INSUFFICIENT FLIGHT DATA..... 64

FIGURE 3.17 - 11/15/2001 HR 2113, RHi HOUR 20 FIELD. A) FILTERED CONTRAIL MASK. LACK OF CONTRAILS (45N 120W) CAUSED BY THREADING (CONTRAIL MASK DOES NOT SEE CONTRAILS IN CLOUDS). B) FLIGHTS EXAMINED, C) FILTERED CONTRAIL ESTIMATION. CONTRAILS (47N 120W) CAUSED BY INCORRECT CONTRAIL ADVECTION. 65

FIGURE 3.18 - 11/16/2001 HR 1924, RHi HOUR 18 FIELD. A) FILTERED CONTRAIL MASK. LACK OF CONTRAILS (35N 96W, 35N 90W) CAUSED BY THREADING (CONTRAIL MASK DOES NOT SEE CONTRAILS IN CLOUDS). B) FLIGHTS EXAMINED, C) FILTERED CONTRAIL ESTIMATION. LACK OF CONTRAILS (45N 95W) CAUSED BY INSUFFICIENT FLIGHT DATA. 66

FIGURE 3.19 - 11/16/2001 HR 2095, RHi HOUR 20 FIELD. A) FILTERED CONTRAIL MASK. CONTRAILS CAUSED BY THREADING (SOME CONTRAILS ARE CLOUDS, AND SOME CLOUDS BLOCK OUT CONTRAILS). B) FLIGHTS EXAMINED, C) FILTERED CONTRAIL ESTIMATION. CONTRAILS (47N 120W) CAUSED BY INCORRECT CONTRAIL ADVECTION (NOTE THERE WERE NO FLIGHTS AT 42N 120W).	67
FIGURE 3.20 - 11/17/2001 HR 1906, RHi HOUR 18 FIELD. A) FILTERED CONTRAIL MASK. B) FLIGHTS EXAMINED, C) FILTERED CONTRAIL ESTIMATION. LACK OF CONTRAILS CAUSED BY INCORRECT RHi FIELDS (THERE ARE CLOUDS IN THE SATELLITE IMAGE, AND HERE RHi < 100%).	68
FIGURE 3.21 - 11/17/2001 HR 2077, RHi HOUR 19 FIELD. A) FILTERED CONTRAIL MASK. B) FLIGHTS EXAMINED, C) FILTERED CONTRAIL ESTIMATION. LACK OF CONTRAILS (45N 110W, 35N 115W) CAUSED PARTIALLY BY INCORRECT RHi FIELDS (THERE ARE CLOUDS IN THE SATELLITE IMAGE, AND HERE RHi < 100%), PARTIALLY BY INSUFFICIENT FLIGHT DATA.	69
FIGURE 3.22 - 11/18/2001 HR 1888, RHi HOUR 18 FIELD. A) FILTERED CONTRAIL MASK. CONTRAILS (ALL) CAUSED BY THREADED (STRIATED CLOUDS). B) FLIGHTS EXAMINED, C) FILTERED CONTRAIL ESTIMATION. LACK OF CONTRAILS (45N 90W) CAUSED BY INSUFFICIENT FLIGHT DATA.	70
FIGURE 3.23 - 11/18/2001 HR 2059, RHi HOUR 19 FIELD. A) FILTERED CONTRAIL MASK. CONTRAILS (45N 117W) CAUSED BY THREADING. B) FLIGHTS EXAMINED, C) FILTERED CONTRAIL ESTIMATION. LACK OF CONTRAILS CAUSED BY INCORRECT RHi FIELD.	71
FIGURE 3.24 – PERCENT AREA (.XX) POTENTIALLY COVERED BY CONTRAILS AS A FUNCTION OF MINIMUM PERCENT RHi SATURATION NEEDED FOR CONTRAILS TO PERSIST. EACH DAY IS CALCULATED FROM RUC DATA AT 18 UTC.	73
FIGURE 3.25 - PERCENT AREA (.XX) POTENTIALLY COVERED BY CONTRAILS AS A FUNCTION OF MINIMUM PERCENT RHi SATURATION NEEDED FOR CONTRAILS TO PERSIST. EACH DAY IS CALCULATED FROM UM DATA AT 18 UTC.	73
FIGURE 3.26 – PERCENT OF CRUISE SFC AS A FUNCTION OF ALTITUDE AND MACH NUMBER, AVERAGED FOR FIVE AIRCRAFT/ENGINE COMBINATIONS. RECALL THAT SAGE SFC CHANGES LITTLE WITH ALTITUDE, SO THE SAGE CURVE WOULD BE A STRAIGHT LINE AT Y = 1.	74
FIGURE 4.1 - THE NORTHERN HEMISPHERE RELATIVE HUMIDITY AT 250 hPa (ABOUT 34000FT) AT 00Z ON 18 FEBRUARY 1999 (DATA COURTESY OF BRIAN HOSKINS, THE EUROPEAN CENTRE FOR MEDIUM RANGE WEATHER FORECASTS)	80
FIGURE 4.2 - AIRCRAFT TYPES FOR ETMS CONTINENTAL ROUTES, VARYING ORIGIN DESTINATION PAIR, NOV 12-18 2003	81
FIGURE 4.3 - AIRCRAFT TYPES FOR ETMS TRANSATLANTIC ROUTES, VARYING ORIGIN DESTINATION PAIR, NOV 12-18 2003	81
FIGURE 4.4 - 11/12/2001 ETMS FLIGHTS EXAMINED	83
FIGURE 4.5 – CONTRAILS ESTIMATED FOR FLIGHTS IN FIGURE 4.4. RHi IS FROM RUC DATA, HOUR 18.	83
FIGURE 4.6 - 11/12/2003 ETMS FLIGHTS EXAMINED	84
FIGURE 4.7 – CONTRAILS ESTIMATED FOR FLIGHTS IN FIGURE 4.6. RHi IS FROM UM DATA, HOUR 18.	84

FIGURE 4.8 - EXAMPLES FCA/FEA. EACH BLOCK IS A "BAD" AREA, SUCH AS A THUNDERSTORM OR AN AREA OF HIGH HUMIDITY, THAT PLANES COULD BE ASKED TO REROUTE AROUND. PICTURE COURTESY OF MATT MAKI (VOLPE).....	88
FIGURE 4.9 - ETMS ROUTES FOR LAX TO JFK. BLUE INDICATE ALL THE ROUTES FOR 11/12-18/2003. YELLOW INDICATES THE REROUTES CHOSEN.....	89
FIGURE 4.10 – REROUTES CHOSEN FOR LAX TO JFK AND RHi FOR 11/12/2001 HR 18. NOTE THAT SOME OF THESE ROUTES CAME FROM 5/13/2001 AND 10/13/2001 INSTEAD OF JUST FROM 11/12/2001. A VISUAL INSPECTION OF THE REROUTES SHOWS THAT CHANGING BETWEEN REROUTES CAN SIGNIFICANTLY ALTER CONTRAIL PERSISTENCE.....	89
FIGURE 4.11 – ETMS ROUTES FOR EGLL TO JFK. BLUE INDICATE ALL THE ROUTES FOR 5/13/2001, 10/13/2001, AND 11/12-18/2003; NOTE HOW OVER A HUNDRED FLIGHTS LINE UP ON A COUPLE TRACKS. RED INDICATES THE “MIDDLE” NORTH ATLANTIC ROUTE CHOSEN. YELLOW INDICATES TRACKS OFFSET BY ONE DEGREE. RED AND YELLOW TRACKS WERE USED AS THE REROUTES.	90
FIGURE 4.12 - REROUTES CHOSEN FOR EGLL TO JFK AND RHi FOR 11/12/2003 HR 18. A VISUAL INSPECTION OF THE REROUTES SHOWS THAT CHANGING BETWEEN REROUTES CAN ALTER CONTRAIL PERSISTENCE; WHEN THE JET STREAM IS SHAPED DIFFERENTLY, THIS CAN LEAD A SIGNIFICANT ALTERATION IN CONTRAIL PERSISTENCE.	90
FIGURE 4.13 – SAMPLE MACH NUMBERS FOR THE CUSTOM TRAJECTORIES.....	93
FIGURE 4.14 – SAMPLE ALTITUDES FOR THE CUSTOM TRAJECTORIES	93
FIGURE 4.15 - CONTRAILS ESTIMATED FOR ALL CUSTOM REROUTES ON NOVEMBER 12, 2001. RHi IS FROM RUC DATA, HOUR 18.	95
FIGURE 4.16 - CONTRAILS ESTIMATED FOR ALL CUSTOM REROUTES ON NOVEMBER 12, 2003. RHi IS FROM UM DATA, HOUR 18.	96
FIGURE 4.17 – TRADEOFF CONTRAILS PERSISTING COMPARED TO THE TIME, FUEL BURN, AND TOTAL OPERATING COSTS FOR LAX TO JFK ON 11/17/2001 0000 UTC. ALL VALUES ARE GIVEN AS PERCENTS OF THE AVERAGE ETMS VALUE FOR THREE HOURS SURROUNDING 11/17/2001 0000 UTC.....	100
FIGURE 4.18 – TRADEOFF CONTRAILS PERSISTING COMPARED TO THE TIME, FUEL BURN, AND TOTAL OPERATING COSTS FOR EGLL TO JFK ON 11/17/2003 1200 UTC. ALL VALUES ARE GIVEN AS PERCENTS OF THE AVERAGE ETMS VALUE FOR THREE HOURS SURROUNDING 11/17/2003 1200 UTC.....	100
FIGURE A.1 - ILLUSTRATION OF SMALL SCALE CONTRAIL PHYSICS PROCESS.....	112
FIGURE A.2 - ILLUSTRATION OF THE SCHMIDT-APPLEMAN PROCEDURE	114
FIGURE A.3 - ILLUSTRATION OF THREE POSSIBLE SCENARIOS OF AMBIENT CONDITIONS AND ENGINE EXIT CONDITIONS.....	114
FIGURE A.4 - ILLUSTRATION OF THE SCHUMANN HYPOTHESIS	115
FIGURE A.5 – VARIOUS WATER AND ICE SATURATION PRESSURE CURVES	119
FIGURE A.6 - CONTRAIL FACTOR LINE, WITH AND WITHOUT CHANGING SPECIFIC HEAT	120
FIGURE A.7 - TURBULENT PLUME GROWTH ON STANDARD AIRPLANE. THE BLUE LINE IS WHERE CONTRAILS FORM (0.36 SECONDS) AND THE GREEN LINE IS MAXIMUM SATURATION POINT OF THE EXHAUST AND ENTRAINED AIR.	121
FIGURE A.8 – EXAMPLE OUTPUT, CONTRAIL FORMS AND PERSISTS.....	122
FIGURE C.1 - DRAG COEFFICIENT OF EXAMPLE SAGE AIRCRAFT	126
FIGURE C.2 - THEORETICAL DRAG RISE, INCLUDING COMPRESSIBILITY DRAG (M4 TERM)	126

FIGURE C.3 – PERCENT DIFFERENCE FROM ACTUAL FUEL BURN AT VARYING ALTITUDES. “OLD” VALUES ARE PRE-COMPRESSIBILITY EFFECTS, “NEW” VALUES ARE POST COMPRESSIBILITY EFFECTS. NOTE HOW BOTH OAG AND ETMS ARE SYSTEMATICALLY INCREASED. SINCE THE ORIGINAL OAG WAS SET FOR AN AGGREGATE PERCENT ERROR OF ZERO, THIS MEANS THAT THE OAG ESTIMATION WOULD WORSEN.....	130
FIGURE D.1 - SFC VERSUS ALTITUDE AT VARYING MACH NUMBER, B757-300	132
FIGURE D.2 – SFC VERSUS ALTITUDE AT VARYING MACH NUMBERS, B767-200	133
FIGURE D.3 – PERCENT CHANGE IN SFC WITH RESPECT TO ALTITUDE, B767-200.	133
FIGURE D.4 - SFC VERSUS ALTITUDE AT VARYING MACH NUMBERS, B767-300	134
FIGURE D.5 – PERCENT CHANGE IN FUEL FLOW WITH RESPECT TO ALTITUDE, B767-300.....	134
FIGURE D.6 – THRUST SPECIFIC FUEL CONSUMPTION AT CRUISE AND TAKEOFF FOR VARIOUS TURBOPROPS	136
FIGURE E.1 – DIFFERENCES IN LATITUDE AND LONGITUDE FOR THREE DIFFERENT MINIMIZE-DISTANCE METHODS.....	137
FIGURE F.1 - NOAA-16 SATELLITE IMAGE AND MATCHING CONTRAIL MASK (WHITE PIXEL INDICATES CONTRAIL FORMATION), NOVEMBER 12, 2001 1827 UTC.....	139
FIGURE F.2 - NOAA-16 SATELLITE IMAGE AND MATCHING CONTRAIL MASK (WHITE PIXEL INDICATES CONTRAIL FORMATION), NOVEMBER 12, 2001 1996 UTC.....	140
FIGURE F.3 - NOAA-16 SATELLITE IMAGE AND MATCHING CONTRAIL MASK (WHITE PIXEL INDICATES CONTRAIL FORMATION), NOVEMBER 12, 2001 2167 UTC.....	140
FIGURE F.4 - NOAA-16 SATELLITE IMAGE AND MATCHING CONTRAIL MASK (WHITE PIXEL INDICATES CONTRAIL FORMATION), NOVEMBER 13, 2001 1809 UTC.....	141
FIGURE F.5 - NOAA-16 SATELLITE IMAGE AND MATCHING CONTRAIL MASK (WHITE PIXEL INDICATES CONTRAIL FORMATION), NOVEMBER 13, 2001 1978 UTC.....	142
FIGURE F.6 - NOAA-16 SATELLITE IMAGE AND MATCHING CONTRAIL MASK (WHITE PIXEL INDICATES CONTRAIL FORMATION), NOVEMBER 13, 2001 2148 UTC.....	143
FIGURE F.7 - NOAA-16 SATELLITE IMAGE AND MATCHING CONTRAIL MASK (WHITE PIXEL INDICATES CONTRAIL FORMATION), NOVEMBER 14, 2001 1791 UTC.....	144
FIGURE F.8 - NOAA-16 SATELLITE IMAGE AND MATCHING CONTRAIL MASK (WHITE PIXEL INDICATES CONTRAIL FORMATION), NOVEMBER 14, 2001 1960 UTC.....	145
FIGURE F.9 - NOAA-16 SATELLITE IMAGE AND MATCHING CONTRAIL MASK (WHITE PIXEL INDICATES CONTRAIL FORMATION), NOVEMBER 14, 2001 2131 UTC.....	146
FIGURE F.10 - NOAA-16 SATELLITE IMAGE AND MATCHING CONTRAIL MASK (WHITE PIXEL INDICATES CONTRAIL FORMATION), NOVEMBER 15, 2001 1773 UTC.....	147
FIGURE F.11 - NOAA-16 SATELLITE IMAGE AND MATCHING CONTRAIL MASK (WHITE PIXEL INDICATES CONTRAIL FORMATION), NOVEMBER 15, 2001 1942 UTC.....	148
FIGURE F.12 - NOAA-16 SATELLITE IMAGE AND MATCHING CONTRAIL MASK (WHITE PIXEL INDICATES CONTRAIL FORMATION), NOVEMBER 15, 2001 2113 UTC.....	149
FIGURE F.13 - NOAA-16 SATELLITE IMAGE AND MATCHING CONTRAIL MASK (WHITE PIXEL INDICATES CONTRAIL FORMATION), NOVEMBER 15, 2001 2283 UTC.....	150
FIGURE F.14 - NOAA-16 SATELLITE IMAGE AND MATCHING CONTRAIL MASK (WHITE PIXEL INDICATES CONTRAIL FORMATION), NOVEMBER 16, 2001 1755 UTC.....	151
FIGURE F.15 - NOAA-16 SATELLITE IMAGE AND MATCHING CONTRAIL MASK (WHITE PIXEL INDICATES CONTRAIL FORMATION), NOVEMBER 16, 2001 1924 UTC.....	152
FIGURE F.16 - NOAA-16 SATELLITE IMAGE AND MATCHING CONTRAIL MASK (WHITE PIXEL INDICATES CONTRAIL FORMATION), NOVEMBER 16, 2001 2095 UTC.....	153

FIGURE F.17 - NOAA-16 SATELLITE IMAGE AND MATCHING CONTRAIL MASK (WHITE PIXEL INDICATES CONTRAIL FORMATION), NOVEMBER 16, 2001 2265 UTC..... 154

FIGURE F.18 - NOAA-16 SATELLITE IMAGE AND MATCHING CONTRAIL MASK (WHITE PIXEL INDICATES CONTRAIL FORMATION), NOVEMBER 17, 2001 1738 UTC..... 155

FIGURE F.19 - NOAA-16 SATELLITE IMAGE AND MATCHING CONTRAIL MASK (WHITE PIXEL INDICATES CONTRAIL FORMATION), NOVEMBER 17, 2001 1906 UTC..... 156

FIGURE F.20 - NOAA-16 SATELLITE IMAGE AND MATCHING CONTRAIL MASK (WHITE PIXEL INDICATES CONTRAIL FORMATION), NOVEMBER 17, 2001 2077 UTC..... 157

FIGURE F.21 - NOAA-16 SATELLITE IMAGE AND MATCHING CONTRAIL MASK (WHITE PIXEL INDICATES CONTRAIL FORMATION), NOVEMBER 17, 2001 2247 UTC..... 158

FIGURE F.22 - NOAA-16 SATELLITE IMAGE AND MATCHING CONTRAIL MASK (WHITE PIXEL INDICATES CONTRAIL FORMATION), NOVEMBER 18, 2001 1720 UTC..... 159

FIGURE F.23 - NOAA-16 SATELLITE IMAGE AND MATCHING CONTRAIL MASK (WHITE PIXEL INDICATES CONTRAIL FORMATION), NOVEMBER 18, 2001 1888 UTC..... 160

FIGURE F.24 - NOAA-16 SATELLITE IMAGE AND MATCHING CONTRAIL MASK (WHITE PIXEL INDICATES CONTRAIL FORMATION), NOVEMBER 18, 2001 2059 UTC..... 161

FIGURE F.25 - NOAA-16 SATELLITE IMAGE AND MATCHING CONTRAIL MASK (WHITE PIXEL INDICATES CONTRAIL FORMATION), NOVEMBER 18, 2001 2229 UTC..... 162

LIST OF TABLES

TABLE 2.1, TOP – 36501 FLIGHTS IN OCTOBER 2000, WITH BADA 3.3, NO WEATHER, NO COMPRESSIBILITY EFFECTS.....	31
TABLE 2.2, BOTTOM – 1306 FLIGHTS ON OCTOBER 5, 2000 WITH BADA 3.5, WEATHER, COMPRESSIBILITY EFFECTS.....	31
TABLE 2.3 - AVERAGES AND 95% CONFIDENCE INTERVALS OF THE PERCENT DIFFERENCE FROM ACTUAL FUEL BURN BEFORE AND AFTER WEATHER IMPLEMENTATION.....	43
TABLE 2.4 - AVERAGES AND 95% CONFIDENCE INTERVALS OF THE PERCENT DIFFERENCE FROM ACTUAL FUEL BURN BEFORE AND AFTER SAGE UPDATES.....	43
TABLE 2.5 – EXCERPT FROM TABLE ES-1: ECONOMICS VALUES FOR USE IN ANALYSES: AIRCRAFT OPERATING COST [25]. MORE SPECIFIC VALUES (E.G. 2-ENGINE NARROW BODY) ARE FOUND IN [25]. VALUES IN 2005 UNITED STATES DOLLARS.....	48
TABLE 2.6 - CHOSEN FUEL BURN AND TIME COSTS FOR EACH ORIGIN-DESTINATION PAIR	49
TABLE 3.1 - LATITUDE AND LONGITUDE RANGES OF THE RUC AND UM DATA USED IN THIS STUDY	73
TABLE 3.2 – PERCENT DIFFERENCE FROM ACTUAL FUEL BURN, AVERAGED OVER 1702 FLIGHTS ON OCTOBER 5, 2000.....	75
TABLE 3.3 - DISTANCE OF CONTRAIL ESTIMATED FROM VARIOUS SCENARIOS, BEFORE AND AFTER SFC CHANGE	76
TABLE 4.1 – ORIGIN DESTINATION PAIRS CHOSEN, GIVEN BY FAA CALL SIGNS.	79
TABLE 4.2 - AIRCRAFT CHOSEN FOR EACH OF THE ORIGIN-DESTINATION PAIRS	82
TABLE 4.3 - ETMS ESTIMATIONS FOR CONTINENTAL FLIGHTS, AVERAGED OVER 11/12/2001 & 11/15-18/2001	85
TABLE 4.4 - ETMS ESTIMATIONS FOR TRANSATLANTIC FLIGHTS, AVERAGED OVER 11/12-18/2003	86
TABLE 4.5 - PERCENT CHANGE OF AVERAGE CUSTOM REROUTE OUTPUTS COMPARED TO AVERAGE CURRENT PRACTICE OUTPUTS FOR TRANSATLANTIC FLIGHTS.....	96
TABLE 4.6 – AVERAGE CUSTOM REROUTE CONTRAILS COMPARED TO CURRENT PRACTICE OUTPUTS FOR TRANSATLANTIC FLIGHTS. THIS TABLE GIVES THE PERCENT OF THE FLIGHT AS PERSISTENT CONTRAILS (INSTEAD OF A PERCENT REDUCTION OR INCREASE). THIS IS DONE DUE TO THE PLETHORA OF ZEROS IN BOTH ETMS AND CUSTOM FLIGHTS.....	98
TABLE 4.7 – COST OF MITIGATING ALL CONTRAILS FROM ETMS ROUTES. NOTE THIS IS A SUMMATION OVER THE COSTS OF REDUCING CONTRAILS FOR ALL FLIGHTS, NOT AN AVERAGE.	99
TABLE 4.8 - COST OF MITIGATING CONTRAILS IN CLEAR SKIES FROM ETMS ROUTES. NOTE THIS IS A SUMMATION OVER THE COSTS OF REDUCING CONTRAILS FOR ALL FLIGHTS, NOT AN AVERAGE.	99
TABLE 4.9 - CALCULATED COSTS FOR ALL SCENARIOS. ALL NUMBERS ARE GIVEN AS FRACTIONS OF THE ETMS VALUE.....	103
TABLE 4.10 - FRACTION REDUCTION OF CONTRAIL PERSISTENCE CHOSEN FOR TABLE 4.9	104
TABLE 4.11 – COST OF MITIGATING ALL CONTRAILS FROM MINIMUM FUEL BURN CUSTOM REROUTES. NOTE THIS IS A SUMMATION OVER THE COSTS OF REDUCING CONTRAILS FOR ALL FLIGHTS, NOT AN AVERAGE.	105

TABLE 4.12 - COST OF MITIGATING CONTRAILS IN CLEAR SKIES FROM MINIMUM FUEL BURN CUSTOM REROUTES. NOTE THIS IS A SUMMATION OVER THE COSTS OF REDUCING CONTRAILS FOR ALL FLIGHTS, NOT AN AVERAGE.	105
TABLE A.1 - MEAN CHARACTERISTICS OF CIRRUS CLOUDS	111
TABLE A.2 – THE CHANGE IN RELATIVE HUMIDITY (%) FOR THE MAXIMUM OF 99% CONFIDENCE INTERVAL.....	117
TABLE A.3 - VARIOUS SATURATION PRESSURE EQUATIONS	118
TABLE A.4 - MEAN RUC RELATIVE HUMIDITY AS A FUNCTION OF CLOUD COVER, COURTESY OF DR. DAVID DUDA (NASA LANGLEY, VA).	123
TABLE C.1 - CHANGE IN MACH NUMBER DUE TO WINDS, BRITISH AIRWAY 747-400 CFDR DATA (993 FLIGHTS).....	129
TABLE C.2 - CHANGE IN MACH NUMBER DUE TO SPEED OF SOUND, BRITISH AIRWAY 747-400 CFDR DATA (993 FLIGHTS).....	129
TABLE C.3 - 1306 AMERICAN AIRLINES FLIGHTS WITH A COMBINATION OF COMPRESSIBILITY EFFECTS AND WEATHER	129
TABLE G.1 – AVERAGE CUSTOM REROUTE CONTRAILS COMPARED TO CURRENT PRACTICE OUTPUTS FOR TRANSATLANTIC FLIGHTS. NOTE THAT THE FLIGHT DISTANCE OF BOTH FLIGHTS ARE THE SAME, SO BOTH COMPARISON METRICS (% OF FLIGHT BY DISTANCE AND OVERALL DISTANCE OF FORMATION) YIELD THE SAME RELATIVE CHANGE.	163
TABLE G.2 – CURRENT PRACTICE (ETMS) BEST AND WORST CASE ESTIMATIONS FOR CONTINENTAL FLIGHTS, OVER 11/12/2001 & 11/15-18/2001. RESULTS MAY BE FROM DIFFERENT FLIGHTS.....	164
TABLE G.3 – CURRENT PRACTICE (ETMS) BEST AND WORST CASE ESTIMATIONS FOR TRANSATLANTIC FLIGHTS, OVER 11/12-18/2003. RESULTS MAY BE FROM DIFFERENT FLIGHTS.	165
TABLE G.4 - CUSTOM REROUTE BEST CASE SCENARIO FOR CONTRAIL PERSISTENCE FOR EACH ORIGIN-DESTINATION PAIR. THESE NUMBERS ARE CALCULATED FROM THE AVERAGE OVER ALL TIMES EXAMINED (10 FOR CONTINENTAL, 14 FOR TRANSATLANTIC). COST WAS USED AS A TIEBREAKER.....	166
TABLE G.5 - CUSTOM REROUTE BEST CASE SCENARIO FOR CONTRAIL PERSISTENCE (IN CLEAR SKIES) FOR EACH ORIGIN-DESTINATION PAIR. THESE NUMBERS ARE CALCULATED FROM THE AVERAGE OVER ALL TIMES EXAMINED (10 FOR CONTINENTAL, 14 FOR TRANSATLANTIC). COST WAS USED AS A TIEBREAKER.....	167
TABLE G.6 - CUSTOM REROUTE SCENARIO FOR CONTRAIL PERSISTENCE (IN CLEAR SKIES) FOR EACH ORIGIN-DESTINATION PAIR. THIS AVERAGE IS CALCULATED USING ALL THE CUSTOM REROUTES WITH DECREASED CONTRAIL PERSISTENCE.	168
TABLE G.7 - CUSTOM REROUTE SCENARIO FOR CONTRAIL PERSISTENCE (IN CLEAR SKIES) FOR EACH ORIGIN-DESTINATION PAIR. THIS AVERAGE IS CALCULATED USING ONLY THE STEP CLIMB CUSTOM REROUTES WITH DECREASED CONTRAIL PERSISTENCE.....	169

NOMENCLATURE

Constants

C _p	specific heat	= 1004 J/(kg K)
E	R _{air} / R _{water}	= 0.622
R	radius of earth	= 6369 km
Q	heating value of fuel	= 4.29 * 10 ⁷ J/kg

General Variables

AR	aspect ratio
ΔC _{Dc}	compressibility drag
C _{Dc}	drag rise associated with compressibility effects
C _{D0}	form drag
C _L	lift coefficient
C _{Lmindrag}	lift coefficient corresponding to minimum drag
e	Oswald efficiency factor
FB	fuel burn
M	Mach number
M _{crit}	= M _{CC} = crest critical Mach number
M _{DIV}	= M _{DD} = divergence Mach number
P ₀	ambient pressure
qcsweep	quarter-chord wing sweep
RH	relative humidity with respect to water
RHi	relative humidity with respect to ice
S	wing surface area
SFC	specific fuel consumption (jets)
sup	supercritical factor
t _c	mean thickness to chord ratio
Thrust	thrust
TSFC	thrust specific fuel consumption (turboprops)
W	weight
η	engine efficiency
ρ	density

Specific to Aviation Model

C _{D0_CR}	= parasitic drag coefficient in BADA (cruise)
C _{D2_CR}	= induced drag coefficient in BADA (cruise)
C _{f1}	= fuel flow coefficient in BADA #1
C _{f2}	= fuel flow coefficient in BADA #2
C _{fer}	= cruise fuel flow coefficient in BADA
M _{BADA}	= BADA cruise Mach number
deltaM _i	= change in Mach number from the head to tail of a chord
M _i	= Mach number in the middle of the chord
delta t _i	= change in time from the head to tail of a chord
delta V _i	= change in velocity from the head to tail of a chord
V _i	= velocity in the middle of the chord

Specific to Current Research

M_{H_2O}	mass of water output
Percent	percent of RH _i saturation at which contrail persist
V_{TRUE}	true velocity
V_{GRS}	ground velocity
V_{WIND}	wind velocity aloft, headwind is positive

GLOSSARY

ARM - Atmospheric Radiation Measurement Program
AVHRR - Advanced Very High Resolution Radiometer
BADA - Base of Aircraft Data
CFDR - Computer Flight Data Recorder
DTR - Diurnal Temperature Range
ECMWF - European Centre for Medium Range Weather Forecasting
ETMS - Enhanced Traffic Management System
FAA - Federal Aviation Administration
FCA - Flow Constrained Area
FEA - Flow Evaluation Area
GMT - Greenwich Mean Time
HPSS - High Pressure Spool Speeds
IPCC - Intergovernmental Panel on Climate Change
IR - infrared radiances
ISO - International Organization for Standardization
ISSR - Ice-super-saturated region
MIT - Massachusetts Institute of Technology
NASA - National Air and Space Administration
NAT - North Atlantic Track
NCEP - National Centers for Environmental Prediction
NOAA - National Oceanic and Atmospheric Administration
OAG - Official Airline Guide
RH - relative humidity with respect to water
RH_i - relative humidity with respect to ice
RUC - Rapid Update Cycle meteorological data
SAGE - System for Assessing Global Emissions
SFC - Specific Fuel Consumption
TDS - Traffic Display Situation
TSFC - Thrust Specific Fuel Consumption
UM - Unified Model of the U.K. Meteorological Office
UTC - Universal Time Conversion
VOLPE - Volpe National Transportation Systems Center, Environmental Measurements and Modeling Division

CHAPTER 1: INTRODUCTION

Recent updates to the IPCC estimates of radiative forcing contributions from aircraft have raised concerns about the impacts of contrails and aviation-induced cirrus on climate [1]. Within four to six hours after initial formation, contrails, if they persist, may evolve into aviation-induced cirrus. Figure 1.1 shows example contrail evolution over Albuquerque, New Mexico. Over Europe and North America, the effect of these line-shaped contrail cirrus has been estimated to be as high as 0.10W/m^2 , twice that of non-water vapor aircraft emissions (Figure 1.2). Other effects include decreasing the diurnal temperature difference [2].

The amount of contrail formation depends upon the number, type, and trajectory (Mach number, altitude, meteorological conditions) of aircraft flown. Although technical and operational improvements have decreased overall fuel consumption, increased demand has outweighed these advances. Air traffic in the troposphere, where humidity levels are such that contrails may form, is projected to continue to increase [1]. Additionally, more efficient engines will cause contrails to occur more frequently and over a larger altitude range for the same amount of air traffic.

There are currently only limited capabilities for evaluating the extent of global contrail coverage and assessing technology, operations and policy options for reducing contrail coverage if it is found to be a significant environmental impact. Previous studies range in degree of reliability. Some reports employ unrealistic flight profiles and trajectories; Williams et al. employs inappropriate models for the change in fuel burn as a function of altitude and Mach number [3]. More realistic studies include accurate flight performance, but do not include meteorological data; in a critique of the Williams work, Boeing [4] used proprietary aircraft performance models to describe cruise performance, but did not include wind data. Other realistic studies include accurate meteorological data, but assumed flight performance and trajectories. For example, Minnis et al. [5] describe a method to calculate whether a contrail will form and persist along certain routes based on an estimated propulsive efficiency.

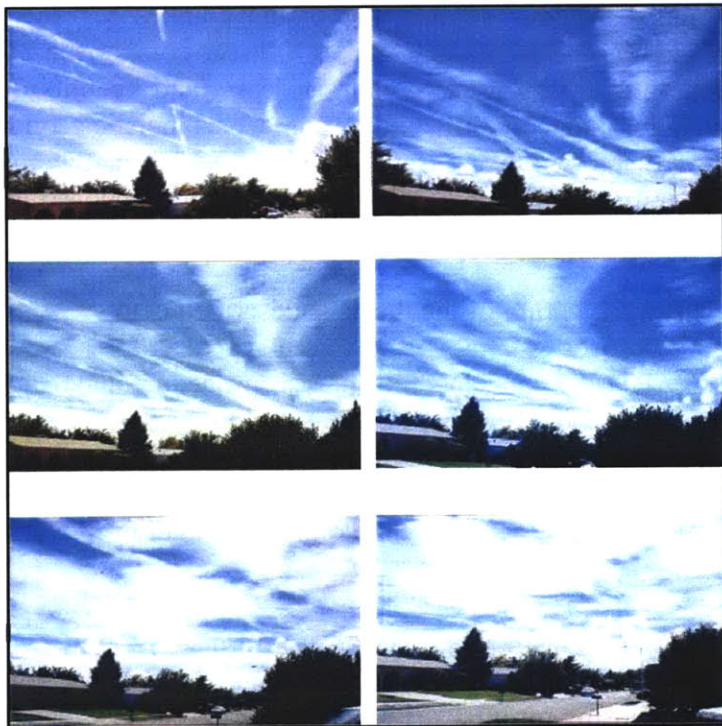


Figure 1.1 - Contrail Evolution in Albuquerque, NM [6]

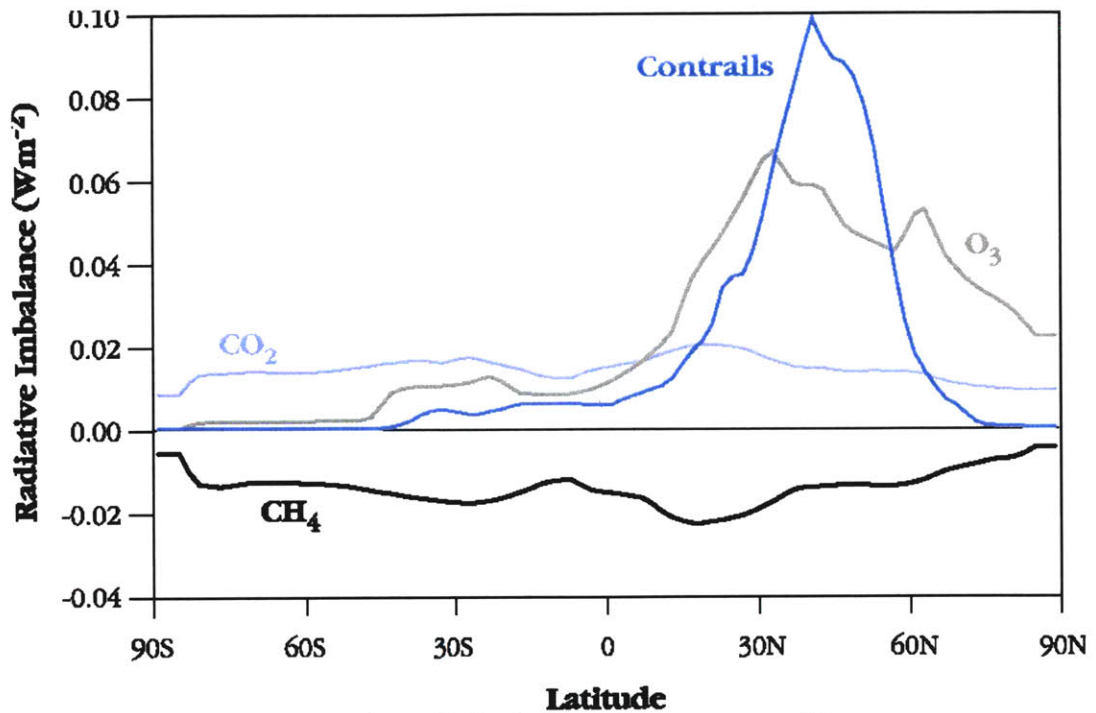


Figure 1.2 - Radiative imbalance at tropopause [7]

This thesis provides a model to assess operational options for reducing contrail coverage. Unlike previous studies, the model couples realistic flight performance with best-available meteorological data and makes a direct comparison of contrail estimates to satellite imagery. The model was used to estimate costs and benefits of operational strategies for contrail and aviation-induced cirrus mitigation. Costs include economic performance information (e.g. crew costs) and fuel burn. Benefits are measured relative to percent reduction in contrail formation. Operational strategies investigated include unconstrained flight and both lateral and altitude adjustments on existing flights/ trajectories.

The organization of the thesis is described below.

CHAPTER 2: presents the analysis procedure and data used. This includes a description of the contrail model, updates to the aviation system model, description of the meteorological data, and a brief discussion of the cost analysis and benefit criterion used to reroute the aircraft.

CHAPTER 3: assesses the contrail estimation model through comparison to satellite contrail data.

CHAPTER 4: includes extended information on two contrail mitigation case studies. The first involves U.S. continental flights, and the second involves transatlantic flights. The processes for choosing reroutes differ in these two case studies.

Research conclusions, summaries, and recommendations are contained in CHAPTER 5:.

The primary contributions of this thesis are:

- Identification of key areas for future research through assessment of contrail estimates against NASA satellite images.
- Rigorous estimation of fuel burn and time penalties to reduce contrail and aviation-induced cirrus cloudiness.
- Implementation of the contrail method into a researcher version of the FAA System for Assessing Global Emissions (SAGE).
- Improvement of the fuel burn and emissions modeling in the researcher version of the FAA SAGE model through equation updates and inclusion of meteorological data.

CHAPTER 2: ANALYSIS PROCEDURE AND DATA

2.1. CONTRAIL MODEL

Contrails are line-shaped clouds produced by aircraft engine exhaust at high altitudes. Depending on the temperature and the amount of moisture in the air at the aircraft altitude, contrails evaporate quickly (if the humidity is low) or persist and grow (if the humidity is high) [8].

The physics of contrail formation are described through the Schmidt-Appleman procedure and the Schumann Hypothesis.

2.1.1. Schmidt-Appleman procedure

The Schmidt-Appleman procedure for estimating contrail formation was independently proposed by Schmidt and Appleman (1953) [9]. It states that contrails form when the exhaust and entrained air pass through a thermodynamic state that is saturated with respect to liquid water (droplets form) and then into a state that is saturated with respect to ice (droplets freeze). If the ambient conditions are saturated with respect to ice, the contrail will persist. Figure 2.1 graphically represents the Schmidt-Appleman Procedure by tracing out the thermodynamic path of the particles from the engine exit to the ambient conditions.

Depending on the ambient conditions and the engine exhaust characteristics, the contrail factor line can move. Figure 2.2 shows three different sets of ambient conditions and engine characteristics. The ambient conditions are denoted by the red dot. The contrail factors are denoted by the red line.

In Case A, the particles do not pass through a state that is supersaturated with respect to water. Hence the water never condenses, never hardens into ice, and so a contrail does not form.

In Case B, the particles pass through a state that is supersaturated with respect to water. The water then condenses, and freezes into ice. However, but the ambient conditions are not saturated with respect to ice. So, when the particles reach equilibrium with the surrounding atmosphere, they evaporate. Hence a contrail forms, but does not persist.

In Case C, the particles pass through a state that is supersaturated with respect to ice. Unlike Case B, the ambient conditions are supersaturated with respect to ice. So when the particles reach equilibrium with the surrounding atmosphere, they remain solid. Hence a contrail forms and persists¹.

¹ Most of the water vapor in a contrail comes from the surrounding ice-supersaturated region (ISSR). As the contrail develops into aviation-induced cirrus, it can spread through the ISSR. ISSR size can limit the final aviation-induced cirrus size; in small ISSRs (e.g. 1km wide) the condensation would spread throughout the entirety of the ISSR. In larger ISSRs, the aviation-induced cirrus will not fill the ISSR. Due to the high uncertainties surrounding aviation-induced cirrus formation, the evolution into cirrus will be not examined in this thesis.

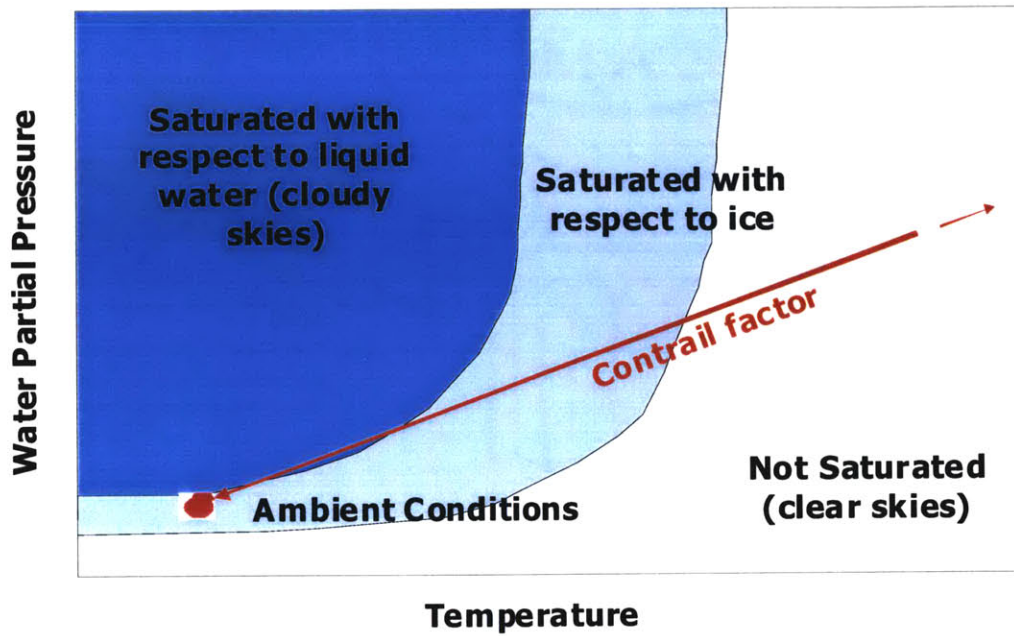


Figure 2.1 - Illustration of the Schmidt-Appleman Procedure

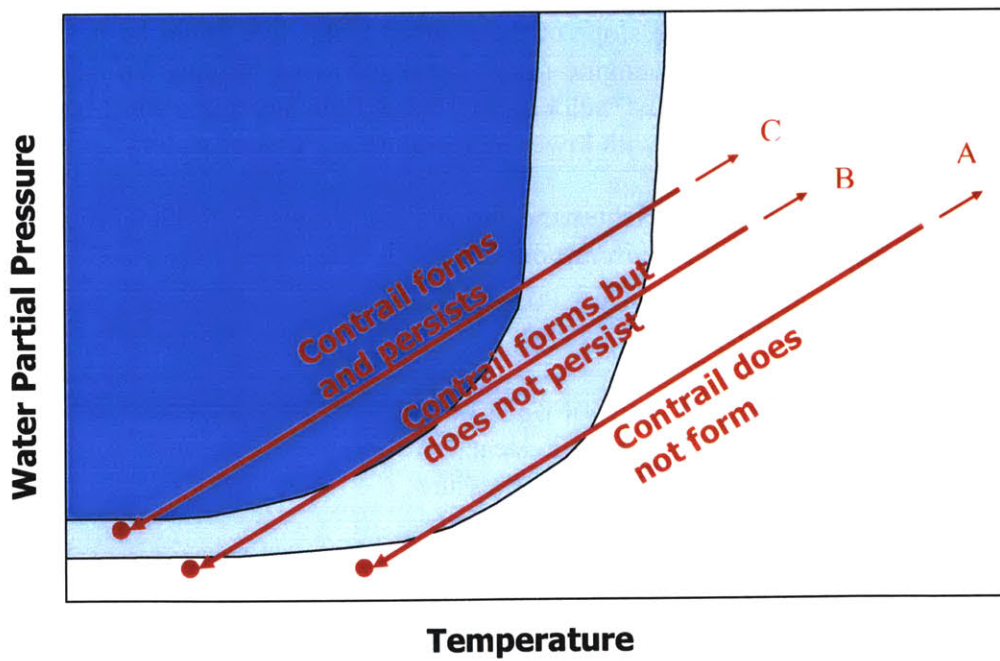


Figure 2.2 - Illustration of three possible scenarios of ambient conditions and engine exit conditions.

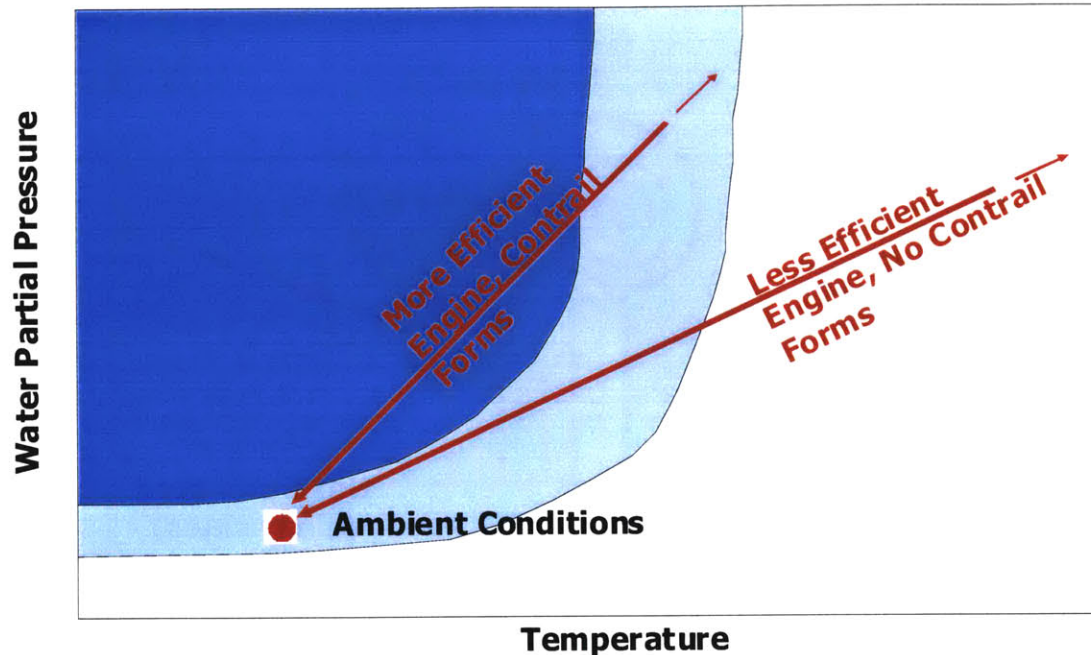


Figure 2.3 - Illustration of the Schumann Hypothesis

2.1.2. Schumann Hypothesis

In 1996 Schumann proposed that the slope of the contrail factor line could be described using the overall efficiency of the aircraft engine [10]. This holds true because an airplane engine with a higher overall efficiency (thrust*velocity/fuel mass flow*heating value) has a different thermodynamic state in the exhaust (with lower temperature per unit of water)².

Through thermodynamic arguments, Schumann showed that the slope of the contrail factor line can be related to the efficiency of the aircraft engine:

$$\frac{dw}{dT} = \frac{M_{H_2O} * C_p * P_o}{FB * E * Q * (1-\eta)} \quad (2.1)$$

Where M_{H_2O} = mass of water output

C_p = Specific Heat

P_o = Ambient Pressure

FB = Total Fuel Burn

E = $R_{air} / R_{water} = 0.622$

Q = Heating value of fuel

η = Overall efficiency \equiv (Thrust*V)/(Fuel Mass Flow*Q)

Figure 2.3 depicts the implications of this hypothesis. Note the slopes are exaggerated to more clearly depict Schumann's hypothesis.

² The overall efficiency should not be confused with other efficiencies, such as the propulsive efficiency and the thermal efficiency. The overall efficiency implies that better engines, though using less fuel for the same thrust power, produce the same amount of water at a lower exhaust temperature. The overall efficiency is the product of the propulsive and thermal efficiencies.

2.1.3. Application

First a model was developed to estimate the formation of contrails and aviation-induced cirrus clouds from aircraft. The model chosen was the Schmidt-Appleman procedure, modified by the Schuman hypothesis. This model was further improved through use of an empirical saturation curve (Sonntag) and mass-averaged moist air specific heat. Given local meteorological conditions, aircraft fuel burn, aircraft overall propulsion efficiency, and fuel characteristics, this model:

- Calculates whether a contrail will form
- Calculates whether that contrail will persist
- Reports contrail formation as percentage of distance traveled
- Differentiates between contrails forming in clouds and in clear skies

Due to the complexity of contrails, several characteristics were not fully addressed:

- The varying shapes/sizes of contrails. This study will calculate the time and fuel burn cost for a particular length of contrail, and disregard width and shape issues. For the assessment against satellite data, the varying shapes/sizes are a more important issue; however, due to the inability of simple models to predict these features, the shapes/sizes were be ignored.
- Sub-grid scale variability in meteorological data. Williams 2005 [15] applied an adjustment factor to their measure of potential contrail fraction to account for this variability. This study uses different metrics, so does not apply a correction factor.
- Optical depth. It is recognized that different contrails will have different optical depths, and hence cause different radiative forcing. This is a relatively difficult characteristic to predict, and is not addressed in this study.
- Overlapping contrails. At any one time, only 10-15% of the tropopause consists of ice-supersaturated regions (see Section 3.3.1). Satellite images indicate that the average contrail size is less than 10km (one pixel size in the NASA satellite images). As shown in Section 4.2, aircraft travel along many different trajectories, and winds quickly advect the contrails. These factors suggest that for a first order estimate it is appropriate to ignore overlapping contrails.
- The movement of contrails after formation. For the purposes of comparing model estimates to satellite data, winds are assumed to be invariant from time of formation.
- Aviation-induced cirrus cloudiness. The evolution of contrails into aviation-induced cirrus cloudiness is a difficult atmospheric fluid dynamics problem, beyond the scope of this study.
- The environmental effect of contrails is highly uncertain and is not addressed.

Background on this model and the theories behind it have been provided in APPENDIX A.:

2.2. AVIATION SYSTEM MODEL

To estimate contrail formation, an aircraft model estimating aircraft efficiency and the emissions index of water is needed. This study used the fuel burn and emissions module of the FAA's System for Assessing Global Emissions (SAGE).

This chapter briefly describes SAGE, and discusses improvements made to enable this study to be completed. For extensive descriptions of the SAGE model, please refer to the Lee thesis [11].

2.2.1. Model Background

2.2.1.1. Purpose

SAGE is a computer model developed for the FAA by the Volpe National Transportation Systems Center (Environmental Measurements and Modeling Division), MIT and the Logistics Management Institute (LMI). It is intended to be an internationally-accepted computer model used for estimating aircraft emissions and evaluating the effects of different policy and technology scenarios on aircraft performance, aviation-related emissions, costs, and industry responses [11]. The performance objectives for SAGE Version 1 were to compute aircraft performance, fuel burn and emissions of CO₂, H₂O, NO_x, HC, and CO at each point along the flight trajectory. From an aircraft level to airport, regional and global levels, the model is capable of various analyses such as:

- Implementation of new aircraft technology
- Improvements to air traffic control/ airspace capacity
- Enhancements to airport infrastructure
- Improvements in aircraft operations (e.g. increased NO_x certification standards, continuous descent approaches, derated takeoffs)

2.2.1.2. Model Structure

The model structure of SAGE is shown in Figure 2.4. SAGE consists of individual modules (e.g. aerodynamics, engine thrust, etc.) that interact to create a fuel burn estimate. This structure allows for relative ease in improving the model (discussed in Sections 2.2.2-2.2.5).

An important consideration of the model structure is how the flights are represented. In SAGE databases, trajectory data exist in two forms. Radar data are from the Enhanced Traffic Management System (ETMS), which mainly cover North America and Western Europe. For cases where radar data are not available, flight trajectories and vertical and horizontal dispersion, all as a function of stagelength, were developed by analyzing thousands of ETMS flights. These trajectories are then used in each scheduled flight in the Official Airline Guide (OAG) when radar data do not exist. In the SAGE 2000 analysis, the total number of ETMS and OAG flights modeled were 4,524,728 (17%) and 21,899,800 (83%), respectively. For this study, ETMS flights were readily available for all areas examined. Therefore, in all cases radar and pilot reporting data were used to define the baseline trajectory of the aircraft.

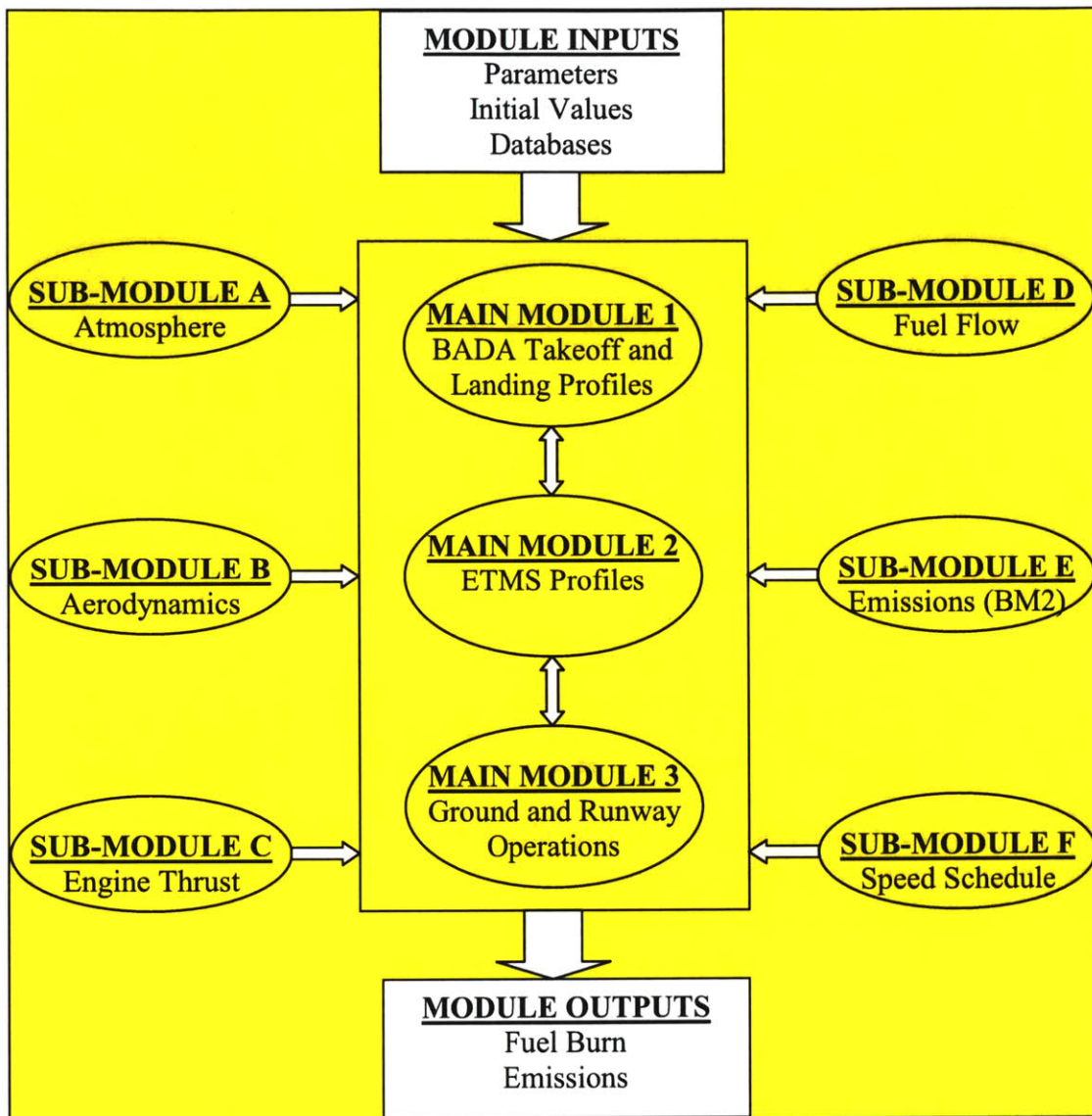


Figure 2.4 - Pictorial model of SAGE [11]

A second important consideration is the use of the Base of Aircraft Data (BADA) to replicate various aircraft. Each aircraft is identified and assigned an engine/airframe type, corresponding to unique performance coefficients in BADA. This database works well at cruise, but performance is poorer at off-cruise conditions. For rerouting purposes, the BADA methods and coefficients need to accurately reflect off-cruise conditions. Improvements to BADA to address off-cruise performance are discussed in Section 2.2.1.4.

2.2.1.3. Example Output

Summing all the ETMS and OAG flights allows one to make global fuel burn estimates. The results are aggregated into 1° x 1° x 1km world grids. Figure 2.5 shows the global 2000 fuel burn plot.

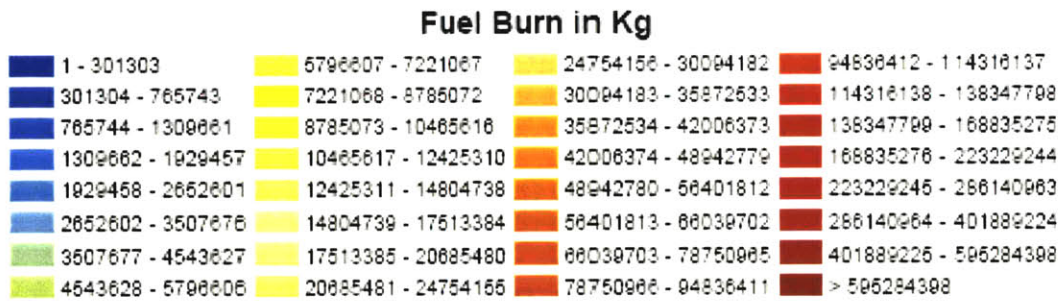
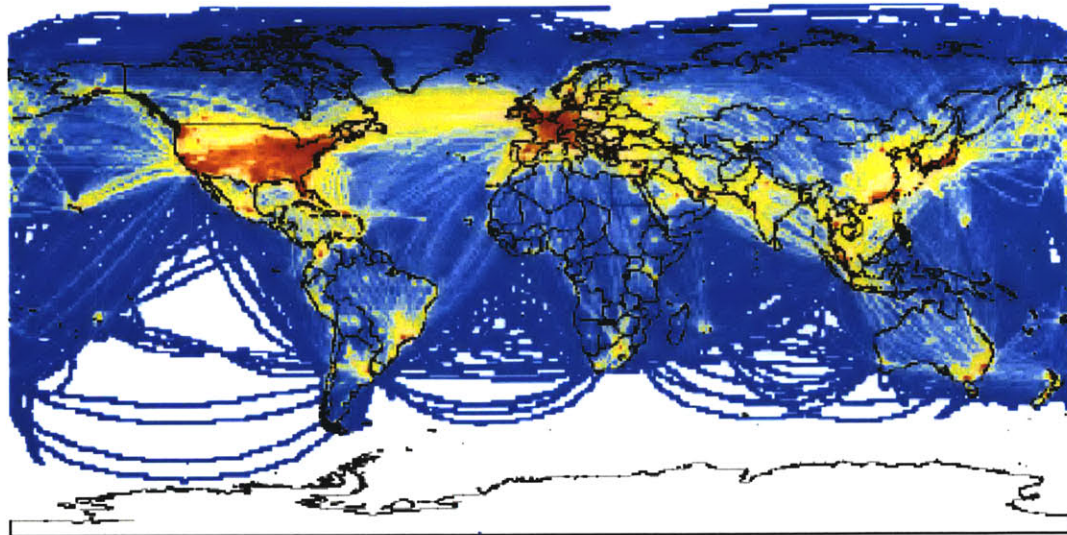


Figure 2.5 - SAGE global 2000 fuel burn plot (1° by 1°, all altitudes aggregated) [11]

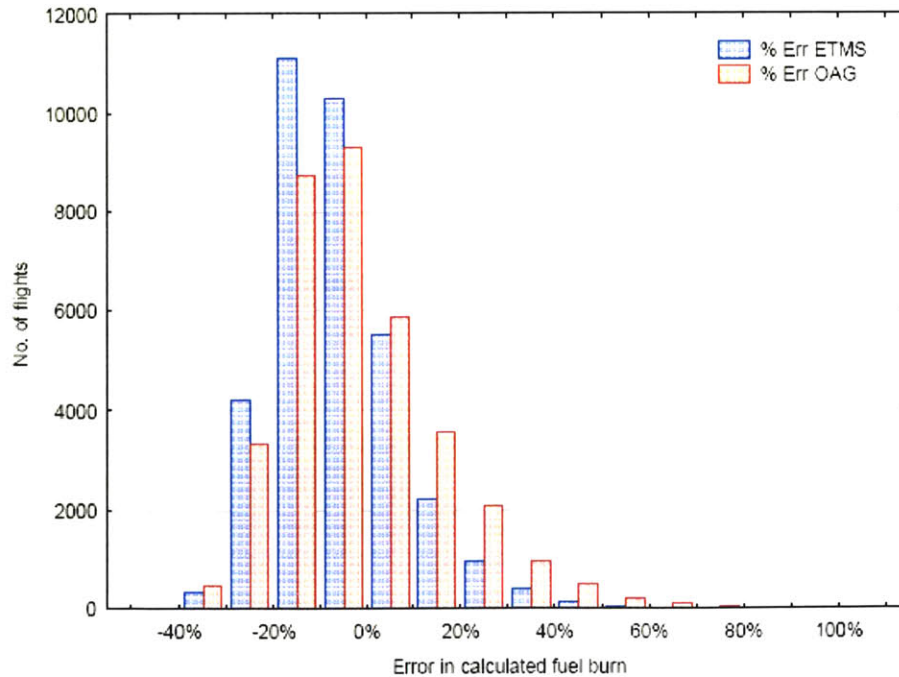


Figure 2.6 - Histogram results of SAGE fuel burn comparisons to airline-reported data [11]

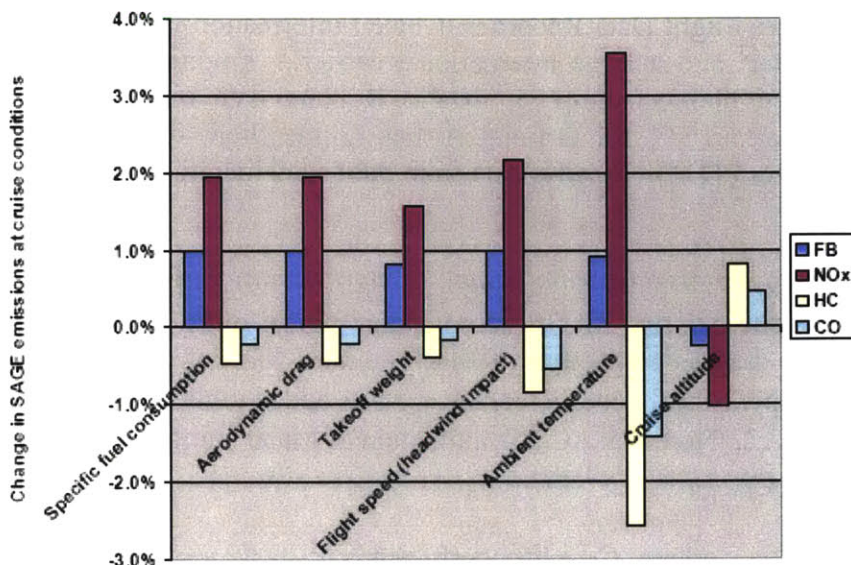


Figure 2.7 – Changes in SAGE emissions due to 1% increase in key input variables (Cruise at 35,000 ft, M0.8, all aircraft types in SAGE) [11]

2.2.1.4. Uncertainty in SAGE Model

Figure 2.6 gives a histogram of how SAGE estimates compare to proprietary fuel burn data provided by airlines. Since the ETMS routes provide high confidence in airplane trajectory, other factors cause this uncertainty. Lee [11] identified the largest contributors to error as shown in Figure 2.7.

When examining fuel burn, these uncertainties average to produce a fuel burn estimate to within $-5.7 \pm 18.7\%$ of reported fuel burn for ETMS flights [11, p.67]. However, contrail formation is dependent on flight-to-flight variations. To accurately estimate contrail formation, the model needs to capture aircraft performance with changes in altitude and Mach number. Hence there was the need to assess (and improve where possible) these components of the modeling methodology employed in SAGE.

Each of these uncertainties listed in Figure 2.7 was addressed separately. The cruise altitude was not of concern, since ETMS data were used. Flight speed and ambient temperature were added through meteorological data. The initial weight was modified based on flight length. The remaining uncertainties lie in the aerodynamic equation and engine equation (specific fuel consumption). To address these remaining issues, improvements to the aerodynamic model (allowing changes in cruise performance with changes in altitude to be more accurately estimated) and filters on the ETMS chorded data were added. The engine equations were also examined in depth, but an improved correction could not be found to better capture changes in engine performance as a function of Mach number and altitude. The impact of the uncertainty in engine performance on contrail prediction was assessed by a parametric study reported in Section 3.3.2; the uncertainty was found to not have a significant effect on the conclusions of this thesis.

Several sources of data were used to create the model updates (described further in Sections 2.2.2-2.2.5). Computer Flight Data Recorder (CFDR) information included data from a large North American carrier³ and a large international carrier⁴. Engine data included turboprop data⁵, and jet specific fuel consumption data⁶. Routing data included Enhanced Traffic Management radar data (ETMS), Official Airline Guide flight data (OAG), and Traffic Display System reroutes (TDS). Finally, data from published literature were used.

2.2.2. Improvements to the Aerodynamic Model: Compressibility Effects

It was observed that the existing SAGE aerodynamic model did not include compressibility effects, and therefore drag as a function of Mach number was not appropriately represented. To correct this, a compressibility coefficient (ΔC_{Dc}) was added to the drag coefficient equation, resulting in Equation 2.2. Note that ΔC_{Dc} is a function of Mach number to the fourth power.

$$C_D = C_{D0_CR} + C_L^2 * C_{D2_CR} + \Delta C_{Dc} \tag{2.2}$$

- where C_L = lift coefficient
- ΔC_{Dc} = compressibility drag
- C_{D0_CR} = parasitic drag coefficient in BADA (cruise)
- C_{D2_CR} = induced drag coefficient in BADA (cruise)

No theoretical calculation of ΔC_{Dc} existed, hence an empirical solution was used. The compressibility effects applied to SAGE consisted of the Kroo method [13] with the crest critical Mach number (M_{cc})⁷ equal to the Base of Aircraft Data (BADA) cruise Mach number. To account for weather effects and errors in the radar data, an upper cap was employed on the range of Mach numbers where C_{Dc} was computed; chords with Mach numbers higher than 104.6% of the BADA cruise Mach number did not use the compressibility effects. The calculation of ΔC_{Dc} is shown in Equations 2.3-2.5.

$$X = M / M_{BADA} \tag{2.3}$$

$$Y = X-1 \tag{2.4}$$

Relation	ΔC_{Dc}	(2.5)
----------	-----------------	-------

$X \geq 1.0$	$0.001000 + 0.02727*Y - 0.1952*Y^2 + 19.09*Y^3$
$1.0 > X \geq 0.95$	$0.001000 + 0.02727*Y + 0.4920*Y^2 + 3.573*Y^3$
$0.95 > X \geq 0.8$	$0.0007093 + 0.006733*Y + 0.01956*Y^2 + 0.01185*Y^3$
$0.8 > X \geq 0.5$	$0.00013889 + 0.00055556*Y + 0.00055556*Y^2$
$0.5 > X$	0

- where M = Mach number
- M_{BADA} = BADA cruise Mach number

Background on this model and the theories behind it have been provided in APPENDIX B:

³ Over 40,000 flights in fleet in Oct 2000. A306, B722, B738, B752, B762, B763, B772, DC10, F100, MD80, MD90

⁴ 993 flights of B747-400

⁵ Confidential, courtesy of a major engine company

⁶ Confidential, courtesy of a major engine company

⁷ M_{crit} , also M_{CC} , is the crest critical Mach number, the freestream Mach number at which the local Mach number on the crest of the airfoil becomes supersonic.

2.2.3. Cruise Velocity Filter

The next improvement was made to the ETMS data chords. Occasionally the data contained unexplainable spikes. For instance, the change in velocity (ΔV_i) would be extremely high or low, in turn resulting in high fuel burn. Previously, SAGE discarded these flights as “bad flights”. A check was required that would replace these bad chords and allow SAGE to keep these flights.

The best practice was to limit $\Delta V_i/V_i$ ⁸. First a 68% confidence interval of $\Delta V_i/V_i$ was calculated from international airline data. Then the filter consisted of two steps:

1. In ETMS, identify all flights outside this interval ($-0.088 < \Delta V_i/V_i < 0.088$).
2. Assume these flights have faulty radar data. Report ΔV_i as 0 and recalculate V_i .

Table 2.1 shows that the cruise velocity filter produces little or no change in estimated fuel burn compared to measured airline fuel burn. Since many previously discarded flights (on order of 20% of ETMS flights) can now be run, the fix was implemented for use in the next version of SAGE.

As the contrail model included an updated version of BADA (BADA 3.5), meteorological data, and compressibility effects, Table 2.2 reports the effect of the cruise velocity filter with these additions. The overall improvement of the estimation is caused by the combination of all the updated factors. Examining the flights with the worst fuel burn estimation showed that “bad chords” would have been corrected by winds. Consequently, the cruise velocity filter will not be necessary in future versions of SAGE that include weather.

Table 2.1, top – 36501 flights in October 2000, with BADA 3.3, no weather, no compressibility effects

	Percent reduction +/- 95% confidence interval	
Before	-6.82 +/- 58.55%	
After	-6.83 +/- 58.76%	
Change	-0.01	+0.21%

Table 2.2, bottom – 1306 flights on October 5, 2000 with BADA 3.5, weather, compressibility effects

	Percent reduction +/- 95% confidence interval	
Before	2.56 +/- 24.23%	
After	2.70 +/- 24.67%	
Change	+0.14	+0.44%

⁸ Note this is the same as putting a limit on $\Delta M_i/M_i$.

2.2.4. Engine Equation

The engine model in SAGE consists of one equation from BADA, the specific fuel consumption (SFC) equation. This varied depending on aircraft type (jet, turboprop, or piston), altitude, and whether the engine is idling. The veracity of the specific fuel consumption equation was individually examined for each aircraft type, but research time was weighted by percent fuel burn; jets make up over 97% of the annual fuel burn, and over 85% of the flights⁹, and therefore will be given preferential treatment here. Turboprops and pistons are examined briefly in APPENDIX D:

In SAGE, jet fuel flow in kg/sec is given as:

$$\begin{aligned} & \text{Below 7620 m:} \\ & \text{Fuel Flow} = C_{f1} / 60000 * (1 + 1.9438*V / C_{f2}) * \text{Thrust} \end{aligned} \quad (2.6)$$

$$\begin{aligned} & \text{Above 7620 m :} \\ & \text{Fuel Flow} = C_{f1} / 60000 * (1 + 1.9438*V / C_{f2}) * C_{fcr} * \text{Thrust} \end{aligned} \quad (2.7)$$

This equation can be broken up into specific fuel consumption (SFC) and thrust:

$$\text{Fuel flow} = \text{SFC} * \text{Thrust} \quad (2.8)$$

$$\begin{aligned} & \text{Below 7620 m:} \\ & \text{SFC} = C_{f1} / 60000 * (1 + 1.9438*V / C_{f2}) * \text{Thrust} \end{aligned} \quad (2.9)$$

$$\begin{aligned} & \text{Above 7620 m :} \\ & \text{SFC} = C_{f1} / 60000 * (1 + 1.9438*V / C_{f2}) * C_{fcr} * \text{Thrust} \end{aligned} \quad (2.10)$$

One disturbing trend occurs due to the C_{fcr} coefficient; the specific fuel consumption has a step increase or decrease through an altitude of 7620 meters. A second (but lesser) concern was that the same engine will perform differently on two different aircraft.

However, these concerns could easily be due to incorrect BADA coefficients, as opposed to an incorrect equation. Hence to verify the reliability of the SAGE SFC model, several data sources and alternative models were obtained. It was assumed that the SAGE aerodynamic model (with compressibility effects) was correct, and all calculations were conducted assuming steady level flight (thrust equals drag). Furthermore, it was assumed that the engine model was independent of the aerodynamic model, hence SFC was a function of altitude and Mach number only. Lastly, engines were assumed to function at the same non-dimensional operating point, hence performance could be scaled with standard non-dimensional parameters. (Note that the final two assumptions were later shown to be incorrect.)

⁹ SAGE 2003 data: Pistons negligible. Turboprops account for 2.3% of fuel burn, and 23.7-23.9% of flights. Jets account for remaining 97% of fuel burn.

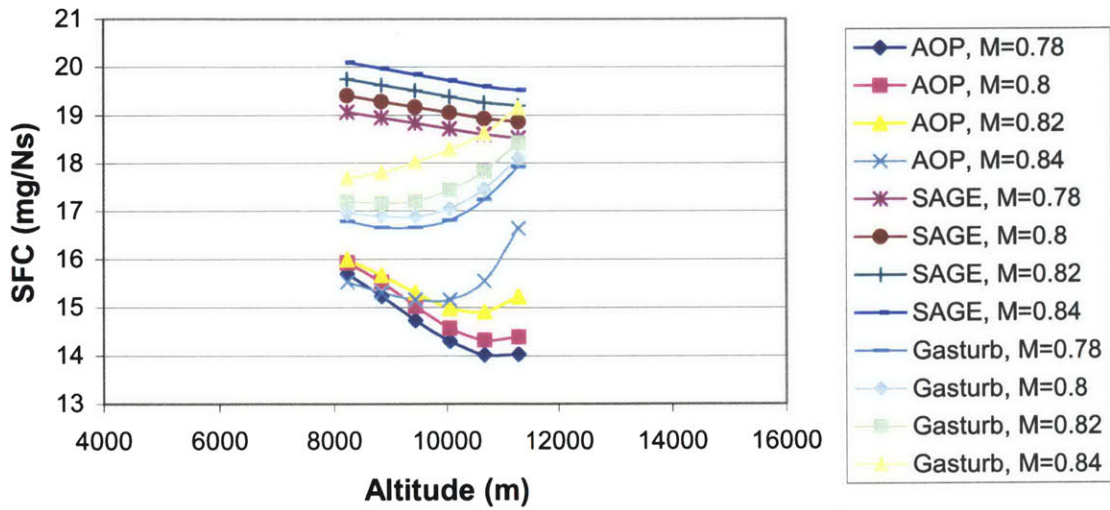


Figure 2.8 - SFC versus altitude at varying Mach numbers, B767-200

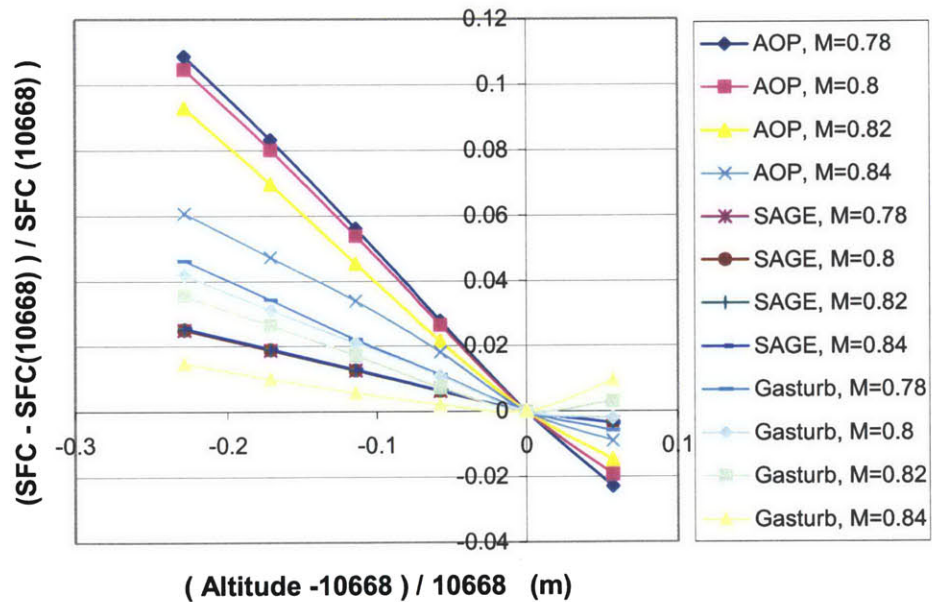


Figure 2.9 – Percent change in SFC with respect to altitude, B767-200.

Cruise: altitude = 10668m, Mach=0.78M

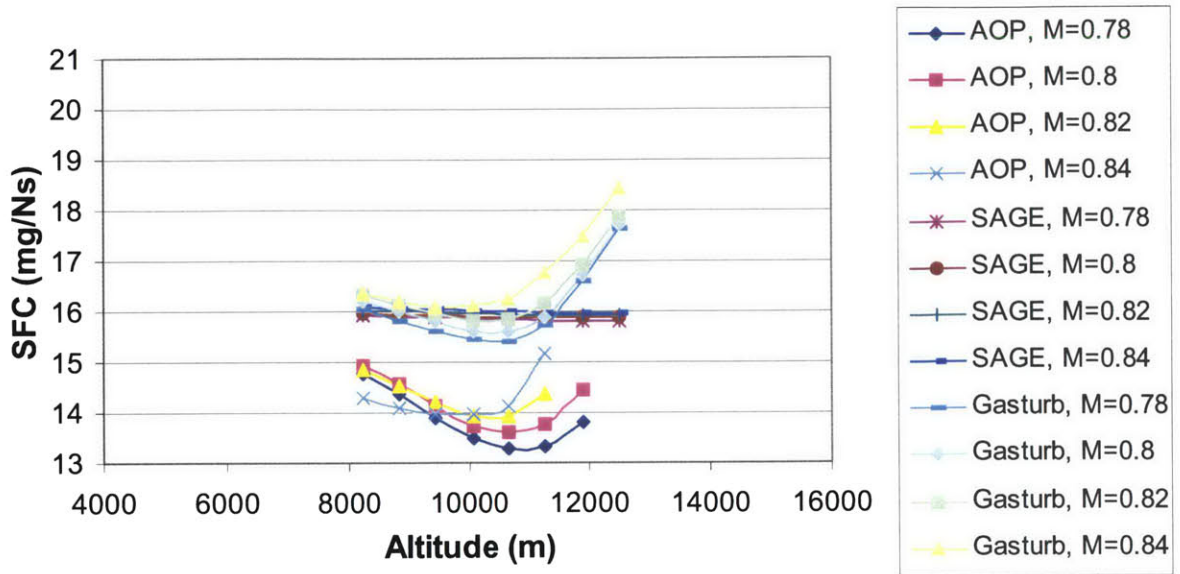


Figure 2.10 - SFC versus altitude at varying Mach numbers, B767-300

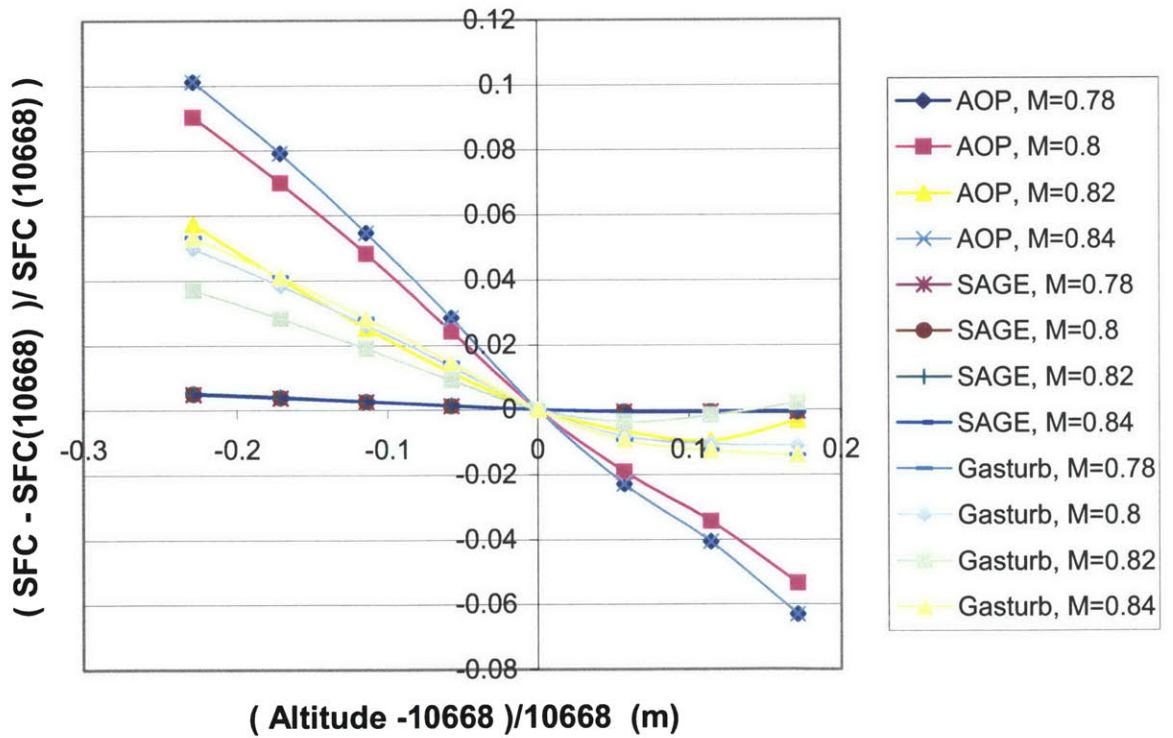


Figure 2.11 – Percent change in fuel flow with respect to altitude, B767-300.

Cruise: altitude = 10668m, Mach=0.8M

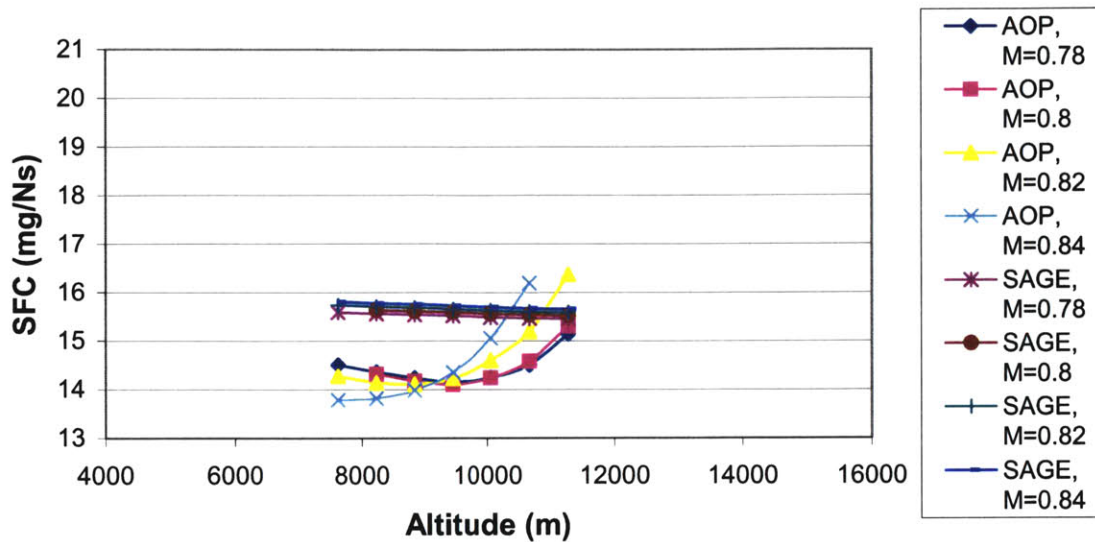


Figure 2.12 - SFC versus altitude at varying Mach number, B757-300

First the current SAGE model was examined against aircraft operating manual data¹⁰ and a higher fidelity model¹¹ to identify relative reliability. Figure 2.12- Figure 2.10 present SFC versus altitude for the three aircraft listed in the aircraft operating manual. The B757-300 figure does not have a GasTurb curve because the engine cycle deck was not completed. Although it was assumed that SFC was independent of net thrust, net thrust was held constant between SAGE and GasTurb.

The relatively straight SAGE curves do not capture the curved trends of the aircraft operating manual. GasTurb does a better job, but overestimates specific fuel consumption in both cases. More specifically, trends with Mach number and altitude were examined. In both the aircraft operating manual and GasTurb, as Mach number increased, SFC increased. SAGE did not capture the magnitude of change in SFC between Mach numbers. With regard to altitude,

¹⁰ An aircraft operating manual was obtained for the B57-300 (RB211-535E4B), B767-200 (CF6-80A), and B767-300 (CF6-80C2B6). It contained EPR, N1, specific range, and fuel flow per engine as a function of mass, altitude, and Mach number. For most of the study, this data source was considered a gold standard. However, insight from Prof. Robert Liebeck (MIT) indicated that assumption was may not be correct. Often the aircraft operating manual numbers are based on the first engine design. As the engine design changes or the engine matures, the reported numbers do not.

¹¹ GasTurb version 9 is a standard one-dimensional engine cycle deck which uses thermodynamic equations to calculate SFC. In order to obtain output, the user must first create the appropriate engine deck. This requires identifying the type of engine (two-spool unmixed flow, three-spool mixed flow, etc.), obtaining relevant data for the engine, and modifying input values to create the engine cycle deck. Some care must be taken in modifying the input values; efficiencies must be sensibly chosen to create a physically-realizable engine. Seven cycle decks were created by a previous MIT student, (CF6-50C, CFM56-3B, Ge90-90B, JT8D-9, PW2037, JT9D-7, and tayMK620-15). Three cycle decks were created to match the aircraft in the aircraft operating manual (CF6-80C2B6, CF6-80A, RB211-535E4B). One of these, the RB211, was not examined in depth due to lack of data.

SAGE failed to capture the slope or magnitude of either the aircraft operating manual data or the engine cycle deck. Furthermore, SAGE did not have the upturn pictured near 11000 m. Additionally, although the relative trend in change in SFC from cruise conditions was captured (see Figure D.3 and Figure D.5), the magnitudes were not.

In summary, general SAGE SFC trends did not correlate well with the AOP trends. Further examination showed this was not due to unrealistic high-pressure spool speeds, the efficiency maps, or to incorrect assumptions (specific fuel consumption is a function of altitude and Mach number only, and engines function at the same non-dimensional operating point). Most likely a combination of these factors caused the discrepancy.

Background on failed attempts to improve the engine model are provided in APPENDIX D:

2.2.5. Additional Factors

During processing, the aviation system model was updated from SAGE V1.1 and V1.5. Most changes (listed in APPENDIX B:) did not affect this study. The remainder of this section lists additional factors which will be improved in future versions of the aviation system model:

Flight Data Set - The flight data set used has a significant impact on contrail estimations; missing flights will cause errors in estimating contrail persistence. For the assessment against satellite data, only United States continental flights were used, but not international flights departing from or arriving in the United States. Increasing the set of flight data used will improve contrail estimations.

Air traffic control constraints - This study does not take into account air traffic control constraints. The sky is crowded, and reducing available highways or North Atlantic tracks from 5 to 3 may impair the ability of the aircraft to travel from origin to destination. Hence to avoid contrails, some aircraft would be forced to fly outside not only their normally preferred envelope, but their contrail-mitigating preferred envelope.

Chord Lengths - Comparison of SAGE with the satellite images (discussed in depth in CHAPTER 3:) indicates that the typical contrail length is shorter than the SAGE chord lengths. This occurs because the chord lengths are longer than the typical gradients in the meteorological data; averaging the head and tail chord components will not accurately reflect intermediate conditions. Decreasing the chord lengths employed by SAGE to roughly one degree lengths (70-100 km) would allow a better estimation of contrails, and will be employed in future versions of SAGE.

2.3. METEOROLOGICAL DATA

Contrail formation is sensitive to meteorological conditions. Although SAGE had provided for the future addition of meteorological data, as of September 2003, this work remained

incomplete. To first order, SAGE used the International Organization for Standardization (ISO) Standard atmospheric conditions. This lacks wind and relative humidity approximations. Since relative humidity is necessary for contrail estimation, meteorological data was needed. The humidity estimates are uncertain. In the context of contrail formation, this uncertainty has been addressed in the literature. Sausen et al. [14] break the region in question into a grid. If the humidity is greater than 60% in a grid box, and an airplane flies through that area, the entire area becomes a contrail. The expected contrail cover is then the product of the air mass coverage and the fuel consumption rate in the same region [1, p.91]. This assumes that all the aircraft have the same efficiency. Williams et al. improve upon the Sausen technique by relating the contrail formation to air traffic density [15]. Minnis et al. [4] have a different method, which calculates whether a contrail will form or persist along certain routes based on an estimated overall engine efficiency, an emissions index of water, and the more reliable Rapid Update Cycle (RUC) meteorological data.

Compared to these techniques, this study provides an improved method of calculating contrail formation and persistence. First, the emissions index of water and the type-specific engine efficiency are reported along each chord of the SAGE model. Then, the temporally and spatially matching RHi is obtained from the meteorological data sets. Consequently, the model can calculate whether a contrail will form and persist at a specific location in the atmosphere.

Several sources of meteorological data were considered for this research. Upon the advice of researchers Dr. David Duda and Dr. Patrick Minnis at the NASA Langley Research Center in Virginia, initial studies began with the 40km Rapid Update Cycle (RUC) data for the CONUS region. As it became apparent that this region would not encompass transatlantic flights, the Unified Model of the U.K. Meteorological Office (UM) was used. According to the researchers at NASA Langley, although significant uncertainty remains, both of these data sets contain the best available relative humidity estimates for their latitude/longitude ranges.

2.3.1. Rapid Update Cycle (RUC) Data

The Rapid Update Cycle (RUC) is an atmospheric prediction system comprised primarily of a numerical forecast model and an analysis system to initialize that model. The RUC has been developed to serve users needing short-range weather forecasts. RUC runs operationally at the National Centers for Environmental Prediction (NCEP).

Initially RUC data was obtained from Dr. Duda and Dr. Minnis at NASA Langley Research Center. More complete data was available through a United States program called the Atmospheric Radiation Measurement Program (ARM) (for dates November 12-18, 2001 and October 2000). Recently, the RUC data resolution has improved from 40 to 20 kilometers. This study uses 40km data on the advice of NASA Langley; the higher resolution 20km data have altered values of humidity which aid in cloud prediction, but are considered less realistic for contrail estimations.



Figure 2.13 - RUC data coverage, map adapted [16]

Lower Left, 16.281N, 126.1378W
 Upper Left, 54.1731N, 139.8563W

Lower Right, 17.34N, 69.0371W
 Upper Right, 55.4818N, 57.3794W

The RUC data are constructed using a meteorological data model which uses measured data as inputs. The RUC covers the lower 48 United States and adjacent areas of Canada, Mexico, and oceanic areas. The grid is a subset of the AWIPS Lambert Conformal Grid (AWIPS/GRIB grid 215). Figure 2.13 shows the coverage of the RUC model estimates. The 40-km grid (AWIPS grid ID 236) has 151 by 113 points. The estimates are given hourly, with the 23rd hour missing.

Key features of RUC/MAPS include [17]:

- The RUC uses a hybrid isentropic-sigma vertical coordinate in which most of the atmosphere is resolved on isentropic surfaces (defined by constant virtual potential temperature) except for layers near the ground where terrain-following (sigma) coordinates are used.
- high-frequency (every 1h) 3-d objective analyses over the contiguous United States
- high-frequency (every 1h) short-range weather model forecasts (out to 12 h) in support of aviation and other mesoscale weather forecast users
- assimilation of data from
 - commercial aircraft (relayed through ACARS - Aircraft Communications, Addressing, and Reporting System)
 - wind profilers (404 and boundary-layer 915 MHz)
 - rawinsondes and special dropwindsondes
 - surface reporting stations and buoys
 - RASS (Radio Acoustic Sounding System) - experimental
 - VAD (velocity-azimuth display) winds from NWS WSR-88D radars
 - GOES total precipitable water estimates
 - SSM/I total precipitable water estimates
 - GPS total precipitable water estimates
 - GOES high-density visible and IR cloud drift winds

An example RHi field (relative humidity with respect to ice) is given in Figure 2.14.

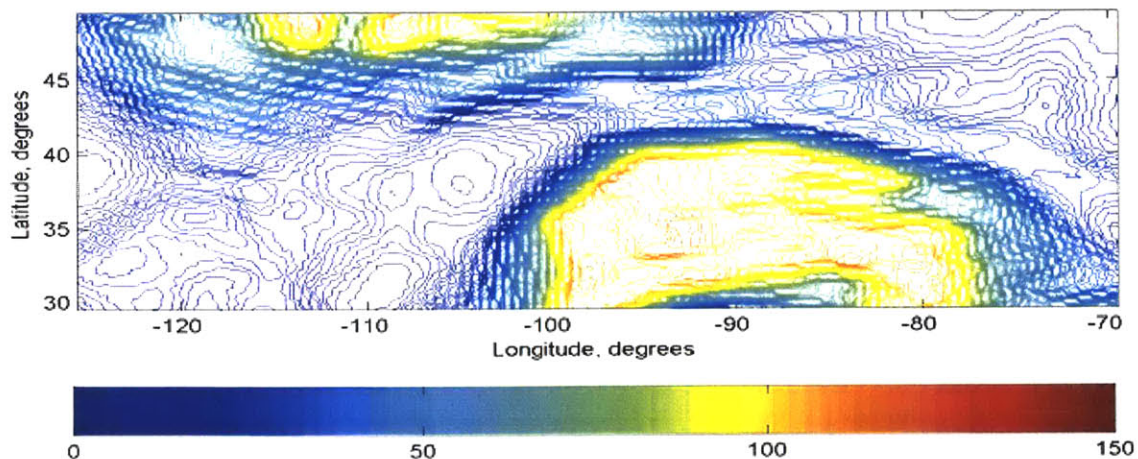


Figure 2.14 - Relative Humidity with respect to ice. 2/5/2002, hour 13, altitude 10972.8, from RUC data

2.3.2. Unified Forecast / Climate Model (UM) Data

The Unified Forecast / Climate Model (UM) is used for modeling the atmosphere and/or the ocean. It is a highly-configurable suite of modules written by the U.K. Meteorological Office, which is used for modeling the atmosphere and/or the ocean. Although many physical processes (such as advection, radiation, convection, precipitation and boundary layer turbulence) are considered in the UM, the modular nature of the code enables the user to include only those sections appropriate to the current application. The UM is operated and maintained by the Numerical Weather Prediction division of the U.K. Meteorological Office.

The Unified Model atmospheric estimates used for this research project were obtained from Dr. Brian Hoskins and Dr. Peter Clark of the University of Reading, England. They provided raw binary output from the UM model for June 27, 2004 and November 12-18, 2003. The data covers the globe, and is of 60km resolution. The operational Unified Model is currently run four times per day, at 00Z, 06Z, 12Z and 18Z, producing three-hour analyses and forecasts [18].

An example RH_i field (relative humidity with respect to ice) is given in Figure 2.15.

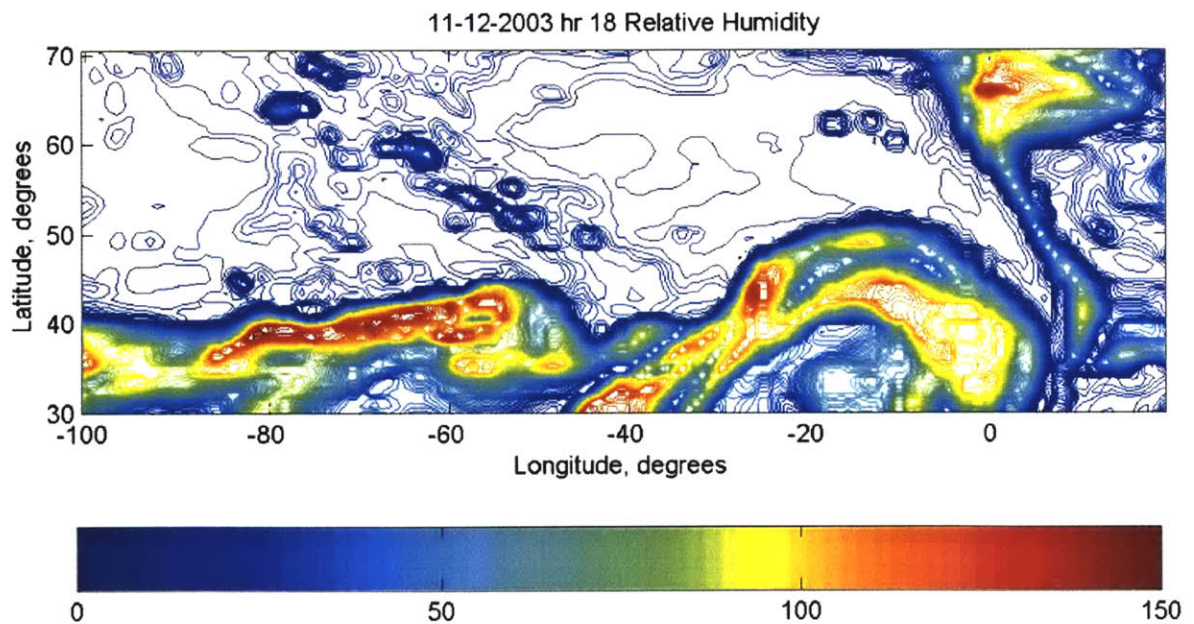


Figure 2.15 - Relative Humidity with respect to ice. 11/12/2003, hour 18, altitude 10972.8, from UM data

2.3.3. Processing Meteorological Information for SAGE Use

For use in SAGE, the meteorological information needed to be in a format such that meteorological fields could be extracted by interpolation (bilinear latitude/longitude, linear altitude, linear time). This required individual processing for the RUC and for the UM information. For instance, the RUC estimates were converted from pressure levels to altitude levels, and from random points into a $\frac{1}{4}$ degree linear grid. The UM estimates were converted into a $\frac{3}{4}$ degree linear grid, taking into account the orography. Additionally, the UM information contained specific humidity, which was converted to relative humidity using the Wexler-Sonntag relations described in Section A.2.2.

These outputs were verified against independent wind source data [19] & [20] and NASA Langley RHi plots. One example comparison is shown in Figure 2.16 and Figure 2.17.

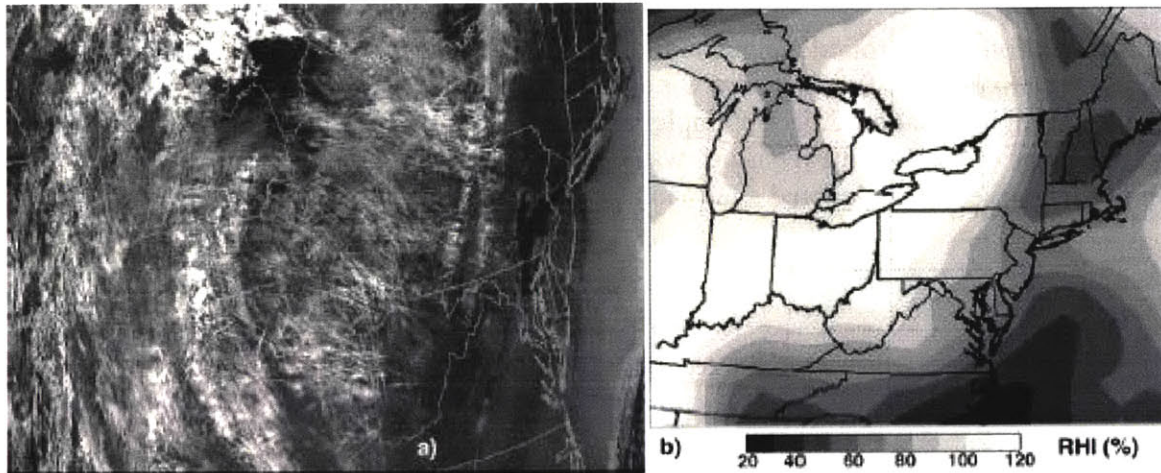


Figure 1. Contrails and humidity over northeastern USA, 18 November 2001. (a) Terra MODIS T11-T12 image, 1624 UTC. (b) 225-hPa RHI (%) from RUC reanalysis, 1600 UTC.

Figure 2.16 - Contrails and humidity over northeastern USA, 18 November 2001. (a) Terra MODIS T11-T12 image, 1624 UTC. (b) 225-hPa RHI (%) from RUC reanalysis, 1600 UTC [21]

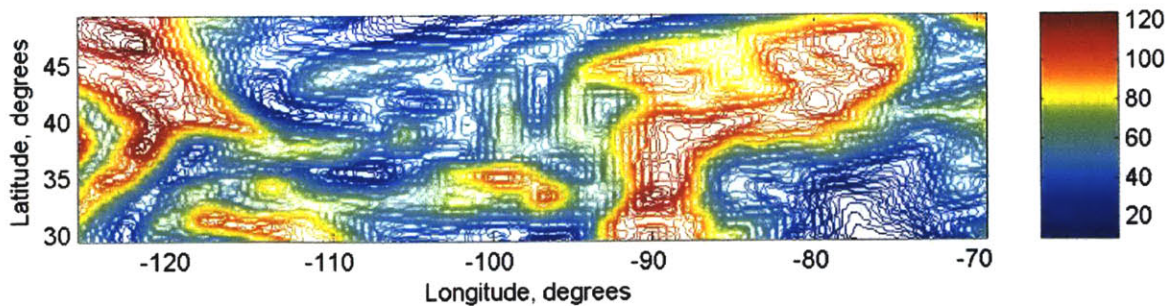


Figure 2.17 - Relative Humidity with respect to ice. 11/18/2001, hour 16, altitude 10972.8, from RUC data

2.3.4. Implementation

Though SAGE had been prepared for meteorological inputs, more adaptations were necessary. The addition of temperature, pressure, and humidity involved querying a database. However, the addition of winds was more involved. The overall assumptions made include:

- The flight is broken up into segments, called chords. The beginning point of each chord is referred to as the head, and the end point of the chord is referred to as the tail. Along a chord, the bearing at the head and tail are equivalent.
- Along chords, the aircraft will travel the shortest distance between two points. On a sphere, this is the great circle distance (see APPENDIX E:).
- Along a chord, averaging the head and tail components supplies an average wind vector for the chord.
- The true pressure and temperature (as opposed to ideal equations) are used everywhere. No winds are in effect during takeoff, since the bearing is unknown.
- Vertical winds are neglected.

In SAGE, both the ground velocity and the true velocity (a.k.a. the relative velocity, the velocity relative to the frame where wind speed is zero) are used. These two velocities can be related through Equation 2.6. To implement this equation, the component of the wind along the trajectory of the aircraft (bearing) was calculated¹². A positive V_{WIND} denoted a headwind, while a negative V_{WIND} denoted a tailwind.

$$V_{_TRUE} = V_{GRS} + V_{WIND} \quad (2.6)$$

where $V_{_TRUE}$ = true velocity
 V_{GRS} = ground velocity
 V_{WIND} = wind velocity aloft, headwind is positive

SAGE runs two types of flights; Enhanced Traffic Management System (ETMS), where ground velocity is given, and Official Airline Guide (OAG), where true velocity is given¹³. Each flight required a separate implementation of Equation 2.5. Additionally, SAGE was updated to reflect winds; aerodynamic and engine portions of SAGE use true velocity (both in velocity and change in velocity), and the time length of the chord (Δt_i) uses ground velocity.

2.3.5. Filtering of ETMS Flight Bearings (Latitude & Longitude)

In order to apply Equation 2.5, the aircraft bearing was needed. The bearing calculation for OAG was trivial, since the trajectories were specified. On the other hand, the ETMS flights used raw positioning data. The data were reported in a mosaic-style fashion, with each instrument's range of data slightly overlapping the ranges of surrounding instruments. Near the boundaries of the instrument's range, the data were less reliable.

¹² Winds were given as either N-S, E-W components, or as a magnitude and direction. For the latter, the direction is given in the navigational sense, where North is 0°, East is 90°, South is 180°, and West is 180°.

¹³ Note that any flight created without knowledge of wind data would fall in the OAG category. Hence all reroutes created were run as OAG flights.

Table 2.3 - Averages and 95% confidence intervals of the percent difference from actual fuel burn before and after weather implementation

	Before (BADA 3.5, transonic)	After (BADA 3.5, transonic, weather, no checks)	After (BADA 3.5, transonic, weather, checks)
1306 Large Carrier Flights	-3.36 +/- 33.13%	2.92 +/- 25.27%	2.70 +/- 24.67%
Same Flights without Honolulu	-3.29 +/- 33.18%	3.04 +/- 25.19%	2.82 +/- 23.45%

Table 2.4 - Averages and 95% confidence intervals of the percent difference from actual fuel burn before and after SAGE updates

	No Additions	With compressibility effects, meteorological data, filtering of flight bearings
1306 Large Carrier Flights	-7.87 +/- 26.95%	2.70 +/- 24.67%
Same Flights without Honolulu	-6.82 +/- 28.80%	2.82 +/- 23.45%

ETMS points were reported everywhere, including within the areas of mosaic overlap. This mosaic overlapping caused consecutive latitude and longitudes to be incorrectly reported to such an extent, that at times the aircraft reportedly flew backwards. Other times, the latitude or longitude was reported as constant. This problem was alleviated through two checks:

1. Pre-SAGE check: Chords with the same time stamp were identified, and most values were averaged. Any delta values (changes along the chord from the beginning to the end, such as the change in velocity) were dropped to prevent high fuel burns.
2. During SAGE check: If the bearing changed between chords by more than 120 degrees, or direct North, South, East, or West is reported, the bearing of the previous chord was used.

Table 2.3 shows the averages and 95% confidence intervals for percent difference from fuel burn before and after the weather implementation¹⁴. The ETMS data set consists of 1306

¹⁴ The average and standard deviation are calculated according to the standard 2000 excel formats. Assuming a normal distribution, confidence intervals (95% and 99%) can be obtained from the standard deviation. A 95% confidence is 1.96 times the standard deviation. A 99% confidence interval is 2.56 times the standard deviation.

United States flights from a large North American airline on October 5, 2000. The weather input consists of 0.25x0.25 degree horizontal resolution and 1000ft vertical resolution RUC output on October 4-6, 2000. Only ten of these flights (origin or destination Honolulu) exited the meteorological data region, and hence have been separated out¹⁵. Furthermore, these flights were DC-9s, which previous research has indicated have high uncertainties in BADA performance estimates.

2.3.6. Summary of SAGE Changes

Table 2.4 shows the summary of SAGE changes employed in the contrail study. In both cases SAGE v1.1 was run with BADA 3.5, and the cruise velocity filter was not used. The combination of all changes decreases both the standard deviation and magnitude of average percent error of fuel burn estimation. This in turn creates more reliable contrail estimations.

2.4. COST-BENEFIT ASSESSMENT METHODS

Before employing the contrail estimation model, a brief discussion is presented of the methods for assessing the costs and benefits of rerouting aircraft to reduce contrail formation.

2.4.1. Background

To effectively assess the rerouting of aircraft, one must understand the inherent costs. Any requirement to move the aircraft to off-optimal cruise locations needs to take into account the necessary tradeoffs in fuel burn and time costs. Chapter 10 of Padilla's Optimizing Jet Transport Efficiency [22] gives an excellent discussion of cruise economy. As can be seen in Figure 2.18, the optimal flight path is a tradeoff of fuel and time costs. This tradeoff occurs not only for Mach number, but each component of flight; altitude, trajectory, aircraft, cargo (weight) limits. Average fuel burn and time costs are well documented.

Suppose that contrail formation is given a cost of X dollars per mile of formation in clear skies, and Y dollars per mile of formation in cloudy skies.¹⁶ With the addition of contrail formation as described in 2.1, SAGE can calculate contrail formation at the chord level. Hence given a contrail cost, the aircraft could be rerouted to a new optimum speed and flight path (Figure 2.19).

Currently, a contrail cost has not been defined. Not only would this contrail cost be a function of time and fuel costs, but ideally it would also be a function of environmental effects. As explained in 2.1, this study does not address environmental effects. Instead, this study identifies the contrail cost as a function of time and fuel costs; a reduction of x amount of contrail formation costs \$y in fuel and \$z in time.

¹⁵ Note that all ten of the Hawaiian flights were DC-9s. Previous research [11] has shown that the fuel burn prediction for DC-9s are incorrect due to incorrect BADA coefficients.

¹⁶ Note that study does not encompass the evolution of the contrails following formation. A better contrail cost would be a function of optical depth, diffusion rate, altitude of formation, and existence of clouds.

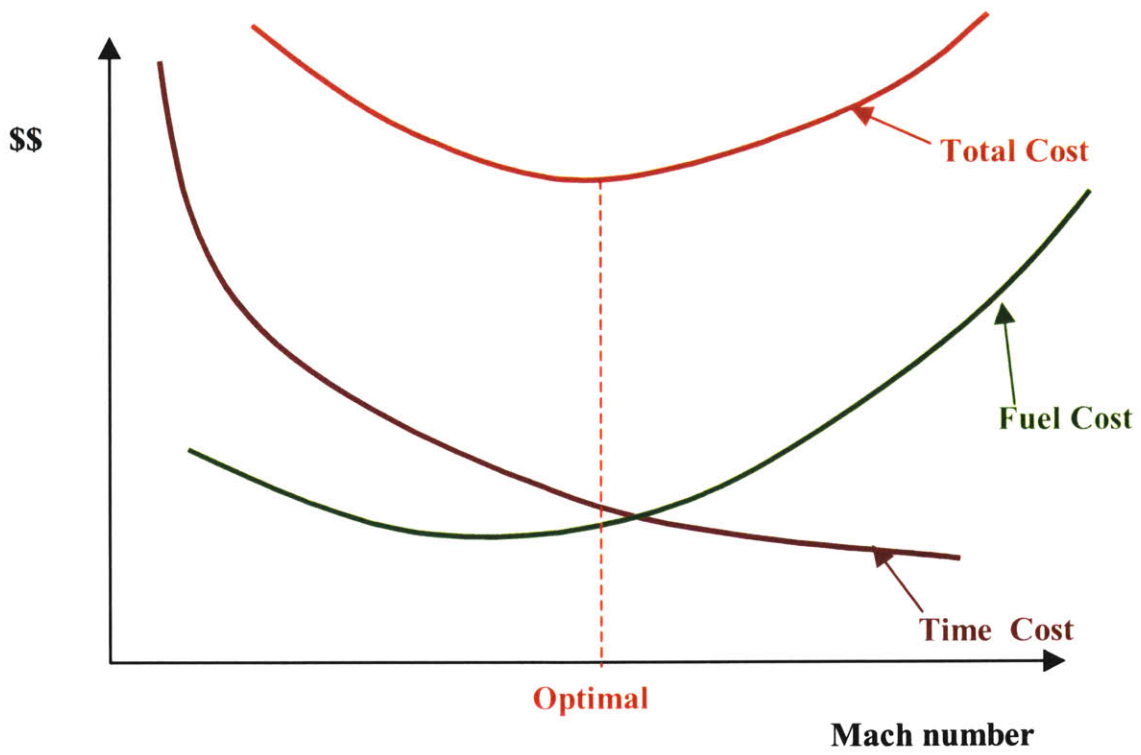


Figure 2.18 - The tradeoff between fuel and time cost, adapted from [22]

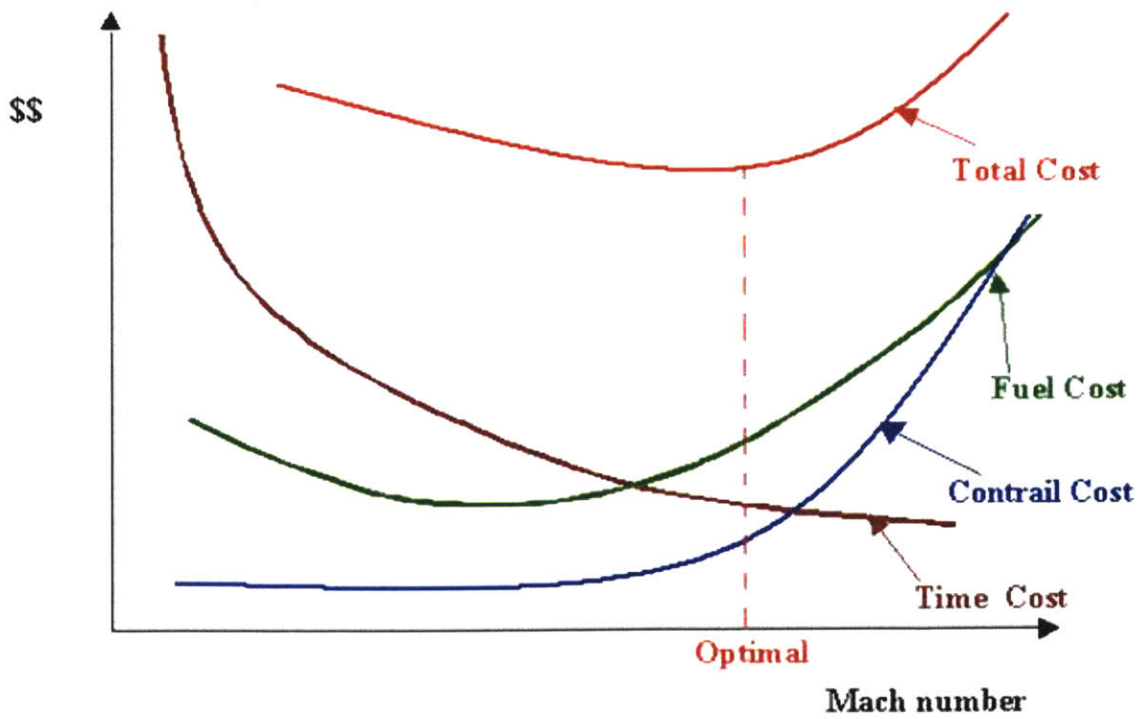


Figure 2.19 - The tradeoff between fuel, time, and (randomly assigned) contrail cost

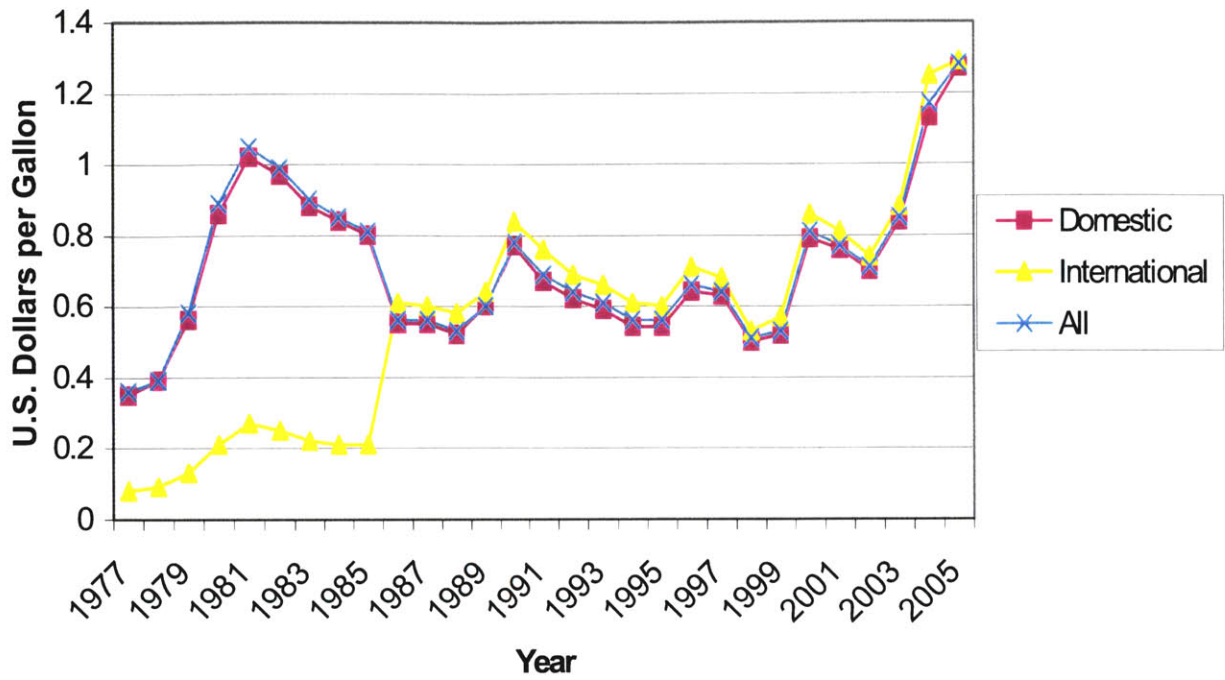


Figure 2.20 – Bureau of Transportation Statistics Airline Fuel Cost (1977-2005), as of March 29, 2005 [23]. Note that these data do not account for inflation.

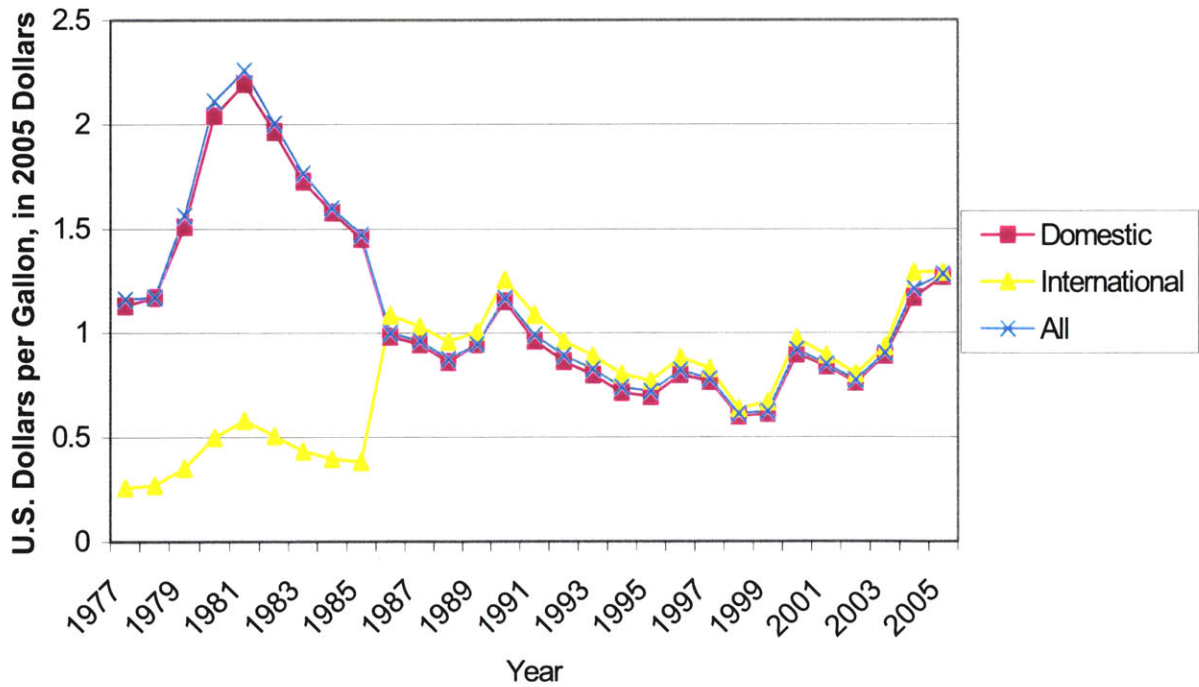


Figure 2.21 – Figure 2.20, converted in 2005 U.S. Dollars [24]

2.4.2. Cost Data

To determine the costs of rerouting aircraft, the aviation system model was modified as described in CHAPTER 2:. Then flights could be flown to ascertain fuel burn and time costs of rerouting to mitigate contrails. Costs were assigned as follows:

2.4.2.1. Fuel Costs

Fuel costs have been well-documented through the years, and the Bureau of Transportation Statistics offers an on-line update of airline fuel costs per gallon from 1977 until 2005, for international, domestic, and total fuel costs [22]¹⁷. Figure 2.20 and Figure 2.21 show these data. Since domestic and international categories were separately defined for each year, the appropriate temporal and spatial fuel burn cost could be assigned to each flight.

For instance, we can briefly examine three example flights. A flight on November 13, 2001 from Los Angeles to New York would use the “Domestic” 2001 fuel cost. A flight on October 23, 2000 from London to Madrid would use the “International” 2000 fuel cost. And finally, a flight on March 13, 2003 from New York to London would use the “All” 2003 fuel cost (because both domestic and international)¹⁸.

2.4.2.2. Time Costs

FAA requires quarterly averages of operating costs to be reported for each aircraft type. This includes, but is not limited to, maintenance, pilot/crew costs, and depreciation. Using these data, the FAA has created economic values for use in cost studies (recent values are listed in Table 2.5). Note that these data do not account for inflation; all data were converted into 2005 United States dollars (as of March 28, 2005).

¹⁷ The mass of one gallon of fuel depends on the temperature. According to Pratt & Whitney, JP-4 has a density of 0.751-0.802 kg/liter at 15°C [24.5], or 2.843-3.036 kg/US gallon. For the purposes of this study, it is assumed that commercial airlines choose a fuel of a density of 2.939 kg/US gallon.

¹⁸ One might argue that the flights from United States to countries abroad could be broken up by the origin city into domestic and international fuel costs. This was not done since it was assumed that the international fuel costs accounted for this.

**Table 2.5 – Excerpt from Table ES-1: Economics Values for Use in Analyses: Aircraft Operating Cost [25].
More specific values (e.g. 2-engine narrow body) are found in [25]. Values in 2005 United States dollars.**

Physical Units	Value	Year	In USD2005
Large (Form 41) Passenger Carriers:			
Variable Operating Cost per Hour	\$2,096	2002	\$2,276
Fixed Cost per Hour	640	2002	695
Total Cost per Hour	2,736	2002	2,970
Large (Form 41) Cargo Carriers:			
Variable Operating Cost per Hour	4,339	2002	4,711
Fixed Cost per Hour	1,583	2002	1,583
Total Cost per Hour	5,922	2002	6,429
Regional (Form 41) Passenger Carriers:			
Variable Operating Cost per Hour	3,218	2002	3,494
Fixed Cost per Hour	1,008	2002	1,094
Total Cost per Hour	4,226	2002	4,588
Regional (Form 41) Cargo Carriers:			
Variable Operating Cost per Hour	3,235	2002	3,512
Fixed Cost per Hour	702	2002	762
Total Cost per Hour	3,938	2002	4,275
Form 298-C Alaskan Carriers:			
Variable Operating Cost per Hour	359	2001	396
Fixed Cost per Hour	108	2001	119
Total Cost per Hour	467	2001	515
Form 298-C Non-Alaskan Carriers:			
Variable Operating Cost per Hour	622	2001	686
Fixed Cost per Hour	256	2001	282
Total Cost per Hour	878	2001	969
General Aviation:			
Variable Operating Cost per Hour	394	2003	418
Fixed Cost per Hour	672	2003	713
Total Cost per Hour	1,006	2003	1,068
Military:			
Total Cost per Hour	6,640	2002	7,209

2.4.3. Application

Fuel burn costs were assigned to the individual origin-destination pairs based on the year flown. Time costs (sum of total fixed costs and crew costs) were assigned to the individual origin-destination pairs based on the aircraft type and year flown. The cost index (ratio of time cost per hour to fuel cost per pound, after Padilla [22]) was also computed, but was not compared to industry data. Results are shown in Table 2.6.

Table 2.6 - Chosen fuel burn and time costs for each origin-destination pair¹⁹

Origin-Destination	Aircraft	Year	Fuel Burn (US05/gallon)	Time (US05/hour)	Cost Index (\$ per hr/\$ per lb)
ATL-DFW	B712	2001	\$ 0.84	\$1226	\$9472.89
ATL-LAX	B764	2001	0.84	2069	15986.47
ATL-LGA	B752	2001	0.84	1226	9472.89
ATL-ORD	B752	2001	0.84	1226	9472.89
BOS-LAX	B762	2001	0.84	2069	15986.47
DFW-LAX	B752	2001	0.84	1226	9472.89
DFW-LGA	B752	2001	0.84	1226	9472.89
JFK-LAX	B762	2001	0.84	2069	15986.47
LAX-BOS	B752	2001	0.84	1226	9472.89
LAX-DFW	B752	2001	0.84	1226	9472.89
LAX-JFK	B762	2001	0.84	2069	15986.47
LGA-ORD	B733	2001	0.84	1226	9472.89
MIA-SEA	B763	2001	0.84	2069	15986.47
SEA-MIA	B763	2001	0.84	2069	15986.47
BOS-EGLL	B744	2003	0.90	4043	29034.58
BOS-LFPG	A343	2003	0.90	4043	29034.58
EDDF-JFK	B742	2003	0.90	4043	29034.58
EDDF-ORD	B763	2003	0.90	2069	14858.41
EGLL-BOS	B744	2003	0.90	4043	29034.58
EGLL-JFK	B744	2003	0.90	4043	29034.58
EGLL-ORD	B772	2003	0.90	2069	14858.41
JFK-EDDF	B763	2003	0.90	2069	14858.41
JFK-EGLL	B744	2003	0.90	4043	29034.58
JFK-LFPG	B763	2003	0.90	2069	14858.41
LFPG-JFK	B763	2003	0.90	2069	14858.41
LFPG-ORD	A343	2003	0.90	4043	29034.58
ORD-EDDF	B763	2003	0.90	2069	14858.41
ORD-EGLL	B744	2003	0.90	4043	29034.58
ORD-LFPG	B763	2003	0.90	2069	14858.41

¹⁹ Attempting to follow the FAA paper... All jets are “large” since they have greater than 10 tons cargo capacity. Number of engines and aircraft width (wide or narrow) is identified through BADA.

CHAPTER 3: ASSESSMENT OF CONTRAIL ESTIMATION PROCEDURE AGAINST SATELLITE DATA

An important contribution of this thesis is made through the comparison of the contrail estimations to satellite data. This is the first study to take thousands of radar tracks and type-specific aircraft models and “fly” these through weather estimates, and then directly compare contrail estimations to satellite observations. This is important because there is very high uncertainty in both the estimation and the sensing of contrails, and this provides a useful contribution for understanding uncertainties in both.

3.1. CONTRAIL MASKS

Contrail formation can be detected in infrared satellite observations. Figure 3.1 shows three sets of satellite data and matching relative humidity with respect to ice (RH_i). As to be expected, the clouds form in areas of high humidity. At RH_i ~ 100%, contrails can be seen (evinced best by the top photo).

Creating an algorithm to identify contrails from satellite data was beyond the scope of this project. Instead, satellite contrail data were supplied by NASA Langley, courtesy of Dr. David Duda and Dr. Patrick Minnis (Figure 3.2 and Figure 3.3) using methods presented by Mannstein et al. [28].

3.1.1. Description

Data were provided for the 17-24 Universal Time Conversion (UTC) for the week of November 12-18, 2001. These consisted of three subsections:

1. Terra tracks for NOAA-16 satellite²⁰. These depict the satellite path over the Earth (Figure 3.2) [26].
2. Satellite infrared radiances (IR) from the Sun-synchronous *NOAA-16* Advanced Very High Resolution Radiometer (AVHRR) 1-km imager (Figure 3.3, right). Only the evening overpasses were provided (17-24 UTC), in which the satellite passed over the Earth from south to north. Hence the satellite images provided were flipped east to west [27].
3. Contrail masks (Figure 3.3, left). The satellite data sets for deriving the contrail coverage consist of the *NOAA-16* data and multispectral 1-km data from the MODerate Resolution Imaging Spectroradiometer (MODIS) on the *Terra* satellite [27].

Note that 11/13/2001 and 11/14/2001 had satellite images missing regions of data through the middle of the image. Hence these days, though run, were not closely examined. All satellite images and contrail masks (numbers 2 and 3) are given in APPENDIX F:.

²⁰ NOAA stands for National Oceanic and Atmospheric Administration

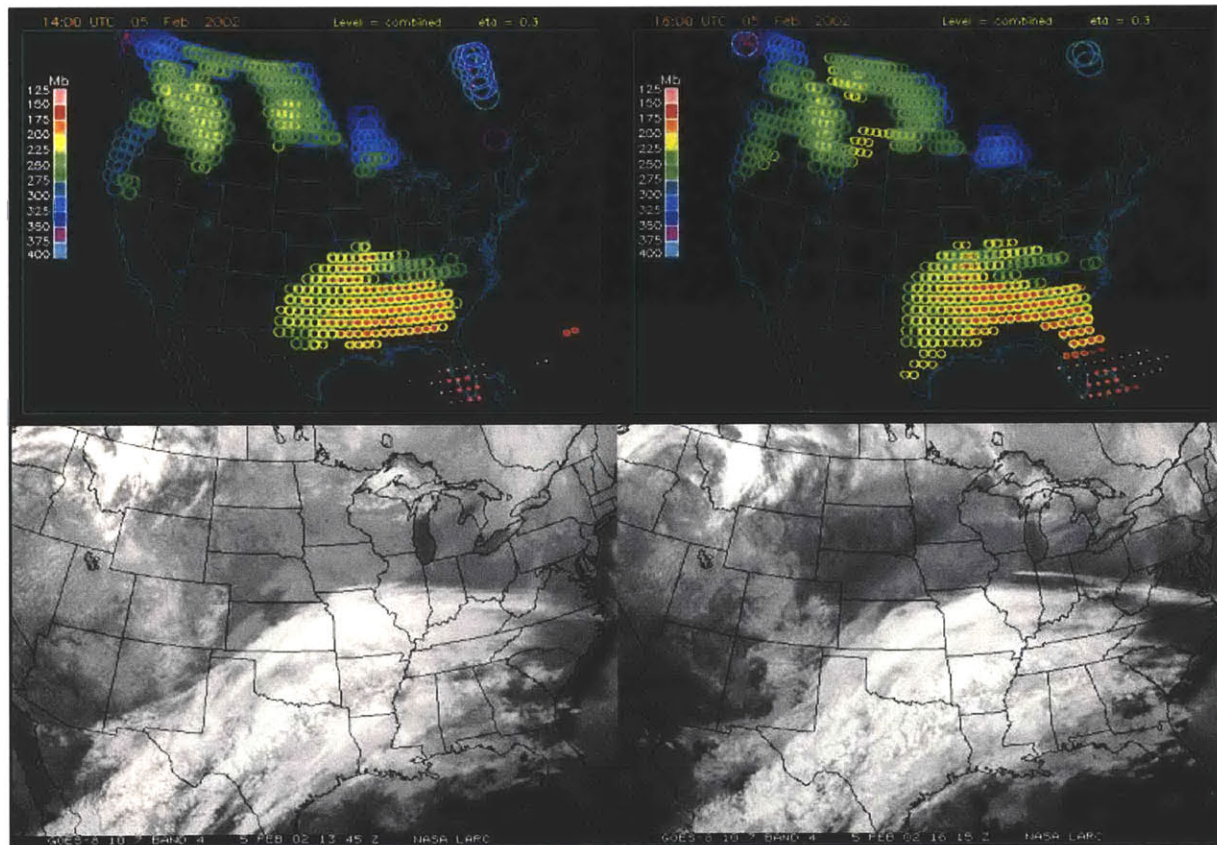
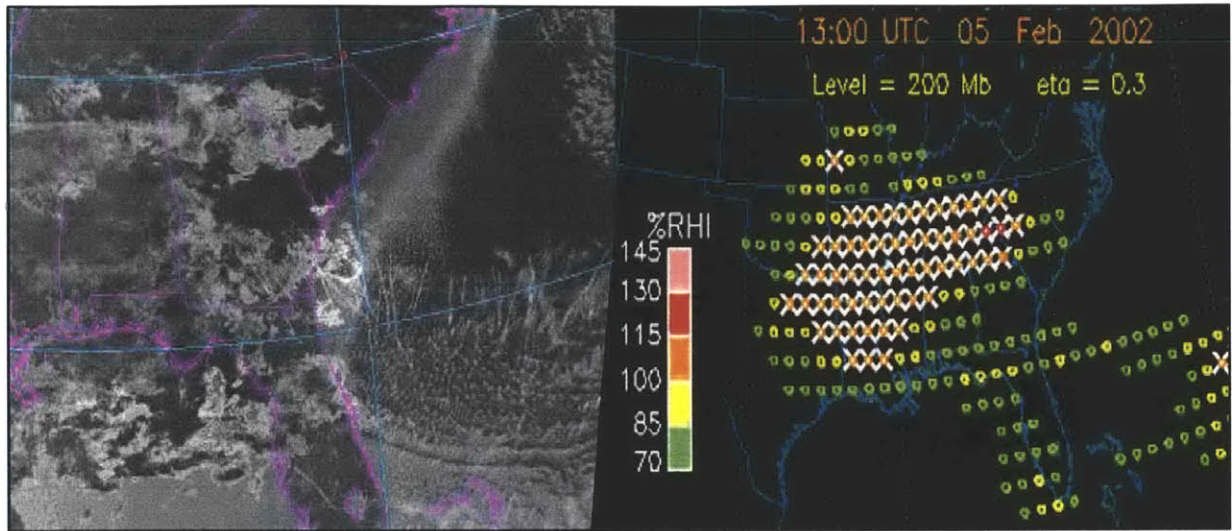


Figure 3.1 - Three sets of satellite data and matching humidity data [28]

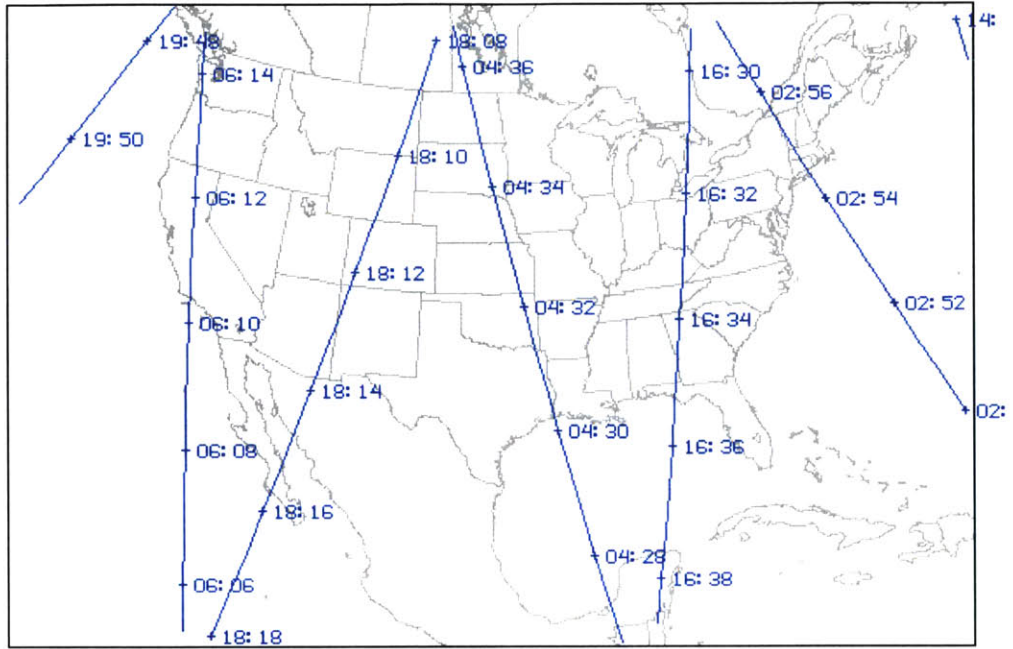


Figure 3.2 - Terra tracks for NOAA-16 satellite, November 18, 2001 [26].

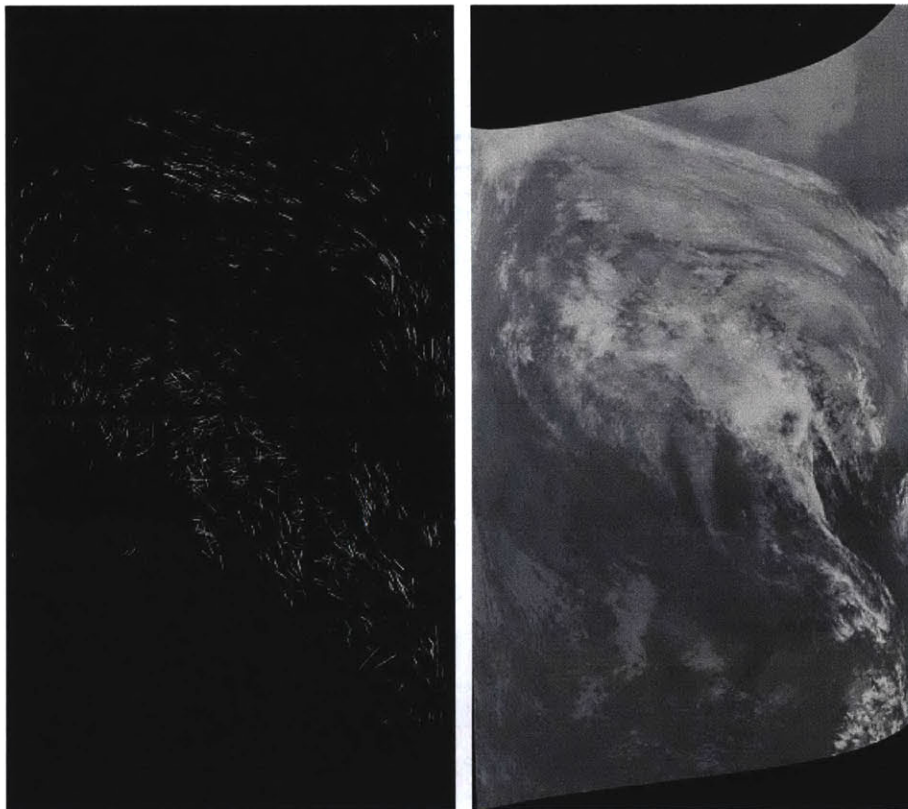


Figure 3.3 - NOAA-16 satellite image and matching contrail mask (white pixel indicates contrail formation), November 18, 2001 1888 UTC. Note that the satellite image is reversed from east to west. This occurs due to the direction the satellite passes overhead.

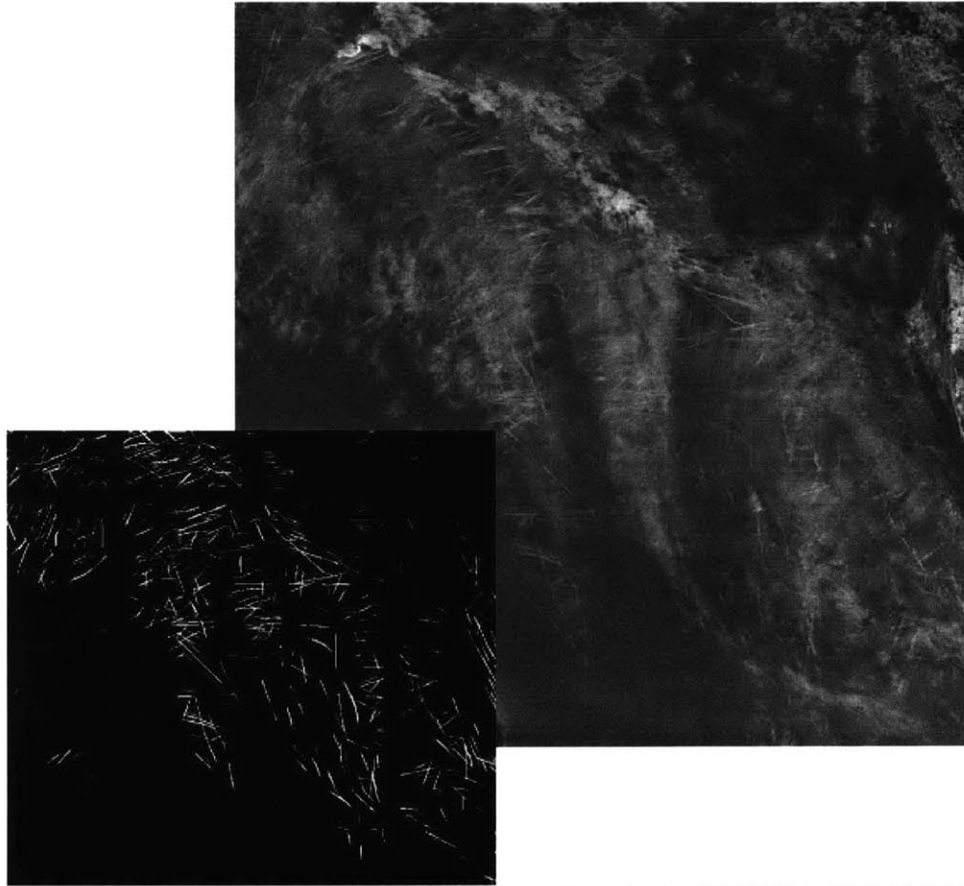


Figure 3.4 - Portion of difference image and matching contrail mask for 11/18/2001, 1888 UTC (Middle of Figure 3.3). In this case, contrails appear to be correctly identified in many cases.

3.1.2. Caveats

As the contrail identification is integral to comparison of actual and estimated contrails, a brief description of the contrail identification scheme is necessary. Young contrails have a smaller crystal size than regular clouds, and hence have a higher IR transmissivity (brightness) in the $10.8\mu\text{m}$ image as compared to the $12\mu\text{m}$ image. Hence a brightness differencing scheme can be used to identify all image pixels which may be contrails: $10.8\mu\text{m}$ minus $12\mu\text{m}$ brightness temperature difference. Figure 3.4 gives an example of a difference image and matching contrail mask. Note that in this example, the contrail mask appears to correctly isolate contrails from the surrounding cirrus.

However, using only a temperature differencing technique could identify singular pixels, edges of clouds, or ground features. A second property of contrails is their linear features, especially at a young age. Hence a linear filter was introduced to help filter non-contrail particles. Extended information on processing techniques is described by Mannstein et al. [28].

There is only limited confidence in the ability of these techniques to identify contrails. Young contrails (less than about 50 minutes) and weak contrails are too small to be noticed by the satellites, and therefore are not identified. Older contrails (greater than 2.5 hours) have begun to lose their linear features, so would also not be identified (even though the crystal size may still be small).

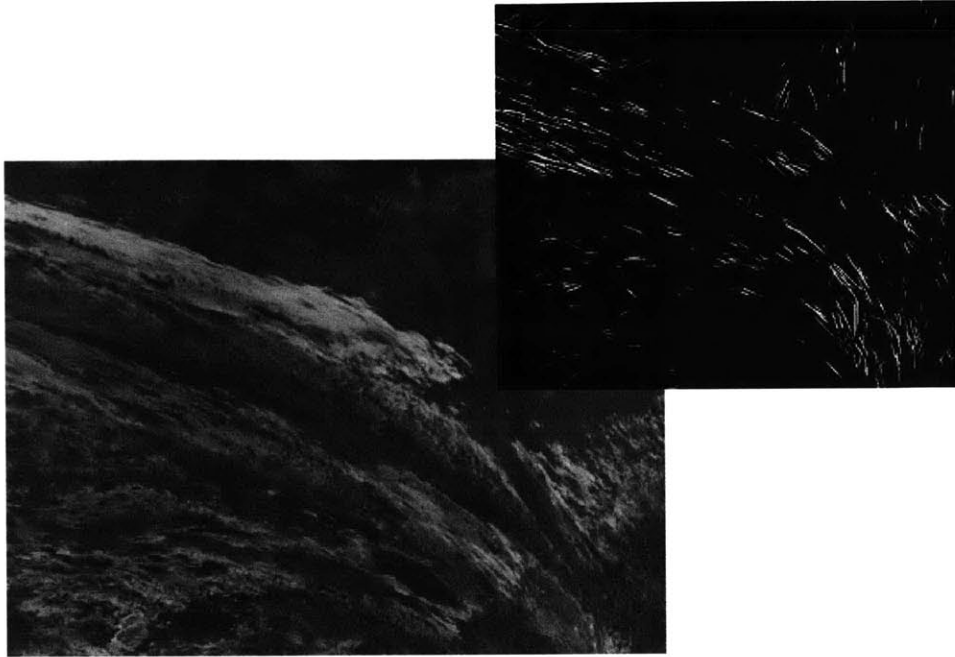


Figure 3.5 - Portion of difference image and matching contrail mask for 11/18/2001, 1888 UTC (Upper right of Figure 3.3). In this case, striated cirrus cloud formation is misidentified as contrails.



Figure 3.6 - Portion of difference image and matching contrail mask for 11/12/2001, 1827 UTC (Middle left of Figure F.1). In this case, striated cirrus cloud formation is misidentified as contrails.

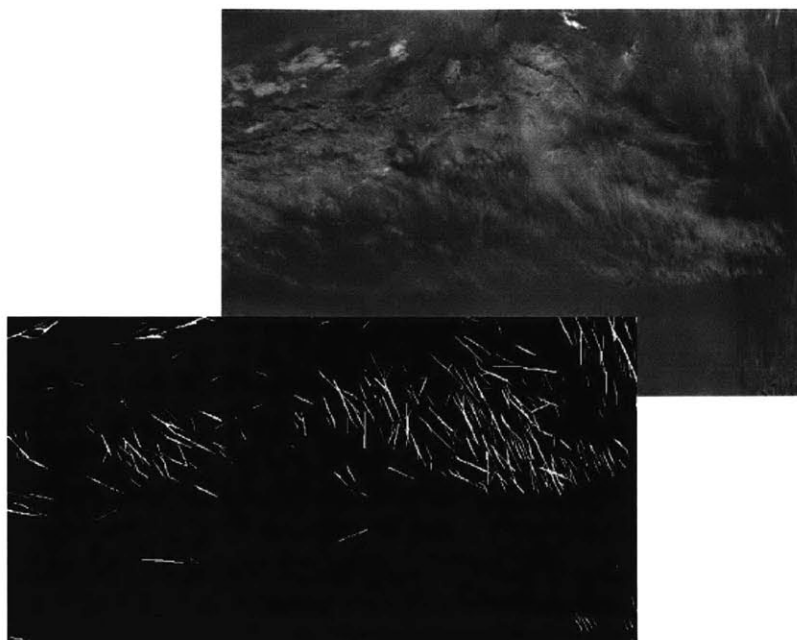


Figure 3.7 - Portion of difference image and matching contrail mask for 11/15/2001, 1827 UTC (Middle right of Figure F.11). In this case, striated cirrus cloud formation is misidentified as contrails.

Misdetection can occur due to elongated cirrus streaks near the edge of cloud systems, or due to linear ground features. According to Mannstein et al. [28], the contrail algorithm has a detection efficiency (defined as the ratio of correct contrail detections to the amount of all visually recognized contrails) of 30-50%, with a misidentification rate of 0.1%. This study identifies a much higher misidentification rate, and also calls into question the RHi data.

3.1.2.1. Misidentification as Contrail

Although contrails become clearer in the difference image, striated cirrus clouds can be misidentified as contrails. Figure 3.5 shows an example of such a misidentification (note this is the same day as Figure 3.4). Visual comparison of the contrail masks to satellite data (see APPENDIX F:) shows that the misidentification rate is high, perhaps on order of 40-50%. Other examples are given in Figure 3.5, Figure 3.6, and Figure 3.7.

3.1.2.2. Accuracy of RHi data

This study was able to independently assess the positive mis-identification rate of the contrail mask algorithm against the finest resolution RHi data. First, contrail mask data and contrail estimation data were transferred into specific latitude and longitude points²¹. Next these figures were overlaid on RHi images. Figure 3.8 and Figure 3.9 show the contrail mask data on November 12, 2001 at 1996 hours, universal time. Note that the first figure contains all the satellite data, while the second figure is filtered to contain only some of the data (filter denoted by crosses). The filtering methods were provided by NASA Langley, and consist of removing points a) outside the satellite image range, and b) near the edges of the image where curvature is high (when scan angle magnitude is greater than 50°) [29].

²¹ Courtesy of Rabi Palikonda, NASA Langley.

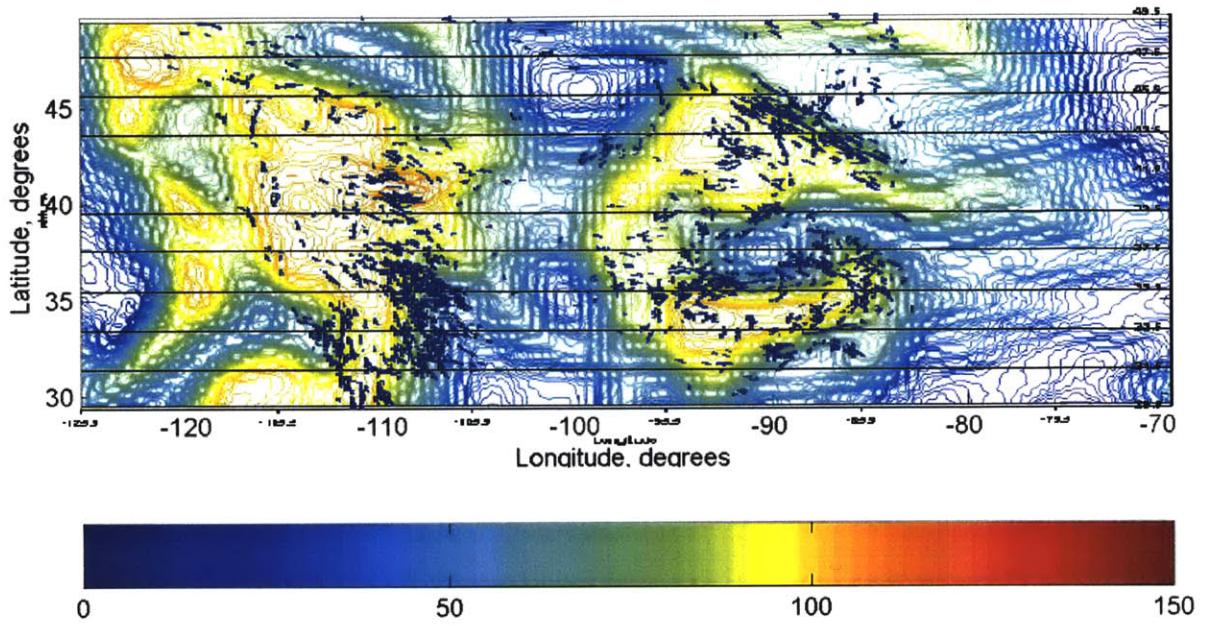


Figure 3.8 - All points of the satellite image (11/12/2001 hr 1996). RHi (hour 19 field).

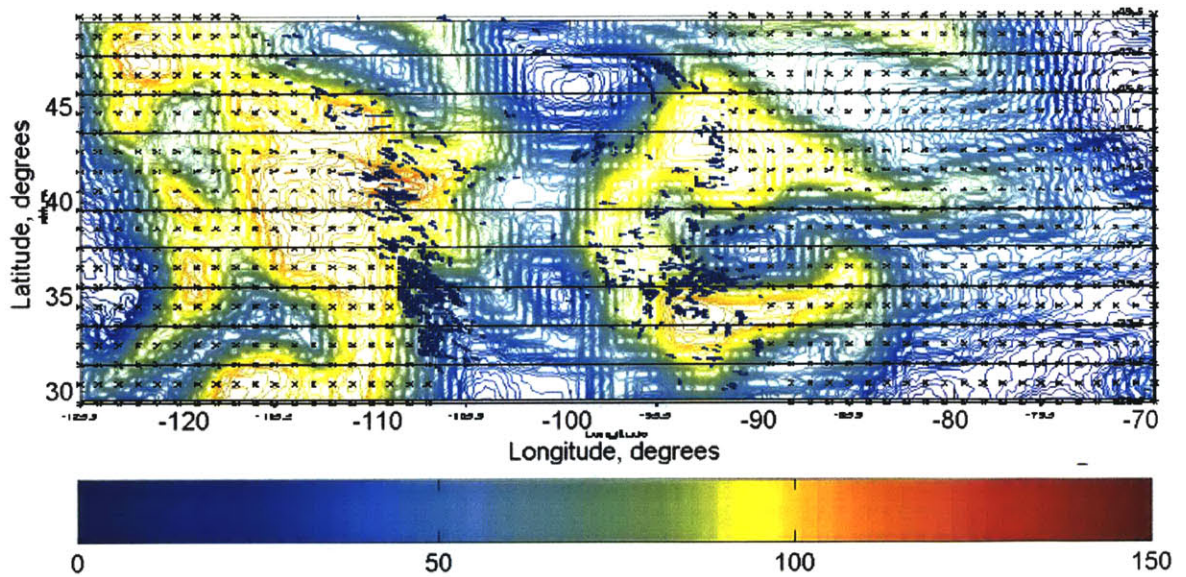


Figure 3.9 - The high confidence regions of the satellite image (11/12/2001 hr 1996). RHi (hour 19 field). Note that crosses indicate the area of nonexistent or uncertain satellite pixels.

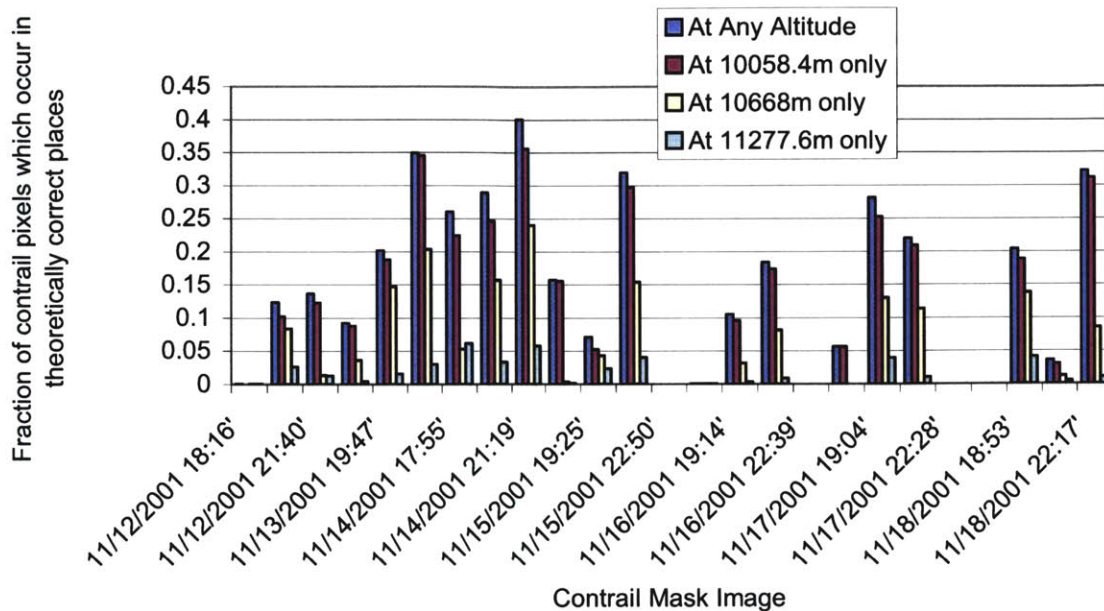


Figure 3.10 - Fraction of contrail pixels which occur in theoretically correct places (i.e. where $RH_i > 100\%$). The “at any altitude” category encompasses all contrail pixels which could have occurred at any of the flight levels examined.

Theoretically, solid particles (clouds and/or contrails) should sublime at $RH_i < 100\%$ ²². Visual comparison of the contrail masks to satellite data (see APPENDIX F:) shows that the contrail pixels are usually either contrails or clouds; they are rarely ground features. Consequently, an accurate RH_i data set would be expected to have $RH_i > 100\%$ in most areas of contrail pixels.

Visual examination of Figure 3.8 and Figure 3.9 shows that this does not occur; contrails pixels appear in areas of $RH_i < 100\%$. Similar results are obtained for the other days examined as shown in Figure 3.4 and Figure 3.7. Figure 3.10 shows the fraction of contrail mask pixels that appear in areas of $RH_i > 100\%$ for three flight levels for all days examined. Based on this comparison, 60-90% of the contrail pixels occurred in a vertical column where they should not. Some of the misidentification occurs because only three altitudes were examined; but as contrails occur most often at or near these flight levels, changing the flight levels should not change the misidentification rate.

This exercise demonstrates that the RH_i fields, although representative, do not accurately portray the true RH_i fields on a given day in 2001.

²² In the literature, the threshold can be variously placed as somewhere between 95-105% [27], although there is high uncertainty. A recent conference concerning “Cirrus Clouds and their Supersaturated Environment” highlights the uncertainty in contrail and cirrus cloud predictions [35]. As noted by Spichtinger [12], some of the ice-supersaturated regions are sub-grid scale. Although recognized, these regions are ignored for the purposes of this study.

3.2. COMPARISON OF ESTIMATED CONTRAILS AND CONTRAIL MASK

In order to compare the satellite images and the model estimations, temporally- and spatially-matched ETMS flights were chosen (from United States continental flights). These flights were simulated in the updated SAGE model, and contrail formation was estimated.

3.2.1. Advection of Estimated Contrails

Since the contrail mask only extracted contrails from 50-150 minutes in age, it became relevant to examine wind advection of the estimated contrails²³. Given an invariant wind of 20 m/s, a 150-minute-old contrail could move 180km (approx. 2 degrees). Hence it was determined that advection was needed.

However, over the course of 2.5 hours (the age of the oldest contrail identified by the contrail mask algorithm), it was demonstrated that the winds could change dramatically. For one day of 2001 continental flights, wind magnitude changed by 70 +/- 274 %, and direction changed by -7 +/- 67 degrees. For one day of 2003 transatlantic flights, wind magnitude changed by 87 +/- 357 %, and direction changed by 5 +/- 66 degrees. This change, though significant, resulted in less than a degree (~ 50 km) of movement. Consequently, for this study only a first order advection was applied; the contrail was assumed to travel the same velocity in the same direction for the entirety of its lifetime.

3.2.2. Sample Day

Figure 3.11 and Figure 3.12 show the set of continental flights that temporally match the contrail mask image. Specifically note the absence of flights around the edges of the figure; contrails will not be estimated here, but might occur due to international flights.

3.2.3. Alignment of Estimated Contrail Data With Contrail Mask

Comparisons were made for 53,844 U.S. continental flights performed during the week of November 11/12-18, 2001. Generally, areas of contrail formation are consistent between the contrail mask and the estimated contrail data. Where the images are not consistent, the estimated contrails match well with the RHi fields. The discrepancies can be attributed to:

- *Incorrect representation of RHi gradients with altitude* – In some of the satellite images, contrails appeared in areas of RHi < 100%, a physically unrealizable occurrence. Some confusion lies in the representation of the RHi data field. The RHi fields shown here for comparison purposes are for 11km, and hence do not capture gradients in altitude. (Note however, that the full Rhi fields as a function of altitude were used for the analysis of the simulated flights, but only one altitude is shown in the

²³ Note that the data were given in degrees (latitude/longitude) and the contrails would advect a distance (km). Consequently, an equation converted degrees to distance was needed. Given lower and upper latitudes as Φ_1 and Φ_2 and R as the radius of the Earth (~6369km):

$$\text{Latitude distance} = R * \pi / 180$$

$$\text{Longitude distance} = (\text{Latitude distance}) * \cos(\Phi)$$

$$\text{Area (swept out by a one degree by one degree box)} = 2 * \pi / 360 * R^2 * (\cos(\Phi_1 + 90) - \cos(\Phi_2 + 90))$$

figure.) Through an altitude range of 9.5 – 12.5 km (common U.S. flight levels), the RHi fields could vary in location by several degrees. Hence contrails could appear to be located in physically unrealizable spots, but just be removed in altitude from the RHi field depicted²⁴.

- *Incorrect RHi fields* – The RHi fields in the meteorological data are imperfect reconstructions of the true RHi fields. Contrails cannot appear in an area where RHi <100%; they should have advected with the RHi field and evaporated as they passed out of an area of high RHi. For instance, the northeast curve (50N 100W, Figure 3.9) appears in an area where RHi < 100%. Looking at hour 16 of the RUC data, it is possible that contrails could have formed in these locations. However, the contrails should have advected with the RHi field, and evaporated as they passed out of an area of high RHi.
- *Threading* – The contrail mask incorrectly reported contrails, in what NASA Langley terms “threading”. Often these the “contrails” are a mixture of striated cloud formations and linear ground features. Threading will also be used to refer to areas where the clouds are so thick that contrails are not identified. The southwest corner (32N 105W, Figure 3.9) is a case of “threading”; returning to the original images (Figure 3.3), we can see that the “contrails” are a mixture of striated cloud formations and linear ground features.
- *Insufficient flight data* – Recall that this study examined continental U.S. flights only. Neglecting international flights leads to an underestimate of persistent contrails, especially at the edges of the United States. For instance, contrails would form to the southeast (30N 85W) or at the northern border (49N, 100W) where there were no flights (according to Figure 3.11); these may be caused by international flights.
- *Incorrect contrail advection* – A shearing of contrails will appear due to a multitude of aircraft traveling the same route; a better contrail advection model may more correctly locate these contrails.

3.2.4. Extended Results

The following are extended results from comparisons the contrail mask and the estimated contrail data (Figure 3.13-Figure 3.23). Each page contains the filtered contrail mask, the map of flights examined, and the filtered estimated contrail data. The filter is based on the “good” points of the satellite data (as determined by NASA Langley), and is denoted by crosses. Where pertinent, the caption will briefly describe discrepancies in the images.

Contrail mask data were available for the entire week of 11/12-18/2001. Unfortunately, some hours are not presented in this section. For instance, the days of 11/13/2001 and 11/14/2001 had a section of data points missing in the middle of the contrail image. This caused an incorrect comparison, and hence these days were not examined in detail. Also, some hours reported contrails outside the set of flights examined, so these days were not examined.

Finally, note that the colorbar is constant in all RHi graphs, so is listed only once on each page.

²⁴ It is suspected that areas of RHi which are relatively constant with respect to altitudes are large cloud structures, and hence have more reliable RHi fields. However, this is unproven, and therefore this possibility will be ignored.

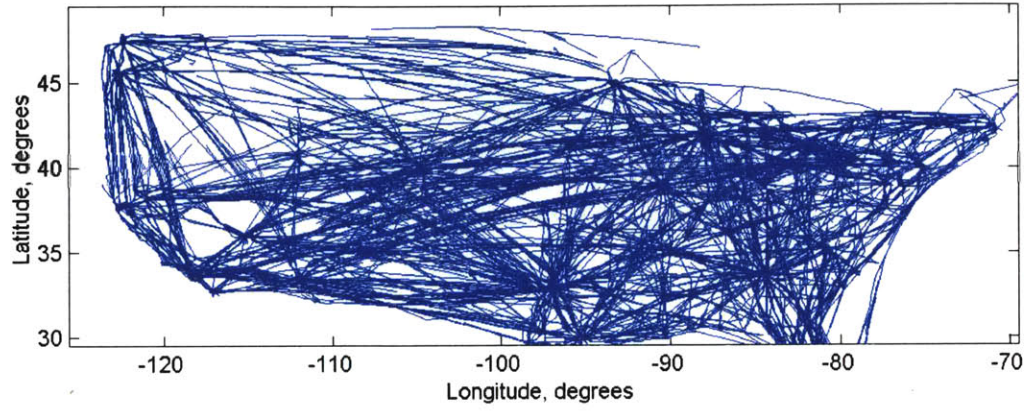


Figure 3.11 - Continental US flights on 11/12/2001 which temporally overlap with data in Figure 3.9.

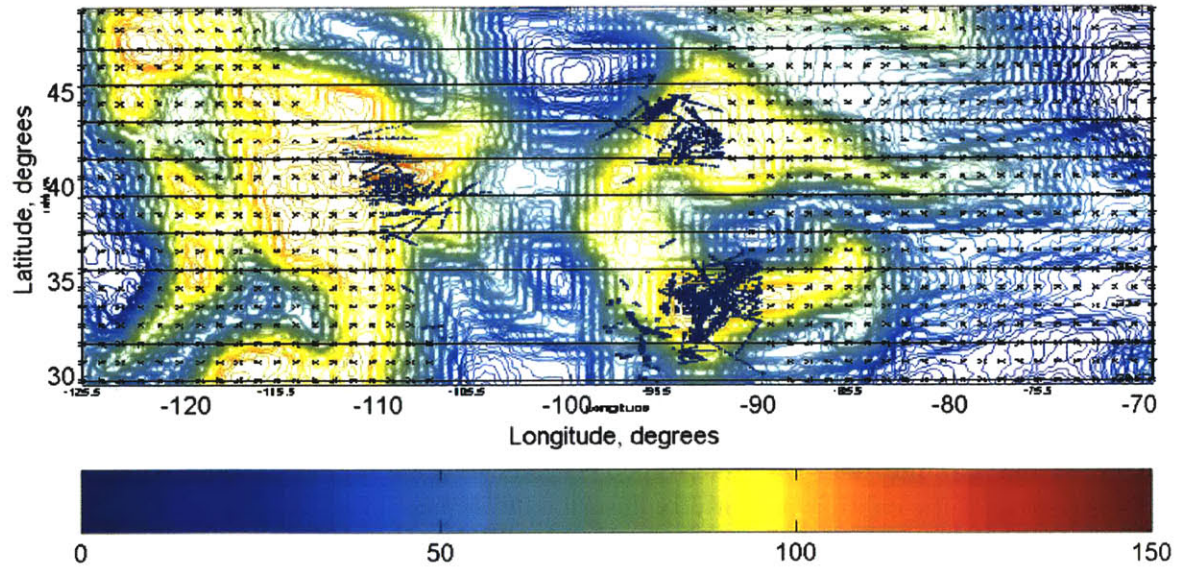


Figure 3.12 – SAGE estimated contrails, filtered by contrail mask filter. (11/12/2001 hr 1996). RHi (hour 19 field).

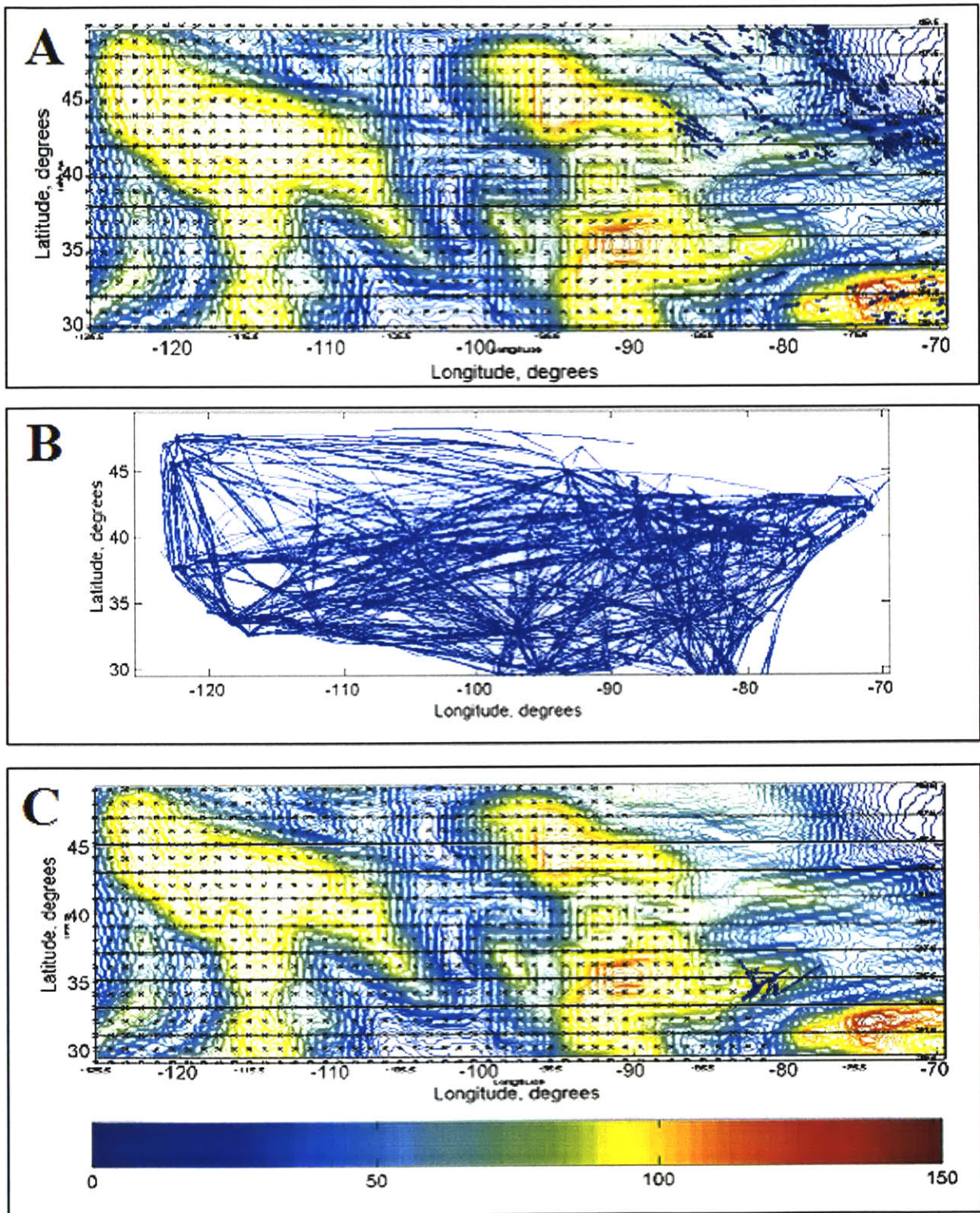


Figure 3.13 - 11/12/2001 hr 1827, RHi hour 16 field. A) Filtered contrail mask. Contrails (45N 75W) caused partially by threading. B) Flights examined, C) Filtered contrail estimation. Lack of contrails caused partially by insufficient flight data.

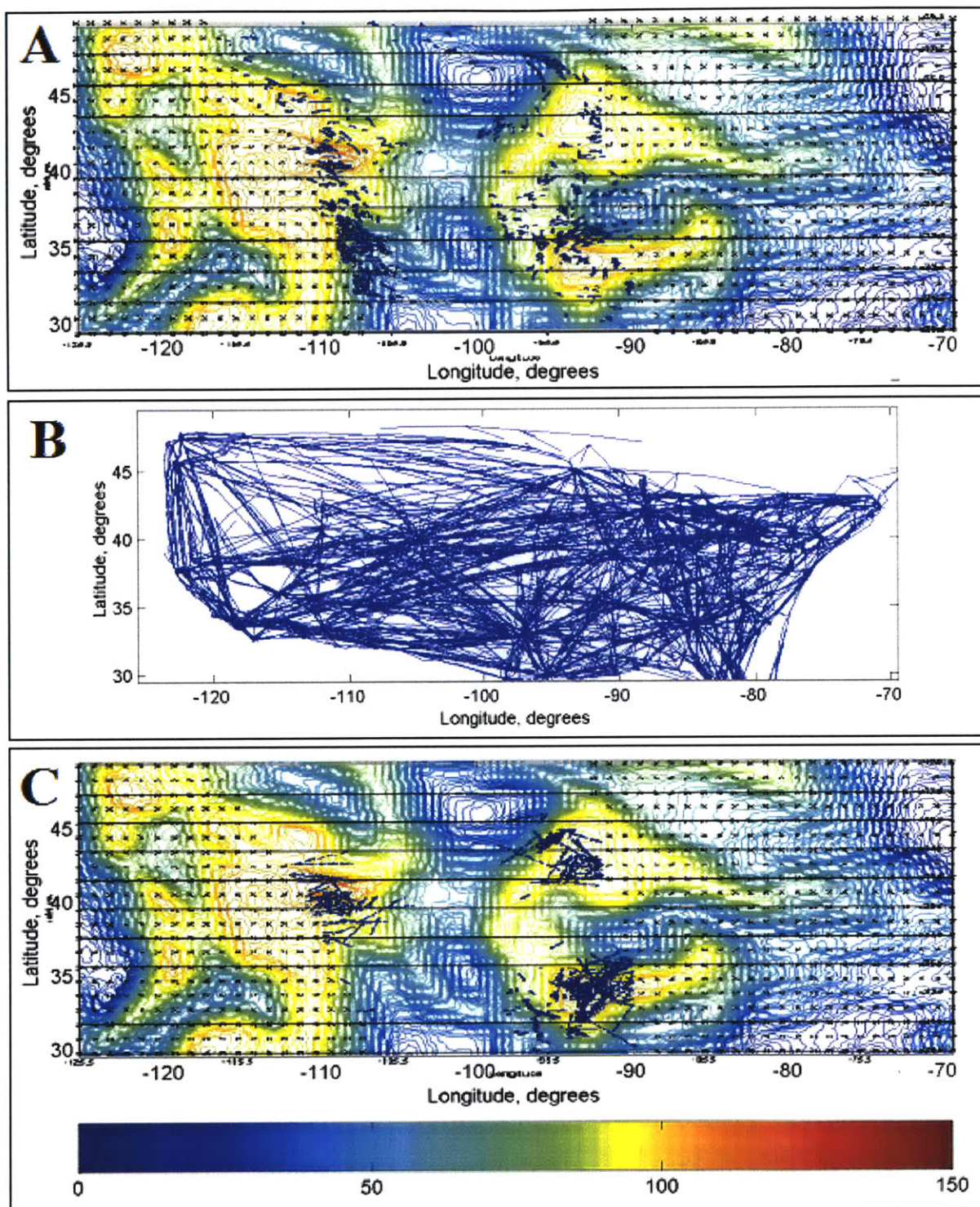


Figure 3.14 - 11/12/2001 hr 1996, RH_i hour 19 field. A) Filtered contrail mask. Contrails (47N 100W) caused by incorrect RH_i field (temporally changing). Contrails (32N 110W) caused by threading. B) Flights examined, C) Filtered contrail estimation.

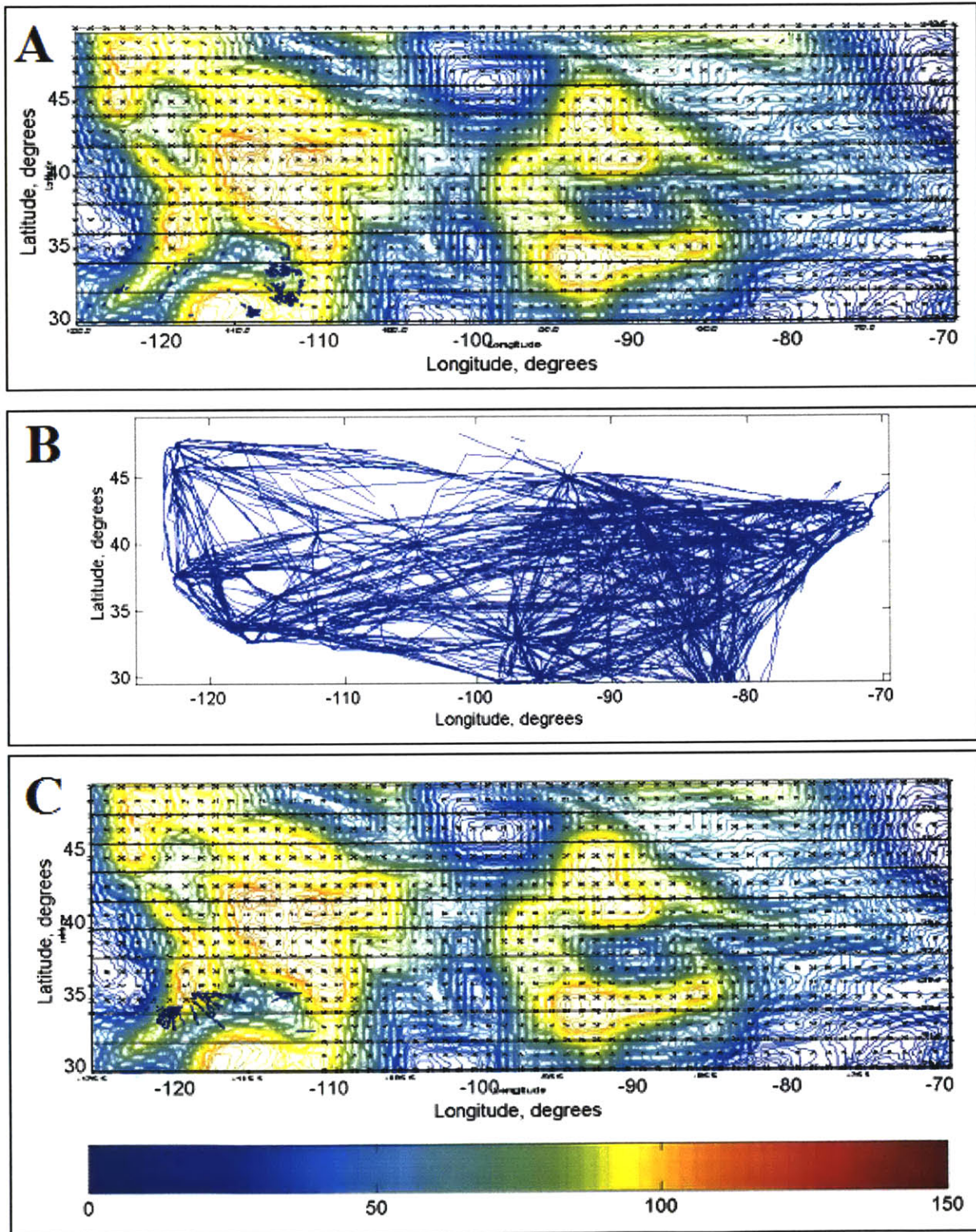


Figure 3.15 - 11/12/2001 hr 2167, RHi hour 20 field. A) Filtered contrail mask. B) Flights examined, C) Filtered contrail estimation. Contrails (32N, 120W) caused by incorrect RHi field (bad in general). Lack of contrails s (32N 112W) caused by insufficient flight data.

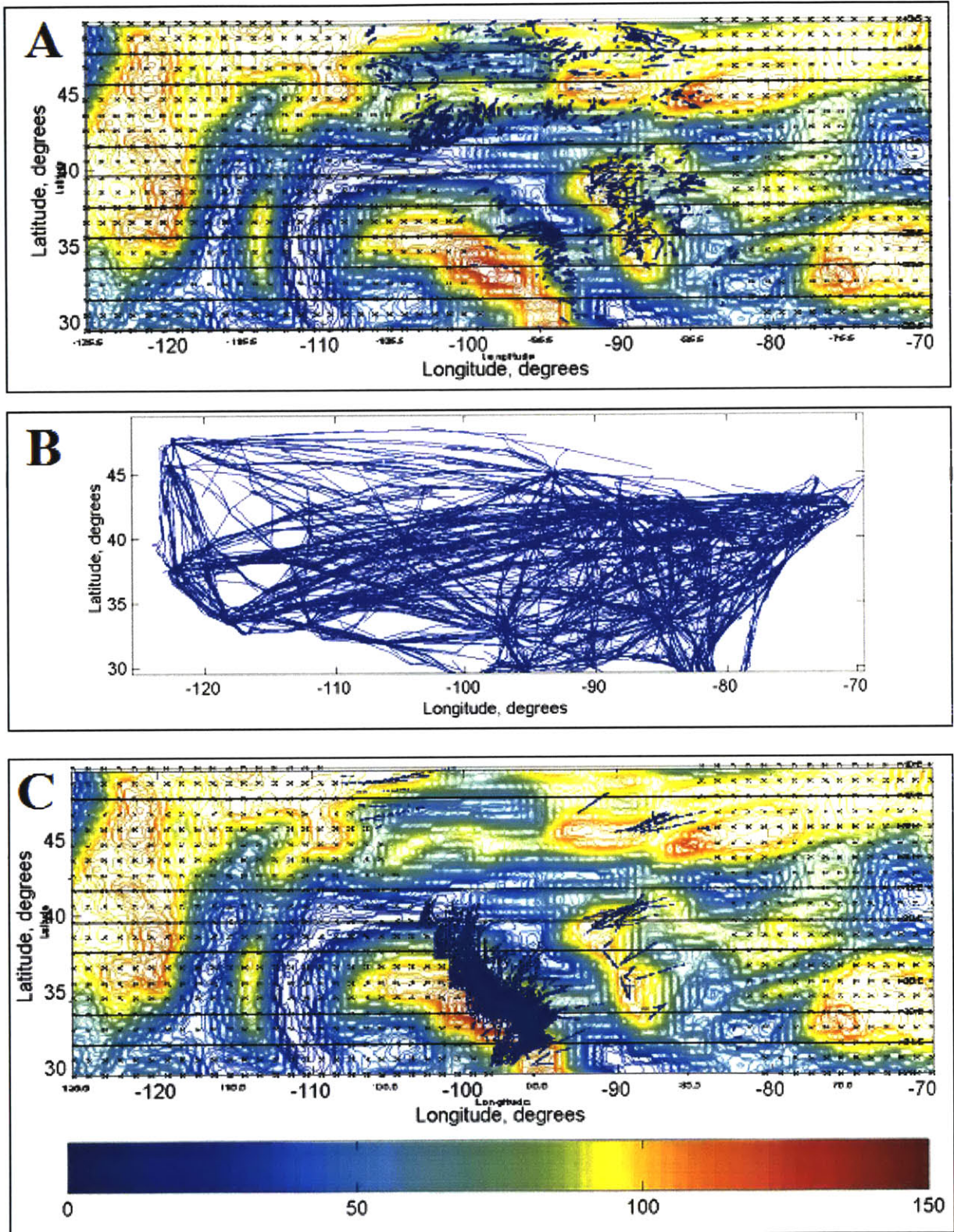


Figure 3.16 - 11/15/2001 hr 1942, RHi hour 18 field. A) Filtered contrail mask. B) Flights examined, C) Filtered contrail estimation. Contrails (35N 96W, 35N 90W) caused by incorrect contrail advection. Lack of contrails (45N 95W) caused by insufficient flight data.

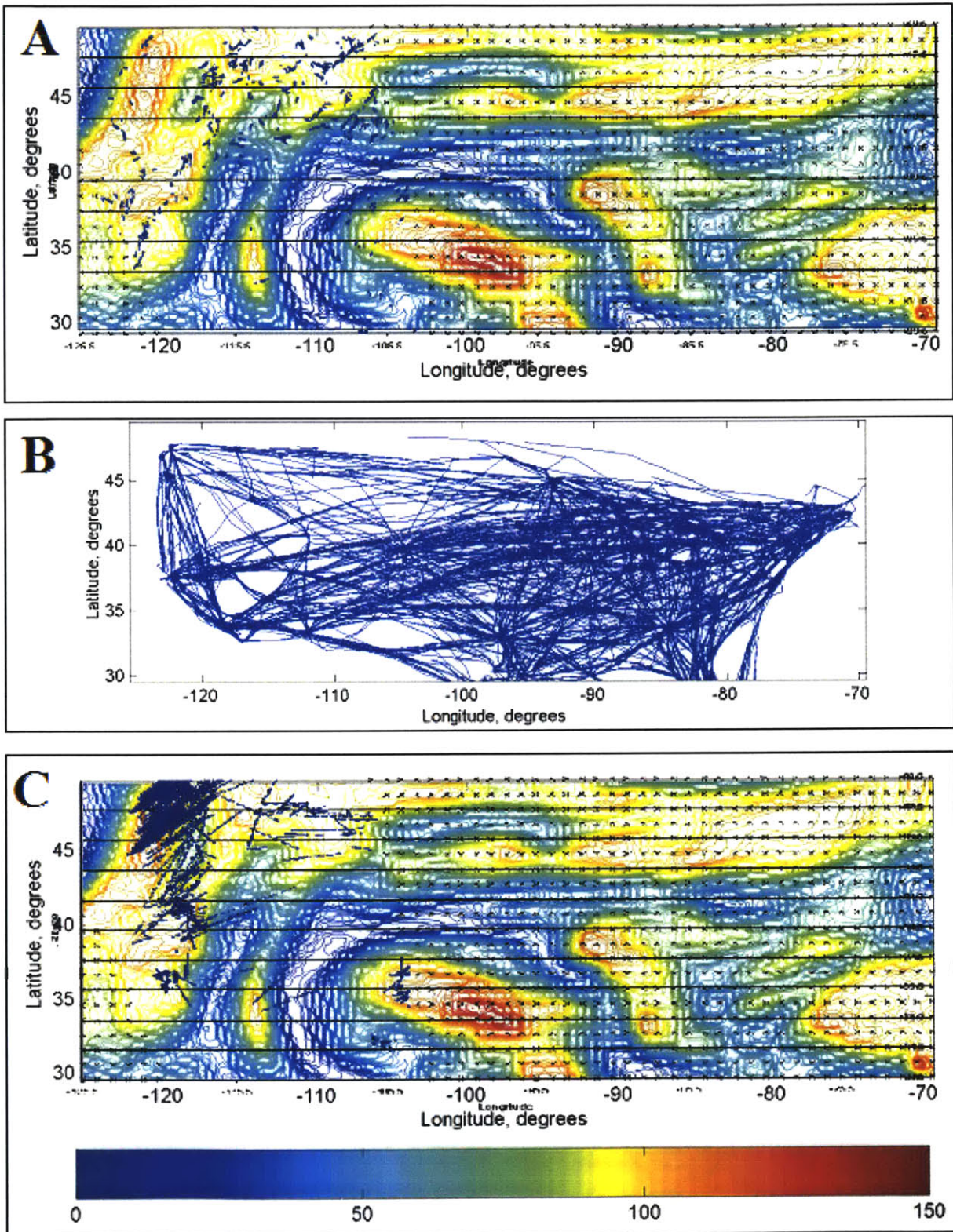


Figure 3.17 - 11/15/2001 hr 2113, RHi hour 20 field. A) Filtered contrail mask. Lack of contrails (45N 120W) caused by threading (contrail mask does not see contrails in clouds). B) Flights examined, C) Filtered contrail estimation. Contrails (47N 120W) caused by incorrect contrail advection.

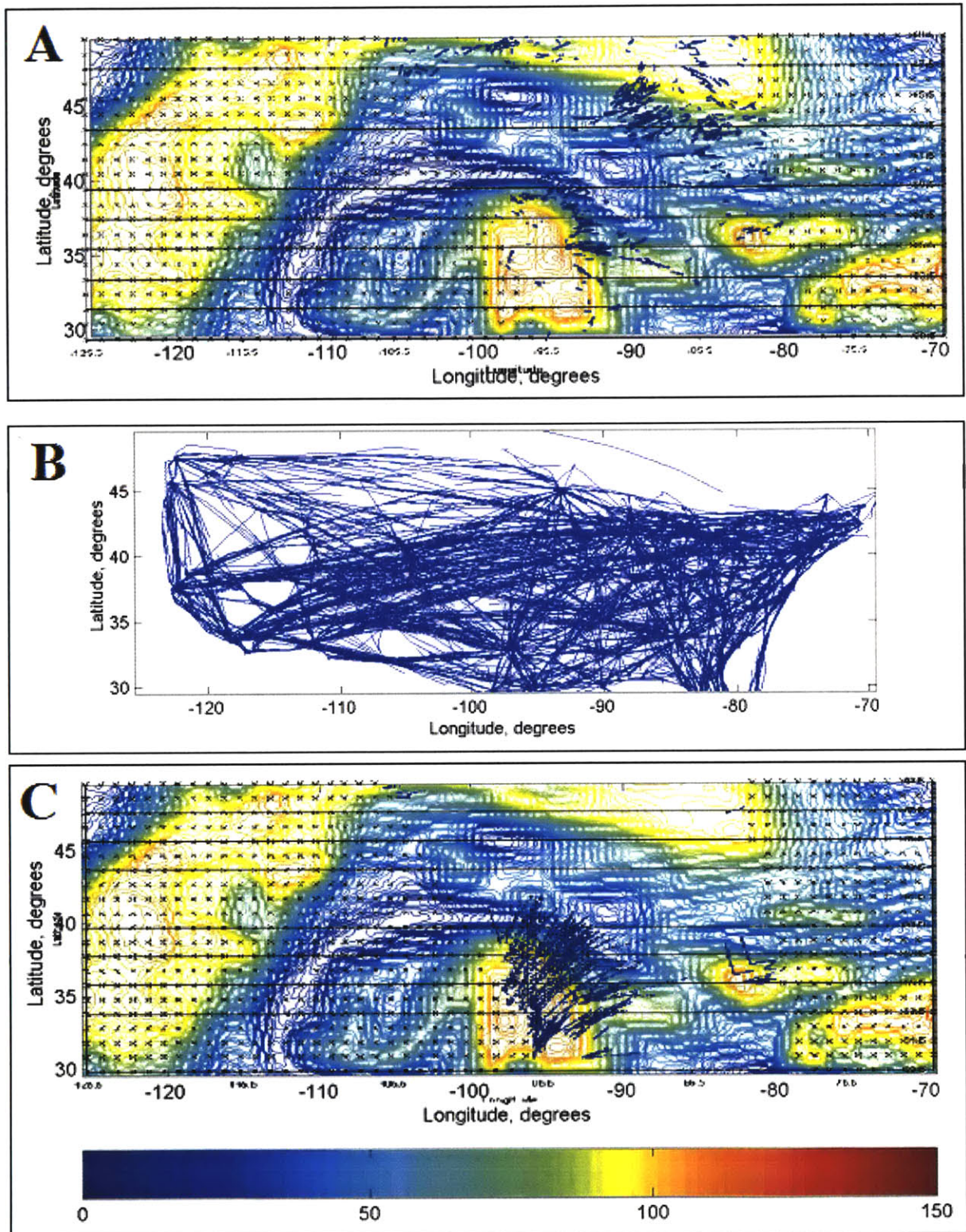


Figure 3.18 - 11/16/2001 hr 1924, RHi hour 18 field. A) Filtered contrail mask. Lack of contrails (35N 96W, 35N 90W) caused by threading (contrail mask does not see contrails in clouds). B) Flights examined, C) Filtered contrail estimation. Lack of contrails (45N 95W) caused by insufficient flight data.

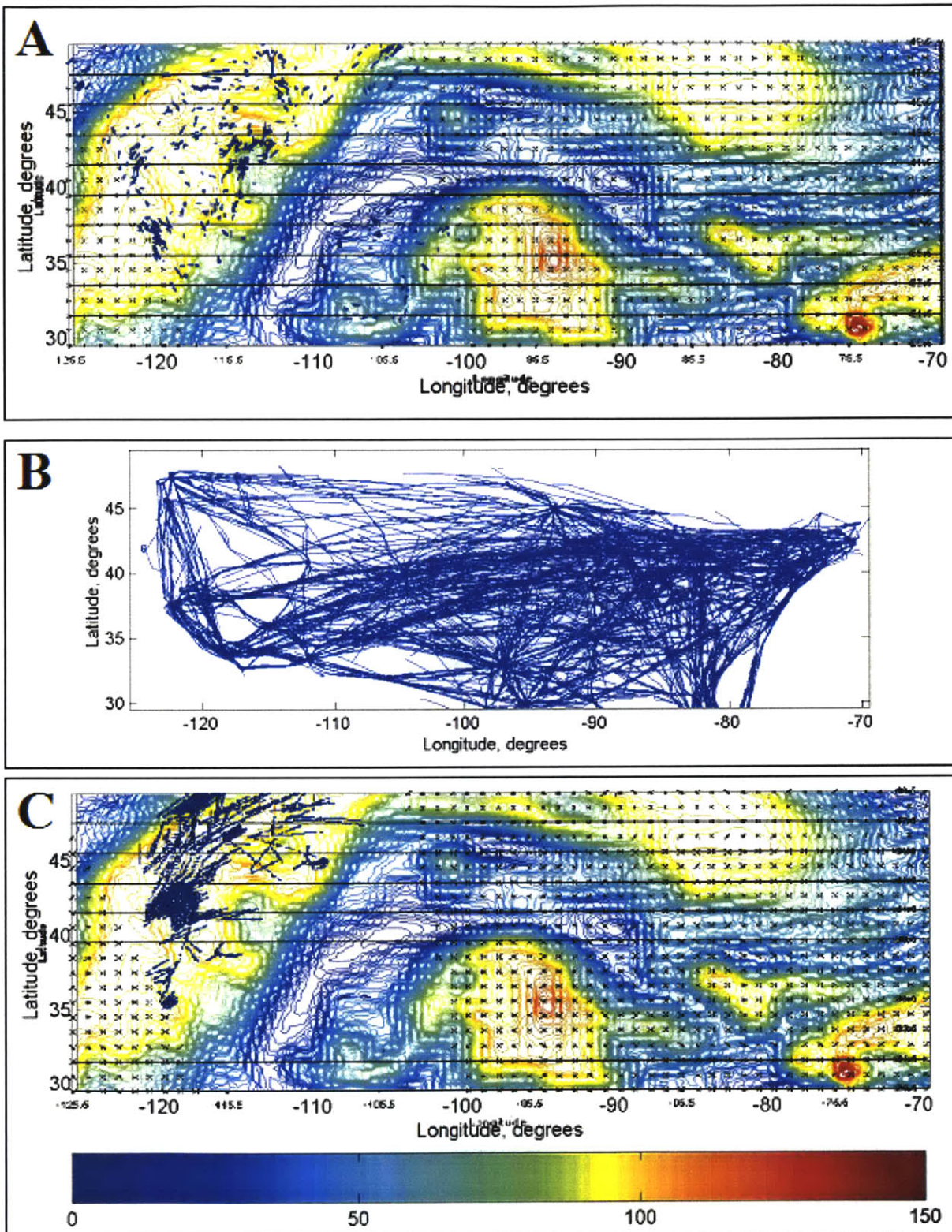


Figure 3.19 - 11/16/2001 hr 2095, RHi hour 20 field. A) Filtered contrail mask. Contrails caused by threading (some contrails are clouds, and some clouds block out contrails). B) Flights examined, C) Filtered contrail estimation. Contrails (47N 120W) caused by incorrect contrail advection (note there were no flights at 42N 120W).

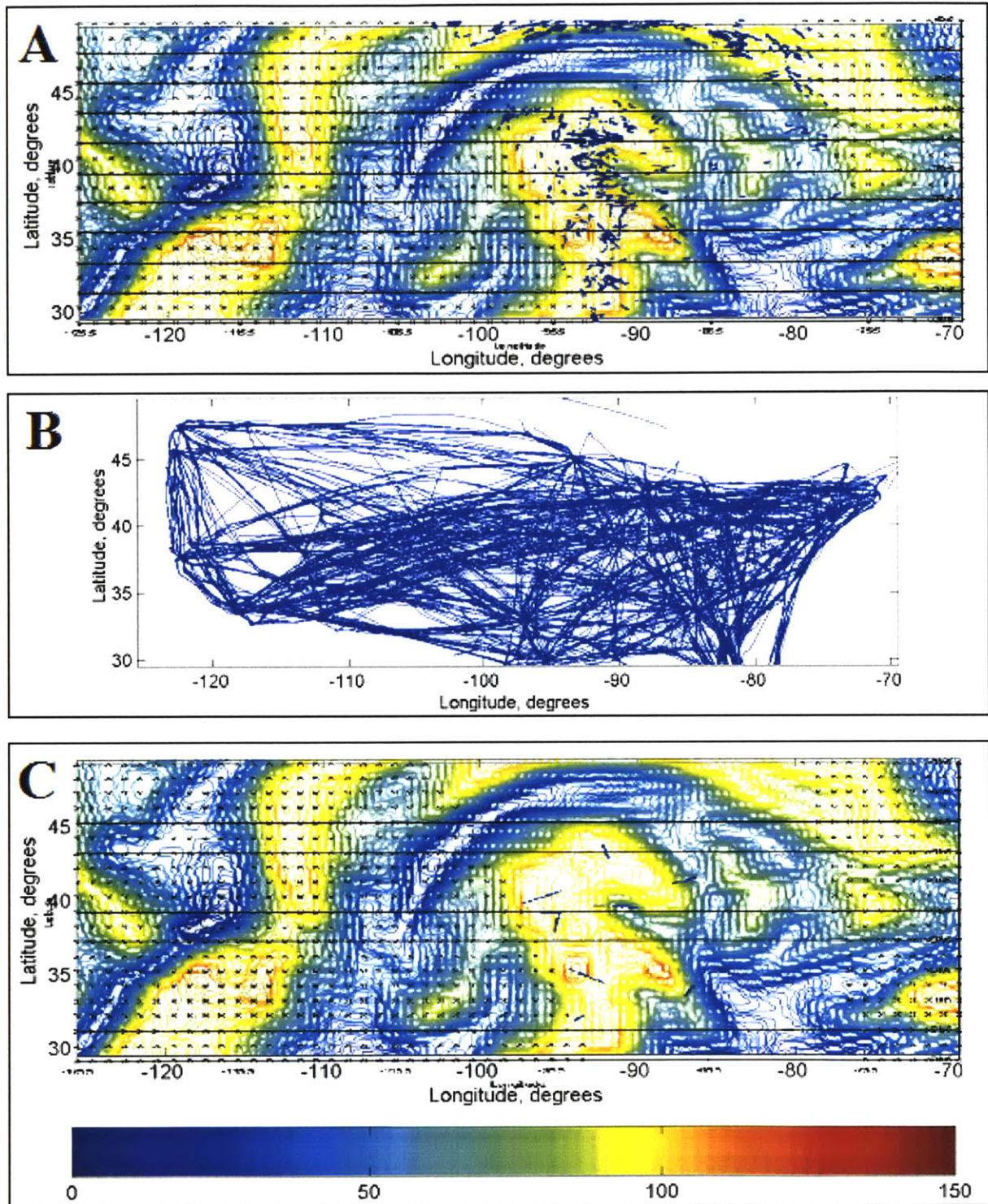


Figure 3.20 - 11/17/2001 hr 1906, RHi hour 18 field. A) Filtered contrail mask. B) Flights examined, C) Filtered contrail estimation. Lack of contrails caused by incorrect RHi fields (there are clouds in the satellite image, and here RHi < 100%).

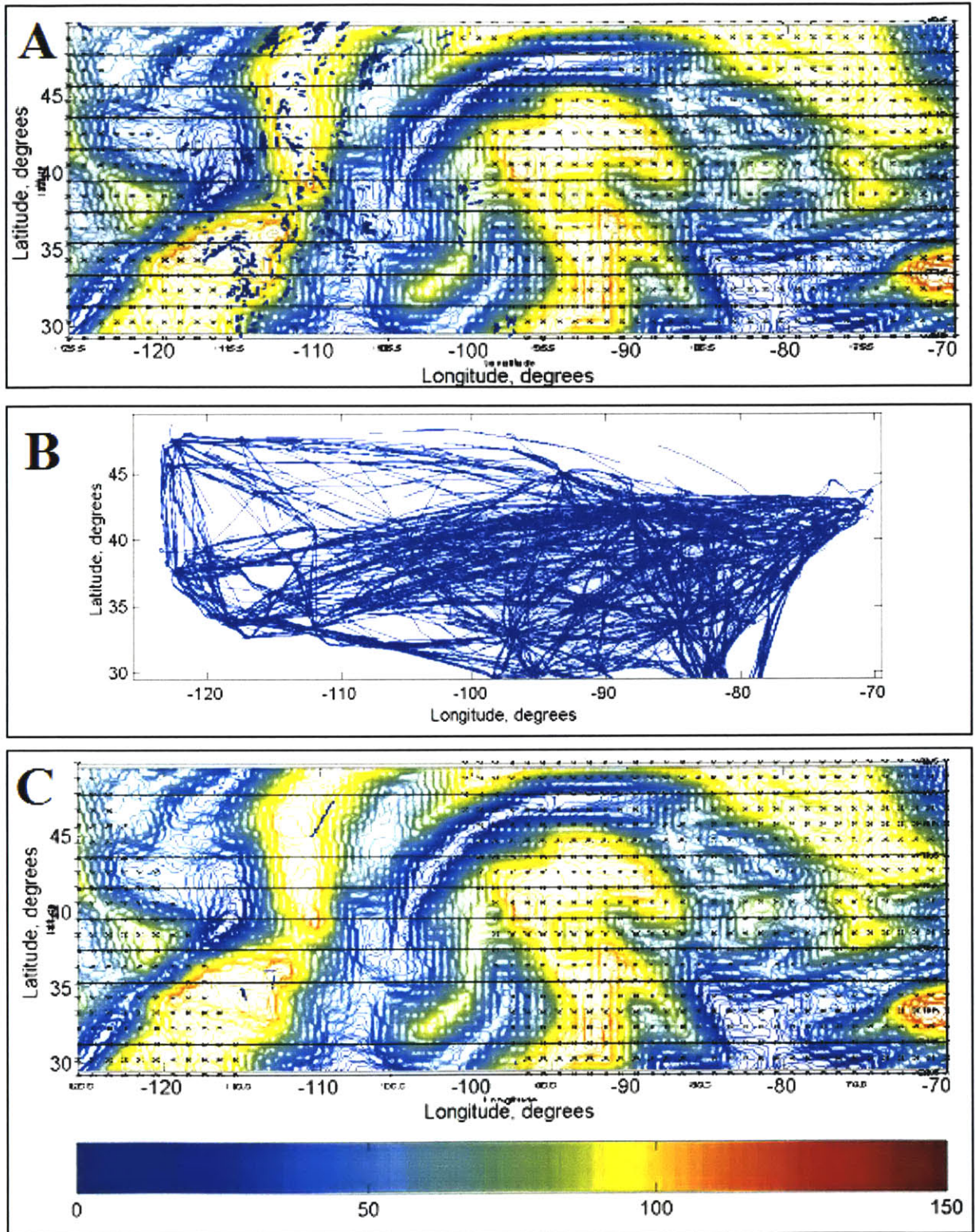


Figure 3.21 - 11/17/2001 hr 2077, RHi hour 19 field. A) Filtered contrail mask. B) Flights examined, C) Filtered contrail estimation. Lack of contrails (45N 110W, 35N 115W) caused partially by incorrect RHi fields (there are clouds in the satellite image, and here RHi < 100%), partially by insufficient flight data.

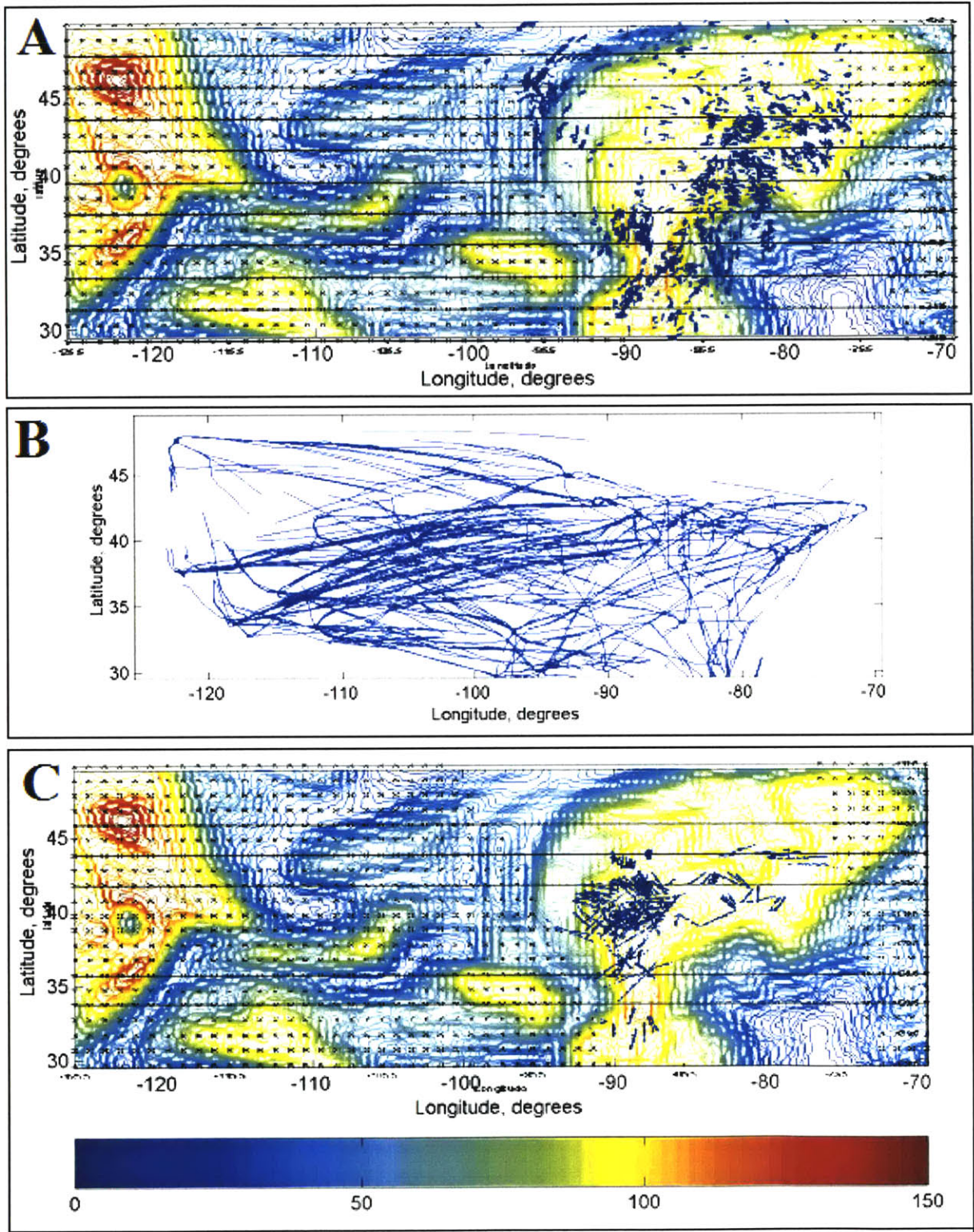


Figure 3.22 - 11/18/2001 hr 1888, RHi hour 18 field. A) Filtered contrail mask. Contrails (all) caused by threaded (striated) clouds. B) Flights examined, C) Filtered contrail estimation. Lack of contrails (45N 90W) caused by insufficient flight data.

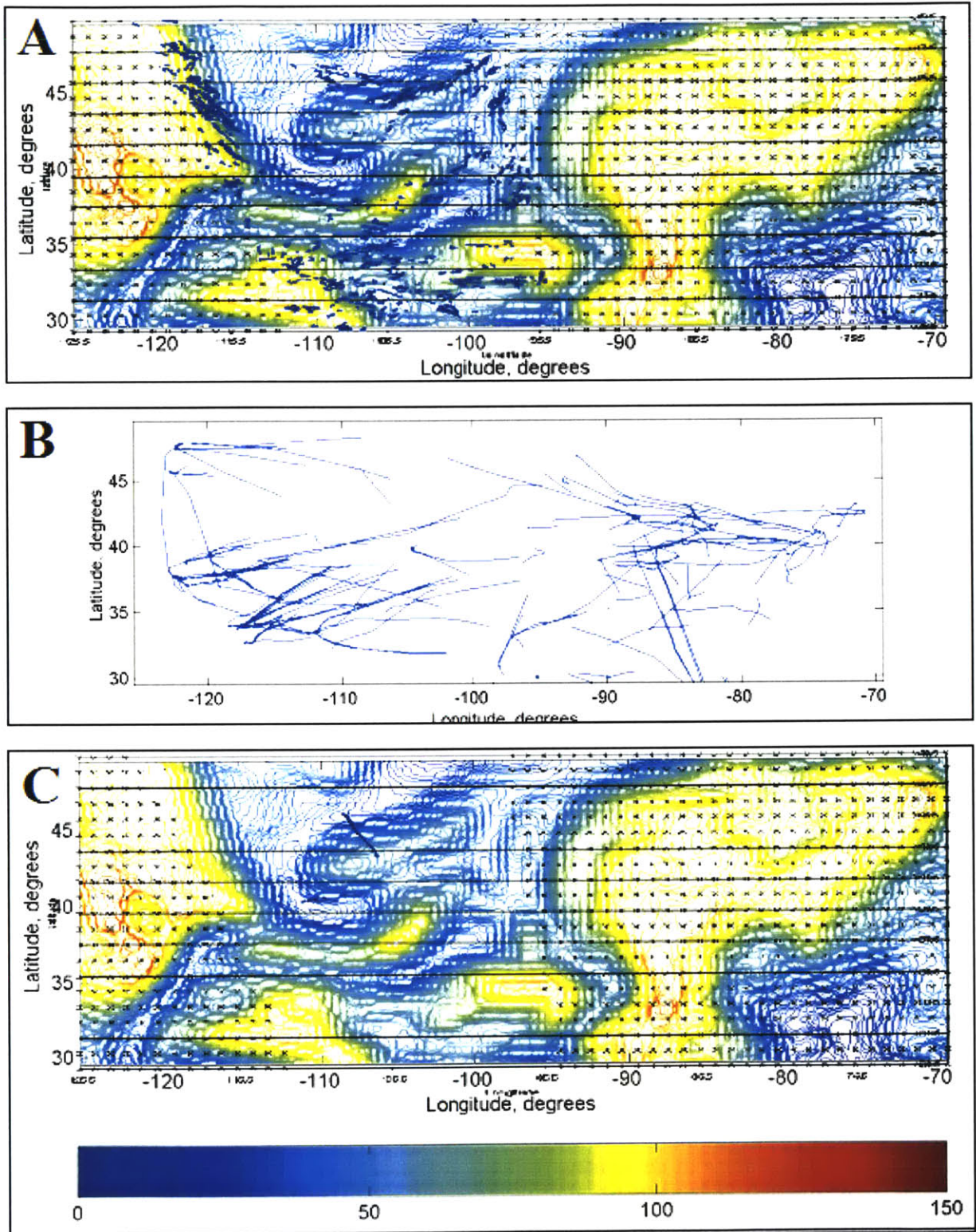


Figure 3.23 - 11/18/2001 hr 2059, RHi hour 19 field. A) Filtered contrail mask. Contrails (45N 117W) caused by threading. B) Flights examined, C) Filtered contrail estimation. Lack of contrails caused by incorrect RHi field.

3.3. SENSITIVITY OF RESULTS TO AVIATION SYSTEM MODEL

3.3.1. Percent of RHi Saturation at Which Contrails Persist

One important parameter in the contrail model is the percent of RHi saturation at which contrails persist. For homogeneous nucleation, this threshold percent is thought to be 140-160% [5]. However, contrails are formed primarily through heterogeneous nucleation. In the literature, the threshold is variously placed as somewhere between 95-105% [27]. The current value in the aviation system model is 100%.

Assuming the threshold varied from 90-110%, one can calculate the extent of ground coverage over which contrails could form. It is possible that lowering the requisite threshold would cause more clouds in general, and thus keep steady the amount of contrails in clear skies. However, this possibility is not addressed in this analysis. Further, this analysis assumes that the aircraft/engine efficiency is nearly uniform, so one can calculate the relative change in persistent contrail formation based solely on a change in the threshold value of saturation with respect to ice.

Figure 3.24 and Figure 3.25 depict the RUC and UM data sets, respectively. The areas chosen are the same as used elsewhere in this study, and are listed in Table 3.1. The effect of changing the persistence threshold varies between the UM and RUC data sets. This occurs because the gradients of RHi in the transatlantic are sharply defined by the jet stream, and hence changing the threshold has little effect. Since the gradients of RHi are less sharply defined in the RUC data, the increase in area is larger.

Based on this analysis, if the persistence threshold was allowed to vary from 90-110%, transatlantic regions supporting persistent contrails could vary between 52-150% in terms of area. Continental results could vary between 13-166% of the currently estimated coverage area. As the flight coverage is close to uniform, therefore, this serves as an estimate for the potential variation in estimated linear length of persistent contrails due to uncertain knowledge of the RHi persistence threshold.

If the persistence threshold was allowed to vary as literature suggests from 95-105%, transatlantic results could vary between 75-125% in terms of area supporting contrails and this then serves as an estimate of the potential change of the estimated length of persistent contrails. Continental results could vary between 51-135% of the currently estimated length of persistent contrails.

Thus, the persistence threshold is one of the largest uncertainties in our model. However, it should be noted that areas of decreasing RHi are near each other. Since reroutes tend to avoid large areas of the sky, it is probable that rerouting to avoid 100% RHi would also reroute to avoid 95% RHi. Hence although the persistence threshold can greatly affect contrail formation (and validation against satellite data), it will have a less significant effect on the cost-benefit assessment of rerouting to reduce contrails.

Table 3.1 - Latitude and longitude ranges of the RUC and UM data used in this study

Data Set	Latitude Range	Longitude Range
RUC	30.5N - 49.5N	125.5W - 69.5W
UM	30.5N - 70.5N	100.5W - 19.5E

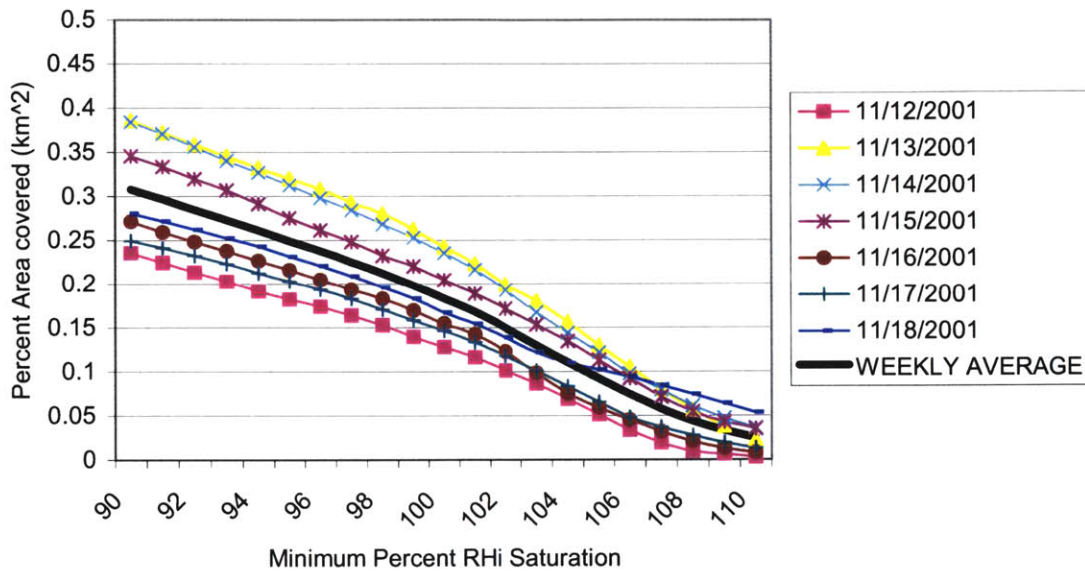


Figure 3.24 – Percent area (.xx) potentially covered by contrails as a function of minimum percent RHi saturation needed for contrails to persist. Each day is calculated from RUC data at 18 UTC.

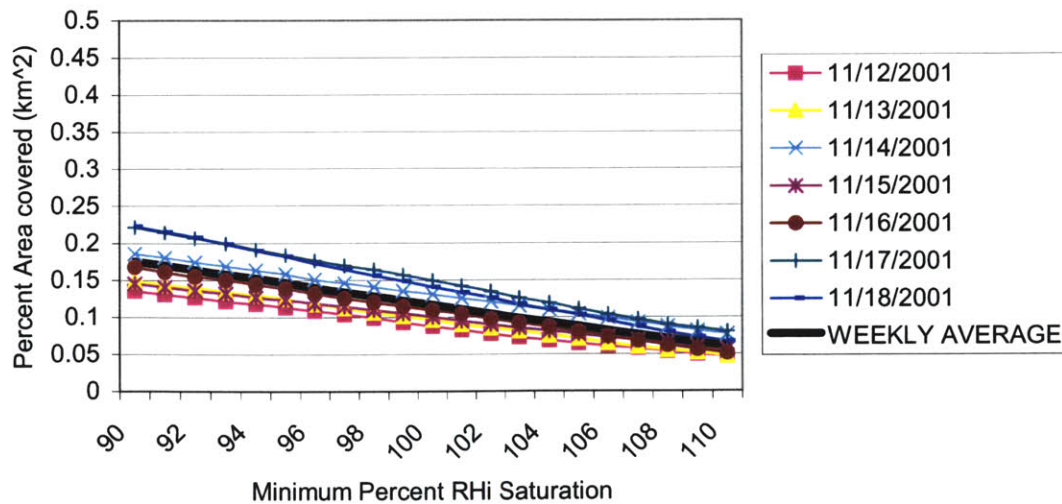


Figure 3.25 - Percent area (.xx) potentially covered by contrails as a function of minimum percent RHi saturation needed for contrails to persist. Each day is calculated from UM data at 18 UTC.

3.3.2. Aviation System Model

The aviation system model, SAGE, contains many assumptions and uncertainties. As discussed briefly in Section 2.2.4, it was recognized that the specific fuel consumption (SFC) equations inaccurately capture off-cruise trends in altitude and Mach number. To obtain a rough estimate of the sensitivity of contrail persistence to SFC, the higher fidelity model (GasTurb) was run on five engine/aircraft combinations²⁵. Note that GasTurb fails to replicate aircraft operating manual data, but more closely approaches these data than the current SAGE practice.

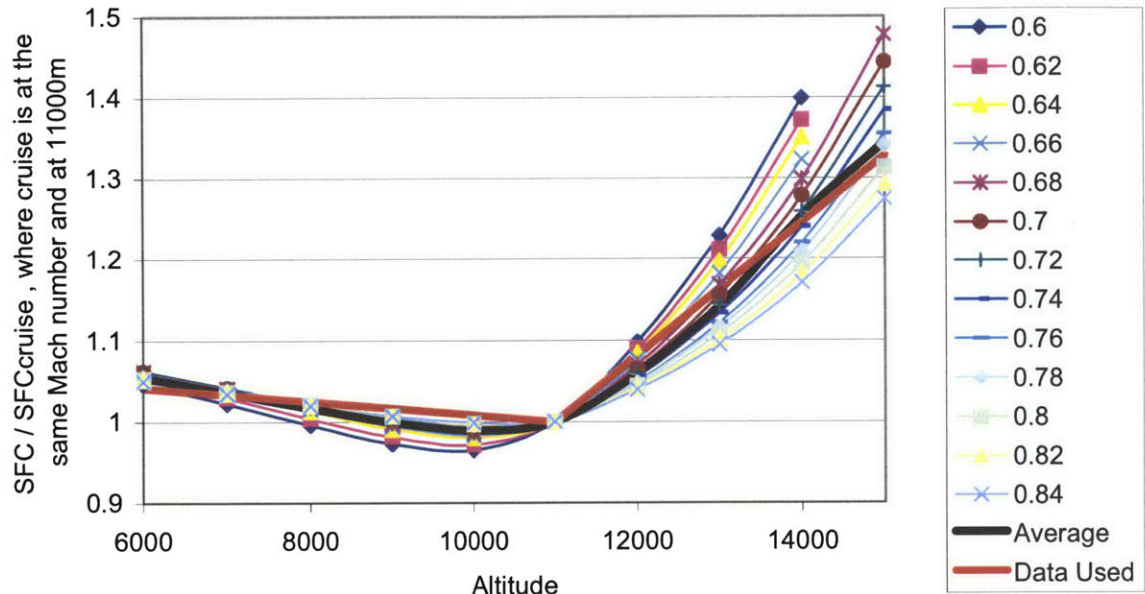


Figure 3.26 – Percent of cruise SFC as a function of altitude and Mach number, averaged for five aircraft/engine combinations. Recall that SAGE SFC changes little with altitude, so the SAGE curve would be a straight line at $y = 1$.

Relation (jets only)	Corrected Fuel Flow	
$h_i < 7000$	no correction	
$7000 < h_i < 11000$	$(-0.000008 \cdot (h_i - 11000) + 1) \cdot f_{i_{cruise}}$	
$11000 < h_i < 15000$	$(0.000008 \cdot (h_i - 11000) + 1) \cdot f_{i_{cruise}}$	
$15000 < h_i$	no correction	(3.1)

Where h_i = altitude

$f_{i_{cruise}}$ = SAGE fuel flow at 11000m and same Mach

²⁵ A30B/CF6-50C, B737-300/CFM56-3Bc, B727-200/GE90-90B, B737-200/JT8D-9, B757-200/PW2037

Table 3.2 – Percent difference from actual fuel burn, averaged over 1702 flights on October 5, 2000

	Average (%)	Standard Deviation (%)
SAGE V1.1	0.0202	17.6629
SAGE V1.1 + Eq. 3.1	3.2018	18.383
SAGE V1.5	-2.196	14.601

First it was assumed that SFC was independent of the mass of the aircraft. Figure 3.26 shows the percent of cruise SFC by altitude and Mach number, averaged over the five aircraft types. Subsequent averaging over Mach number produces the black curve, while employing a moving average over Mach number gives the two-slope function shown in red (and Equation 5.1). Note that Eq. 3.1 increases SAGE SFC at nearly all altitudes and Mach numbers, hence increasing fuel burn.

To test the effect of Eq. 3.1 on contrail estimation, flights with known fuel burn (from data supplied by a major airline) were examined. The best possible meteorological data (RUC) were used. If at any point the mass of the aircraft dropped below the minimum mass necessary to fly (the sum of the empty weight and the necessary fuel to fly at this weight), the flight was discarded. These dropped flights amounted to about twice the normal amount, and were ignored. No trends were noted in stage length or aircraft type, indicating that for an average of the long-haul continental flights that were considered, altitude is not a strong function of stage length or aircraft type.

Table 3.2 shows the results of applying Eq. 3.1. Previous to this addition, SAGE V1.1 estimated overall fuel burn with small bias, but large standard deviation. Including Eq. 3.1 increased fuel burn by several percent, while the standard deviation remained nearly the constant. The same rough change in the engine equation was applied to all the continental flights on 11/12/2001. The change in fuel burn before and after the addition of Eq. 3.1 was a little lower than the October flights: a 2.25% increase instead of a 3.2% increase.

With a more accurate representation of SFC, the standard deviation is expected to decrease. SAGE V1.5, used in CHAPTER 3: and CHAPTER 4:, systematically underestimates fuel burn²⁶. Supposing that Eq. 3.1 affects SAGE V1.5 in the same manner as SAGE V1.1, improving the engine equations would decrease the bias in the estimated fuel burn and further decrease standard deviation.

The result of an increase in fuel burn can be directly related to contrail estimation. Since the emissions index of H₂O is fixed in Boeing Method 2, the only input to the contrail model that changes is the efficiency. If fuel burn increases while all other variables remain constant, then efficiency decreases. Using the Schumann hypothesis, the contrail formation will decrease. Note that in subsequent chords, the reduced weight would be reflected in a reduced thrust and could result in an increase in fuel burn which would outweigh the reduced thrust.

²⁶ Note that the full version of SAGE V1.5 accounts for some of this bias by increasing the initial fuel estimates as a surrogate for fuel tankering. However, this study assumed no fuel tankering, and hence was completed using the researcher version of SAGE V1.5, which did not increase initial weight.

Table 3.3 - Distance of contrail estimated from various scenarios, before and after SFC change

		Distance of Contrails Predicted (nm)	
		All	Clear Skies
ETMS 10-5-2000	NO CHANGE	64.80 +/- 151.58	20.65 +/- 101.72
	WITH SFC CHANGE	64.80 +/- 151.63	20.35 +/- 101.03
ETMS 11-12-2001	NO CHANGE	55.44 +/- 165.98	45.44 +/- 154.54
	WITH SFC CHANGE	55.39 +/- 165.93	45.39 +/- 154.45

Table 3.3 shows the change in contrail persistence values before and after the SFC fix. Although the fuel burn decreases, the reduced weight offsets the change such that a change in the contrail persistence is seen only in fractional distances. As distances are not significant to this precision, the SFC equation is not significant.

Although the uncertainty in change of SFC as a function of altitude and Mach number does not affect contrail formation, it may influence the mitigation results of CHAPTER 4:. Most notably, the increase in fuel burn might result in a different optimal flight (whether choosing by fuel burn or by total operating costs). But without actually implementing the SFC equation, it is uncertain how much the uncertainty in SFC would affect a comparison between two flights.

3.3.3. Meteorological Data

Initial meteorological data were developed from the RUC data, at 0.25x0.25 degree spatial resolution and hourly temporal resolution. If an hour was missing, the previous hour was used. However, the UM data were not available at such a fine resolution; only 0.75x0.75 degree spatial resolution and three-hour temporal resolution. It is unknown how the difference in resolution affects the outcome of the study.

To partially alleviate this uncertainty, the best possible meteorological data were used in all runs, and the two scenarios (continental and international) are presented separately. Both meteorological data sets were checked against outside sources, but it is still unknown whether one data set is better than another. It is recognized that RUC reliability decreases toward the south and over the ocean due to lack of data points. It is similarly expected that the transatlantic data from UM will have a lower reliability due to a lack of data points over the Atlantic Ocean.

Due to staffing constraints, calculations of the sensitivity of SAGE to temporal and spatial resolution of meteorological data have been scheduled for a date following the completion of this thesis. Scenarios include reducing latitude/longitude, altitude, or temporal resolution. If SAGE is to continue the addition of meteorological data, database storage constraints indicate that the current resolution would have to be greatly decreased.

3.4. CONCLUSIONS AND RECOMMENDATIONS FOR FUTURE WORK

In this chapter, the contrail estimation model was used to compare contrail persistence estimations developed using flight data to a method for isolating contrails from satellite data. This unprecedented level of comparison, identified the following issues:

First, it was not possible to match particular contrails observed in the satellite images to origin-destination pairs. The contrails extracted from the satellite images align N-S, while most aircraft routes are aligned E-W. This occurs largely because the contrail mask algorithm identifies both contrails and striated cirrus cloud formations, suggesting limitations in the satellite sensing and extraction methods [28]. Perhaps 40-50% of the contrail pixels are misidentified striated cirrus cloud formations.

Second, it has been demonstrated that 60-90% of the identified contrail pixels (demonstrated to be contrails and clouds) are located in areas where the RHi is theoretically too low. This demonstrates that the RHi fields, although representative, do not accurately portray the true RHi fields on a given day in 2001. Hence at this point in time, it is unknown to what degree the contrail model coupled with actual aircraft flights can be used to accurately estimate contrail formation as given by satellite images/contrail masks

Third, the typical length of the estimated contrails (several degrees) was longer than the typical length of the observed contrails (one degree). This may reflect a limitation of the satellite sensing of the contrails, but it also implies that the chord lengths used within SAGE need to be shortened - at least to the extent to where they are consistent with length-scales observed in the RHi data.

Based on this assessment, the contrail model coupled with measured aircraft flights tracks could not be used to accurately estimate contrail persistence. This is due as much to the limited ability to observe contrails (as a basis for validating the methods) as to uncertainties in the meteorological data and the contrail modeling methods. To improve the model, future work should include:

- Meteorological Data Improvements
 - Update meteorological data, especially RH and RHi fields
 - Improve contrail mask algorithm to remove false positives
 - More precise advection of estimated contrails.
- Contrail Model/Aviation System Model Updates
 - Extend time period of meteorological data in aviation system model (e.g. to a month or year)
 - Decrease chord lengths in the aviation system model
 - Increase the database of flights to include international flights
 - Update engine equation (SFC) to better reflect changes in altitude and Mach number²⁷.

²⁷ Note that with respect to assessing contrail predictions against the contrail masks, the errors in SFC have only a minor effect on uncertainty.

However, these areas of future work are not all relevant for the comparison of two flight track scenarios. In such a comparison, the satellite data is not used. The RHi fields, although not necessarily accurate, are representative of typical large-scale RHi fields (sub-grid scale processes must be ignored, since no data are available). Identification of one time period of origin-destination pairs and potential reroutes eliminates flight database problems. The chord lengths are consistently long in the ETMS flights, so do not affect a comparison of two flights. Only the engine equation may affect the results, and a sensitivity analysis will be used to assess this effect.

Hence, despite the limitations, the contrail estimation model was used as a first order method to assess costs and benefits of operational strategies for contrail mitigation.

CHAPTER 4: ASSESSMENT OF OPERATIONAL STRATEGIES FOR CONTRAIL MITIGATION

To form a contrail, an aircraft must fly through an ice supersaturated region (ISSR). According to Spichtinger [12], ISSRs occur most frequently at mid-latitudes, and during the spring and fall months. Although there is a large variance with altitude, at common aircraft altitudes (altitudes near 215hPa) ISSRs can form nearly anywhere. The mean size of the ISSRs is of order 150km (due to the higher probability of selecting a larger ISSR, the mean size could be as small as 6km).

Figure 4.1 shows global humidity data. Blue areas correspond to clear skies, red areas to cloudy skies. Notice the steep gradients between blue and red areas. Contrail formation will only occur in the ISSRs – the yellow areas.

Since the ISSRs are typically long and thin, and occur with different frequency at different altitudes, attempts to reroute around these areas to reduce contrail formation may be attractive. Options would include:

- Flying around the ISSR
- Flying through the thinnest region of the ISSR
- Flying above the ISSR, in the dryer stratosphere
- Flying at a lower altitude, where the temperature is higher (and hence the water saturation pressure is higher). Here the amount of water needed to reach saturation pressure can be more than the aircraft emits.

4.1. CURRENT PRACTICE

Before assessing costs, the current practice was determined. Fourteen origin destination pairs were studied for continental flights, and fifteen origin destination pairs were studied for transatlantic flights. The pairs were chosen to represent a variety of flights (including N-S and W-E continental flights). The pairs chosen are listed in Table 4.1.

Table 4.1 – Origin destination pairs chosen, given by FAA call signs.

<i>Continental</i>		<i>Transatlantic</i>	
ATL – DFW	JFK – LAX	BOS – ELL	JFK – ELL
ATL – LAX	LAX – BOS	BOS – LFPG	JFK – LFPG
ATL – LGA	LAX – DFW	EDDF – JFK	LFPG – JFK
ATL – ORD	LAX – JFK	EDDF – ORD	LFPG – ORD
BOS – LAX	LGA – ORD	ELL – BOS	ORD – EDDF
DFW – LAX	MIA – SEA	ELL – JFK	ORD – ELL
DFW – LGA	SEA – MIA	ELL – ORD	ORD – LFPG
		JFK – EDDF	

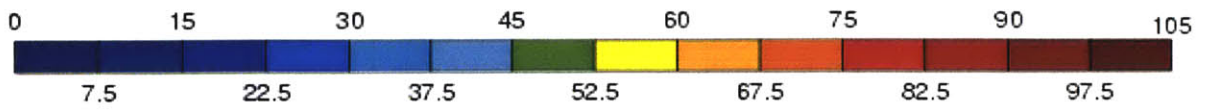
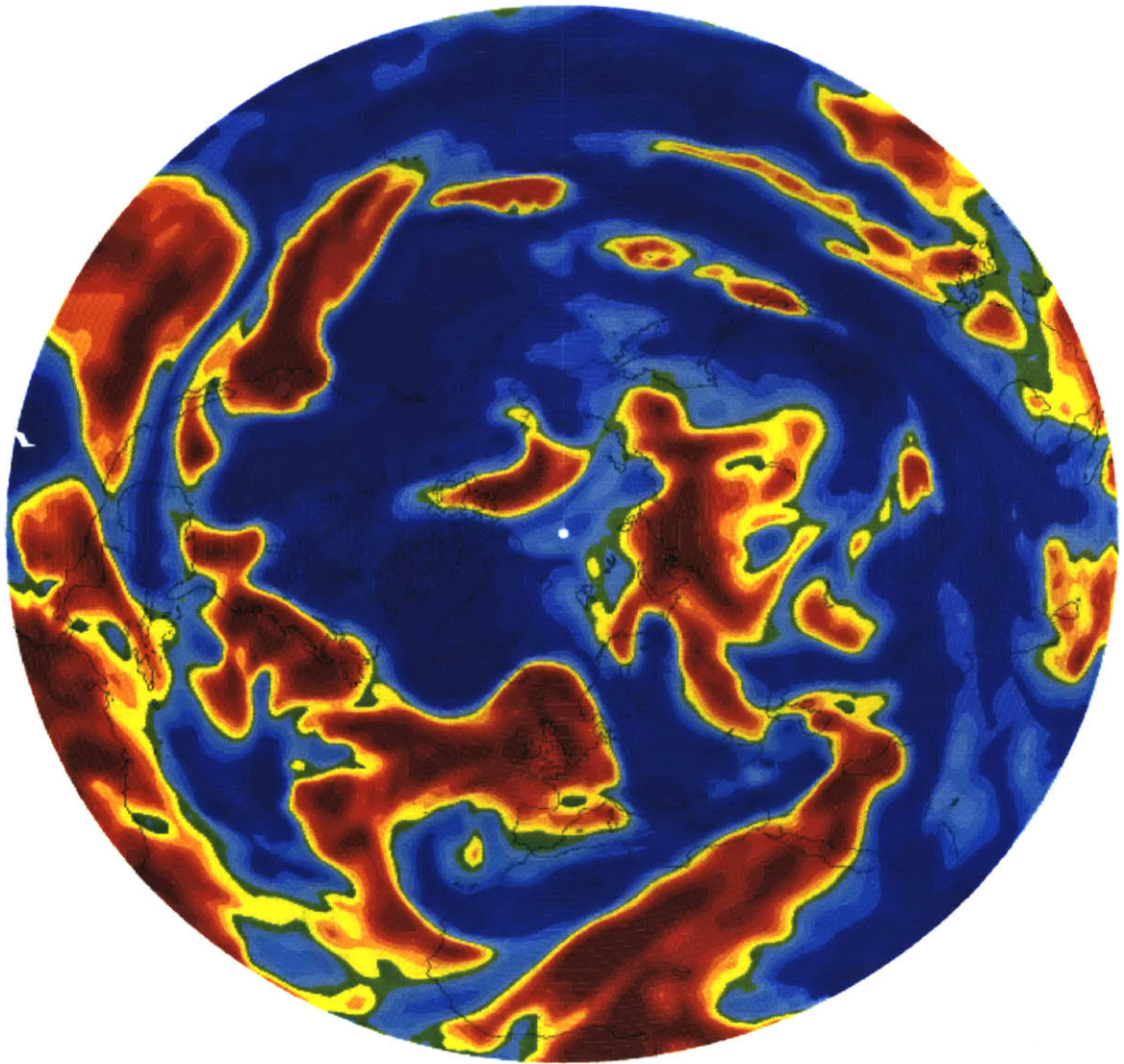


Figure 4.1 - The northern hemisphere relative humidity at 250 hPa (about 34000ft) at 00Z on 18 February 1999 (data courtesy of Brian Hoskins, the European Centre for Medium Range Weather Forecasts)

Then the flights were filtered by aircraft type. Figure 4.2 and Figure 4.3 depict all the aircraft in the ETMS routes for the period of November 12-18, 2003. For each origin destination pair, only flights corresponding to the most common aircraft listed in the ETMS routes were examined.

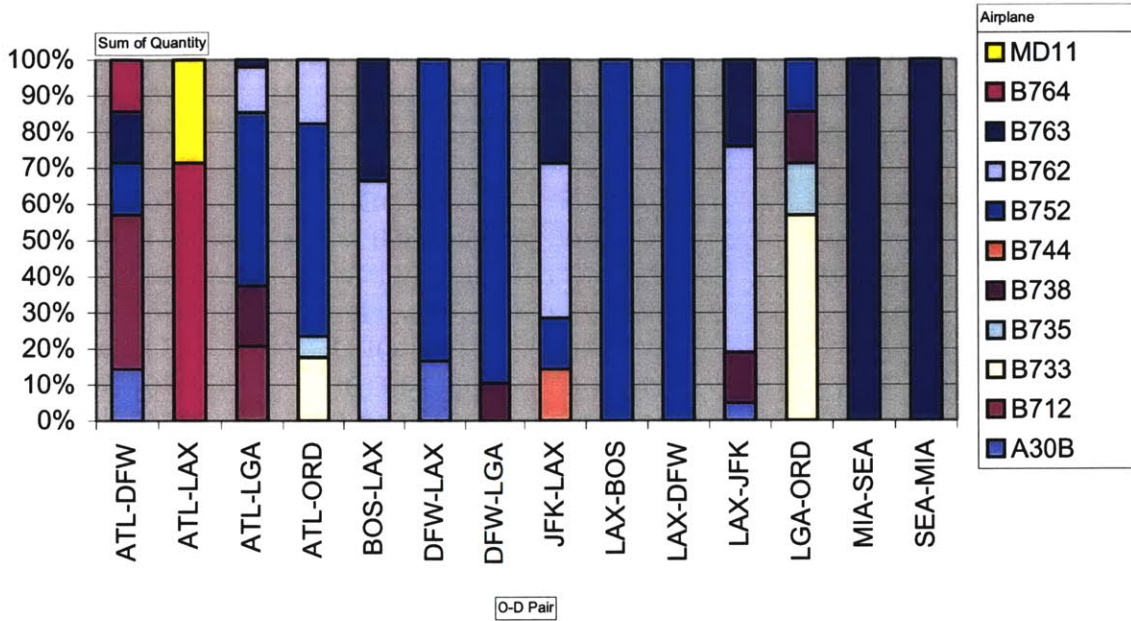


Figure 4.2 - Aircraft types for ETMS continental routes, varying origin destination pair, Nov 12-18 2003

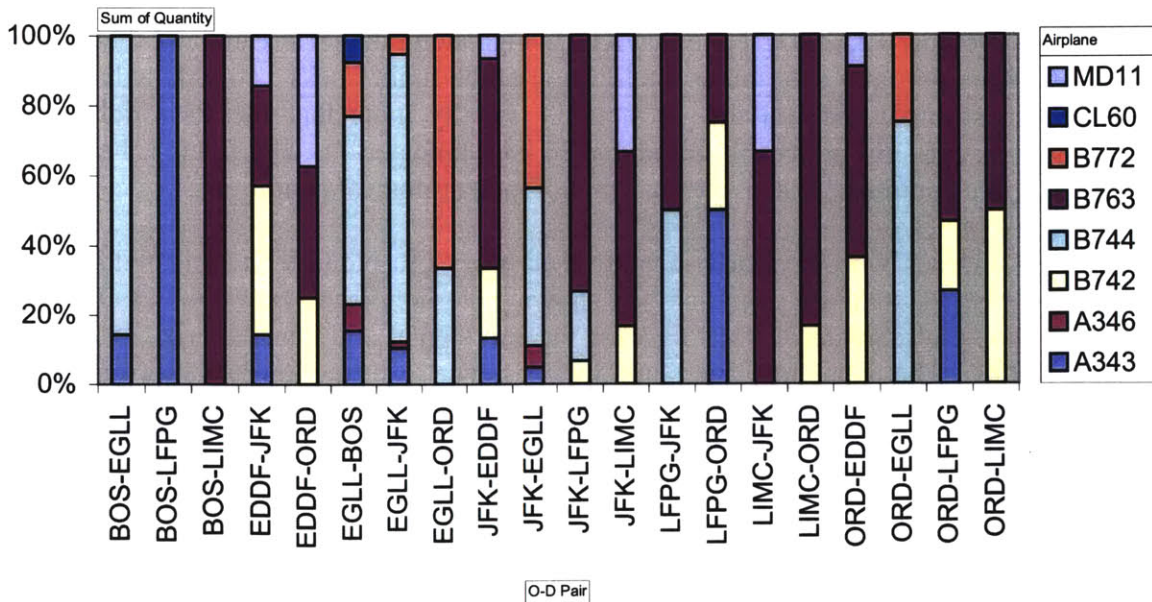


Figure 4.3 - Aircraft types for ETMS transatlantic routes, varying origin destination pair, Nov 12-18 2003

Table 4.2 - Aircraft chosen for each of the origin-destination pairs

Continental Flights		Transatlantic Flights	
O-D pair	Aircraft	O-D pair	Aircraft
ATL-DFW	B717-200	BOS-EGLL	B747-400
ATL-LAX	B767-400	BOS-LFPG	A340-300
ATL-LGA	B757-200	EDDF-JFK	B747-200
ATL-ORD	B757-200	EDDF-ORD	B767-300
BOS-LAX	B767-200	EGLL-BOS	B747-400
DFW-LAX	B757-200	EGLL-JFK	B747-400
DFW-LGA	B757-200	EGLL-ORD	B777-200
JFK-LAX	B767-200	JFK-EDDF	B767-300
LAX-BOS	B757-200	JFK-EGLL	B747-400
LAX-DFW	B757-200	JFK-LFPG	B767-300
LAX-JFK	B767-200	LFPG-JFK	B767-300
LGA-ORD	B737-300	LFPG-ORD	A340-300
MIA-SEA	B767-300	ORD-EDDF	B767-300
SEA-MIA	B767-300	ORD-EGLL	B747-400
		ORD-LFPG	B767-300

Finally, any flight with a chord larger than 1000km was discarded. The resulting flights were examined for contrail persistence estimations. Figure 4.4 and Figure 4.5 show the flights examined and the estimated contrails for continental flights on November 12, 2001. Note that the flights follow highways in the sky, occasionally rerouting to avoid storm systems. Figure 4.6 and Figure 4.7 shows the flights examined and the estimated contrails for transatlantic flights on November 12, 2003. Note that RHi is high along the jet stream, and that the location of the jet stream partially determines the location of the flight tracks²⁸ (flights will alter slightly to catch the strong winds on the jet stream. Finally, note that the RHi fields, although representative, can shift noticeably through a 24 hour time period. The figures shown are all of one day's flights graphed on a single snapshot of meteorological conditions.

All contrail metrics were reported in both clear skies (no clouds) and in total. Due to the processing method, standard deviation was shown pictorially (see Section 4.3.2). Table 4.3 and Table 4.4 give the tabulated ETMS data for the continental and transatlantic flights, averaged over all flights. The data show that contrail persistence is a function of the origin-destination pair, since this can be closely related to humidity fields. The best and the worse flights in fuel burn, time, cost, and contrail persistence are listed in APPENDIX G:.

²⁸ Flights will alter slightly to catch the strong winds on the jet stream. This is more readily apparent some days than others, depending on the location of the jet stream.

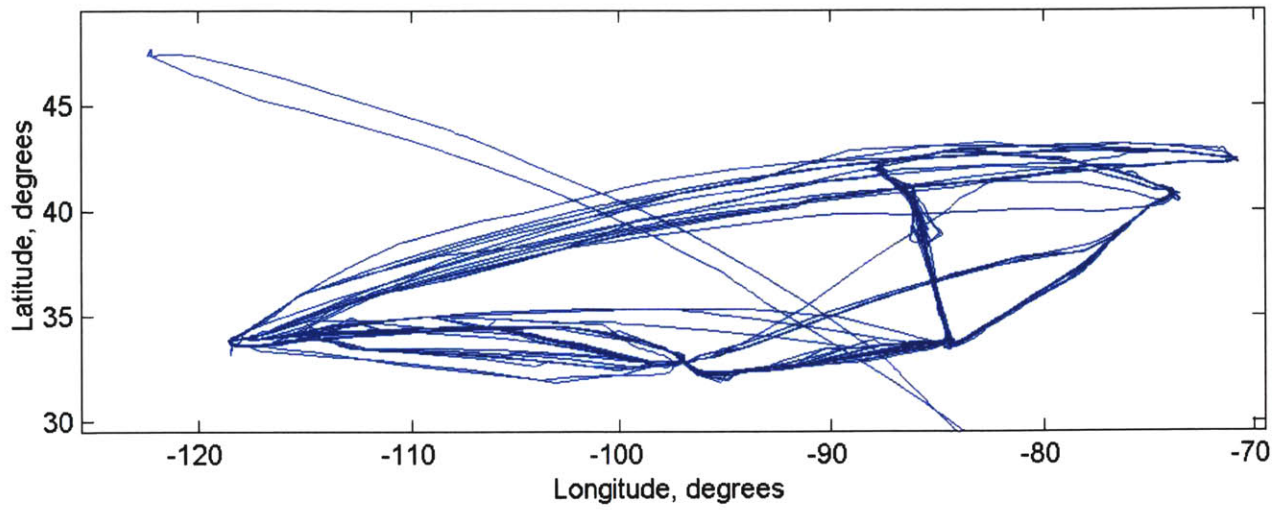


Figure 4.4 - 11/12/2001 ETMS flights examined

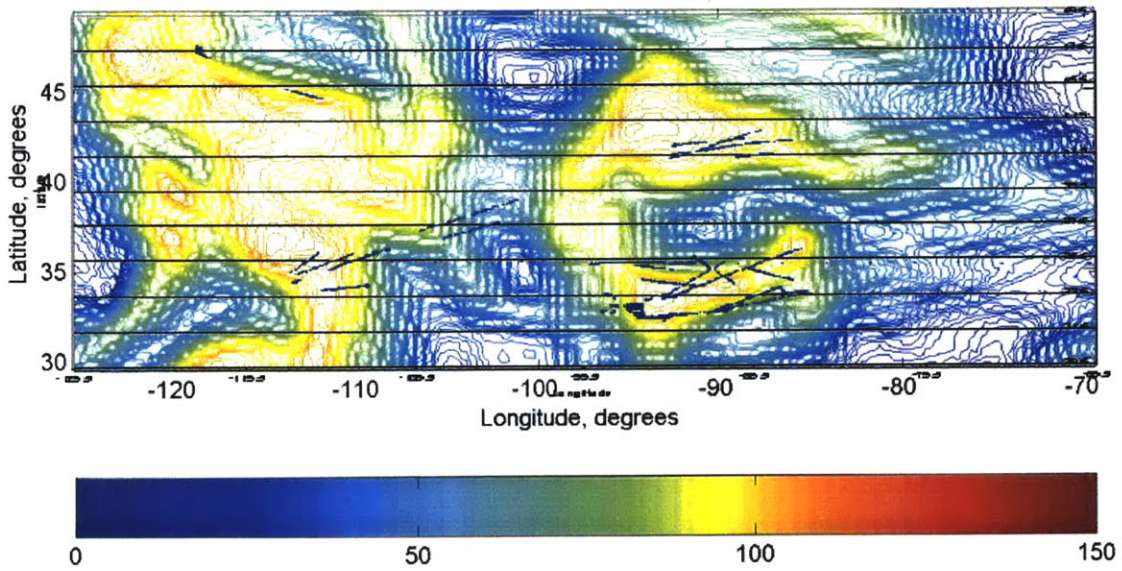


Figure 4.5 – Contrails estimated for flights in Figure 4.4. RHi is from RUC data, hour 18.

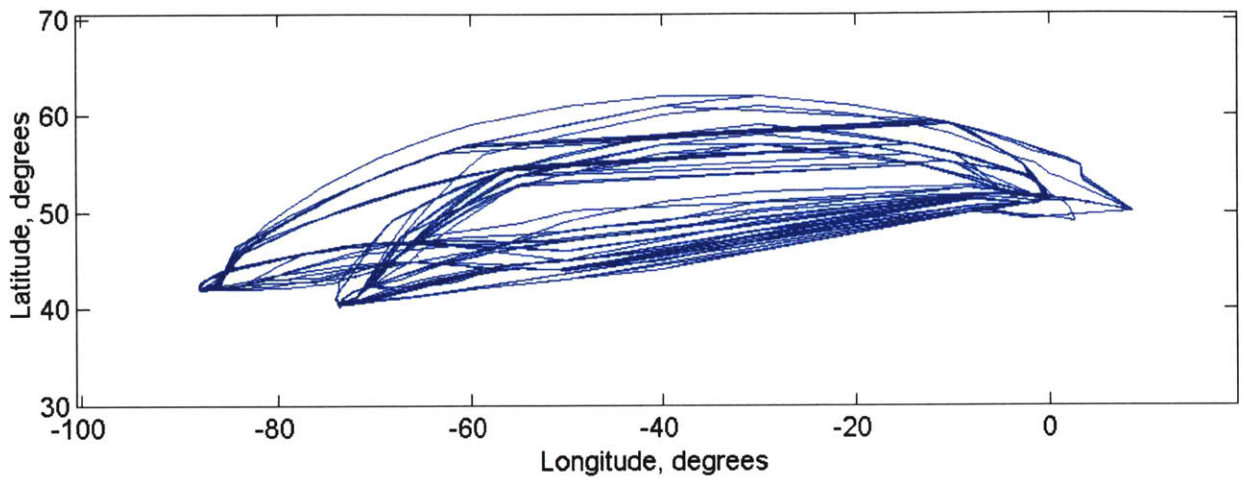


Figure 4.6 - 11/12/2003 ETMS flights examined

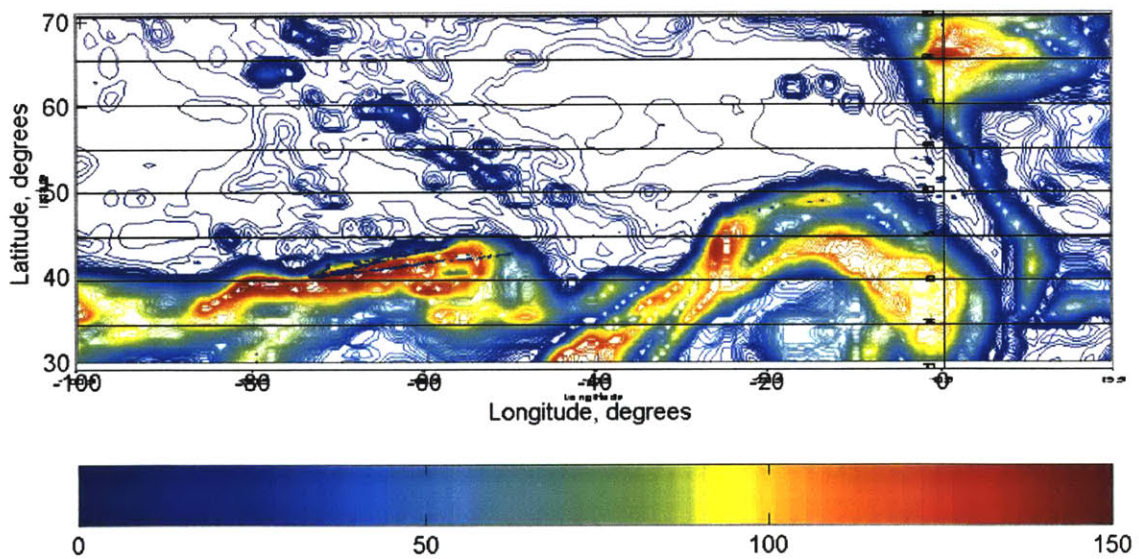


Figure 4.7 – Contrails estimated for flights in Figure 4.6. RH is from UM data, hour 18.

Origin Destination Pair	Time (seconds)	Fuel Burn (kg)	Distance (km)	Contrail Formation (Percentage)	Contrail Formation in Clear Skies (Percentage)	Contrail Formation (km)	Contrail Formation in Clear Skies (km)	Contrails/ Time (km/ second)	Contrails in Clear Skies/Time (km/second)	Contrails/ Fuel Burn (km/kg)	Contrails in Clear Skies/Fuel Burn (km/kg)
ATL-DFW	6554	4327	375	8.2	6.3	31	23	4.6E-03	3.5E-03	7.2E-03	5.5E-03
ATL-LAX	13965	20022	912	0.4	0.4	3	3	2.3E-04	2.3E-04	1.6E-04	1.6E-04
ATL-LGA	6107	5588	376	0.1	0.1	0	0	4.5E-05	4.5E-05	5.0E-05	5.0E-05
ATL-ORD	5803	5284	315	1.3	1.3	4	4	7.7E-04	7.7E-04	7.9E-04	7.9E-04
BOS-LAX	20090	23531	1239	6.8	6.4	85	80	4.2E-03	3.9E-03	3.5E-03	3.3E-03
DFW-LAX	9720	9501	605	3.7	2.6	22	16	2.4E-03	1.7E-03	2.5E-03	1.7E-03
DFW-LGA	10420	9509	682	3.8	3.4	26	24	2.5E-03	2.3E-03	2.7E-03	2.5E-03
JFK-LAX	18623	21902	1173	3.8	3.8	45	45	2.3E-03	2.3E-03	2.0E-03	2.0E-03
LAX-BOS	18308	16993	1231	4.0	4.0	49	49	2.7E-03	2.7E-03	3.1E-03	3.1E-03
LAX-DFW	9344	9069	604	2.0	1.3	12	8	1.3E-03	8.5E-04	1.3E-03	8.7E-04
LAX-JFK	17562	23640	1202	1.8	1.8	22	22	1.3E-03	1.3E-03	9.7E-04	9.7E-04
LGA-ORD	6698	4843	364	8.7	5.8	32	21	4.7E-03	3.1E-03	6.7E-03	4.5E-03
MIA-SEA	20460	25441	1324	9.6	6.6	128	88	6.1E-03	4.2E-03	5.2E-03	3.6E-03
SEA-MIA	18960	26367	1306	4.9	4.9	64	64	3.4E-03	3.4E-03	2.5E-03	2.5E-03

Table 4.3 - ETMS estimations for continental flights, averaged over 11/12/2001 & 11/15-18/2001

Origin Destination Pair	Time (seconds)	Fuel Burn (kg)	Distance (km)	Contrail Formation (Percentage)	Contrail Formation in Clear Skies (Percentage)	Contrail Formation (km)	Contrail Formation in Clear Skies (km)	Contrails/ Time (km/ second)	Contrails in Clear Skies/Time (km/second)	Contrails/ Fuel Burn (km/kg)	Contrails in Clear Skies/Fuel Burn (km/kg)
BOS-EGLL	20717	86754	1601	15.1	14.4	242	230	1.2E-02	1.1E-02	2.9E-03	2.8E-03
BOS-LFPG	21864	54684	1636	14.2	12.9	232	210	1.1E-02	9.7E-03	4.4E-03	4.0E-03
EDDF-JFK	27740	84699	1766	0.2	0.0	4	0	1.3E-04	0.0E+00	4.7E-05	0.0E+00
EDDF-ORD	31800	37921	1947	6.3	5.2	123	102	3.8E-03	3.1E-03	3.3E-03	2.7E-03
EGLL-BOS	24849	64793	1593	9.0	4.8	142	77	5.7E-03	3.1E-03	2.2E-03	1.2E-03
EGLL-JFK	25699	66282	1674	7.8	5.6	131	93	5.0E-03	3.6E-03	2.0E-03	1.4E-03
EGLL-ORD	28862	49422	1931	4.6	3.8	88	73	3.0E-03	2.5E-03	1.8E-03	1.5E-03
JFK-EDDF	24687	45712	1765	9.6	7.5	170	134	7.0E-03	5.5E-03	3.7E-03	2.9E-03
JFK-EGLL	21677	94780	1700	11.5	10.3	196	175	9.1E-03	8.2E-03	2.1E-03	1.9E-03
JFK-LFPG	23416	43445	1722	16.2	14.1	279	243	1.2E-02	1.0E-02	6.4E-03	5.6E-03
LFPG-JFK	28260	29909	1627	0.3	0.0	5	0	1.7E-04	0.0E+00	1.6E-04	0.0E+00
LFPG-ORD	30480	58932	2047	0.6	0.0	11	0	3.7E-04	0.0E+00	2.0E-04	0.0E+00
ORD-EDDF	28340	57309	2091	6.7	5.2	141	110	4.9E-03	3.8E-03	2.5E-03	2.0E-03
ORD-EGLL	25280	120704	1995	9.0	8.5	179	168	7.2E-03	6.8E-03	1.5E-03	1.4E-03
ORD-LFPG	27360	53673	2020	11.5	9.4	231	189	8.6E-03	7.0E-03	4.4E-03	3.6E-03

Table 4.4 - ETMS estimations for transatlantic flights, averaged over 11/12-18/2003

4.2. REROUTE CONSTRUCTION

In order to examine rerouting for contrail mitigation, several alternative routes were assessed. This section describes rerouting scenarios, and the construction of the potential reroutes. The origin-destination pairs and aircraft were chosen to match the ETMS routes in Section 4.1.

4.2.1. Background

Rerouting is the process of altering the trajectory between origin and destination²⁹, and is already done on a daily basis for inclement weather using Flow Constrained Areas (FCA) and Flow Evaluation Areas (FEA) in the Traffic Display Situation (TDS).

First, areas are identified that aircraft need to avoid or may want to avoid. This could be due to inclement weather, turbulence, high humidity, etc. Figure 4.8 shows an example FCA/FEA, where the outlined areas indicate areas to be avoided. After construction, then the FCA/FEA goes into effect. Air traffic controllers will reroute grounded aircraft to avoid the outlined areas. Airborne aircraft may or may not reroute, based on the severity of the weather and their ability to avoid it. The reroutes are pre-agreed between the airlines and the Federal Aviation Administration (FAA). These can include altitude and Mach number changes as well as latitude/longitude changes.

Since FCA/FEAs can be constructed for a variety of reasons, areas of high humidity could be used to construct FCA/FEAs. Unfortunately, MIT could not use archived meteorological data with the FCA/FEA interface for extended analysis. Instead, a representative sample of latitude/longitude reroutes was obtained from the TDS database.

4.2.2. Choosing Latitude/Longitude Trajectories

The first step in creating the custom reroutes was to choose the latitude and longitude.

Over the continental United States, where “highways in the sky” predominate (versus direct routing), current TDS reroutes (2004), past ETMS routes (chosen from 5/13/2001, 10/13/2001, and 11/12-18/2001), and the great circle distance were examined. Example routes for one origin-destination pair are shown in Figure 4.10. The routes show it is possible to reroute around areas of high RH_i.

Over the transatlantic, roughly 4-5 routes are shifted daily based on the location of the jet stream. These are called “North Atlantic tracks” (NATs). However, in this study the trajectories could not be dynamically altered for winds, and therefore could not capture the changes in the jet stream. Instead, a smooth, “middle” track was chosen from the ETMS routes (chosen from 5/13/2001, 10/13/2001, and 11/12-18/2001). One such route is shown in red in Figure 4.11. On the advice of Prof. John Hansman (MIT), the remaining tracks were offset roughly one degree from each other (two north and two south), for a total of five tracks (shown in yellow). The reroutes are shown with RH_i in Figure 4.12.

²⁹ Note that rerouting is a change of trajectory, while diverting is a change of the destination airport.

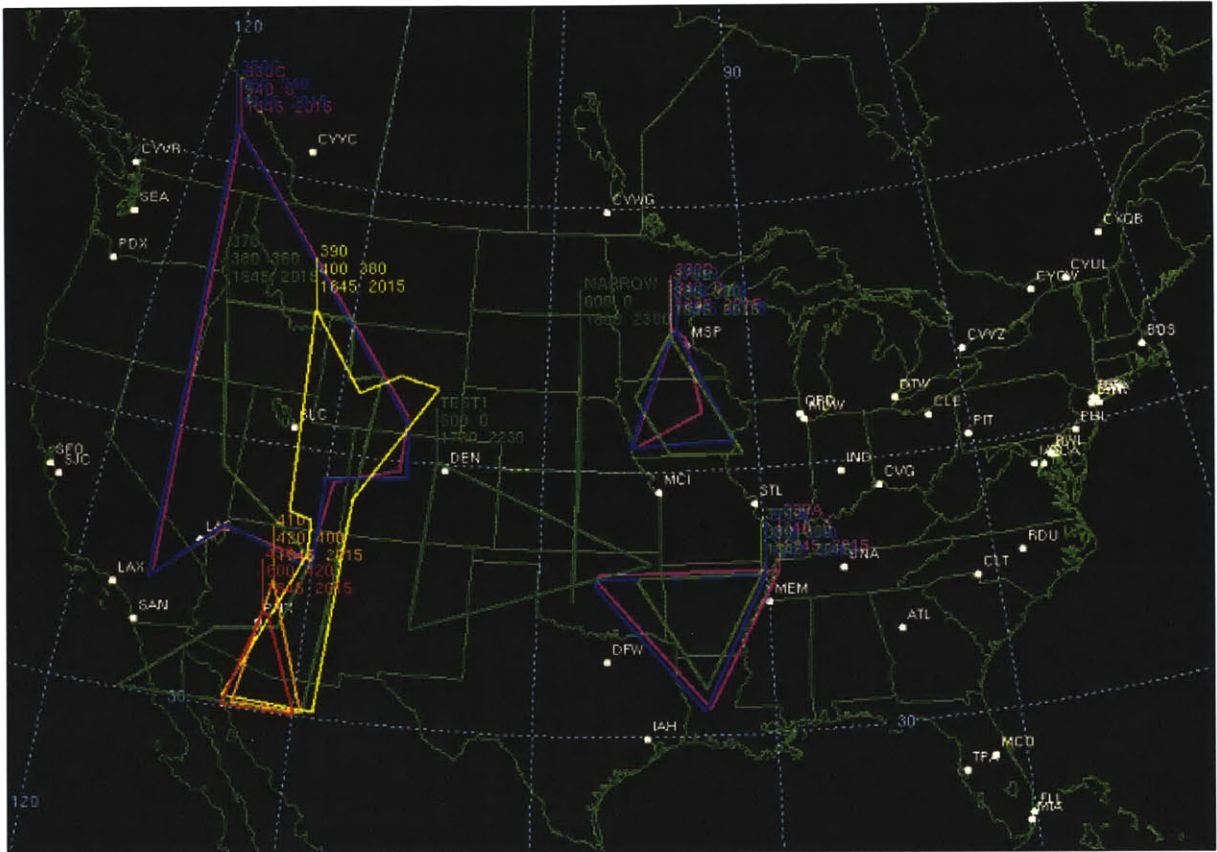


Figure 4.8 - Examples FCA/FEA. Each block is a "bad" area, such as a thunderstorm or an area of high humidity, that planes could be asked to reroute around. Picture courtesy of Matt Maki (Volpe).

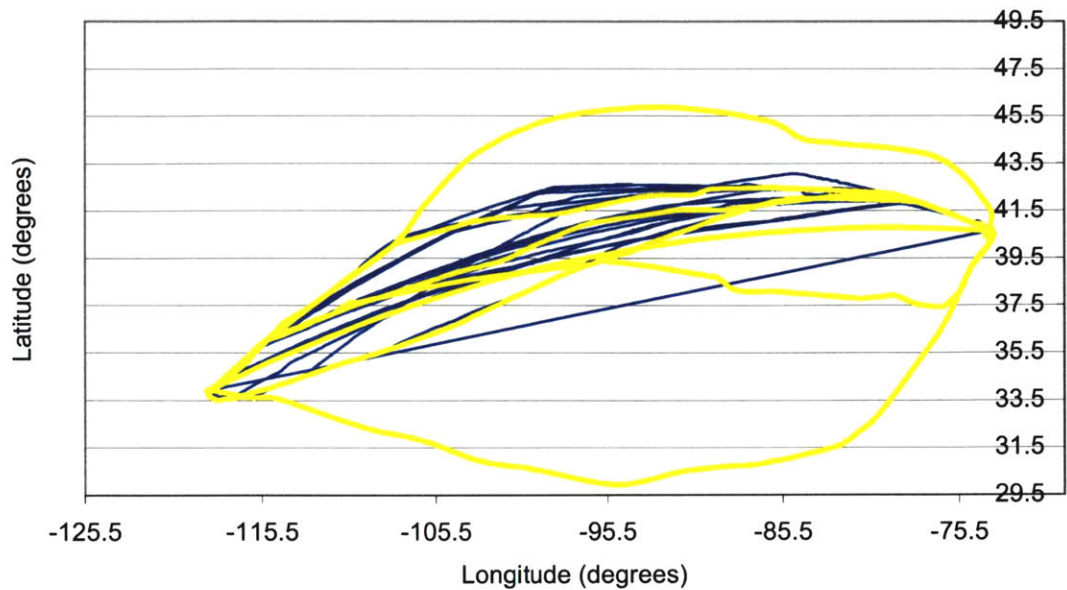


Figure 4.9 - ETMS routes for LAX to JFK. Blue indicate all the routes for 11/12-18/2003. Yellow indicates the reroutes chosen.

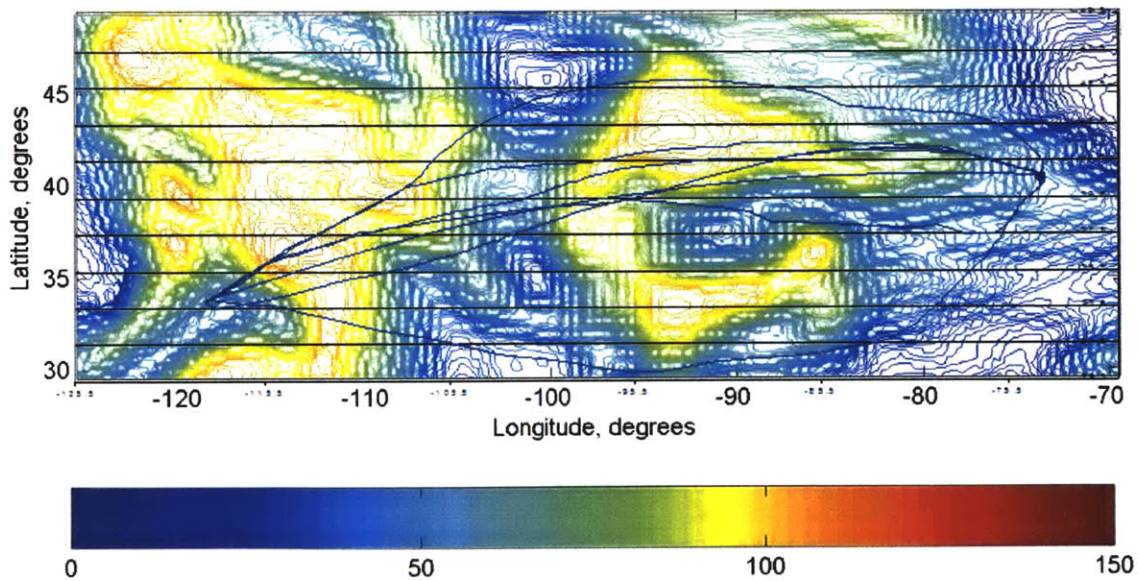


Figure 4.10 – Reroutes chosen for LAX to JFK and RHi for 11/12/2001 hr 18. Note that some of these routes came from 5/13/2001 and 10/13/2001 instead of just from 11/12/2001. A visual inspection of the reroutes shows that changing between reroutes can significantly alter contrail persistence.

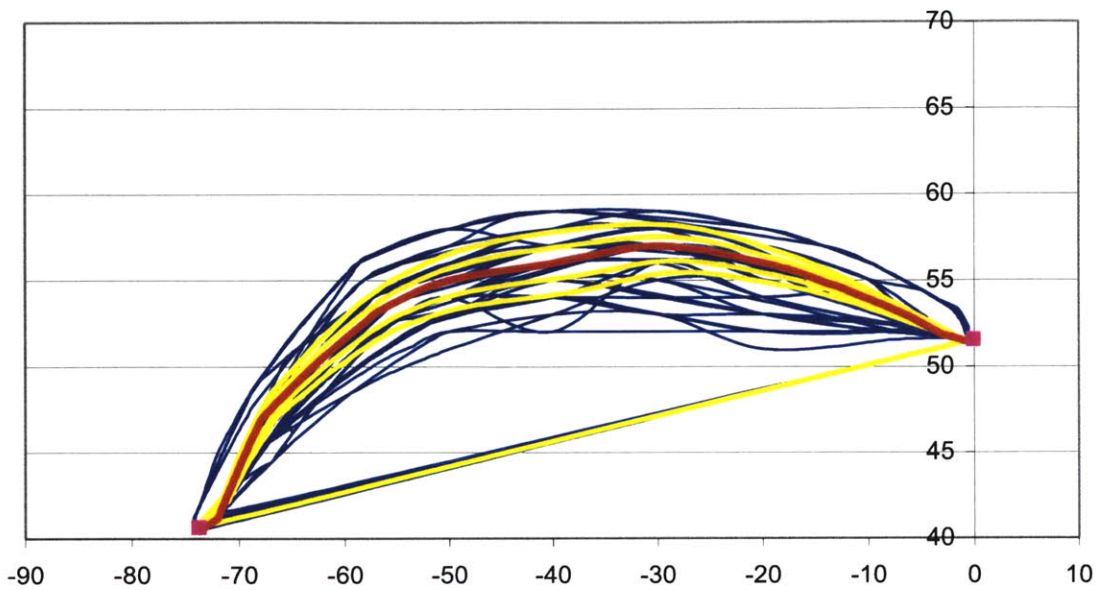


Figure 4.11 – ETMS routes for EGLL to JFK. Blue indicate all the routes for 5/13/2001, 10/13/2001, and 11/12-18/2003; note how over a hundred flights line up on a couple tracks. Red indicates the “middle” North Atlantic Route chosen. Yellow indicates tracks offset by one degree. Red and yellow tracks were used as the reroutes.

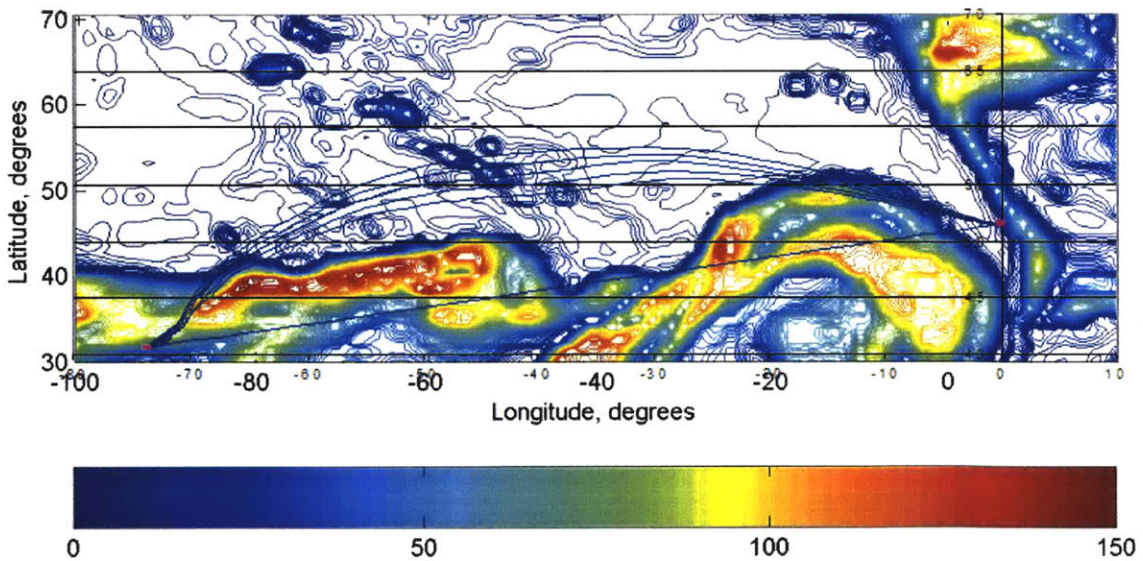


Figure 4.12 - Reroutes chosen for EGLL to JFK and RHI for 11/12/2003 hr 18. A visual inspection of the reroutes shows that changing between reroutes can alter contrail persistence; when the jet stream is shaped differently, this can lead a significant alteration in contrail persistence.

4.2.3. Choosing Altitude/Mach Number Trajectory

For both continental and transatlantic flights, the same altitude and Mach number scenarios were chosen. Using a spreadsheet version of the cruise equations in SAGE, ETMS-like input files were created for each scenario. The only difference between the ETMS and custom routes was the velocity; ETMS flights report ground velocity, while custom flights report true velocity (since meteorological conditions were unknown). Each scenario was created at the flight level above and below the average ETMS cruise altitude.

In a recent paper, Boeing raised concerns regarding Williams's treatment of flights [3], [4]. These issues are addressed in this thesis:

- Realistic operational profiles were used; a variety of altitude and Mach number paths were examined (including step climbs).
- Assumed altitudes were chosen from the average values from *real* flights as recorded on radar. Shorter flights are represented through lower altitudes, and it is assumed that full cruise begins at the first ETMS chord labeled cruise.
- Short-range and long-range flights were examined individually. Additionally, north/south and east/west flights were examined individually.
- Realistic takeoff weights were used, since SAGE accounts for varying takeoff weights through use of the INM and ICAO databases.
- The operational limits of aircraft were better considered through updating the aviation system model equations. Pertinent lacks of sufficient performance data were noted.
- A variety of aircraft and engine types were examined.
- Takeoff and landing trajectories were created in SAGE, so that the extra fuel burn necessary for higher altitude was included in the fuel burn estimates.

The following is a short description of the four operational profiles. Each is shown pictorially in Figure 4.11 and Figure 4.12.

In three of the operational profiles, the aircraft was assumed to fly at conditions corresponding to minimum drag. Because of the very weak dependence of the BADA sfc equations on Mach number and altitude, minimizing drag is a close approximation to minimizing fuel burn (or maximizing specific range). To calculate minimum drag, first the aircraft was assumed to fly at 11000m. Then the Mach number was iterated until a drag minimum was reached. In all cases, the new Mach number was about 0.03-0.05 lower than the BADA cruise Mach number. Next the constant value of aspect ratio times Oswald efficiency ($AR * e$) was calculating using

$$C_D = C_{D_0} + C_L^2 / (\pi * AR * e) + \Delta C_{D_c} \quad (4.1)$$

$$V_{\text{mindrag}} = (W / (1/2 * \rho * S * C_{L_{\text{mindrag}}}))^{1/2} \quad (4.2)$$

$$= (4 * (W/S)^2 * (1/ \rho^2) * (1/C_{D_0}) * (1/ \pi * e * AR))^{(1/4)} \quad (4.3)$$

where W = weight

ρ = density

S = wing surface area

$C_{L_{\text{mindrag}}}$ = lift coef corresponding to minimum drag

C_{D_0} = parasitic drag coefficient in BADA (cruise)

e = Oswald efficiency factor

AR = aspect ratio

ΔC_{D_c} = compressibility drag

Eq. 4.1. After identifying the value of AR^*e , minimum drag conditions could be created by solving Eq. 4.3 for either velocity or altitude as appropriate.

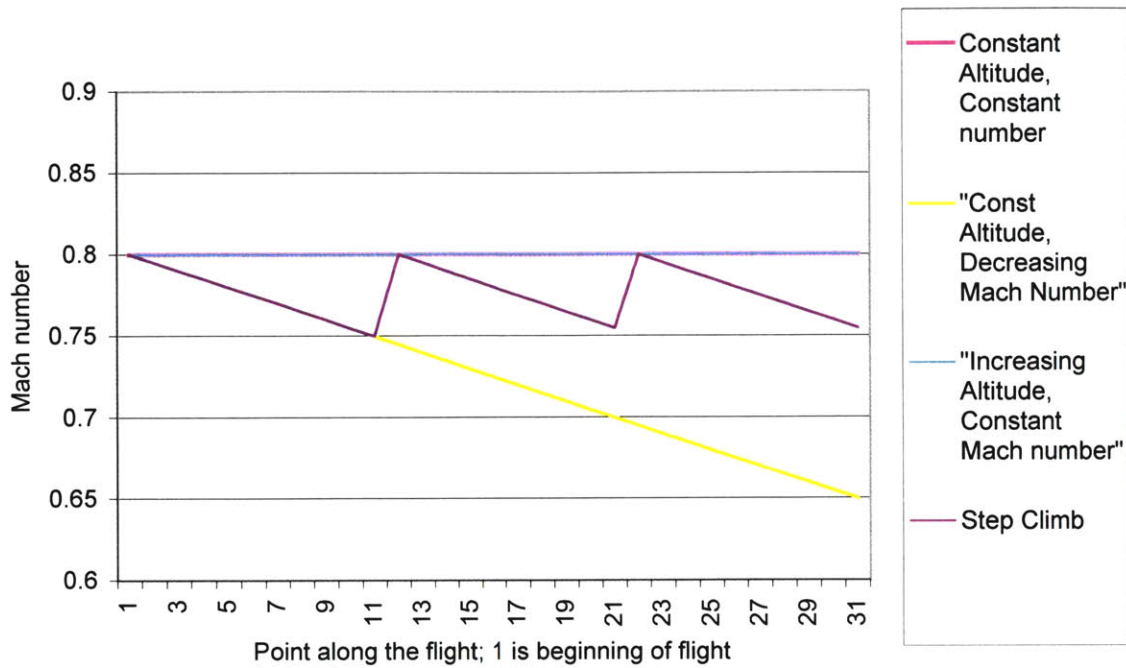


Figure 4.11 – Sample Mach numbers for the Custom Trajectories

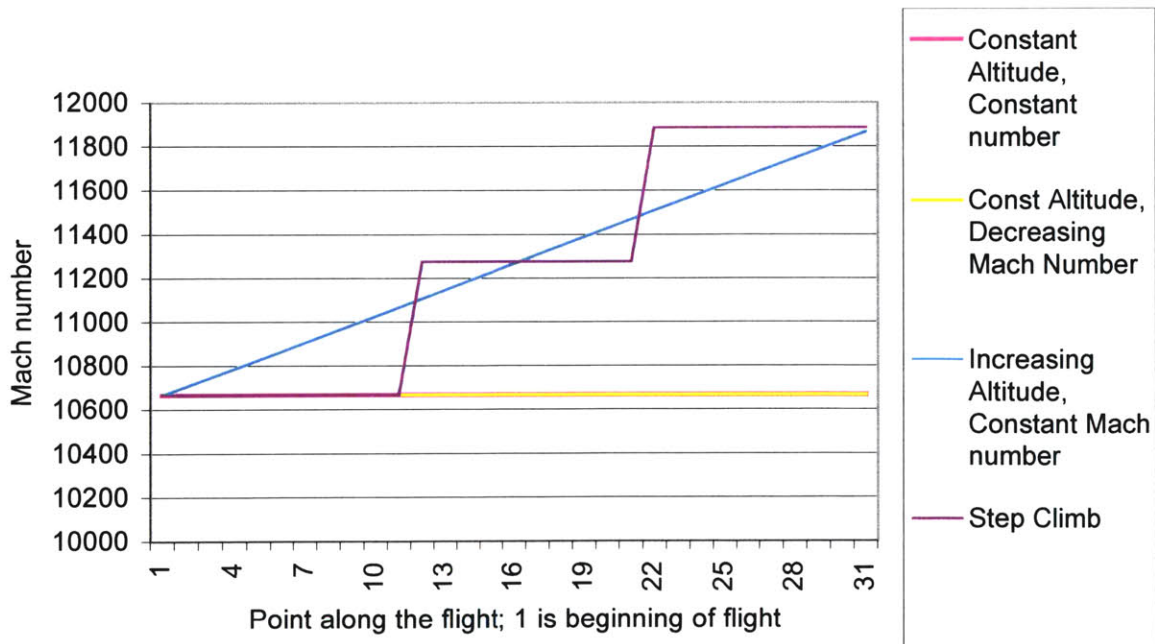


Figure 4.12 – Sample Altitudes for the Custom Trajectories

For each origin-destination pair, two initial altitudes were examined. These were identified as the flight levels just above and just below the average ETMS cruise altitude (where cruise was defined as cruise chords and above 7000m). Lower boundary flight levels were 8534.4m, 8839.2m, 9448.8m, 10058.4m, 10668m. Since the altitude was usually less than 11000m, the Mach number corresponding to minimum drag was decreased more. Visual inspection of the flights showed a decrease of about 0.15 in Mach number, or about 0.1 for the change in altitude and about 0.05 for the change in initial Mach number. The changes in Mach number are consistent with changes in Mach number reported in the literature (Shevell [32], Padilla [22]) for optimizing specific range as a function of altitude

4.2.3.1. Constant Altitude, Constant Mach Number

The simplest reroute trajectory mimicked the way OAG flights are modeled in SAGE (e.g. flights for which ETMS trajectory data are not available). The altitude was assumed constant, at the average cruise altitude of the ETMS data. The Mach number was assumed to be the BADA cruise Mach number.

4.2.3.2. Constant Altitude, Mach Number Corresponding to Minimum Drag

A second reroute trajectory assumed that the aircraft flew at minimum drag conditions, given by Equation 4.2 and 4.3. Although some aircraft companies may choose to fly more quickly due to time costs, this was not accounted for. The initial altitude was the average cruise altitude of the ETMS data. The altitude was held constant, and the Mach number (and hence velocity) was changed according to Equations 4.2-4.3.

4.2.3.3. Constant Velocity, Altitude Corresponding to Minimum Drag

A third reroute trajectory also assumed that the aircraft flew at minimum drag conditions, given by Equation 4.2 and 4.3. The initial altitude and Mach number were assumed to be the same as the constant altitude, constant Mach number flight: the average cruise altitude of the ETMS data, and the Mach number corresponding to minimum drag. The velocity was held constant, and the altitude (and hence Mach number) were changed according to Equations 4.2-4.3.

4.2.3.4. Step Climb

The last reroute trajectory assumed that the aircraft flew with step climbs. The initial altitude and Mach number were assumed to be the same as the constant altitude, constant Mach number flight: the average cruise altitude of the ETMS data, and the Mach number corresponding to minimum drag. When the fuel burn at the next higher flight level was less than the fuel burn at the current flight level, the aircraft initiated a climb. Hence the step climb followed a combination of the two previous trajectories; 4.2.3.2 at each flight level, and then a jump in altitude (similar to 4.2.3.3) when necessary.

4.2.4. Time Period

Choice of time period allowed some minimization of the number of data sets used. The continental flights examined were the same as those in CHAPTER 3; the week of 11/12/2001 to 11/18/2001 (with RUC data), minus the days of 11/13 and 11/14 (recall that the satellite data were not available for this time period). Unfortunately, the same meteorological data set was

unavailable for 2001. Consequently, the transatlantic flights were run on the week of 11/12/2003 to 11/18/2003 (with UM data).

The constructed reroutes were scheduled for 00 and 12 Universal Time Conversion (UTC) on each day. UTC is also known as GMT, or Greenwich Mean Time. For ease in comparison, note that hour 12 UTC corresponds to hour 07 Eastern Standard Time, 08 Eastern Daylight Time, 05 Pacific Standard Time, and 06 Pacific Daylight Time [30].

Figure 4.13 and Figure 4.14 show all the estimated contrails for one day of the custom reroutes.

4.3. RESULTS

To compare the various flights, a metric was needed. When comparing two flights with the same flight distance (i.e. two flights with the same latitude/longitude trajectory), the percentage of the flight (by distance) with persistent contrails was used. To compare different origin-destination pairs, the linear distance of persistent contrails (or contrails/km) was used.

4.3.1. Assessment of Custom Reroutes' Ability to Mimic Current Practice

First the custom reroutes were assessed to see how well they replicated the ETMS routes. One random ETMS flight was identified for each origin-destination pair. Then a custom reroute was created to replicate that ETMS flight as closely as possible:

- The departure time, aircraft type, and latitude/longitude trajectory were taken directly from the ETMS flight to be used in the custom reroute.
- The closest of the four altitude/Mach number trajectories of Section 0 was chosen and used in the custom reroute.
- The starting Mach number was chosen as described in the scenario.
- The starting altitude was chosen to match the ETMS flight.

These custom reroute outputs were compared to their matching ETMS flights. In most cases, the custom reroutes had lower fuel burn and longer time than the ETMS flight (see Table 4.5). For instance, the transatlantic custom reroutes overestimated time by 12.6 +/-17.7% and underestimated fuel burn by -12.1 +/-5.2%. This directly reflects the lack of time costs in the creation of the custom reroute trajectories; the creation process minimized fuel burn, and ignored time. Despite this, the average total cost nearly replicated the actual flights' cost (percent reduction of 0.3 +/- 8%, Table 4.5). This small reduction indicates that airline companies may place a higher price on time than that assumed in 2.4. Otherwise, they would fly more slowly, and save in fuel burn. Due to the inability to precisely identify an altitude/Mach number trajectory, the continental routes were much harder to replicate (and therefore not discussed here). This is consistent with the fact that airline companies are also subject to flight controls on altitude, which makes it difficult to minimize time and fuel burn.

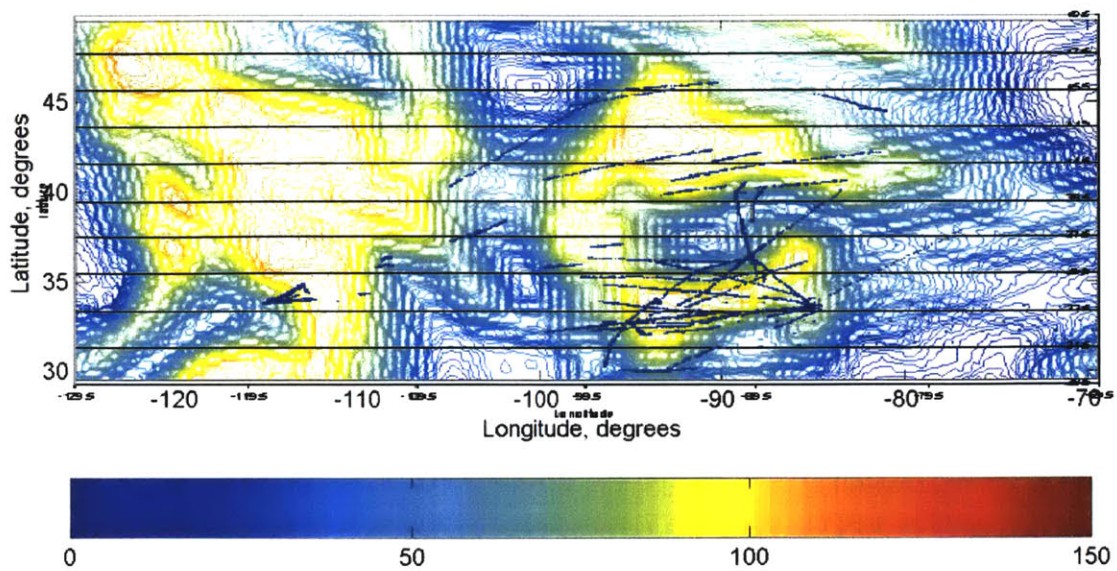


Figure 4.13 - Contrails estimated for all custom reroutes on November 12, 2001. RHi is from RUC data, hour 18.

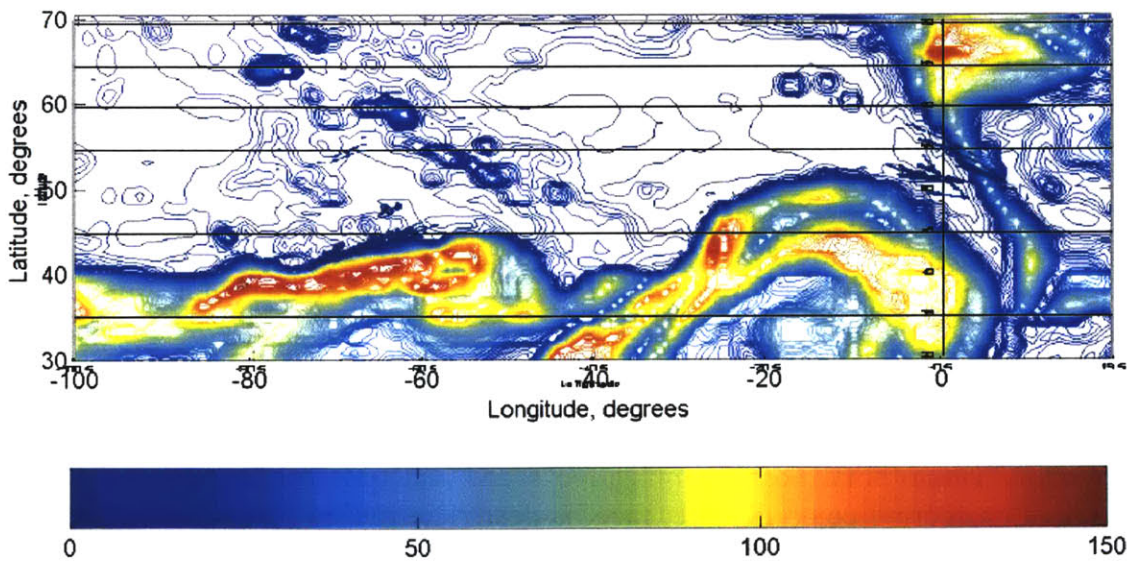


Figure 4.14 - Contrails estimated for all custom reroutes on November 12, 2003. RHi is from UM data, hour 18.

Table 4.5 - Percent change of average custom reroute outputs compared to average current practice outputs for transatlantic flights.

Departure Airport	Arrival Airport	% Increase of Time	% Reduction of Fuel Burn	% Reduction of Cost
BOS	EGLL	35	13	9
BOS	LFPG	38	8	19
EDDF	JFK	1	7	- 3
EDDF	ORD	- 2	7	- 4
EGLL	BOS	-12	15	-13
EGLL	JFK	-12	4	- 9
EGLL	ORD	- 1	11	- 6
JFK	EDDF	20	11	6
JFK	EGLL	35	19	5
JFK	LFPG	17	20	0
LFPG	JFK	2	4	- 2
LFPG	ORD	- 5	13	- 8
ORD	EDDF	31	17	6
ORD	EGLL	18	14	1
ORD	LFPG	24	18	3
Average		12.6 +/-17.7	12.1 +/-5.2	0.3 +/-8.1

Custom short-haul flights, such as ATL-ORD, overestimated both time and fuel burn compared to the ETMS routes. Examination of the chorded data showed that ~50% of the ETMS flight (by ground distance) was spent climbing to or descending from the cruise altitude, while the custom reroute supposed all the cruise chords were spent at the cruise altitude and Mach number. This occurred because the aviation system model dynamically created landing and takeoff trajectories, but did not track for the ground distance traveled and shift the beginning cruise latitude/longitude accordingly. If instead the low percentage of flight at cruise had been replicated (e.g. include a slow climb to altitude instead of the default in the aviation system model), the custom reroute would replicate the ETMS flights better. Future studies would benefit by correcting this for short haul flights.

It has been demonstrated that the custom reroutes are only a first order estimate of the ETMS flights due to decreased Mach number resulting from adopting a fuel burn minimization speed and trajectory versus total cost minimization speed and trajectory. Next contrails are examined. Considering contrail persistence in clear skies and in total for all transatlantic flights and most continental flights, the estimated persistent contrail distance of the custom reroute was within +/-5% of the persistent contrail distance of the current practice routes (see Table 4.6). These could occur because:

- The altitude and Mach number were not accurately portrayed. As these directly relate to fuel burn and efficiency, the contrail estimations would be altered.
- Time differences toward the end of the flight resulted in different RH_i fields. This would have less effect because we have shown that the gradient of RH_i with respect to time is small.

- The engine equation was incorrect. But as demonstrated in Section 3.3.2, this has little effect on the resultant contrail persistence.

Table 4.6 – Average custom reroute contrails compared to current practice outputs for transatlantic flights. This table gives the percent of the flight as persistent contrails (instead of a percent reduction or increase). This is done due to the plethora of zeros in both ETMS and custom flights.

Departure Airport	Arrival Airport	ETMS Flight % of Flight as Contrails	ETMS Flight % of Flight as Contrails (clear skies)	Custom Flight % of Flight as Contrails	Custom Flight % of Flight as Contrails (clear skies)
BOS	EGLL	11.89	9.95	7.30	6.46
BOS	LFPG	18.56	17.99	6.84	6.67
EDDF	JFK	0.00	0.00	0.00	0.00
EDDF	ORD	5.36	5.36	0.00	0.00
EGLL	BOS	6.40	5.38	0.20	0.20
EGLL	JFK	0.83	0.00	7.55	7.32
EGLL	ORD	0.50	0.50	0.00	0.00
JFK	EDDF	0.00	0.00	0.04	0.00
JFK	EGLL	0.59	0.42	0.00	0.00
JFK	LFPG	0.00	0.00	0.00	0.00
LFPG	ORD	0.97	0.00	0.91	0.57
ORD	EDDF	11.22	6.35	4.81	4.81
ORD	EGLL	0.31	0.22	7.40	7.06
ORD	LFPG	33.28	33.11	29.43	28.92

4.3.2. Rerouting, One Flight at a Time

This section explores if all flights could be individually rerouted to avoid contrails, then whether it would be possible to reduce persistent contrails.

Figure 4.15 and Figure 4.16 show example tradeoffs of contrail persistence against fuel burn, time, and total operating cost. Note that there is not a clear trend of these values as a function of contrail distance formed. Rather, the trend is a function of trajectory. This is clearest in the continental case; for the time examined, only one trajectory formed contrails. But, this trajectory produced nearly identical contrail formation regardless of Mach/altitude trajectory. Furthermore, these graphs show that the “best” alternative could greatly decrease contrail persistence with a small reduction of cost. Different days had a different amount of contrail mitigation and reduction/increase of costs.

To estimate costs to reroute individual aircraft, first ETMS flights and custom reroutes were temporally matched³⁰ in an effort to replicate exact meteorological conditions. Then it was assumed that the “best” custom route (which minimized firstly contrail persistence and secondly total operating cost) was flown instead of the current practice. This yielded a cost and contrail difference between ETMS and custom reroutes for all the origin-destination pairs.

³⁰ . For each time that custom reroutes were run, ETMS flights within three hours were considered temporally matching. This time period as chosen because the temporal resolution of the UM data was three hours.

Since the custom reroutes were run at 0000UTC and 1200UTC, a separate cost and contrail difference was calculated for each of these hours on each day examined. If the current practice (ETMS route) yielded the best combination of contrail mitigation and costs, no custom reroute was used. Table 4.7 and Table 4.8 give penalties for the best possible contrail mitigation for all the flights examined (continental of 11/12-18/2001, transatlantic of 11/12-18/2003).

Through this analysis, several conclusions become clear. First, the costs are nearly identical whether mitigating all contrails or just contrails in clear skies. This indicates that the best route for these two cases is typically the same. Secondly, the continental routes have a relatively low cost for rerouting. This occurs because the FAA approved continental reroutes have much larger distances between them than the transatlantic reroutes do, so are less likely to fly the aircraft through the same area of high RH_i. The cost is relatively the same for the different FAA approved reroutes, whereas the cost of the different transatlantic routes varies depending on how close to the jet stream they are. This indicates that rerouting to mitigate contrail formation may be more cost effective if done over the continental United States using the FAA approved reroutes.

Overall, given perfect knowledge of meteorological data and no air traffic controls, if aircraft were individually rerouted, it was possible to mitigate 65%-80% of persistent contrails and simultaneously achieve an average decrease of 5%-7% of the total operating cost for the week in November 2001 for which this analysis was carried out. These reductions are relative to the actual routes flown by the aircraft during this week, reflecting the impact of non-optimal routing not only on contrail formation, but also on fuel burn and operating costs in general..

However, as aircraft are not flown on cost optimal trajectories, the comparison of fuel-minimizing custom reroutes with the ETMS flights yields an over-optimistic view. A better comparison would be custom reroutes against custom reroutes, or ETMS routes against ETMS routes, as described in Section 4.3.4.

Table 4.7 – Cost of mitigating all contrails from ETMS routes. Note this is a summation over the costs of reducing contrails for all flights, not an average.

	% Reduction of Persistent Contrails	% of Nominal Time Costs	% of Nominal Fuel Burn Costs	% Reduction of Total Operating Cost
All Flights	67.3%	103.4%	82.6%	5.7%
Just Continental	80.0%	97.1%	89.6%	6.1%
Just Transatlantic	65.9%	105.2%	81.8%	5.7%

Table 4.8 - Cost of mitigating contrails in clear skies from ETMS routes. Note this is a summation over the costs of reducing contrails for all flights, not an average.

	% Reduction of Persistent Contrails	% of Nominal Time Costs	% of Nominal Fuel Burn Costs	% Reduction of Total Operating Cost
All Flights	67.8%	103.2%	82.5%	5.9%
Just Continental	80.9%	96.5%	88.4%	7.0%
Just Transatlantic	66.3%	105.1%	81.9%	5.7%

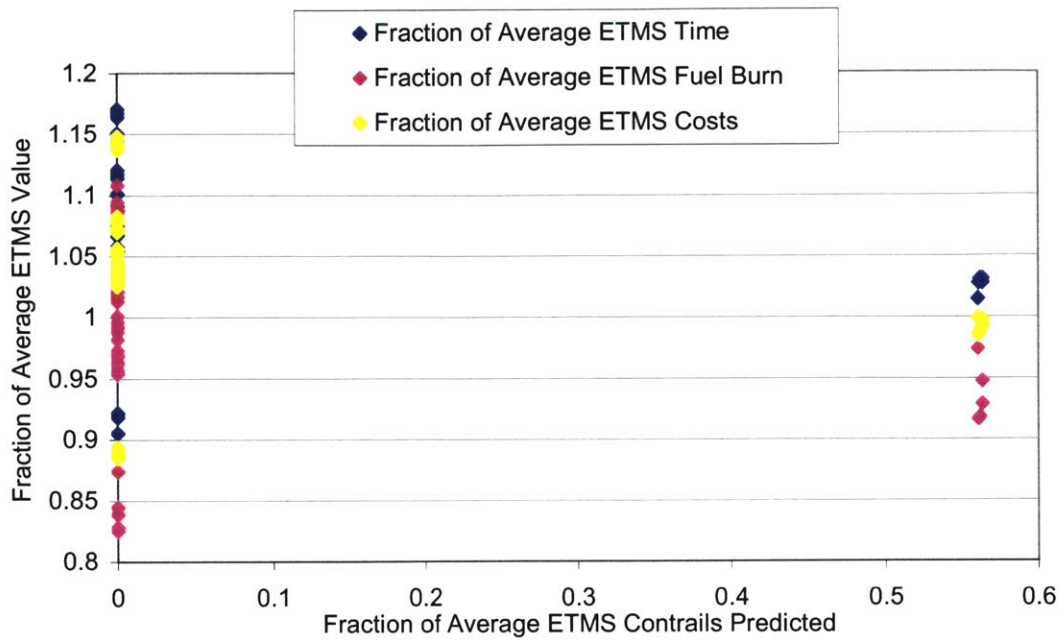


Figure 4.17 – Tradeoff contrails persisting compared to the time, fuel burn, and total operating costs for LAX to JFK on 11/17/2001 0000 UTC. All values are given as percents of the average ETMS value for three hours surrounding 11/17/2001 0000 UTC.

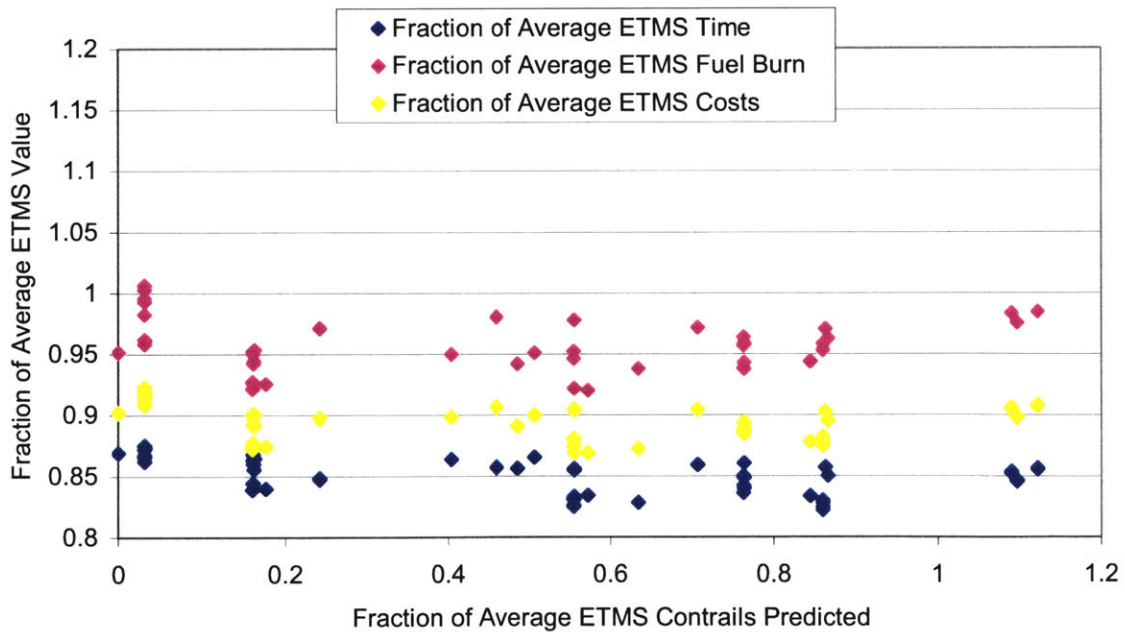


Figure 4.18 – Tradeoff contrails persisting compared to the time, fuel burn, and total operating costs for EGLL to JFK on 11/17/2003 1200 UTC. All values are given as percents of the average ETMS value for three hours surrounding 11/17/2003 1200 UTC.

4.3.3. Rerouting, One Week at a Time

The previous section shows that if all aircraft had been rerouted individually, there would be a significant reduction in persistent contrails. Now let us suppose that only one reroute could be chosen for the entire week. If all the aircraft in this study had flown the same custom reroute(s) for the entire week, there would still be a significant reduction in persistent contrails. This section examines the potential costs for choosing the best custom reroute for the entire week. This approach works well for the transatlantic flights, which have nearly constant RHi fields (always higher RHi toward the south). This does not apply to the continental flights, where the RHi fields are more variable.

Considering each characteristic separately:

Origin Destination Pair - Each origin-destination pair will be examined separately. The average marginal cost will be averaged over all the origin-destination pairs.

Latitude/Longitude Trajectory - For each origin-destination pair, all trajectories that have decreased contrail persistence (in km) compared to the average current practice will be recorded. The best scenario (including altitude/Mach number trajectory) will be examined, as well as an average of the others (in a first order attempt to account for air traffic control constraints). The percent change in time, fuel burn, contrail formation, and cost will be presented.

Aircraft Type – This was addressed through examination of ETMS with the chosen aircraft type only.

Altitude/Mach Number Trajectory – All results with decreased contrail persistence will be reported, regardless of scenario. The best scenario (including the latitude/longitude trajectory) will be examined, as well as an average of the others (in a first order attempt to account for air traffic control constraints). Since the step climb is the most realistic trajectory, it will also be examined separately.

Flight Level Above or Below ETMS Average – All results with decreased contrail persistence will be reported, regardless of scenario. The best scenario (including the latitude/longitude trajectory) will be examined, as well as an average of the others.

Time Period - The results were averaged over all times examined.

In short, this yields the following scenarios for both total contrail persistence and contrail persistence in clear skies:

- Best case scenario for minimal contrail persistence
- Average scenario for all trajectories
- Average scenario for step climbs only

Recalling that one purpose of this study is to assess operational methods to reduce persistent contrails, first all custom reroutes with increased contrail persistence (in km) compared to the current practice were discarded. Some trajectories were more successful at reducing contrail

persistence, and hence systematically reduced contrail formation. This is reflected in which flights were preferentially kept:

Latitude/Longitude Trajectory - For the continental flights, some latitude/longitude trajectories were preferentially kept (no trend). For the transatlantic flights, more northerly routes were preferentially kept.

Altitude/Mach number Trajectory – The constant altitude, constant Mach number trajectory was most favored, with the step climb coming second. The other two trajectories were systematically discarded.

Flight Level Above or Below ETMS Average – Recall that the flight levels allowed for continental flights are 1219m apart, while the flight levels allowed for transatlantic flights are 609m apart. For continental flights, this disparity was large enough such that either a low altitude (too much water partial pressure required to form contrails) or a high altitude (too dry), compared to 10668m, were preferentially kept. For transatlantic flights, these differences were smaller, so since the flights tended toward higher altitudes, the higher altitude was preferentially kept.

With these selected flights, the costs of reducing contrail persistence were calculated. Table 4.9 gives the percent change in time, fuel burn and total operating cost for all the scenarios, and Table 4.10 gives contrail reduction (40-75%). Extended data are listed in APPENDIX G:

Note that some of the custom reroutes chosen for decreased contrail persistence are also cheaper than the current practice. In other words, according to this study it would save airlines money and decrease contrail persistence if the custom reroutes were used. This is a further indication that the airlines either route their aircraft with a different cost index (ratio of cost of time to cost of fuel burn), or are subject to non-cost-optimal ATC controls³¹.

³¹ Assuming that all flights were allowed, the amount of money saved appears to be loosely correlated with aircraft type. For instance, flying custom reroutes with the B747-400 could save ~\$4,000 per flight, while flying custom reroutes with the A340-300 would cost an extra \$5,000 per flight. This suggests that using the standard deviation of the average economic values for each aircraft class is high; individual economic values are required for each aircraft type.

Origin Destination Pair	AVERAGE CUSTOM REROUTES			AVERAGE STEP CUSTOM			BEST BY ALL CONTRAILS			BEST CONTRAILS CLEAR SKIES			
	Fraction of Nominal ETMS time	Fraction of Nominal ETMS fuel burn	Fraction of Nominal ETMS Total Cost	Fraction of Nominal ETMS time	Fraction of Nominal ETMS fuel burn	Fraction of Nominal ETMS Total Cost	Fraction of Nominal ETMS time	Fraction of Nominal ETMS fuel burn	Fraction of Nominal ETMS Total Cost	Fraction of Nominal ETMS time	Fraction of Nominal ETMS fuel burn	Fraction of Nominal ETMS Total Cost	
ATL-DFW		1.16	1.00	1.11	1.03	0.82	0.95	0.97	0.84	0.93	0.97	0.84	0.93
ATL-LAX	NA	NA	NA	NA	NA	NA	NA	NA	NA	NA	0.96	0.90	0.94
ATL-LGA		0.98	0.98	0.98	NA	NA	NA	0.99	0.95	0.97	0.99	0.95	0.97
ATL-ORD		1.07	1.15	1.10	NA	NA	NA	0.90	0.91	0.90	0.90	0.91	0.90
BOS-LAX		1.03	0.98	1.01	1.04	0.97	1.01	0.91	0.85	0.89	0.91	0.85	0.89
DFW-LAX		1.05	0.97	1.01	1.06	0.92	1.00	0.94	0.90	0.93	0.94	0.90	0.93
DFW-LGA		1.08	1.14	1.11	1.09	1.01	1.05	1.07	1.15	1.10	1.07	1.15	1.10
JFK-LAX		1.08	0.99	1.04	1.07	0.98	1.04	1.13	1.03	1.09	1.13	1.03	1.09
LAX-BOS		1.03	0.99	1.01	1.01	0.94	0.98	0.92	0.93	0.92	0.92	0.93	0.92
LAX-DFW	NA	NA	NA	NA	NA	NA	NA	NA	NA	NA	NA	NA	NA
LAX-JFK		1.08	0.97	1.04	NA	NA	NA	1.08	0.97	1.04	1.08	0.97	1.04
LGA-ORD		1.20	0.97	1.11	1.25	0.98	1.15	1.12	0.96	1.06	1.12	0.96	1.06
MIA-SEA		0.93	0.83	0.89	0.93	0.83	0.89	0.93	0.81	0.88	NA	NA	NA
SEA-MIA		1.02	0.88	0.96	NA	NA	NA	0.97	0.86	0.92	0.97	0.86	0.92
BOS-EGLL		1.23	0.82	1.01	1.24	0.80	1.00	1.21	0.78	0.98	1.21	0.78	0.98
BOS-LFPG		1.30	0.90	1.14	1.30	0.87	1.12	1.32	0.88	1.14	1.32	0.88	1.14
EDDF-JFK	NA	NA	NA	NA	NA	NA	NA	NA	NA	NA	NA	NA	NA
EDDF-ORD		0.95	0.95	0.95	0.95	0.92	0.94	1.04	1.00	1.02	1.04	1.00	1.02
EGLL-BOS		0.88	0.94	0.90	0.89	0.93	0.91	0.89	0.93	0.91	0.89	0.93	0.91
EGLL-JFK		0.89	0.95	0.91	0.89	0.94	0.91	0.88	0.92	0.90	0.88	0.92	0.90
EGLL-ORD		0.93	0.93	0.93	0.93	0.90	0.91	0.95	0.93	0.94	0.95	0.93	0.94
JFK-EDDF		1.26	0.75	1.01	1.26	0.75	1.01	1.24	0.74	0.99	1.24	0.74	0.99
JFK-EGLL		1.25	0.77	0.99	1.25	0.77	0.99	1.23	0.76	0.97	1.23	0.76	0.97
JFK-LFPG		1.26	0.80	1.03	1.26	0.75	1.01	1.25	0.74	0.99	1.25	0.74	0.99
LFPG-JFK	NA	NA	NA	NA	NA	NA	NA	NA	NA	NA	NA	NA	NA
LFPG-ORD	NA	NA	NA	NA	NA	NA	NA	NA	NA	NA	NA	NA	NA
ORD-EDDF		1.26	0.71	0.98	1.26	0.71	0.98	1.29	0.73	1.00	1.29	0.73	1.00
ORD-EGLL		1.23	0.73	0.95	1.22	0.72	0.94	1.20	0.72	0.93	1.20	0.72	0.93
ORD-LFPG		1.22	0.75	0.98	1.23	0.72	0.97	1.20	0.71	0.95	1.20	0.71	0.95

Table 4.9 - Calculated costs for all scenarios. All numbers are given as fractions of the ETMS value.

Table 4.10 - Fraction reduction of contrail persistence chosen for Table 4.9

Origin Destination Pair	Change in Contrails , All			Change in Contrails , Clear Skies		
	Average of All	Average of Step	Best of All	Average of All	Average of Step	Best of All
ATL-DFW	0.65	0.12	1.00	0.72	0.03	1.00
ATL-LAX	NA	NA	NA	NA	NA	1.00
ATL-LGA	1.00	NA	1.00	1.00	NA	1.00
ATL-ORD	0.71	NA	0.76	1.00	NA	1.00
BOS-LAX	0.31	0.34	0.68	0.34	0.37	0.83
DFW-LAX	0.60	0.58	1.00	0.48	0.44	1.00
DFW-LGA	0.74	0.64	1.00	0.77	0.69	1.00
JFK-LAX	0.18	0.19	0.38	0.35	0.39	0.67
LAX-BOS	0.50	0.49	0.99	0.52	0.49	1.00
LAX-DFW	NA	NA	NA	NA	NA	NA
LAX-JFK	0.62	NA	0.66	0.63	NA	0.66
LGA-ORD	0.53	0.34	0.96	0.51	0.28	1.00
MIA-SEA	0.14	0.19	0.19	-0.18	-0.12	NA
SEA-MIA	0.18	NA	0.24	0.18	NA	0.24
BOS-EGLL	0.28	0.60	0.70	0.33	0.64	0.72
BOS-LFPG	0.21	0.42	0.51	0.21	0.42	0.52
EDDF-JFK	NA	NA	NA	NA	NA	NA
EDDF-ORD	0.27	0.40	0.66	0.24	0.35	0.67
EGLL-BOS	0.37	0.72	0.85	-0.10	0.54	0.75
EGLL-JFK	0.19	0.30	0.56	-0.05	0.10	0.41
EGLL-ORD	0.30	0.51	0.64	0.26	0.50	0.66
JFK-EDDF	0.34	0.34	0.55	0.24	0.24	0.48
JFK-EGLL	0.45	0.52	0.66	0.45	0.54	0.65
JFK-LFPG	0.23	0.52	0.61	0.20	0.49	0.58
LFPG-JFK	NA	NA	NA	NA	NA	NA
LFPG-ORD	NA	NA	NA	NA	NA	NA
ORD-EDDF	0.44	0.44	0.57	0.36	0.36	0.52
ORD-EGLL	0.44	0.58	0.66	0.45	0.59	0.68
ORD-LFPG	0.38	0.57	0.70	0.31	0.52	0.68
Total Average	0.42	0.44	0.69	0.38	0.39	0.74

Table 4.11 – Cost of mitigating all contrails from minimum fuel burn custom reroutes. Note this is a summation over the costs of reducing contrails for all flights, not an average.

	% Reduction of Persistent Contrails	% Increase of Nominal Time Costs	% Increase of Nominal Fuel Burn Costs	% Increase of Total Operating Cost
All Flights	63.7%	0.7%	3.0%	1.6%
Just Continental	83.6%	1.1%	3.4%	1.9%
Just Transatlantic	56.5%	0.4%	2.8%	1.3%

Table 4.12 - Cost of mitigating contrails in clear skies from minimum fuel burn custom reroutes. Note this is a summation over the costs of reducing contrails for all flights, not an average.

	% Reduction of Persistent Contrails	% Increase of Nominal Time Costs	% Increase of Nominal Fuel Burn Costs	% Increase of Total Operating Cost
All Flights	63.6%	0.7%	2.8%	1.5%
Just Continental	79.2%	1.1%	3.4%	2.0%
Just Transatlantic	58.2%	0.3%	2.5%	1.2%

4.3.4. Comparison of Custom Reroutes

As noted in Section 4.3.1, the custom reroutes tend to underestimate fuel burn and overestimate time. Although contrail costs can be calculated (as in Sections 4.3.2 and 4.3.3), some would argue for a more consistent comparison. Consequently, we now examine tradeoffs within the reroutes themselves; the tradeoff between minimum fuel burn and minimum contrail persistence.

For each temporal set of custom reroutes, first the flight with the minimum fuel burn was identified. Next the flight with the minimum contrail persistence was identified. If two flights had the same minimum contrail persistence, the flight with the minimum fuel burn was chosen. Table 4.11 and Table 4.12 give the average increases in time, fuel burn, and total operating costs. For roughly a 0.5-1% increase in time and 2.5-3.5% increase in fuel burn (or 1-2% increase in total operating cost), 55-85% of the contrails could be mitigated.

A second comparison could be completed within the ETMS routes themselves. First a representative set of ETMS flights could be extracted. Then the time stamps would be altered so each of these flights departed at the same time. Then all the flights could be run simultaneously, and the flight of minimum contrail persistence identified. This is recommended for future work.

4.3.5. Schemes to Reduce Contrail Persistence Levels

It has been shown that the custom reroutes serve as only a first-order simulation of current practice since they were created assuming fuel burn minimization. However, this model can still be used to make first order estimates of the marginal costs of schemes, which might reduce contrail persistence levels by comparing the results for the re-routes to the results for the routes that best approximate current practice.

4.3.5.1. Raising Altitude One Flight Level

Raising the altitude one flight level directly modifies time and fuel burn. Time is increased due to the necessary time to cruise and to decreased velocity (to maintain Mach number). Fuel burn is decreased due to decreased drag at higher altitude, but also increased due to increased climb time. Averaging over the percent differences for all custom reroutes, time is increased by 0.8% and fuel burn is decreased by 3.1%.

Change in contrail persistence depends on the altitude of the two chosen flight levels. If the altitudes are low, then increasing altitude will increase contrail persistence since a smaller partial pressure of water is required for contrail formation. If the altitudes are high, then increasing altitude will decrease contrail persistence (due to decreased humidity at higher altitude). This study indicates that the middle altitude is the tropopause.

In longer flights, such as the transatlantic flights, raising altitude one flight level decreases overall contrail persistence by 14+/-11%, and contrail persistence in clear skies by 6.7+/-12%. This occurs because the average altitude of the ETMS data was at a relatively high altitude.

In shorter flights, such as the continental flights, raising altitude one flight level increased overall contrail persistence by 116+/-109%, and contrail persistence in clear skies by 113+/-90%. This occurred because the average altitude of the ETMS data was lower, and the base contrail persistence was low. When the altitude was raised, the cruise altitude neared the tropopause and formed more contrails. The higher standard deviation occurred because the range of altitudes in the continental data was higher.

As described in Section 3.3.2, changing the engine equation as a function of altitude did not significantly affect contrail persistence. Instead, contrail persistence is highly dependent on the RH_i fields. However, the small changes in fuel burn (3.1%) may be offset by the engine equation.

4.3.5.2. Using a Step Climb Trajectory Instead of Constant Altitude/ Constant Mach Number

According to the average of the custom flights, using a step trajectory instead of constant altitude/constant Mach number will result in a 1.7 +/-1.5% increase in time and a 5.2+/-2.5% decrease in fuel burn. The time increases since it is assumed that at each altitude, Mach number (and hence velocity) steadily decrease until it is more fuel efficient to fly on the next level. The fuel burn decreases because the airplane is allowed to fly at conditions more closely corresponding to minimum drag.

Change in contrail persistence displayed a trend consistent with the altitude study. On longer flights, the step climb decreased overall contrail persistence by 15.4+/- 74.6, and contrail

persistence in clear skies by 12.9+/-78%. However, the shortest flights (ATL-ORD, DFW-LGA) increased overall contrail persistence by 849.8+/- 1687, and contrail persistence in clear skies by 488+/-1529%. This dramatic change occurred because the average ETMS altitudes were low compared to the tropopause, so the baseline contrail estimates were very low.

4.3.5.3. More Northern Routes Over the Transatlantic

Some have suggested that moving the transatlantic aircraft from the most southern route to the most northern route will decrease contrail persistence. This would occur because the RHi fields are always high near the jet stream (other high RHi systems are rare), and the jet stream flows primarily in the south (regardless of the time of year). The contrail model shows that moving all flights to the most northern route would increase time and fuel burn both by 1%, a relatively small amount compared to the sensitivity of the analysis. Yet the effect on contrails is very large; 13+/-15% decrease in contrail persistence, and 16+/-16% decrease in contrail persistence in clear skies. Hence if the northern routes are able to support all the aircraft, a successful scheme to reduce contrail persistence would be to move all aircraft to the most northern routes.

CHAPTER 5: SUMMARY AND RECOMMENDATIONS

5.1. SUMMARY

This thesis created and tested an advanced contrail model. First, the contrail estimation model was used to compare contrail persistence estimates made from measured flight track data to contrail images extracted from satellite data. Then the model was used to assess operational options for reducing contrail coverage. The following conclusions were obtained:

First, it was not possible to match particular contrails observed in the satellite images to origin-destination pairs. The contrails extracted from the satellite images typically align N-S, while most aircraft routes are aligned E-W. This occurs largely because the contrail mask algorithm identifies both contrails and striated cirrus cloud formations, suggesting limitations in the satellite sensing and extraction methods [28]. Perhaps 40-50% of the contrail pixels are misidentified striated cirrus cloud formations.

Second, it has been demonstrated that 60-90% of the identified contrail pixels (demonstrated to be contrails and clouds) are located in areas where the RHi is theoretically too low to support contrail persistence. This demonstrates that the RHi fields, although representative, do not accurately portray the true RHi fields on a given day in 2001. Hence at this point in time, it is unknown to what degree the contrail model coupled with actual aircraft flights can be used to accurately estimate contrail formation as given by satellite images/contrail masks

Third, the typical length of the estimated contrails (several degrees) was longer than the typical length of the observed contrails (one degree). This may reflect a limitation of the satellite sensing of the contrails, but it also implies that the chord lengths used within SAGE need to be shortened - at least to the extent to where they are consistent with length-scales observed in the RHi data.

Fourth, creating custom reroutes based solely on minimization of fuel burn does not replicate the procedure used by airlines. When attempting to apply this process, fuel burn is systematically underestimated and time is systematically overestimated, for a total overestimate of the actual flights' cost by 0.3 +/- 8% (transatlantic only). In order to improve the custom reroute creation, routes need to be created with more input variables (e.g. time costs and winds). Additionally, for short haul flights a smaller percentage of the flight should be spent at cruise. Finally, updating the engine equations to better replicate SFC as a function of altitude and Mach number would further increase the reliability of the custom reroutes fuel burn estimation (but not contrail estimation).

Fifth, the use of published fuel burn and time costs indicates alternate routes would not only decrease contrail formation, but also decrease fuel burn and time costs. Given perfect knowledge of meteorological data and no air traffic controls, if aircraft were individually rerouted, it was possible to mitigate 65%-80% of persistent contrails and simultaneously achieve an average decrease of 5%-7% of the total operating cost for the week in November 2001 for which this analysis was carried out. These reductions are relative to the actual routes flown by the aircraft during this week, reflecting the impact of non-optimal routing not only on contrail formation, but also on fuel burn and operating costs in general. A reduction occurs

even if aircraft are rerouted on a weekly basis; in this case it would be possible to mitigate 40-75% of current practice persistent contrails for an change of -10 to $+5\%$ of the total operating cost. This indicates that either airline companies are highly restricted against preferred routes (air traffic controls), or there are differences between what the airline terms a “time cost” and what was used in this study. For instance, this study did not take into account the passenger’s value of time (desire to get to the destination more quickly).

Sixth, an assessment was also made of the cost of mitigating contrails compared to the custom reroute that minimized fuel burn. In this case, 55%-85% of the contrails could be mitigated, for roughly a 0.5-1% increase in time and 2.5-3.5% increase in fuel burn (or 1-2% increase in total operating cost).

Finally, contrail persistence could be reduced if aircraft are consistently rerouted in certain ways. Examining flights created to minimize fuel burn, one way to reduce contrail persistence is to move the aircraft away from the humid tropopause. Another way would be to fly a route with less fuel burn (e.g. a step climb instead of constant altitude constant Mach number). Over the transatlantic, choosing a more northerly route (with decreased humidity) would also decrease contrail formation.

Key areas of uncertainty that may impact these results include the validity of the contrail identification methods, the validity/range/resolution of the RH_i estimates obtained from the assimilated meteorological data, the advection of contrails over time, the chord lengths in the aviation system model, the value of RH_i assumed as the contrail persistence threshold, the validity of the engine modeling methods, the database of flights examined, and the construction of the custom reroutes. Further, contrail formation is a strong function of latitude and time of year. Therefore, the results cannot be generalized beyond the global regions and times of year that were analyzed.

5.2. RECOMMENDATIONS FOR FUTURE WORK

To improve estimation accuracy, future work should include:

- **Meteorological Data Improvements**
 - Update meteorological data, especially RH and RH_i fields
 - Improve contrail mask algorithm to remove threading (striated cirrus clouds)
 - More precise advection of estimated contrails.
 - Test temporal and spatial resolution of the meteorological data, so that the database can be increased and not overwhelm database storage constraints
 - Identify the value of RH_i at the contrail persistence threshold within $\pm 1\%$
- **Contrail Model/SAGE Updates**
 - Extend time period of meteorological data in aviation system model (e.g. to a month or year)
 - Decrease chord lengths in aviation system model
 - Increase the database of flights to include international flights

- Update engine equation (SFC) to better reflect changes in altitude and Mach number³²
- ETMS/Custom Reroutes
 - Instead of using custom reroutes, change the time stamp on a representative set of ETMS flights such that all flights occur at the same time, then assess mitigation contrail costs
 - Add in a time cost and dynamically create custom reroutes.
 - For short haul flights, spend a smaller percentage of the cruise chords actually at cruise conditions.

³² Note that with respect to assessing contrail estimates against the contrail masks, the errors in SFC have only a minor effect on uncertainty.

APPENDIX A: CONTRAILS AND AVIATION INDUCED CIRRUS CLOUDINESS

Contrails are line-shaped clouds produced by the water in aircraft engine exhaust at high altitudes.

This section describes contrails in depth, and proceeds to describe the method used to evaluate contrail formation.

A.1. CONTRAIL PHYSICS

The combination of water vapor in aircraft engine exhaust and the low ambient temperatures that often exists at these high altitudes allows the formation of contrails. Depending on the temperature and the amount of moisture in the air at the aircraft altitude, contrails evaporate quickly (if the humidity is low) or persist and grow (if the humidity is high) [8].

Consequently, contrail formation is inherently similar to cloud formation. The evolution of contrails into aviation-induced cirrus cloudiness occurs in about 4-6 hours, depending on the winds. After this time period, the resultant clouds are nearly indistinguishable from normal cirrus clouds.

Table A.1 gives the mean characteristics of cirrus clouds. Note that the altitude which cirrus clouds preferentially form is in the range of altitudes that aircraft preferentially fly. Young contrails can be separated from their cloud brethren through their linear features and smaller particle size (10 μ m instead of 15 μ m), but the developing cirrus cloudiness is indistinguishable [4].

Table A.1 - Mean characteristics of cirrus clouds

Thickness	1.5 km
Altitude	9 km
Concentration	30 1/L
Ice Content	0.025 g/m ²
Particle Size	15 μ m
Shape	variable

Small scale contrail physics

1. No clouds, condensation nuclei
2. Water vapor added
3. Water condenses, and either
 - Dissolves the particle and forms a concentrated aqueous solution
 - Forms an aqueous layer on the surface
4. Perturbation causes ice to form

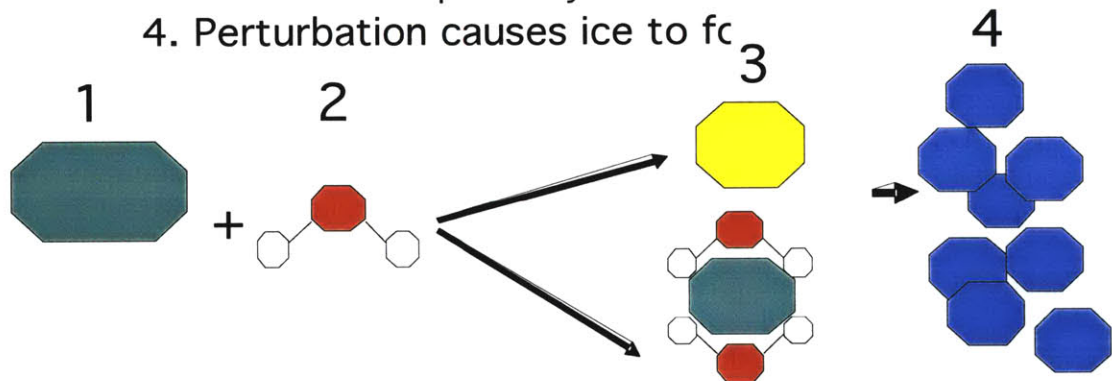


Figure A.1 - Illustration of small scale contrail physics process

A.1.1. Small Scale

On the small scale, contrail formation is similar to any other heterogeneous nucleation process. Figure A.1 depicts the heterogeneous nucleation process.

In the first step, no clouds are present; just condensation nuclei. This is analogous to the upper atmosphere. Storms and temperature inversions cause the troposphere and tropopause to be inundated with potential condensation nuclei. The stratosphere has fewer particles (and ice/water particles) because it is thermally stable.

In the second step, water vapor is added. It is important to note that much of the contrail formation process is dependent on atmospheric water. However since the upper atmosphere is so cold (reaching temperatures of 216 K), the ambient water is frozen as ice. The passage of the aircraft releases water vapor, such that this process may begin.

The next step occurs if the conditions are saturated with respect to water condensing on these nuclei (a function of vapor pressure of water, curvature of the particle). The water either condenses on the particle, or dissolves the particle and forms a concentrated aqueous salt solution.

Even though the conditions may be supersaturated with respect to ice, the activation energy is such that a perturbation is needed to form a contrail. This could be drops hitting each other, a

sound wave, or even vorticity caused by the wingtips of the aircraft. With this perturbation, condensation begins, and continues until the system is no longer supersaturated. Cold temperatures cause the particles to quickly freeze to ice. The result is contrails.

The process may be more readily understood by relating cloud formation to a standard elementary school experiment. In this experiment sugar is dissolved in boiling water. As the water cools, nothing happens. At some point, the water may be supersaturated with respect to sugar, but still nothing happens. Only when a perturbation occurs (e.g. scratching the bottom of the container), will the sugar solidify.

A.1.2. Large Scale

Many areas of the tropopause are supersaturated with respect to ice.³³ The small-scale contrail physics indicate that when the aircraft flies through these areas, a contrail should form.

A.1.2.1. Schmidt-Appleman procedure

The Schmidt-Appleman procedure for estimating contrail formation was independently proposed by Schmidt and Appleman (1953) [9]. It states that contrails form when the exhaust and entrained air passes through a thermodynamic state that is saturated with respect to liquid water (droplets form) and then into a state that is saturated with respect to ice (droplets freeze). If the ambient conditions are saturated with respect to ice, the contrail will persist. Figure A.2 graphically represents the Schmidt-Appleman Procedure by tracing out the thermodynamic path of the particles from the engine exit to the ambient conditions.

Depending on the ambient conditions and the engine exhaust characteristics, the contrail factor line can move. Figure A.3 shows three different sets of ambient conditions and engine characteristics. The ambient conditions are denoted by the red dot. The contrail factors are denoted by the red line.

In Case A, the particles do not pass through a state that is supersaturated with respect to water. Hence the water never condenses, never hardens into ice, and so a contrail does not form.

In Case B, the particles pass through a state that is supersaturated with respect to water. The water then condenses, and quickly freezes into ice. But the ambient conditions are not saturated with respect to ice. So, when the particles reach equilibrium with the surrounding atmosphere, they evaporate. Hence a contrail forms, but does not persist.

In Case C, the particles pass through a state that is supersaturated with respect to ice. But unlike Case B, the ambient conditions are supersaturated with respect to ice. So when the particles reach equilibrium with the surrounding atmosphere, they remain solid. Hence a contrail forms and persists.

³³ The stratosphere is thermally very stable, and hence most particles settle out of it. Therefore, there are very few ice supersaturated regions in the stratosphere. According to Peter Spichtinger, ice super saturated regions of the stratosphere only occur when there is a double tropopause, e.g. along a front.

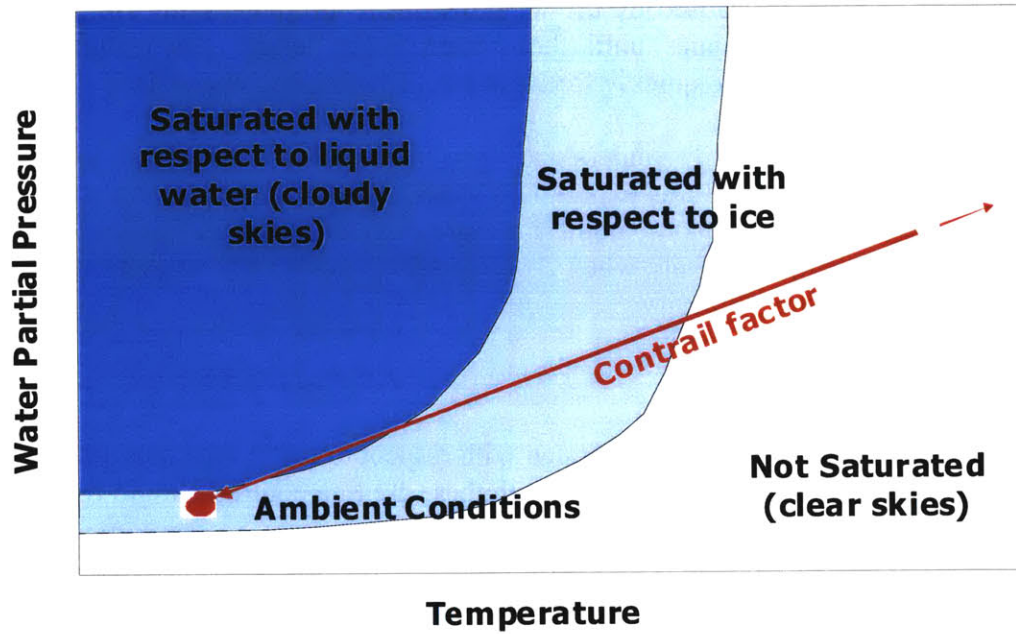


Figure A.2 - Illustration of the Schmidt-Appleman Procedure

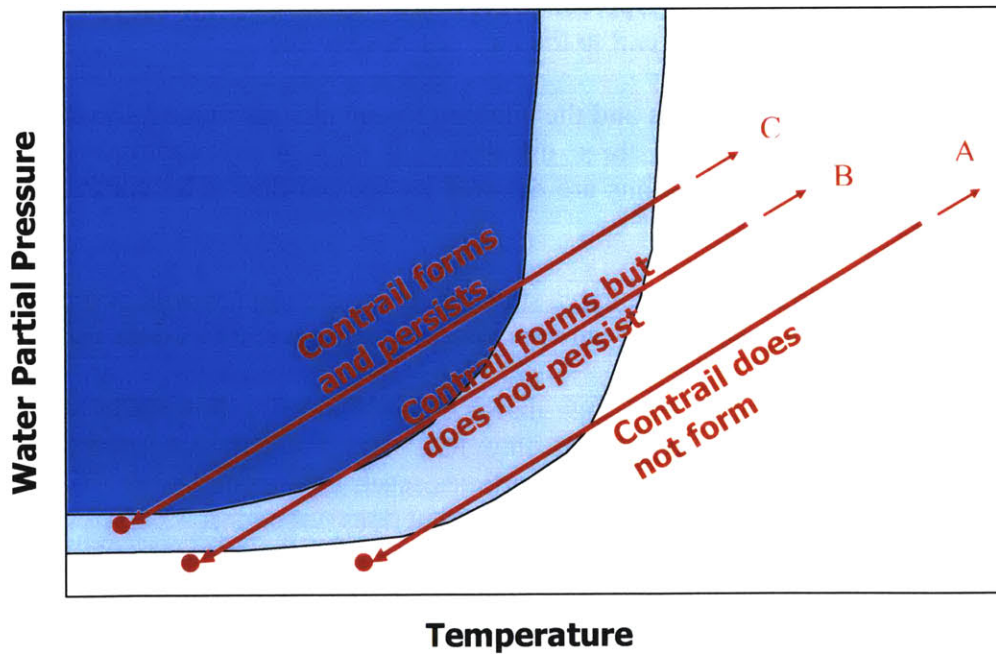


Figure A.3 - Illustration of three possible scenarios of ambient conditions and engine exit conditions.

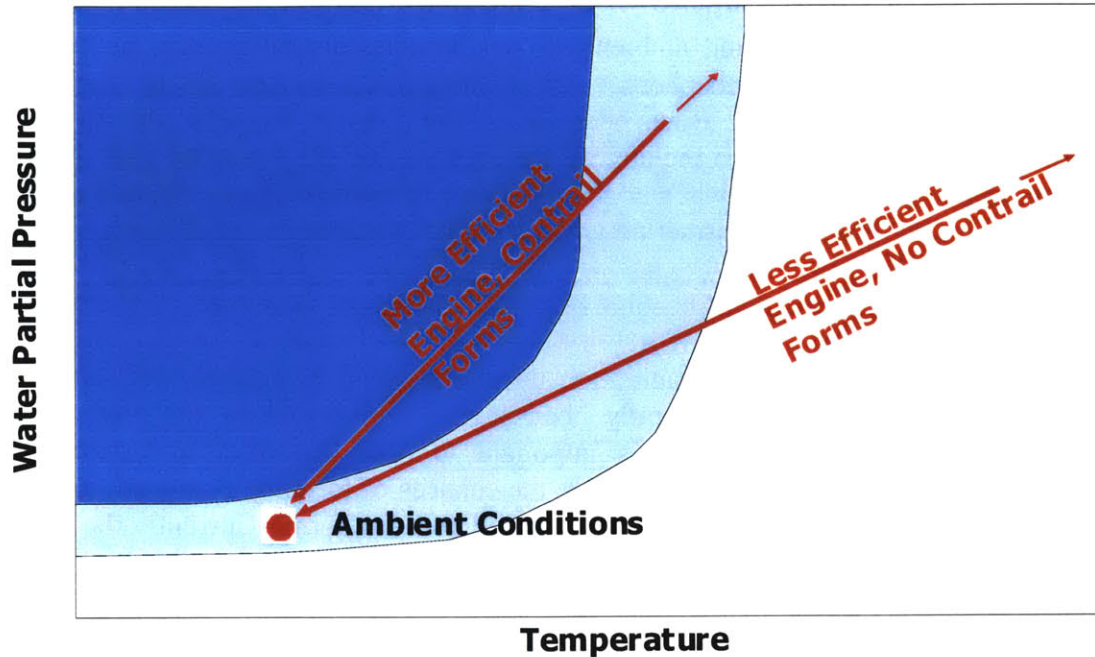


Figure A.4 - Illustration of the Schumann Hypothesis

A.1.2.2. Schumann Hypothesis

In 1996 Schumann proposed that the slope of the contrail factor line could be described using the overall efficiency of the aircraft engine [10]. This holds true because an airplane engine with a higher overall efficiency (thrust*velocity/fuel mass flow*heating value) has a different thermodynamic state in the exhaust (with lower temperature per unit of water)³⁴.

Through thermodynamic arguments, Schumann showed that the slope of the contrail factor line can be related to the efficiency of the aircraft engine:

$$\frac{dw}{dT} = \frac{M_{H_2O} * C_p * P_o}{FB * E * Q * (1-\eta)} \quad (2.1)$$

- Where
- M_{H_2O} = mass of water output
 - C_p = Specific Heat
 - P_o = Ambient Pressure
 - FB = Total Fuel Burn
 - E = $R_{air} / R_{water} = 0.622$
 - Q = Heating value of fuel
 - η = Overall efficiency $\equiv (Thrust * V) / (Fuel\ Mass\ Flow * Q)$

Figure A.4 depicts the implications of this hypothesis. Note the slopes are exaggerated to more clearly depict Schumann's hypothesis.

³⁴ The overall efficiency should not be confused with other efficiencies, such as the propulsive efficiency and the thermal efficiency. The overall efficiency implies that better engines, though using less fuel for the same thrust power, produce the same amount of water at a lower exhaust temperature. The overall efficiency is the product of the propulsive and thermal efficiencies.

A.1.2.3. Role of Other Volatile Particles

Volatile sulfate particles, soot, and ambient aerosol particles are all present in the exhaust stream as it mixes with the atmosphere. All of these particles can act as nuclei in the heterogeneous nucleation process. It has been shown that particles from the aircraft cause the contrail to become visible closer to the aircraft than it would if only ambient particles existed [31]. However, it is not known whether the existence of particles from aircraft impact the “steady-state” contrail that forms farther downstream from the aircraft.

To capture these effects (which will become better understood in the future), this analysis will have a factor describing the percent of RH_i saturation at which contrails persist. If there were solely homogeneous nucleation, the saturation threshold would be roughly 150-200%. The addition of particulates (whether naturally occurring, or introduced by the aircraft) would decrease the saturation threshold. It is important to note that after a certain level of particulates, adding more particulates decreases the chances of forming a contrail; the water is so thinly spread out on so many particles, that a cloud does not form. Currently the saturation threshold for contrail persistence has been set to 100%.

A.2. OTHER CONSIDERATIONS

The calculation of contrail formation has been shown to be complex. Other considerations were examined, as described below.

A.2.1. Addition of Exhaust Water Vapor Increasing Humidity

The addition of water vapor from the aircraft engine exhaust does increase relative humidity. But this level of increase is much smaller than the measurement uncertainty of +/- 1%.

This paper assumes that the addition of water vapor by the aircraft engine exhaust does not increase relative humidity levels. This assumption was tested by calculating the increase in humidity levels from Nov 12-18, 2001 from the total water mass added to the atmosphere during each day of one week. The total water mass added was estimated by SAGE for global 1° by 1° sections.

Assumptions include:

- Altitude at the maximum flight level allowed by the FAA (39000 ft). This will overestimate total humidity increase due to decreased density and pressure.
- Thin slice at this altitude, based on the distance that turbulently mixed water vapor will travel in 120 seconds (~ 150 m). This will overestimate total humidity increase since all water vapor in a vertical column is assumed to be emitted in this section only.
- All water vapor emitted stays in this volume the entire time. This will overestimate total humidity since there would be an outward flux of water vapor.
- The water vapor number corresponding to the maximum of the 99% confidence interval of the entire 1° by 1° sections was used. This will overestimate total humidity increase since most areas would have less aircraft traffic.

Table A.2 shows the increase in relative humidity (in percent) for each day. The change ranges from 0.055 – 0.081%. Summing the water vapor for the entire week (and further assuming that there is not precipitation or natural cloud formation) results in a 0.5% change in relative humidity. Since the areas of highest aircraft traffic (Ohio, and Europe) are naturally moist, it is likely that clouds / precipitation would occur long before the relative humidity is raised enough to form natural clouds.

Table A.2 – The change in relative humidity (%) for the maximum of 99% confidence interval

Maximum of 99% Confidence Interval Mixing Ratio (mass of water vapor per unit mass of dry air)	12-Nov	6.80E-08	Corresponding Change in Relative Humidity (%)	0.07
	13-Nov	6.60E-08		0.07
	14-Nov	7.90E-08		0.08
	15-Nov	7.60E-08		0.08
	16-Nov	7.70E-08		0.08
	17-Nov	5.10E-08		0.05
	18-Nov	5.30E-08		0.06
	Maximum of 99% Confidence Interval, Summed Over the Week			4.70E-07

A.2.2. Ideal vs. Empirical Saturation Curves

When examining whether a contrail will form, some consideration need to be given to the difference between ideal and empirical water and ice saturation curves (Table A.3). A study was conducted comparing Clausius-Clapeyron (ideal) and Goff-Gratch (sample empirical) curves. Clausius-Clapeyron predicts slightly higher water saturation pressures than Goff-Gratch. Hence using Clausius-Clapeyron would underestimate contrail formation.

Although other processes have been assumed to be ideal, using the empirical relations will provide more accurate results. After speaking to Dr. David Duda (NASA Langley Research Center) it was apparent that two newer empirical relations had been constructed: Wexler and Sonntag. Since Sonntag is more widely accepted, this study uses Sonntag.

Table A.3 - Various saturation pressure equations

WATER SATURATION PRESSURES (Pa)	ICE SATURATION PRESSURES (Pa)
<p>Clausius-Clapeyron (Ideal) $2.53 \cdot 10^{11} \cdot \text{EXP}(-5420/T)$</p> <p>Goff-Gratch (Empirical) $10^{(-7.90298 \cdot (T_{sw}/T-1) + 5.02808 \cdot \text{LOG}(T_{sw}/T) - 1.3816 \cdot 10^{-7} \cdot (10^{(11.334 \cdot (1-T/T_{sw}) - 1) + 8.1328 \cdot 10^{-3} \cdot (10^{(-3.49149 \cdot (T_{sw}/T-1) - 1) + \text{LOG}(e_{ws}))})$</p> <p>Sonntag (Empirical) $\text{EXP}(-6096.9385/T + 16.635794 - 0.02711193 \cdot T + 0.00001673952 \cdot T^2 + 2.433502 \cdot \text{LOG}(T)) \cdot 100$</p> <p>Wexler (Empirical) $\text{EXP}(-2991.2729/T^2 - 6017.0128/T + 18.87643845 - 0.028354721 \cdot T + 0.000017838301 \cdot T^2 - 8.4150417 \cdot 10^{-10} \cdot T^3 + 4.4412543 \cdot 10^{-13} \cdot T^4 + 2.858487 \cdot \text{LOG}(T))$</p> <p>Where T = ambient temperature T_{sw} = Boiling Point Temp. of Water e_{ws} = Water Vapor Sat. Pressure at T_o</p>	<p>Clausius-Clapeyron (Ideal) $3.41 \cdot 10^{12} \cdot \text{EXP}(-6130/T)$</p> <p>Goff-Gratch (Empirical) $10^{(-9.09718 \cdot (T_{si}/T - 1) - 3.56654 \cdot \text{LOG}(T_{si}/T) + 0.876793 \cdot (1 - T/T_{si}) + \text{LOG}(e_{io}))}$</p> <p>Sonntag (Empirical) $\text{EXP}(-6024.5282/T + 24.7219 + 0.01061386 \cdot T - 0.000013198825 \cdot T^2 - 0.49382577 \cdot \text{LOG}(T)) \cdot 100$</p> <p>Wexler (Empirical) $\text{EXP}(-5865.3696/T + 22.241033 + 0.013749042 \cdot T - 0.000034031775 \cdot T^2 + 2.6967687 \cdot 10^{-8} \cdot T^3 + 0.6918651 \cdot \text{LOG}(T))$</p> <p>Where T = ambient temperature T_{si} = Ice Point Temp. of Water e_{io} = Ice Vapor Sat. Pressure at T_o</p>

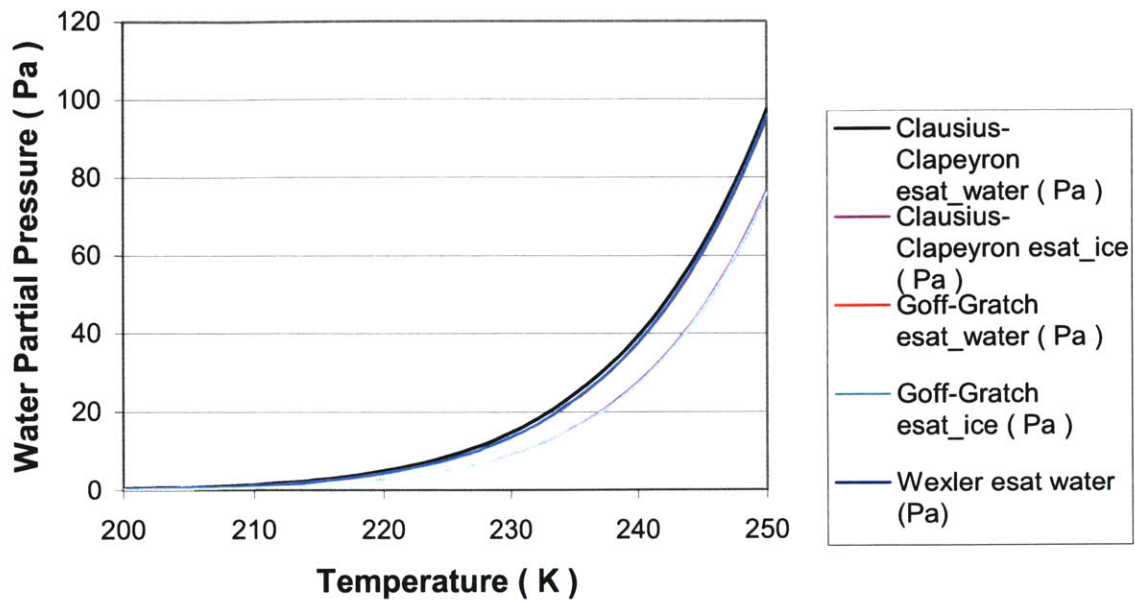


Figure A.5 – Various water and ice saturation pressure curves

Figure A.5 graphs the various saturation pressure curves. Note that they are all nearly identical.

A.2.3. Changing Specific Heat in Contrail Formation Equation

Some have questioned whether the assumption of a constant specific heat at altitude is sufficient. To answer this question, the differences between constant dry air specific heat as well as mass-averaged and pressure-averaged moist air specific heats were examined. All three approaches yield the same contrail line water partial pressure points within +/- .02 for most conditions. Differences are as follows:

- a. Constant dry air specific heat yields the easiest equation.
- b. Pressure-averaged moist air specific heat yields a better approximation, but the pressure averaging is not strictly correct.
- c. Mass-averaged moist air specific heat yields the best approximation, but the equation contains many terms, and therefore would take a much longer time to calculate for each flight.

Although there are slight differences as seen in Figure A.6, these differences are not considered significant. Since calculation time is abundant, this study uses the mass-averaged moist air specific heat.

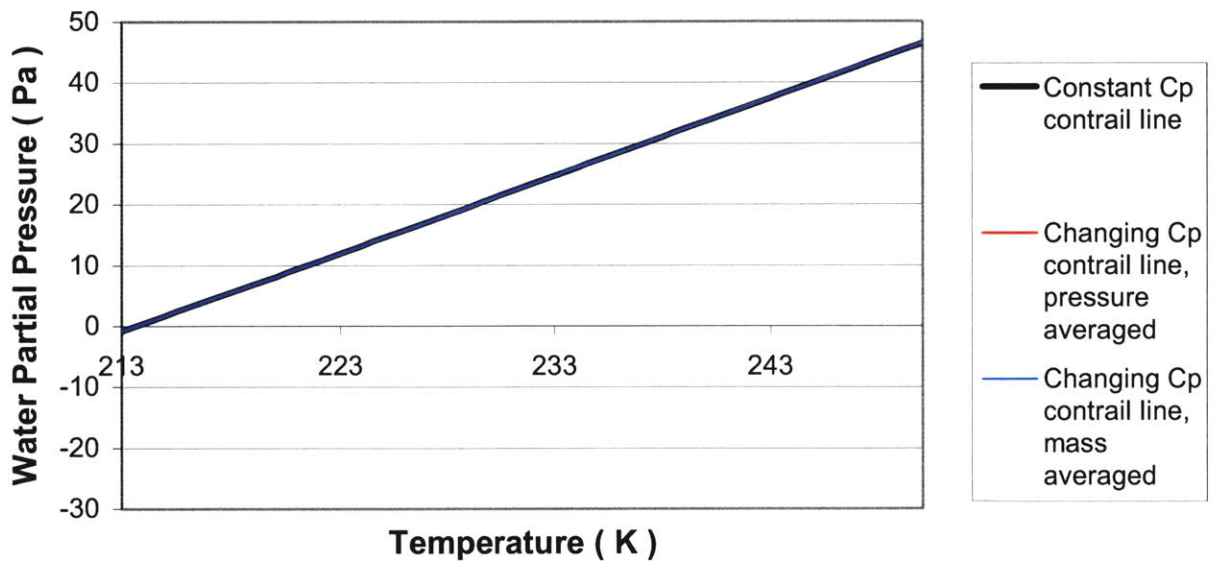


Figure A.6 - Contrail Factor Line, With and Without Changing Specific Heat

A.2.4. Modeling of Emission Plume: Do Engines Affect Each Other?

For one engine to affect another (i.e. cause a contrail when none would have formed before), the plumes must intersect, and the extra water vapor must be enough to produce a contrail where none would have before. Figure A.7 depicts the exhaust evolution (red) on a standard mid-range airplane³⁵ assuming a constant turbulent diffusivity. The blue line is where contrails form (0.36 seconds) and the green line is maximum saturation point of the exhaust and entrained air³⁶. As shown, the plumes do not intersect soon enough for one plume to affect the other.

It should be noted the water and other emissions will be entrained into the wingtip vortices. Hence aircraft with four engines will have only two contrails. However this entrainment into the wingtip vortices is shown to occur beyond the green maximum saturation line.

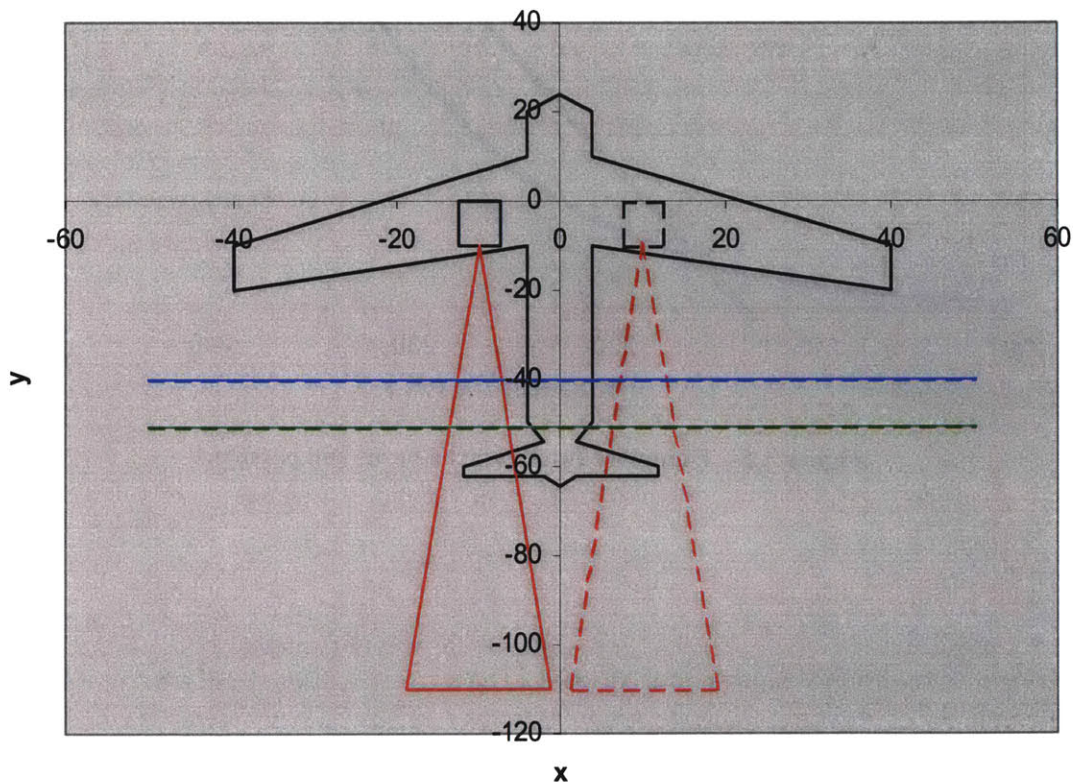


Figure A.7 - Turbulent Plume Growth on Standard Airplane. The blue line is where contrails form (0.36 seconds) and the green line is maximum saturation point of the exhaust and entrained air.

³⁵ Aircraft is not real, just modeled for illustrative purposes. It is modeled simply as 80m long with 124m span, and engines are modeled as 5m x 10m boxes. Engines are 20m apart

³⁶ Estimated using published experimental data [11].

A.3. EXAMPLE OUTPUT

Combining all these assumptions and equations results in Figure A.8. The light blue line indicates the Sonntag ice saturation pressure curve, and the dark blue line indicates the Sonntag water saturation pressure curve. The red diamond indicates the ambient conditions, and the black line is the contrail factor line. In this example, the contrail would form and persist.

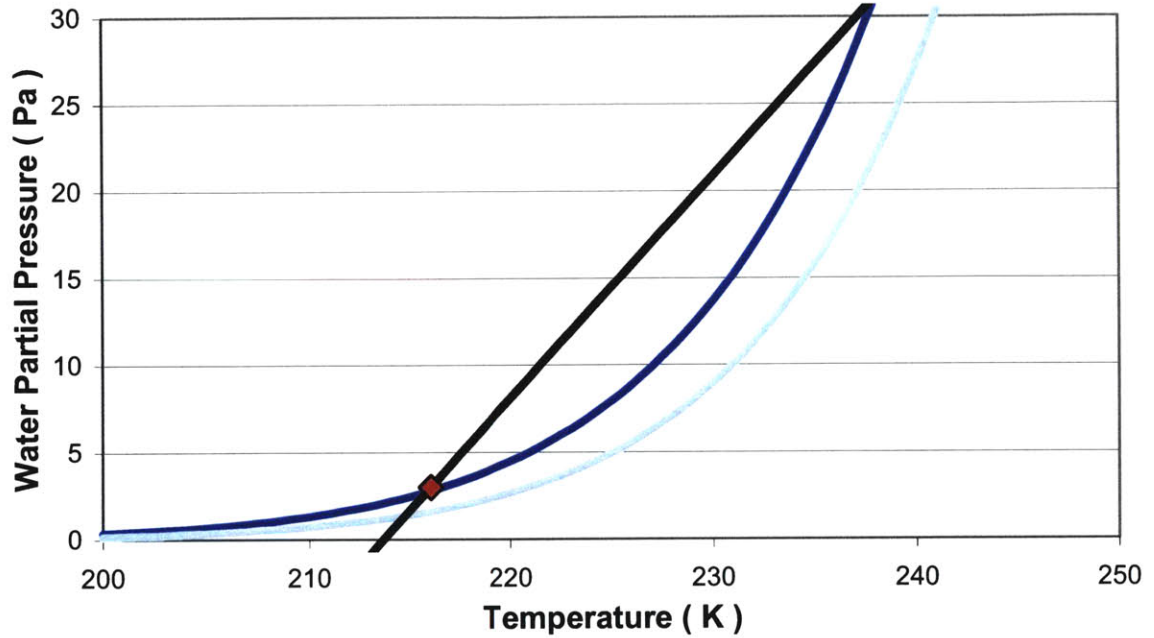


Figure A.8 – Example output, contrail forms and persists.

A.4. CONTRAILS IN CLOUDS

Much research has been developed concerning the radiative effect of contrails. Often the meteorological models severely depress the humidity in a region with clouds, so that a contrail may not form there. However, Minnis noted that since young contrails have smaller particle sizes (10 μm as opposed to 12 μm), they have different optical properties than that of normal clouds. Thus it was considered important to track these contrails, but note that they form in clouds. While nothing can be done if the humidity has been artificially depressed, this study has differentiated between contrails forming in clouds and in clear skies by relating cloud coverage to the relative humidity.

Dr. Stan Benjamin of the NOAA Forecast Systems Laboratory (National Oceanic and Atmospheric Administration, NOAA) pointed out that the relationship between cloud coverage and relative humidity is highly uncertain. So relating cloud formation to a single relative humidity would be improper. Table A.4 gives an empirical relation between relative humidity in the Rapid Update Cycle data (see Section 2.3.1) and cloud formation. According to Duda, the necessary mean Rapid Update Cycle relative humidity for overcast skies is 70%. The Unified Forecast data (see Section 2.3.2) did not depress relative humidity to the same extent as the Rapid Update Cycle data, so an unnamed source reported a higher relation (75% or 80%).

Despite the large gradients of RH_i in clouds, program constraints allowed for a single rule for differentiating clear and cloudy skies. Hence a necessary relative humidity of 75% was chosen for cloudy skies. This underestimated the amount of cloudy skies in the Rapid Update Cycle data, and overestimated the amount of cloudy skies in the Unified Forecast data. With this 75% relationship in place, both the total percent of the flight with contrails and the total percent of the flight with contrails in clouds could be reported. Future research should be directed to creating a better relationship between cloud coverage and relative humidity.

Table A.4 - Mean RUC relative humidity as a function of cloud cover, courtesy of Dr. David Duda (NASA Langley, VA).

	Percent Coverage	Mean RUC relative humidity, 150mb – 400mb
No Cloud	0	39
Clear	1-9	49
Isolated	10-24	56
Scattered	25-49	58
Broken	50-89	63
Overcast	90-100	70

APPENDIX B: CHANGES FROM SAGE V1.1 to V1.5

The following list of additional changes was implemented during the 4th quarter of 2004 and the 1st quarter of 2005 in upgrading SAGE from Version 1.1 to 1.5. Due to computational time constraints, the aviation system model was updated using SAGE Version 1.1, but the results were computed using Version 1.5. Overall, the end result of the V1.5 changes caused a systematic underestimation of fuel burn, but a greatly decreased standard deviation (based on data from major airline company). Note that this list is not comprehensive; only additional changes affecting the contrail estimations were included.

- Changes which increase contrail estimation
Scaling factors have been developed to fill drag coefficient data when it is not available in BADA, instead of using drag polars from cruise. This increases the thrust and fuel flow calculations for takeoff.
- Changes which decrease contrail estimations
Temperature units correction in INM thrust equation. This reduces thrust, and in turn reduces fuel burn, anywhere from 1-10% reduction.

Speed of sound correction to be based on at-altitude conditions rather than sea-level conditions. This was a primary reason for overproducing fuel burn in V1.1, anywhere from 1-20%.
- Impact unknown
The latest BADA (version 3.6) has been implemented. When BADA 3.5 was implemented, specific aircraft either increased or decreased in fuel burn by several percent; BADA 3.6 should cause similar changes³⁷.

³⁷ As BADA creates acronyms for each aircraft type, this footnote will refer to these acronyms only.

The following models were added: DH8A, MD82, B462, B764, B773.

The following models were updated: A30B, A310, A319, A320, A321, A333, A343, B732, B733, B742, B744, B752, AT45, B772.

The synonym file was updated to include additional aircraft types: A3ST, ASTR, B701, C441, GALX, J728, K35A, K35E, L29B, LJ25, LJ60, NIM, PC12, R135, RJ1H, RJ70, P32R, C208, AA5, S76, DC3, BLAS, AEST, EC35, PAY1, PA18, BE55, C170, B461

APPENDIX C: AERODYNAMIC MODEL

C.1. IDENTIFICATION OF THE PROBLEM

Early in the study, a preliminary test of various flight patterns was conducted. These included flying the aircraft at constant altitude and Mach number, at the altitude or Mach number corresponding to the maximum lift coefficient, and in a step climb procedure. Upon running these tests, the aircraft optimized at supersonic Mach numbers. Given that none of the commercial aircraft tested were supersonic aircraft, this was troublesome. To reroute the aircraft to mitigate contrails, the aerodynamic model needed to work well for cruise and off-cruise conditions.

Note that the inclusion of compressibility effects was limited to jet aircraft. Neither turboprops nor pistons cruise near the sonic barrier, so inclusion of compressibility is not necessary.

C.2. DEFINITION OF TRANSONIC DRAG RISE (COMPRESSIBILITY EFFECTS)

Professors Mark Drela, Karen Willcox, and Robert Liebeck (MIT) and Professor Ilan Kroo (Stanford) offered their expertise in solving this problem. Examining the aerodynamic model of SAGE revealed that the calculation of the drag coefficient was correct to second order, but lacked the higher order terms associated with transonic drag rise (an M^4 term). In other words, the drag coefficient equation lacked compressibility effects, so during optimization, unrealistic thrusts and velocities could be reached.

Figure C.1 and Figure C.2 show the difference with and without the compressibility effects. In Figure C.1, SAGE drag coefficients are plotted versus Mach number. Note that the drag continues to decrease through the sonic barrier until supersonic speeds. This does not happen; if it did, all of today's commercial aircraft would fly supersonically to conserve fuel. Figure C.2 shows the theoretical drag coefficient versus Mach number. In this figure, the drag rise associated with the sonic barrier is evident.

Two important parameters for the compressibility effects are M_{crit} and M_{DD} , labeled on Figure C.2. M_{crit} , also M_{CC} , is the crest critical Mach number, the freestream Mach number at which the local Mach number on the crest of the airfoil becomes supersonic. It can be calculated from M_{DIV} , as given by Equation B.1.

$$M_{div} = M_{CC} + 0.004 - M_{div} \tag{B.1}$$

M_{DIV} , also M_{DD} , is the divergence Mach number. It is the Mach number, slightly above M_{CC} , at which the drag of conventional airfoils begins to rise abruptly; the Mach number at which one of the two following conditions hold:

$$\text{Condition 1: } dC_D/dM = 0.1 \tag{B.2}$$

$$\text{Condition 2: } C_D = 0.002 \tag{B.3}$$

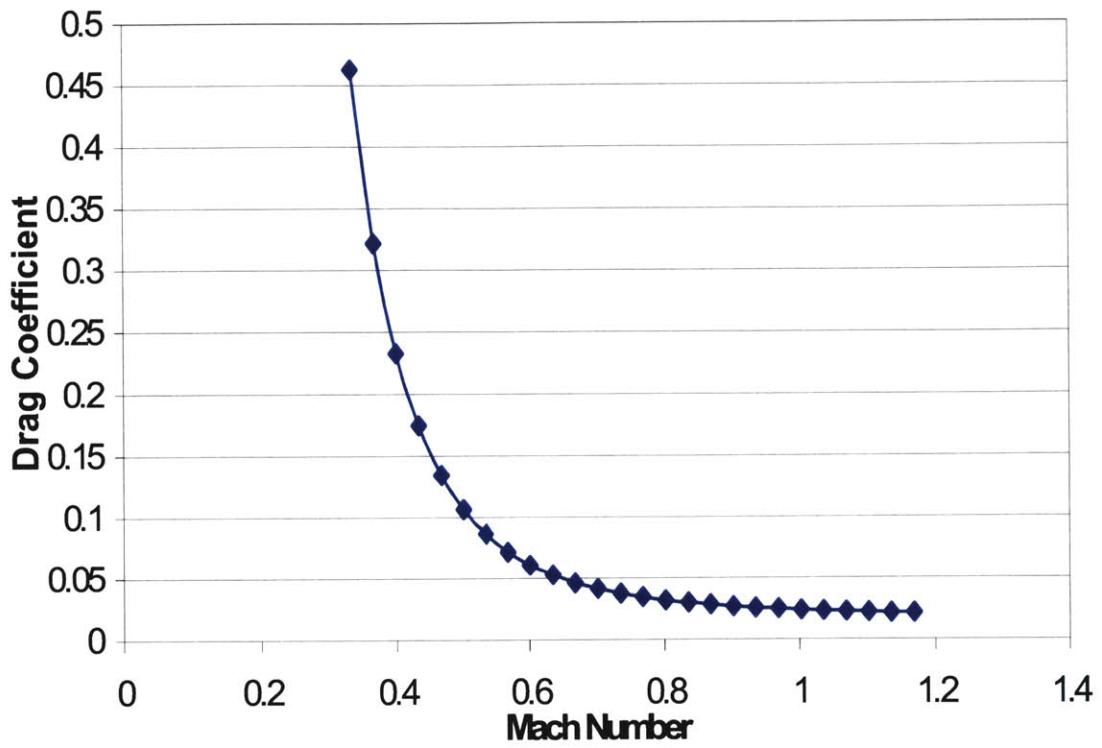


Figure C.1 - Drag coefficient of example SAGE aircraft

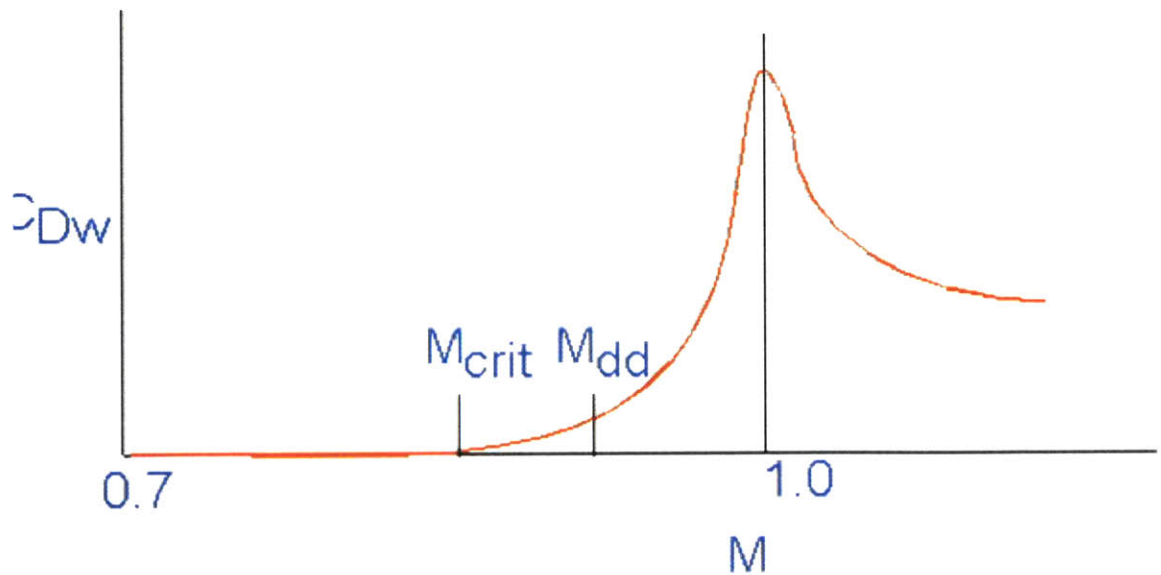


Figure C.2 - Theoretical drag rise, including compressibility drag (M⁴ term)

The drag rise associated with these compressibility effects is termed C_{Dc} , and is applied theoretically as in Equation B.4, and in SAGE as in Equation B.5.

$$C_D = C_{D0} + C_L^2 / (\pi * AR * e) + \Delta C_{Dc} \quad (B.4)$$

$$C_D = C_{D0_CR} + C_L^2 * C_{D2_CR} + \Delta C_{Dc} \quad (B.5)$$

where C_{D0} = form drag
 C_L = lift coefficient
 AR = Aspect Ratio
 e = Oswald planform efficiency factor
 ΔC_{Dc} = compressibility drag
 C_{D0_CR} = parasitic drag coefficient in BADA (cruise)
 C_{D2_CR} = induced drag coefficient in BADA (cruise)

Unfortunately for SAGE, the theoretical derivations of M_{div} and M_{CC} are too complicated to apply to 360+ aircraft types. Additionally, the relationship between C_{Dc} , M_{div} , and M_{CC} is unclear. Hence an empirical fit was needed.

C.3. KROO METHOD

Professor Ilan Kroo (Stanford) has created an empirical calculation of C_{Dc} , henceforth the Kroo Method. His method uses quarter-chord wing sweep, mean thickness to chord ratio, and the supercritical factor. With these factors, M_{CC} and C_{Dc} could be calculated as in Eqs B.6-B.12.

$$\text{cossw} = \cos(\text{qcsweep} * \pi / 180) \quad (B.6)$$

$$\text{clp} = C_L / \text{cossw}^2 \quad (B.7)$$

$$\text{tcp} = t_c / \text{cossw} \quad (B.8)$$

$$M_{CC} = ((.954 - .235 * \text{clp} + .0259 * \text{clp}^2) - (1.963 - 1.078 * \text{clp} + .350 * \text{clp}^2) * \text{tcp} + (2.969 - 2.738 * \text{clp} + 1.469 * \text{clp}^2) * \text{tcp}^2 + (\text{sup}) * .06) / \text{cossw} \quad (B.9)$$

$$X = M / M_{CC} \quad (B.10)$$

$$Y = X - 1 \quad (B.11)$$

Relation	C_{Dc}	(B.12)
$X \geq 1.0$	$0.001000 + 0.02727 * Y - 0.1952 * Y^2 + 19.09 * Y^3$	
$1.0 > X \geq 0.95$	$0.001000 + 0.02727 * Y + 0.4920 * Y^2 + 3.573 * Y^3$	
$0.95 > X \geq 0.8$	$0.0007093 + 0.006733 * Y + 0.01956 * Y^2 + 0.01185 * Y^3$	
$0.8 > X \geq 0.5$	$0.00013889 + 0.00055556 * Y + 0.00055556 * Y^2$	
$0.5 > X$	0	

where qcsweep = quarter-chord wing sweep
 t_c = mean thickness to chord ratio
 sup = supercritical factor
 M = Mach number
 cossw , clp , tcp , X , Y = temporary variables

C.4. ADAPTATION OF KROO METHOD TO SAGE

Initially, the Kroo Method seemed unusable because SAGE did not have values for the quarter-chord wing sweep, thickness to chord ratio, or supercritical factor. However, this difficulty could be eliminated for some aircraft types. A major airline supplied quarter-chord wing sweep and supercritical values for 47 aircraft types, but thickness-to-chord ratio values were closely held proprietary values. Some thickness to chord ratios could be garnered from Shevell [32], but it was clear that the Kroo Method could not be applied to all 360+ aircraft in SAGE.

After testing several scenarios, it was concluded that the cruise Mach number given in BADA is very close to M_{cc} . Using this approximation, the Kroo method could be directly applied in the SAGE model³⁸.

C.5. WEATHER EFFECTS

A large concern was how well the addition of the compressibility correction would work in the absence of meteorological data. Specifically, some questioned whether the wind and/or speed of sound would affect the Mach number. As seen in Table C.1 and Table C.2, differences in wind account for a large difference (and standard deviation) in Mach number, whereas differences in speed of sound account for a smaller difference in Mach number. To account for weather effects, an upper cap was employed on the range of Mach numbers that compute C_{Dc} with compressibility effects.

In order to avoid problems with the meteorological data, several scenarios of M_{CC} and caps were examined. A good cap appeared to be the upper bound of 99% confidence interval of British Airway data, or 104.6% of the BADA Mach cruise number. Before this addition of compressibility effects with this cap, SAGE had a percent difference from reported fuel burn of -5.78 +/- 71.29%. With the addition of this cap, SAGE now had an estimated fuel burn of -1.60 +/- 74.10% percent difference from reported fuel burn.

Recall that when adding a change to the SAGE model, it is preferred for the standard deviation of differences with reported fuel burn to decrease as opposed to the average percent difference from actual. This does not occur with the addition of compressibility effects. However, compressibility effects are known to be relevant, hence not including them would reduce the reliability of the SAGE model. Hence despite the slightly higher 95% confidence interval, they were included.

Consequently, the compressibility effects applied to SAGE consisted of the Kroo method with M_{cc} equal to the BADA cruise Mach number, plus the 104.6% cap on range of Mach numbers. Later examinations coupled weather data and the transonic drag rise. They showed large improvements in average percent difference and standard deviation, as shown in Table C.3.

³⁸ Note that for different aircraft, the compressibility effect is different. Newer aircraft are designed such that the Drag vs. Mach curve increases sharply near the end, like a hockey stick. Hence the cruise Mach number is a good approximation for M_{cc} . Older aircraft have a more gentle rise, hence the cruise Mach and M_{cc} could be far apart.

Table C.1 - Change in Mach number due to winds, British Airway 747-400 CFDR data (993 flights)

	Average +/- 95% Conf.	Minimum	Maximum
Average Mach (true speed), Mcr in BADA is 0.85	0.84 +/- 0.05	0.62	0.89
Average Mach (ground speed), contains winds	0.85 +/- 0.15	0.53	1.14
Difference	-0.01 +/- 0.15	-0.30	0.25

Table C.2 - Change in Mach number due to speed of sound, British Airway 747-400 CFDR data (993 flights)

	Average +/- 95% Conf.	Minimum	Maximum
Real Temperature - ISA Temperature (K)	3.8 +/- 11.4	-14.6	22.3
Real Speed of Sound - ISA Speed of Sound (m/s)	1.9 +/- 6.6	-9.9	14.7
Real Mach number - ISA Mach number	- 0.01 +/- 0.02	-0.03	0.04

Table C.3 - 1306 American Airlines flights with a combination of compressibility effects and weather

	Percent Difference from Actual +/- 95% confidence Interval
Old SAGE (BADA 3.5)	-7.87 +/- 26.95%
Old SAGE w/ compressibility	-3.36 +/- 33.13%
Old SAGE w/ weather	0.75 +/- 32.51%
Old SAGE w/ compressibility, weather	2.70 +/- 24.67%

C.6. TYPE OF FLIGHT: ETMS OR OAG

The inclusion of compressibility effects was designed for ETMS flights. It was not applied to OAG because the altitudes, Mach numbers, and trajectories were already set to produce average fuel burns. The inclusion of compressibility effects would systematically increase fuel burn, hence worsen the OAG predictions. Figure C.3 shows the percent difference from actual fuel burn for these scenarios. Note how ETMS flights are shifted closer to the 0% difference line, while OAG flights are shifted away.

If OAG altitudes, Mach numbers, and trajectories were redistributed to include compressibility effects, then presumably the compressibility effects would be beneficial.

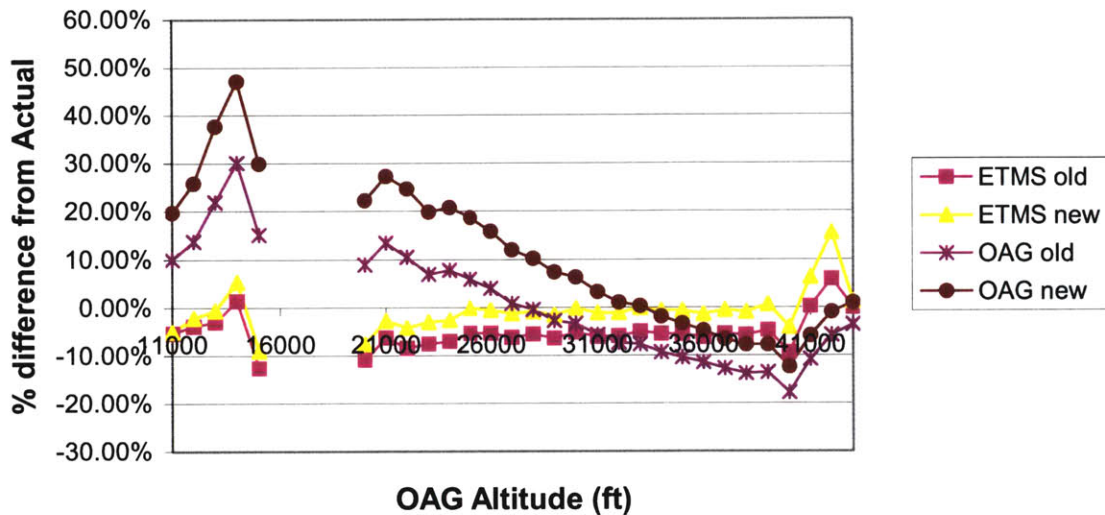


Figure C.3 – Percent difference from actual fuel burn at varying altitudes. “Old” values are pre-compressibility effects, “new” values are post compressibility effects. Note how both OAG and ETMS are systematically increased. Since the original OAG was set for an aggregate percent error of zero, this means that the OAG estimation would worsen.

C.7. FINAL IMPLEMENTATION

The method implemented in SAGE was (Scenario B):

- Inclusion of compressibility effects, taken from Kroo Method
- M_{CC} assumed to be BADA cruise Mach number
- Cap on the range of Mach numbers at $1.046 * \text{BADA cruise Mach number}$

After the compressibility effects were added, the drag curves for the A30B, DC10, and B737-300 were examined to ensure the results reflected theoretical values. They did.

APPENDIX D: ENGINE EQUATION

The engine model in SAGE consisted of one equation, the specific fuel consumption (SFC) equation. This varied depending on aircraft type (jet, turboprop, or piston), altitude (possible multiplication of a cruise coefficient), and whether the engine is idling. The veracity of the specific fuel consumption equation was individually examined for each aircraft type, but research time was weighted by percent fuel burn.

Jets make up over 97% of the annual fuel burn, and over 85% of the flights³⁹, so their equation was most important. Hence this section deals mainly with jets; however a short discussion on turboprops and pistons will follow.

D.1. JETS

In SAGE, jet fuel flow in kg/sec is given as:

Below 7620 m:

$$\text{Fuel Flow} = C_{f1} / 60000 * (1 + 1.9438*V / C_{f2}) * \text{Thrust} \quad (\text{C.1})$$

Above 7620 m :

$$\text{Fuel Flow} = C_{f1} / 60000 * (1 + 1.9438*V / C_{f2}) * C_{fc} * \text{Thrust} \quad (\text{C.2})$$

This equation can be broken up into specific fuel consumption (SFC) and thrust:

$$\text{Fuel flow} = \text{SFC} * \text{Thrust} \quad (\text{C.3})$$

Below 7620 m:

$$\text{SFC} = C_{f1} / 60000 * (1 + 1.9438*V / C_{f2}) * \text{Thrust} \quad (\text{C.4})$$

Above 7620 m :

$$\text{SFC} = C_{f1} / 60000 * (1 + 1.9438*V / C_{f2}) * C_{fc} * \text{Thrust} \quad (\text{C.5})$$

One disturbing trend occurs due to the C_{fc} coefficient; the specific fuel consumption has a step increase or decrease through an altitude of 7620 meters. A second disturbing trend of the model was identified through examining different aircraft equipping the same engine; the same engine will perform very differently on two different aircraft.

However, these concerns could easily be due to incorrect BADA coefficients, as opposed to an incorrect equation. Hence to verify the reliability of the SAGE SFC model, several data sources and alternative models were obtained. It was assumed that the SAGE aerodynamic model (with compressibility effects) was correct, and all calculations were conducted assuming steady level flight (thrust equals drag). Furthermore, it was assumed that the engine model

³⁹ SAGE 2003 data: Pistons negligible. Turboprops account for 2.3% of fuel burn, and 23.7-23.9% of flights. Jets account for remaining.

was independent of the aerodynamic model, hence SFC was a function of altitude and Mach number only. Lastly, engines were assumed to function at same non-dimensional operating point, hence performance could be scaled with standard non-dimensional parameters. (Note that the final two assumptions were later shown to be incorrect.)

First the current SAGE model was examined against aircraft operating manual data⁴⁰ and a higher fidelity model⁴¹ to identify relative reliability. Figure D.2, Figure D.4, and Figure D.1 represent SFC versus altitude for the three aircraft listed in the aircraft operating manual. The B757-300 figure does not have a GasTurb curve because the engine cycle deck was not completed. Although it was assumed that SFC was independent of net thrust, net thrust was held constant between SAGE and GasTurb.

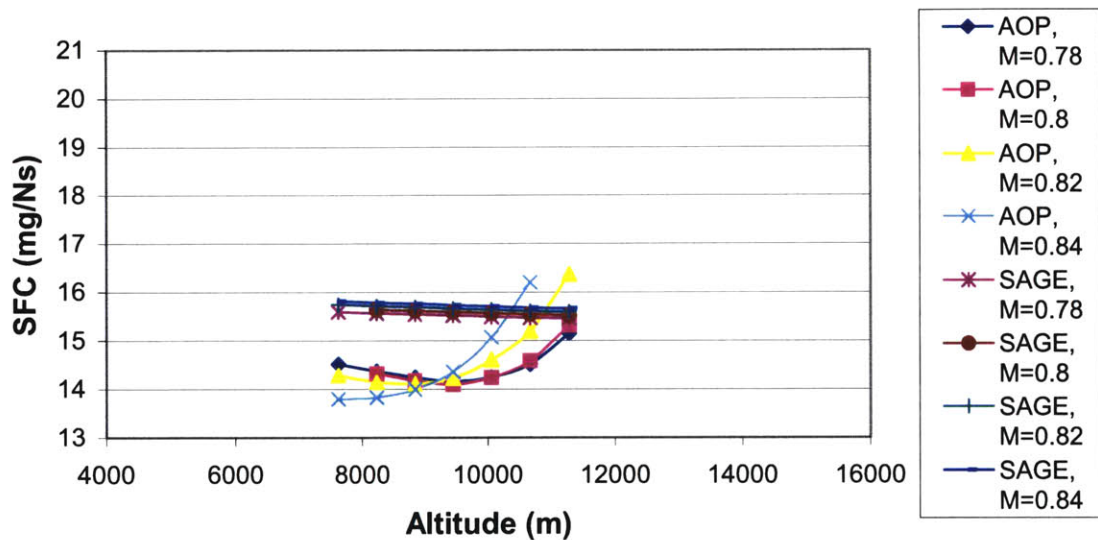


Figure D.1 - SFC versus altitude at varying Mach number, B757-300

⁴⁰ An aircraft operating manual was obtained for the B57-300 (RB211-535E4B), B767-200 (CF6-80A), and B767-300 (CF6-80C2B6). It contained EPR, N1, specific range, and fuel flow per engine as a function of mass, altitude, and Mach number. For most of the study, this data source was considered a gold standard. However, an insight from Prof. Robert Liebeck (MIT) indicated that assumption was incorrect. Often the aircraft operating manual numbers are based on the first engine design. As the engine design changes or the engine matures, the reported numbers do not.

⁴¹ GasTurb version 9 is a standard two-dimensional engine cycle deck which uses thermodynamic equations to calculate SFC. In order to obtain output, the user must first create the appropriate engine deck. This requires identifying the type of engine (two-spool unmixed flow, three-spool mixed flow, etc.), obtaining relevant data for the engine, and modifying input values to create the engine cycle deck. Some care must be taken in modifying the input values; efficiencies must be sensibly chosen to create a physically reliable engine. Seven cycle decks were created by a previous MIT student, (CF6-50C, CFM56-3B, Ge90-90B, JT8D-9, PW2037, JT9D-7, and tayMK620-15). Three cycle decks were created to match the aircraft in the aircraft operating manual (CF6-80C2B6, CF6-80A, RB211-535E4B). One of these, the RB211, was not examined in depth due to lack of data.

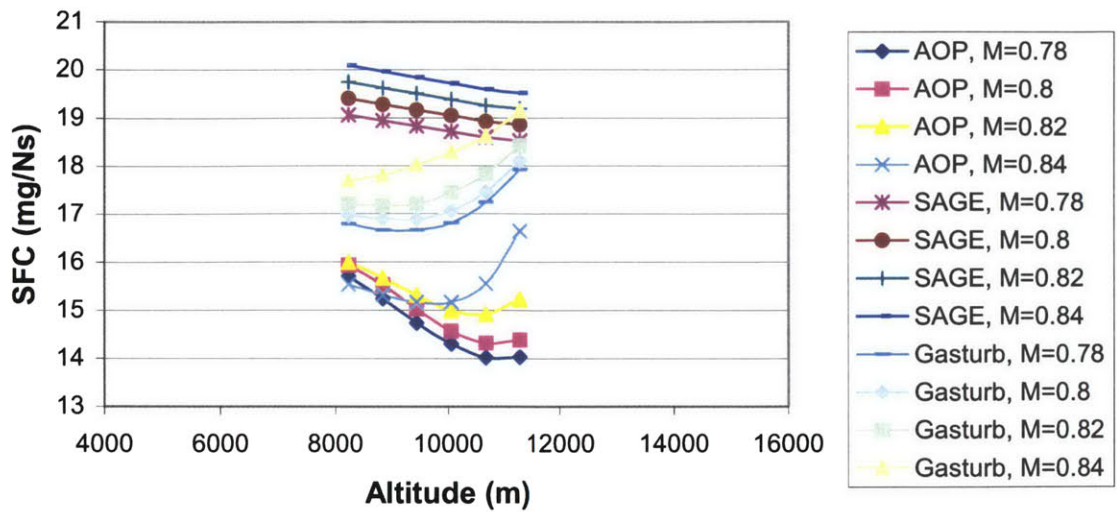


Figure D.2 – SFC versus altitude at varying Mach numbers, B767-200

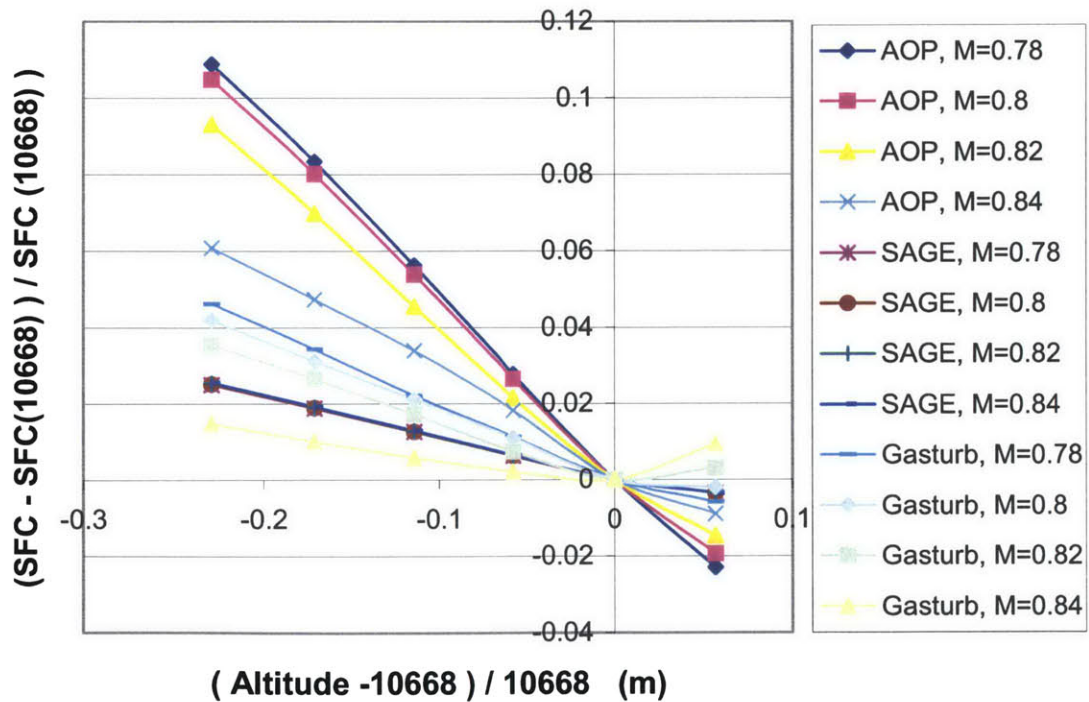


Figure D.3 – Percent change in SFC with respect to altitude, B767-200.

Cruise: altitude = 10668m, Mach=0.78M

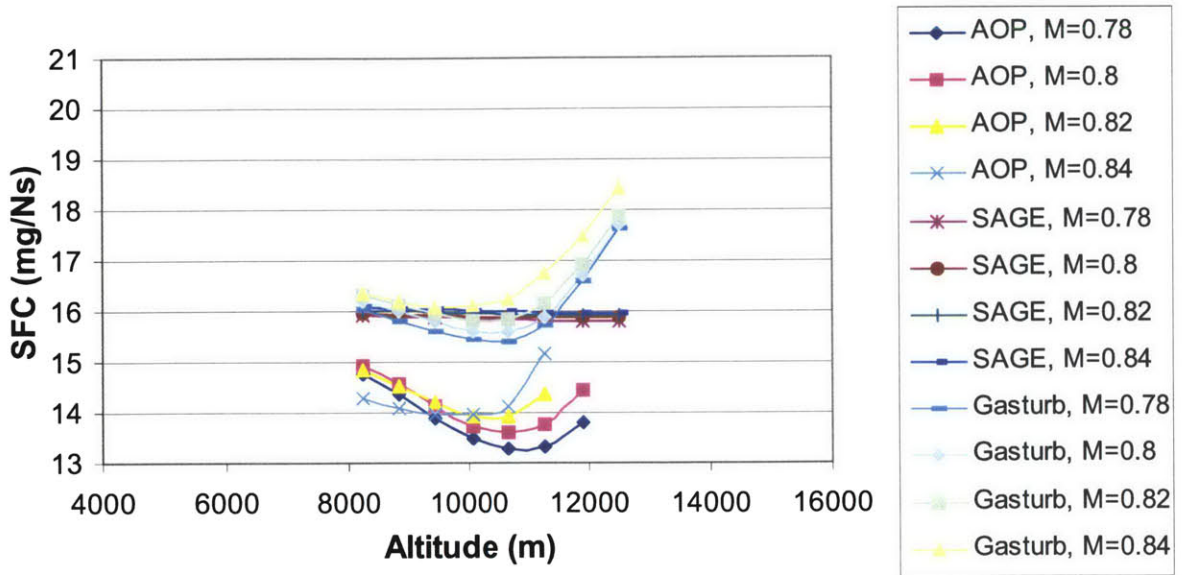


Figure D.4 - SFC versus altitude at varying Mach numbers, B767-300

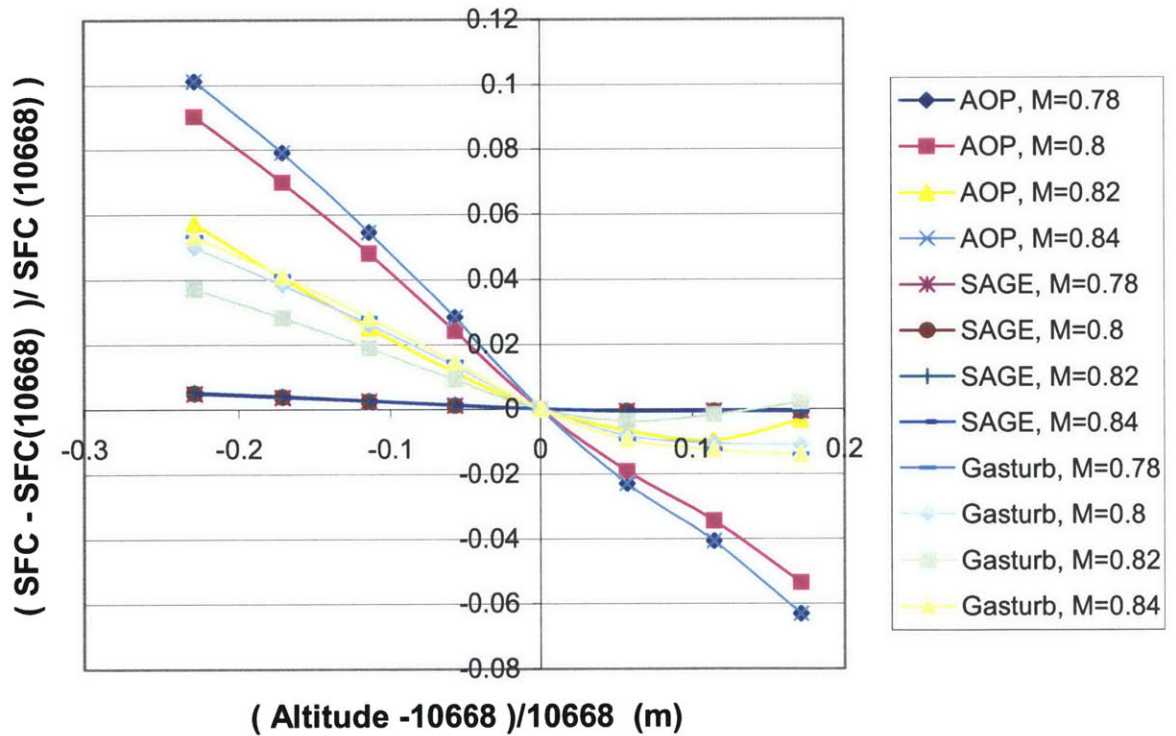


Figure D.5 – Percent change in fuel flow with respect to altitude, B767-300.

Cruise: altitude = 10668m, Mach=0.8M

The relatively straight SAGE curves do not capture the curved trends of the aircraft operating manual. GasTurb does a better job, but overestimates specific fuel consumption in both cases. More specifically, trends with Mach number and altitude were examined. In both the aircraft operating manual and GasTurb, as Mach number increased, SFC increased. SAGE did not capture the magnitude of change in SFC between Mach numbers. With regard to altitude, SAGE failed to capture the slope or magnitude of either the aircraft operating manual data or the engine cycle deck. Furthermore, SAGE did not have the upturn pictured near 11000 m. Additionally, although the relative trend in change in SFC from cruise conditions was captured (see Figure D.3 and Figure D.5), the magnitudes were not.

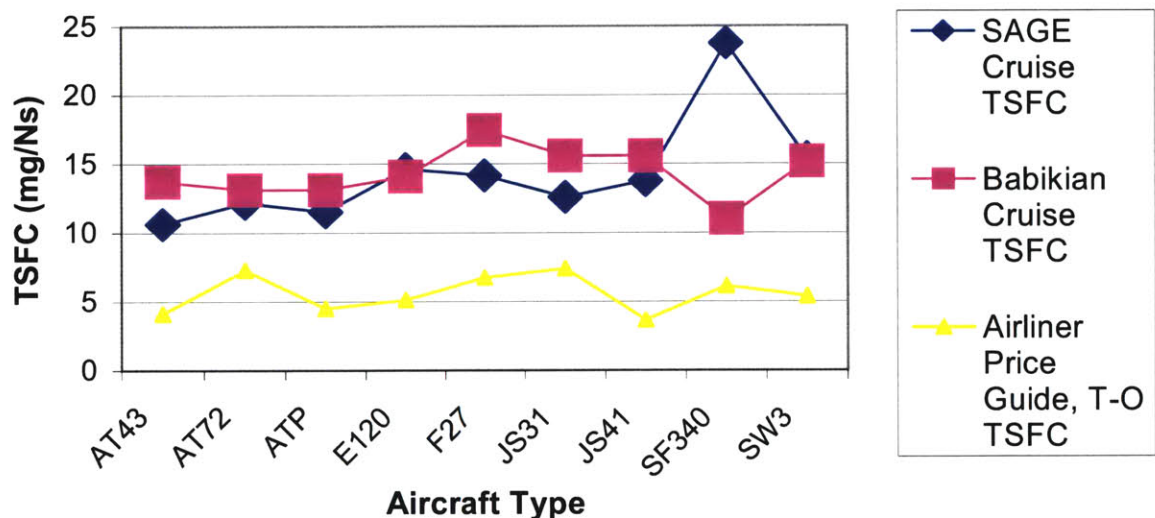
In summary, general SAGE SFC trends did not correlate well with the AOP trends. Further examination showed this was not due to unrealistic high-pressure spool speeds, the efficiency maps, or to incorrect assumptions (specific fuel consumption is a function of altitude and Mach number only, and engines function at the same non-dimensional operating point). Most likely a combination of these factors caused the discrepancy.

To accurately capture the AOP off-cruise performance, the SAGE SFC equation needs correction. However, further gold standard data is lacking.

D.2. TURBOPROPS

Turboprop-engine aircraft make up 2.3% of the fuel burn, so were examined briefly. Using data from a major engine company, an improved model, and published literature [33, 34], the turboprop fuel flow equations were assessed. The thrust estimated by SAGE was consistent with that necessary for steady level flight. However, the thrust specific fuel consumption was not estimated to sufficient accuracy; an idling engine produced zero fuel consumption. Secondly, cruise thrust specific fuel consumption estimates were in error by 3.25 +/- 43.03. Figure D.6 compares TSFC reported in the Babikian paper and in SAGE for nine aircraft types. Note the Airliner Price Guide (yellow) is at take-off instead of cruise; it is added for another comparison. The major engine company data, not shown, is consistent with the Babikian values.

While SAGE incorrectly computes cruise TSFC, it contains the same trends of fuel flow versus thrust as the major engine company data.



AT43 – ATR 42-300

E120 – Brasilia EMB-120

JS41 – BAE Jetstream 41

AT72 – ATR 72

F27- Fokker Friendship

SF340 – Saab-Scania 340

ATP – BAE Advanced Turboprop

JS31 – BAE Jetstream 31

SW3- Fairchild Merlin IVC

Figure D.6 – Thrust specific fuel consumption at cruise and takeoff for various turboprops

D.3. PISTONS

Pistons make up only a small portion of the fuel burn, so were not examined.

APPENDIX E: CALCULATION OF GREAT CIRCLE DISTANCE

Airlines would like to fly aircraft along the shortest distance between the origin and destination to minimize fuel burn. Since the Earth is spherical, we need to examine the shortest distance between two points on the surface of the sphere, the “Great Circle Distance” (Method 1). An extension of the great circle distance occurs when the origin and destination are not at the same radius. In this case, assuming a constant increase in radius, the new path is given by the great circle distance of a sphere with mean radius, centered at a slightly different point (Method 2). The distances between Method 1 and Method 2 are meters for typical flight profiles (see Figure E.1), so we choose the less complex Method 1 for use in SAGE.

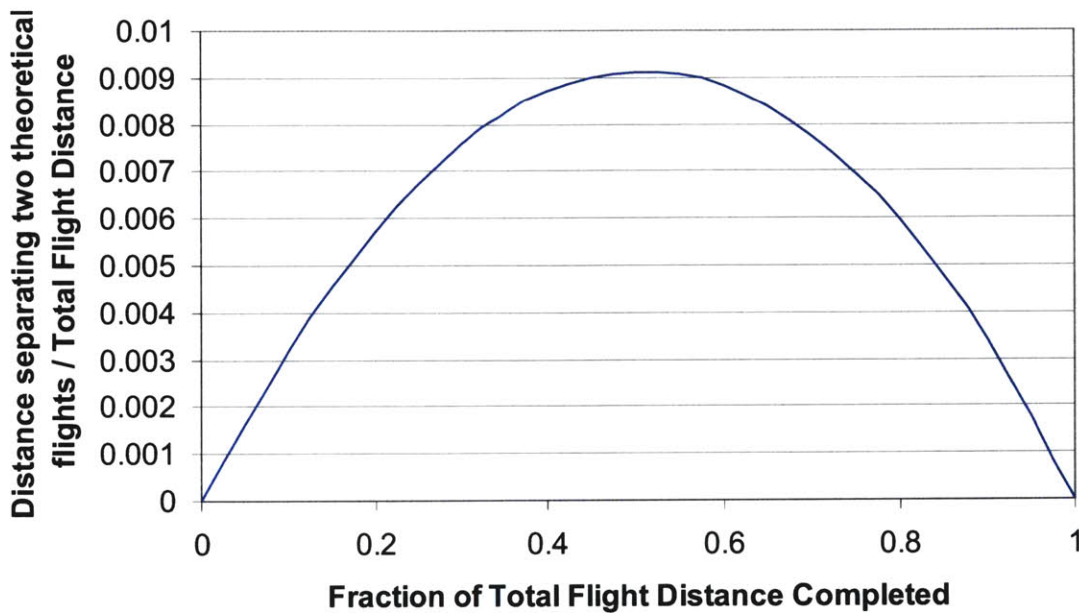


Figure E.1 – Differences in latitude and longitude for three different minimize-distance methods

APPENDIX F: SATELLITE AND CONTRAIL MASK IMAGES

Minnis and Duda of NASA Langley provided satellite IR and contrail mask images for this study. The images are given in this appendix.

Note that all evening images (and hence all images shown) are reversed from east to west. This occurs due to the direction the satellite passes overhead.

Finally, note that 11/13/2001 and 11/14/2001 had satellite images missing regions of data through the middle of the image. Hence these days, though run, were not closely examined.

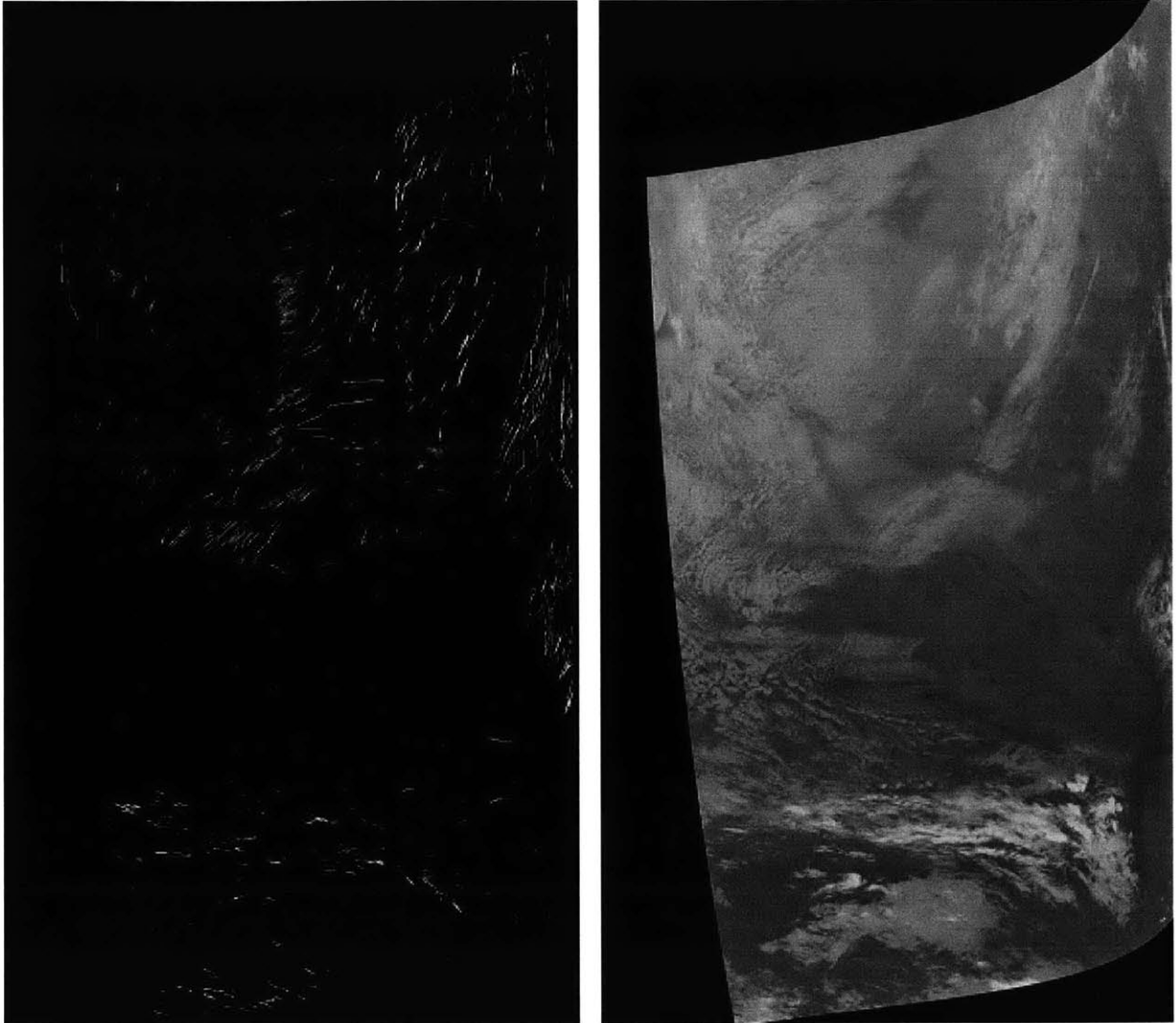


Figure F.1 - NOAA-16 satellite image and matching contrail mask (white pixel indicates contrail formation), November 12, 2001 1827 UTC.

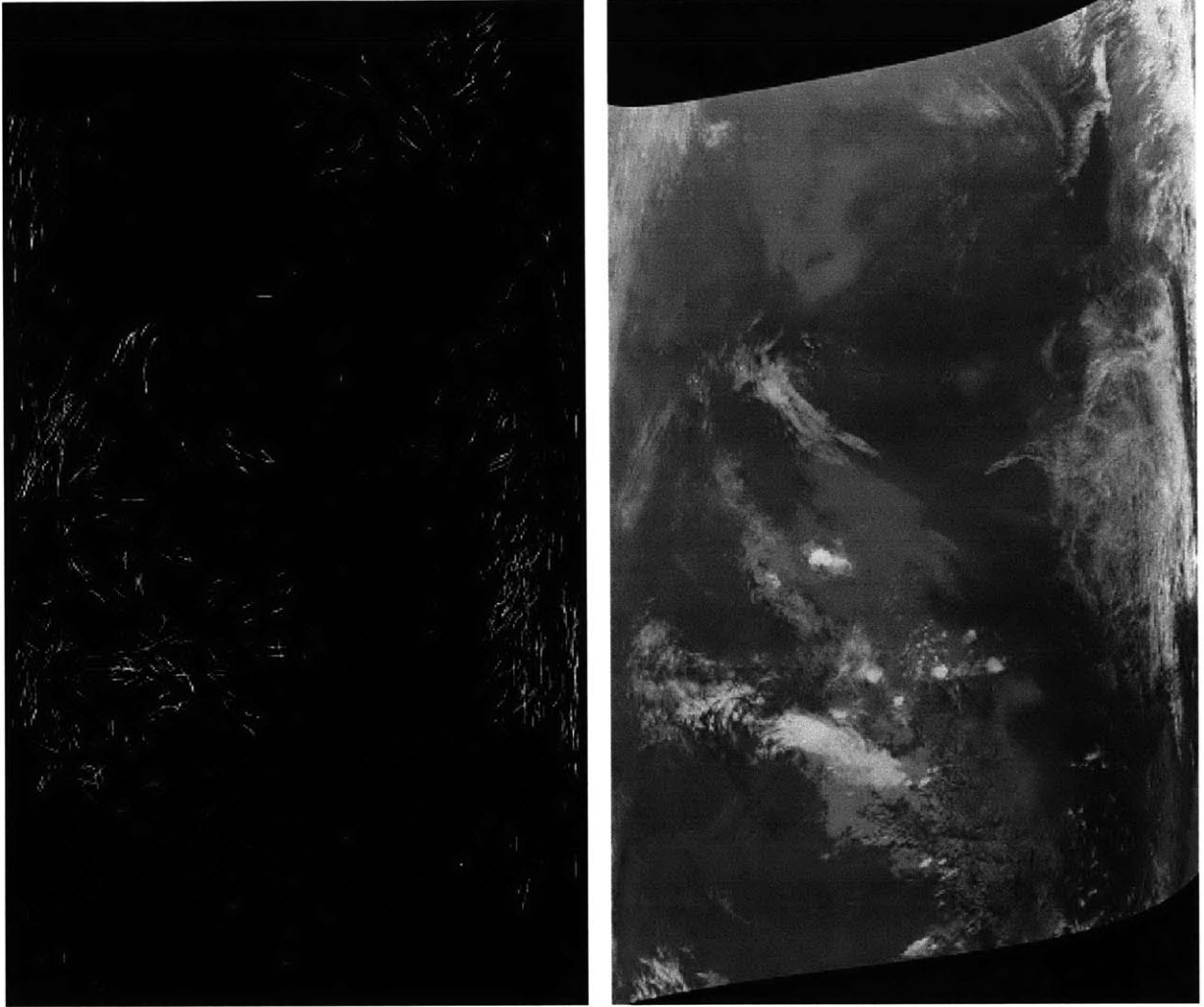


Figure F.2 - NOAA-16 satellite image and matching contrail mask (white pixel indicates contrail formation), November 12, 2001 1996 UTC.

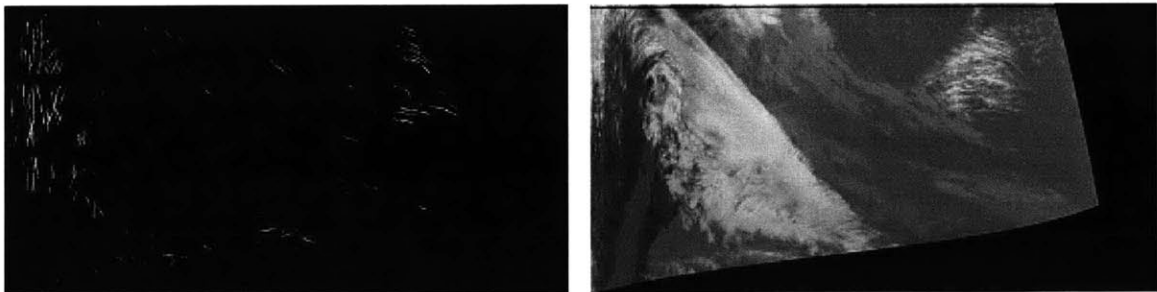


Figure F.3 - NOAA-16 satellite image and matching contrail mask (white pixel indicates contrail formation), November 12, 2001 2167 UTC.

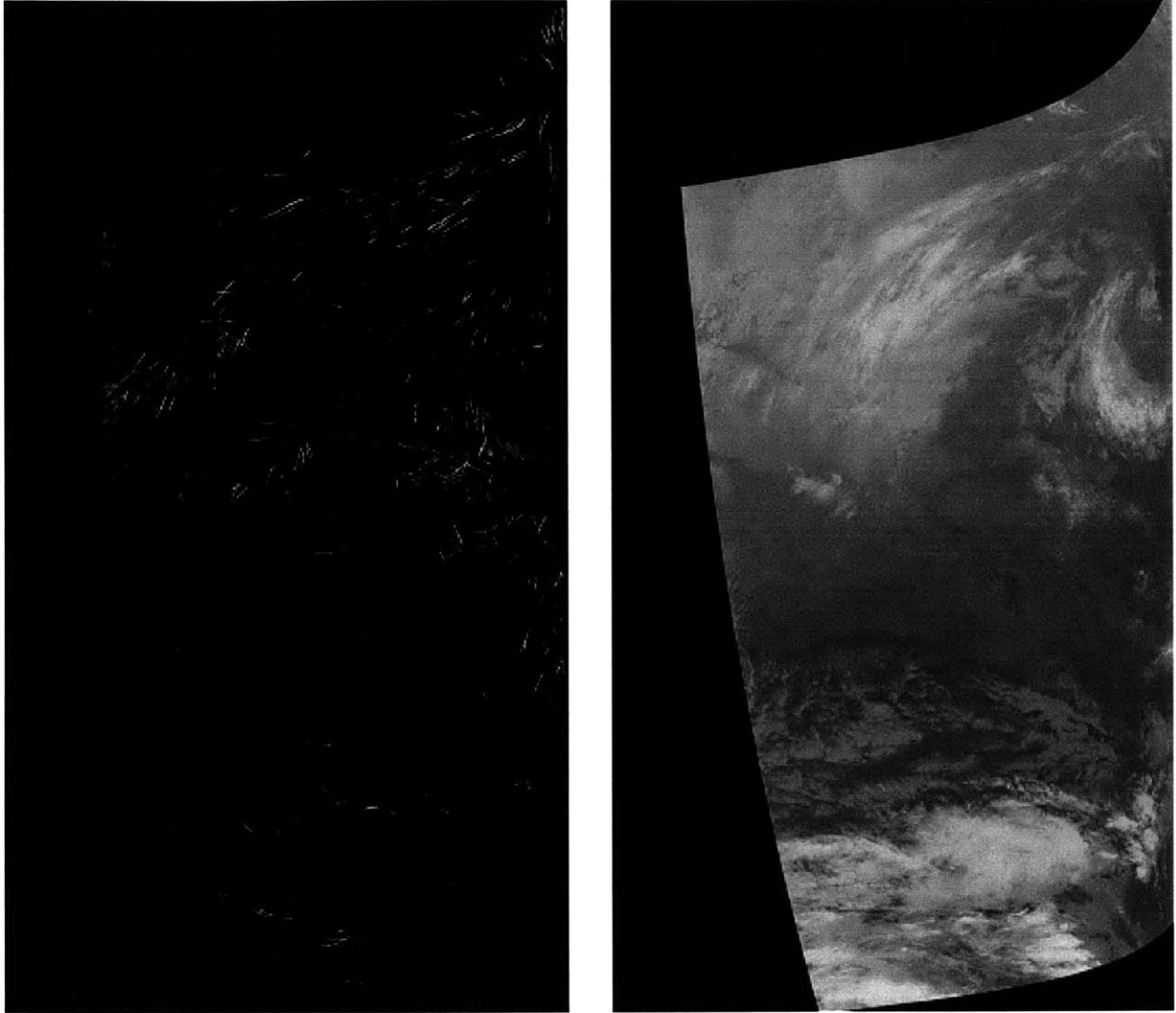


Figure F.4 - NOAA-16 satellite image and matching contrail mask (white pixel indicates contrail formation), November 13, 2001 1809 UTC.

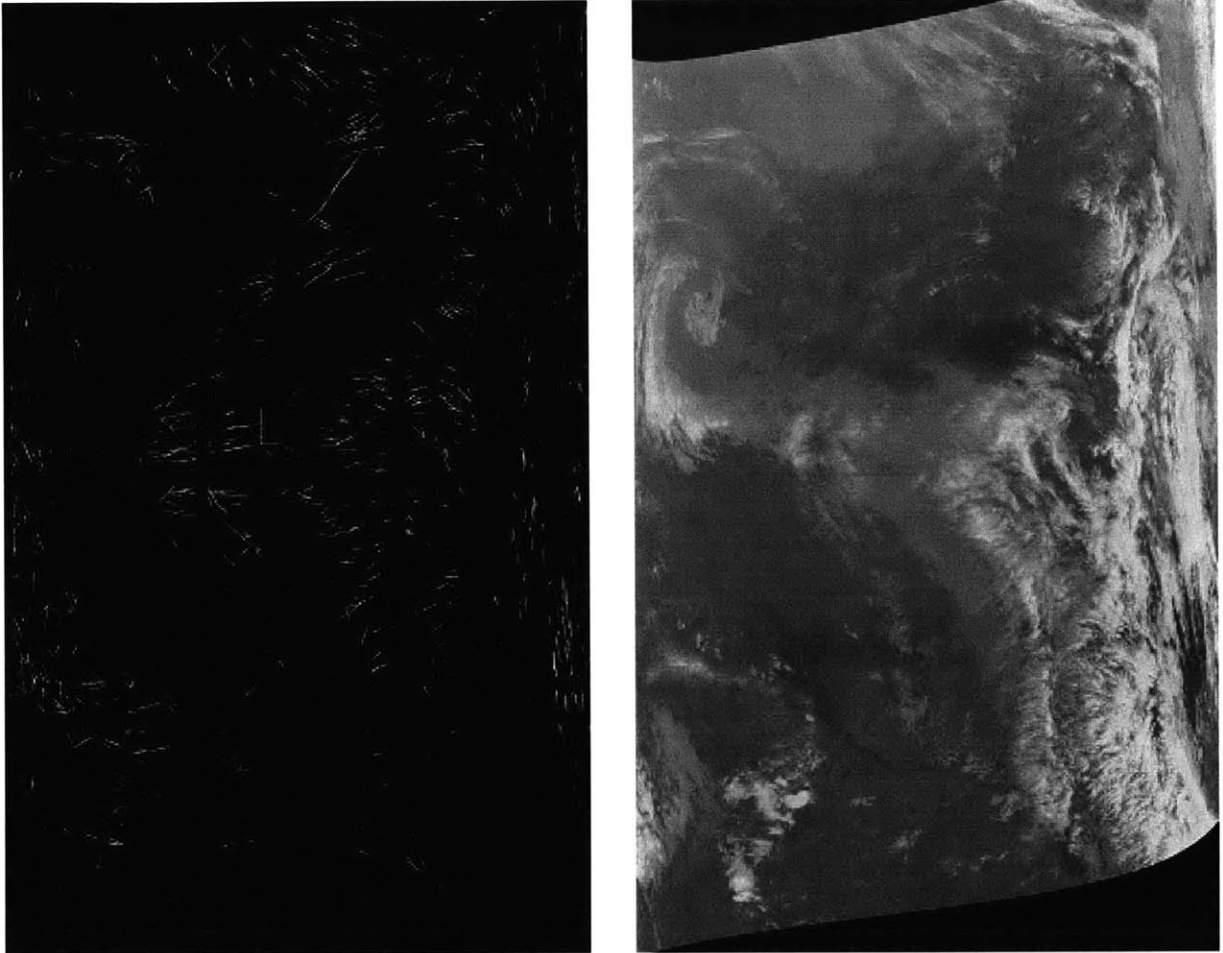


Figure F.5 - NOAA-16 satellite image and matching contrail mask (white pixel indicates contrail formation), November 13, 2001 1978 UTC.

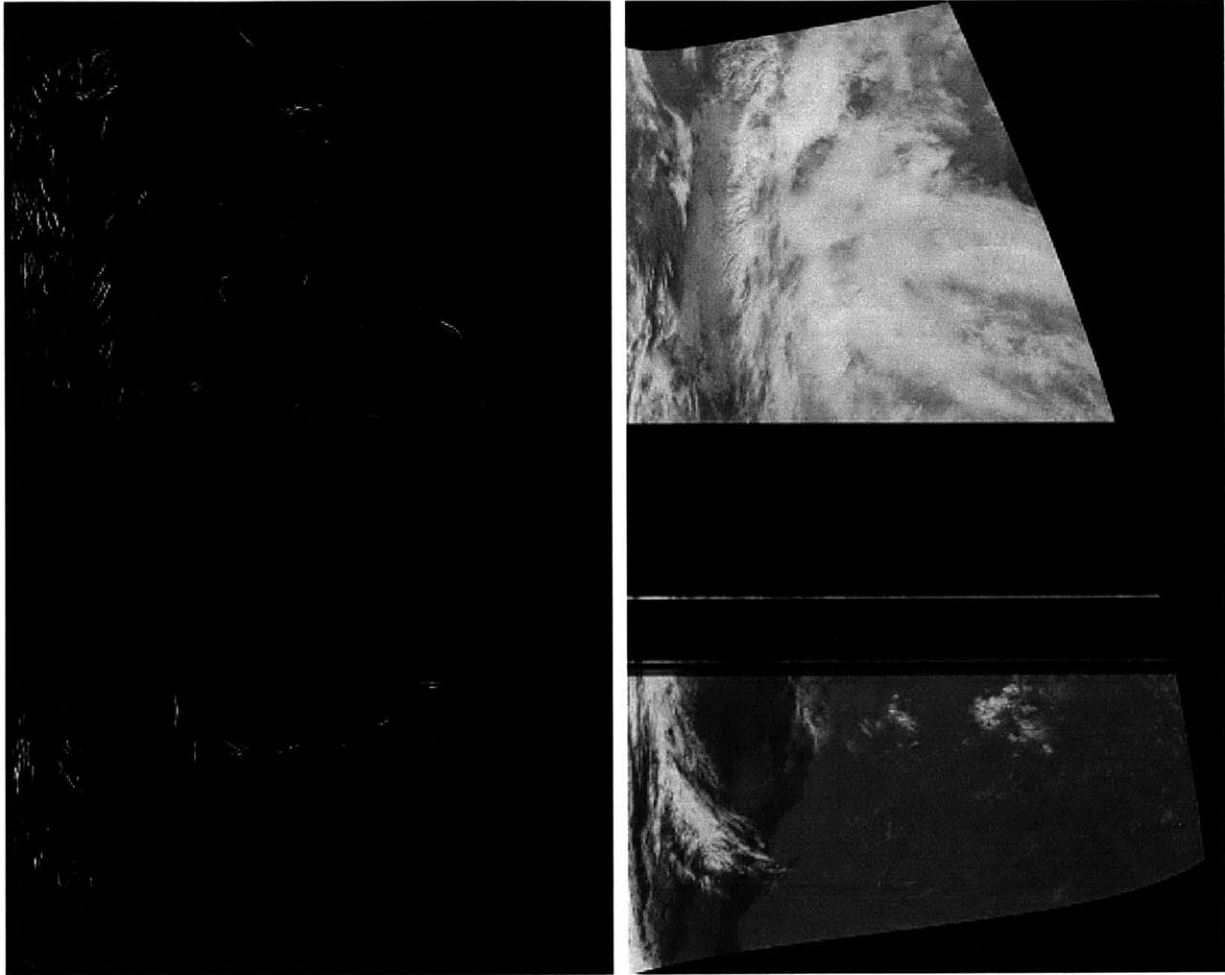


Figure F.6 - NOAA-16 satellite image and matching contrail mask (white pixel indicates contrail formation), November 13, 2001 2148 UTC.

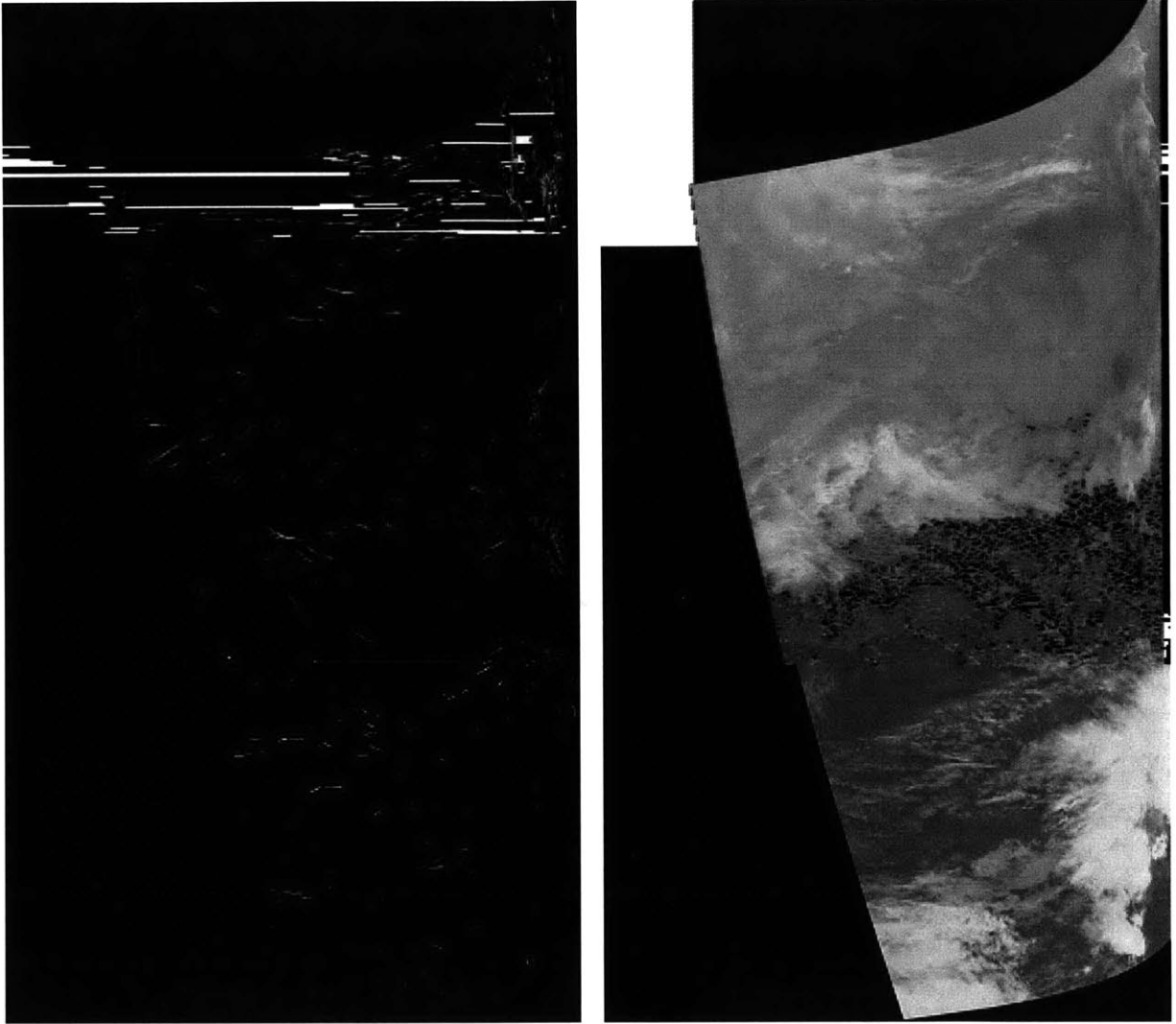


Figure F.7 - NOAA-16 satellite image and matching contrail mask (white pixel indicates contrail formation), November 14, 2001 1791 UTC.

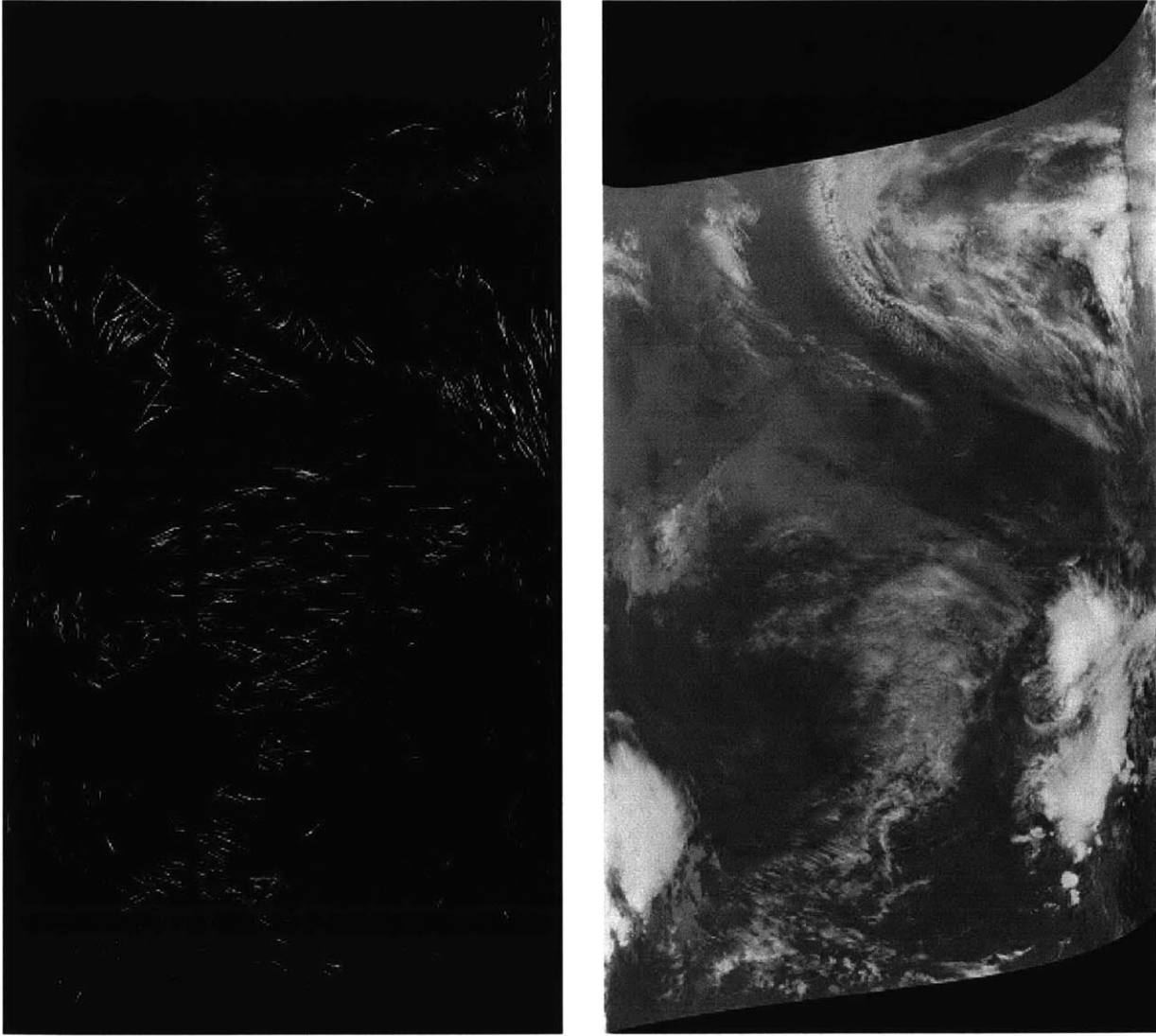


Figure F.8 - NOAA-16 satellite image and matching contrail mask (white pixel indicates contrail formation), November 14, 2001 1960 UTC.

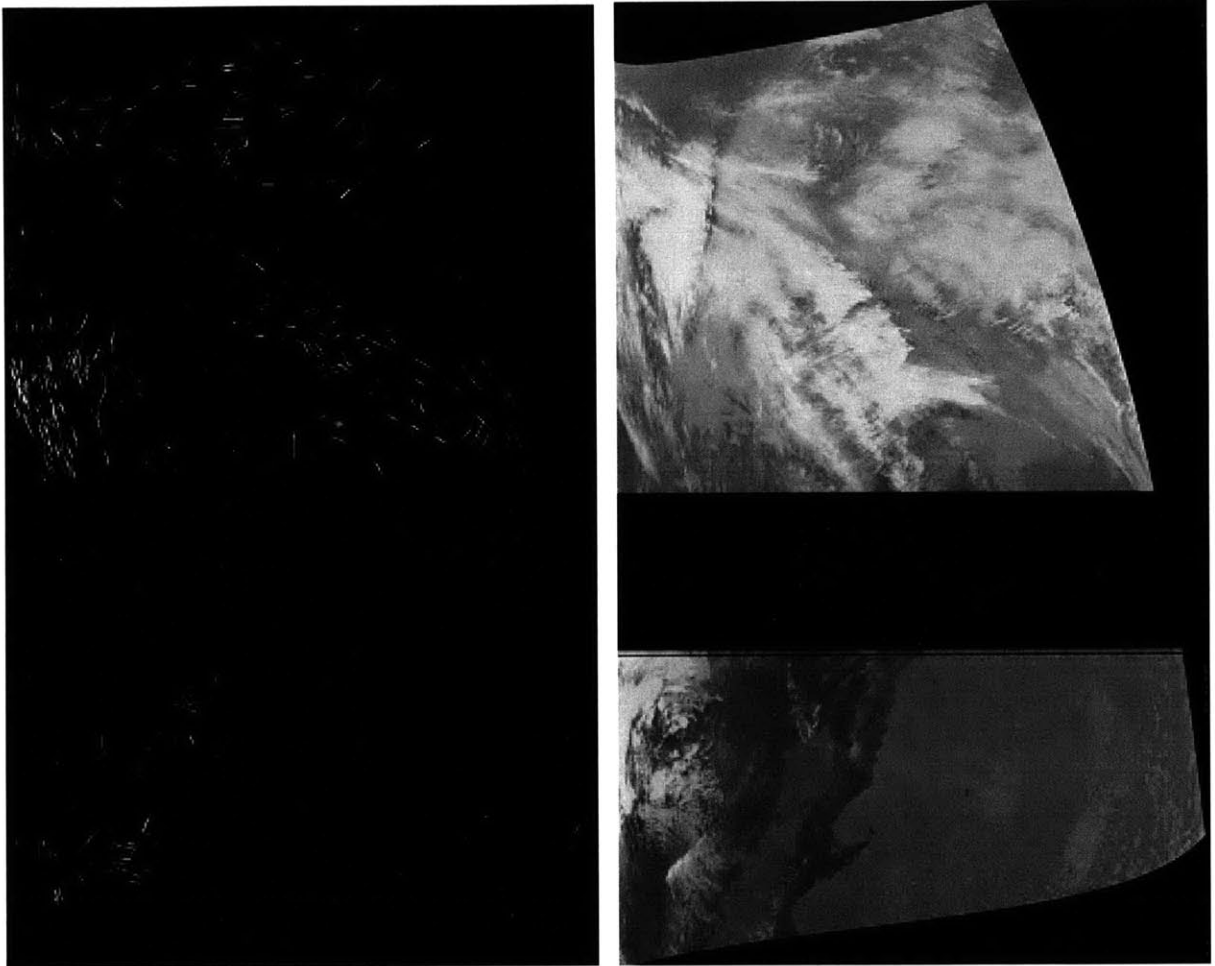


Figure F.9 - NOAA-16 satellite image and matching contrail mask (white pixel indicates contrail formation), November 14, 2001 2131 UTC.

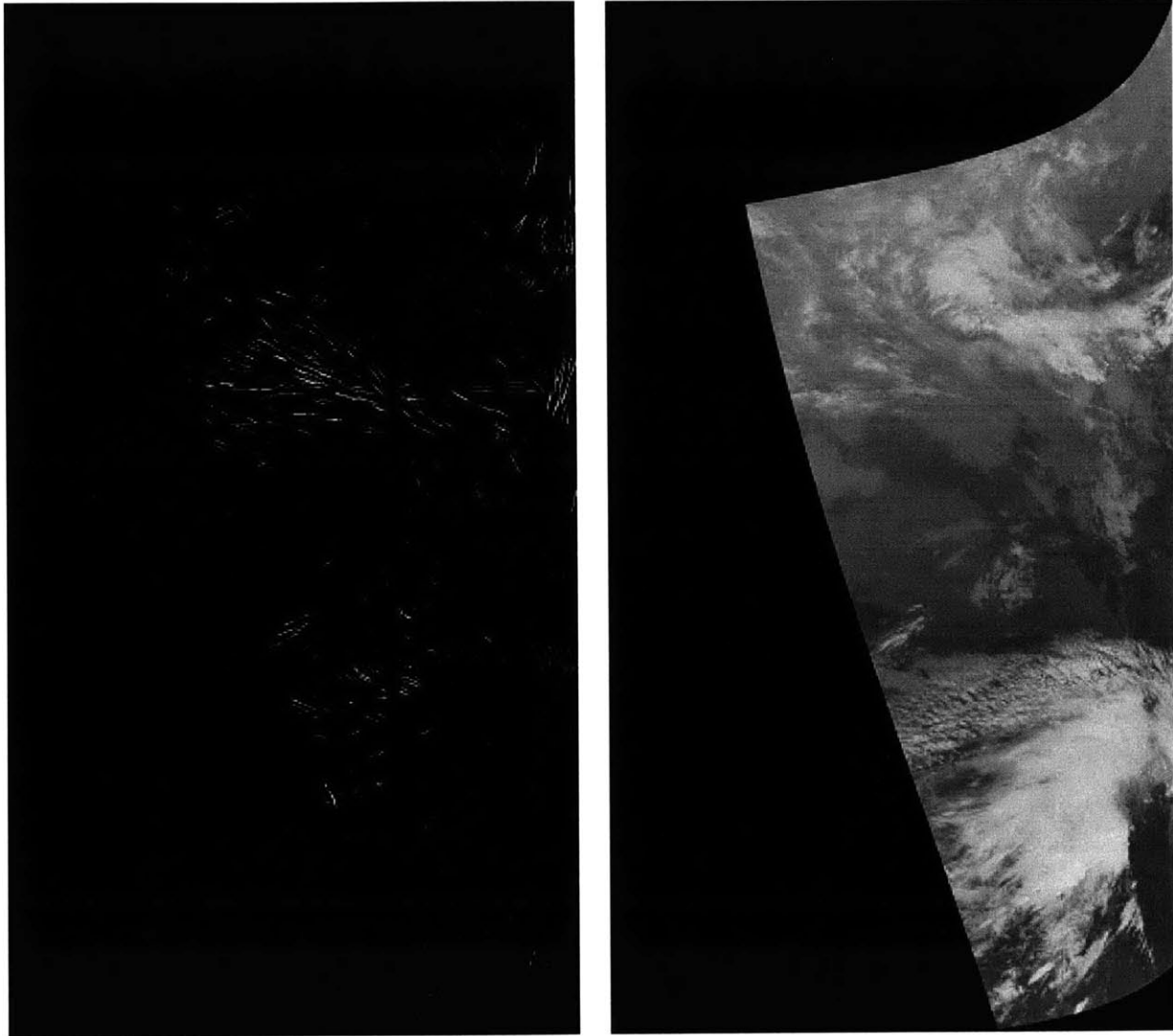


Figure F.10 - NOAA-16 satellite image and matching contrail mask (white pixel indicates contrail formation), November 15, 2001 1773 UTC.

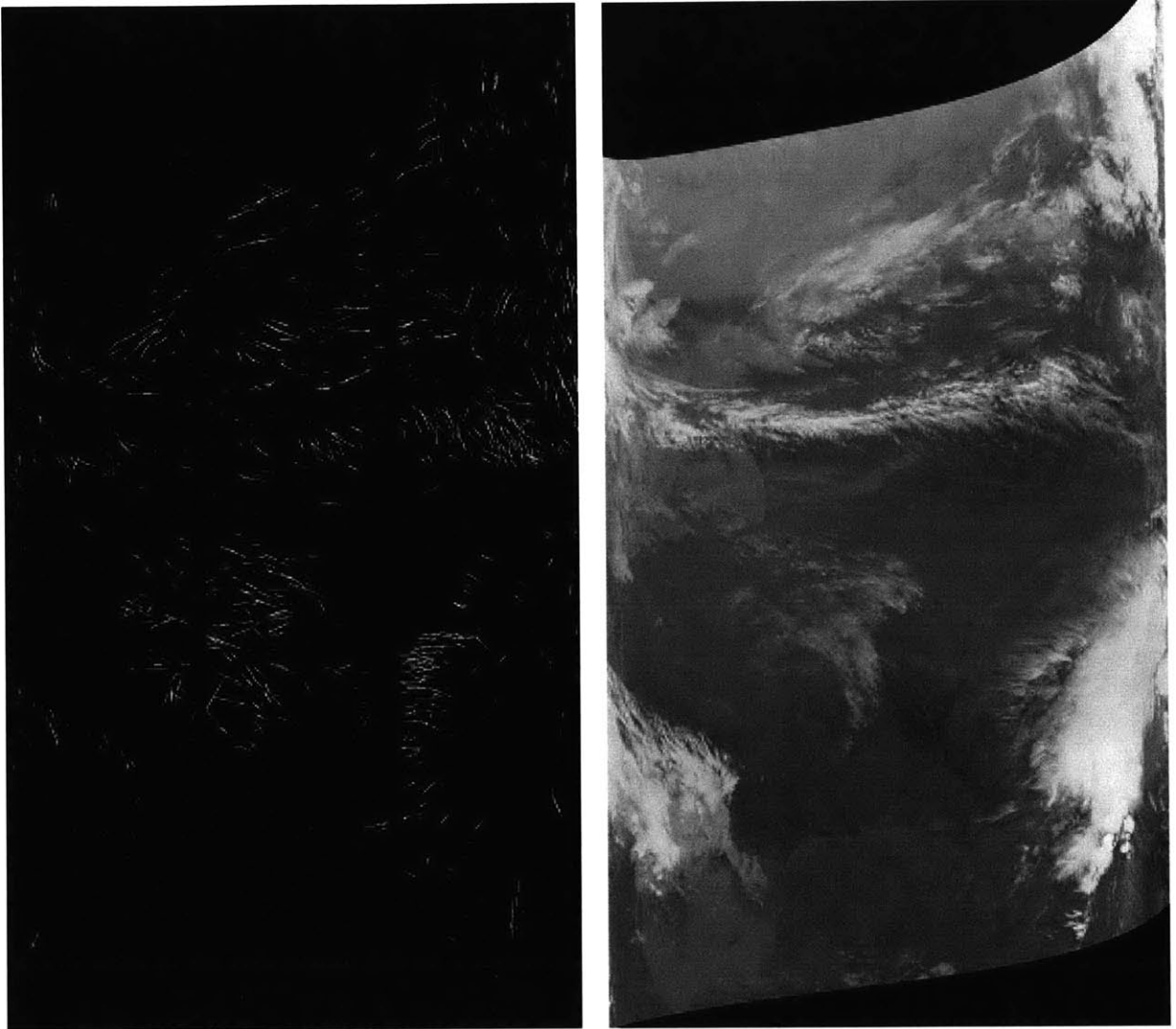


Figure F.11 - NOAA-16 satellite image and matching contrail mask (white pixel indicates contrail formation), November 15, 2001 1942 UTC.

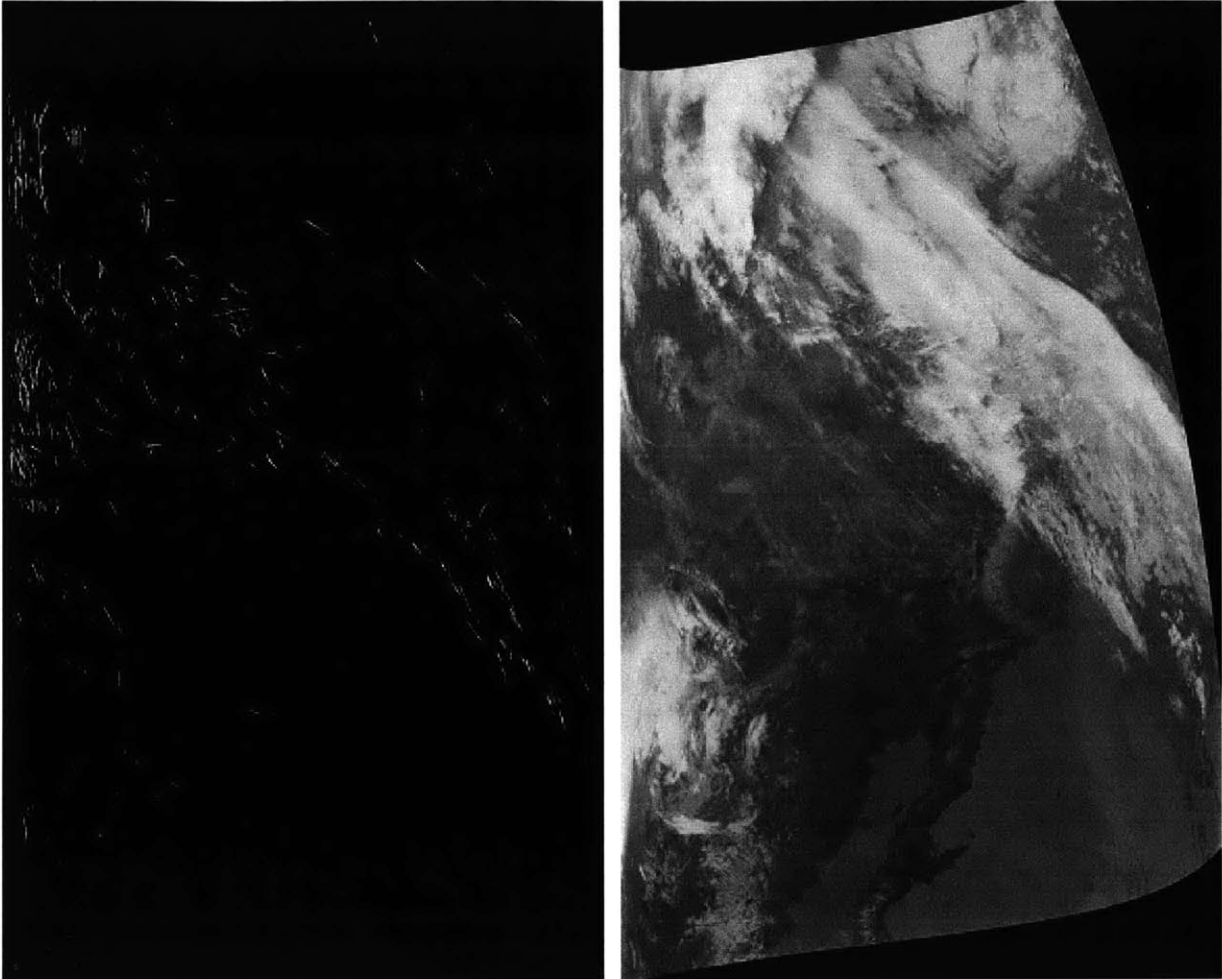


Figure F.12 - NOAA-16 satellite image and matching contrail mask (white pixel indicates contrail formation), November 15, 2001 2113 UTC.

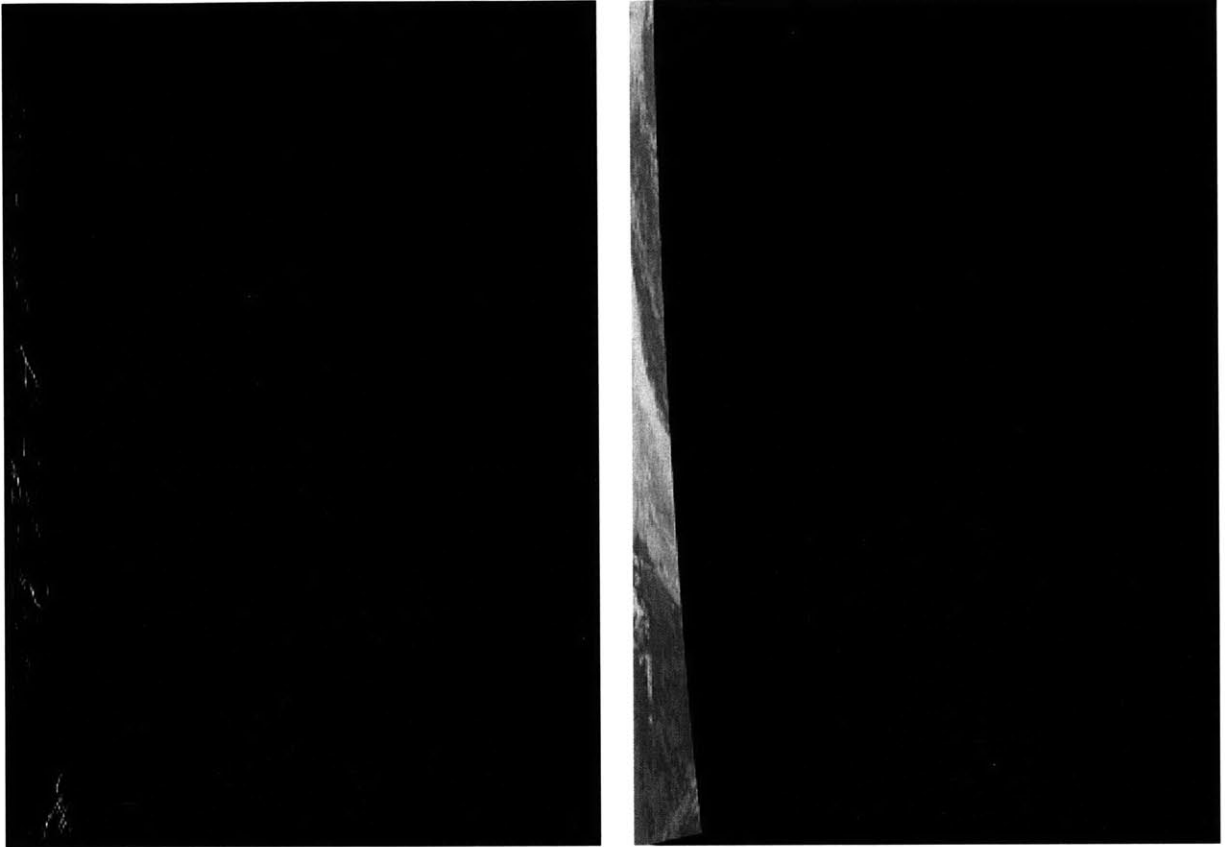


Figure F.13 - NOAA-16 satellite image and matching contrail mask (white pixel indicates contrail formation), November 15, 2001 2283 UTC.

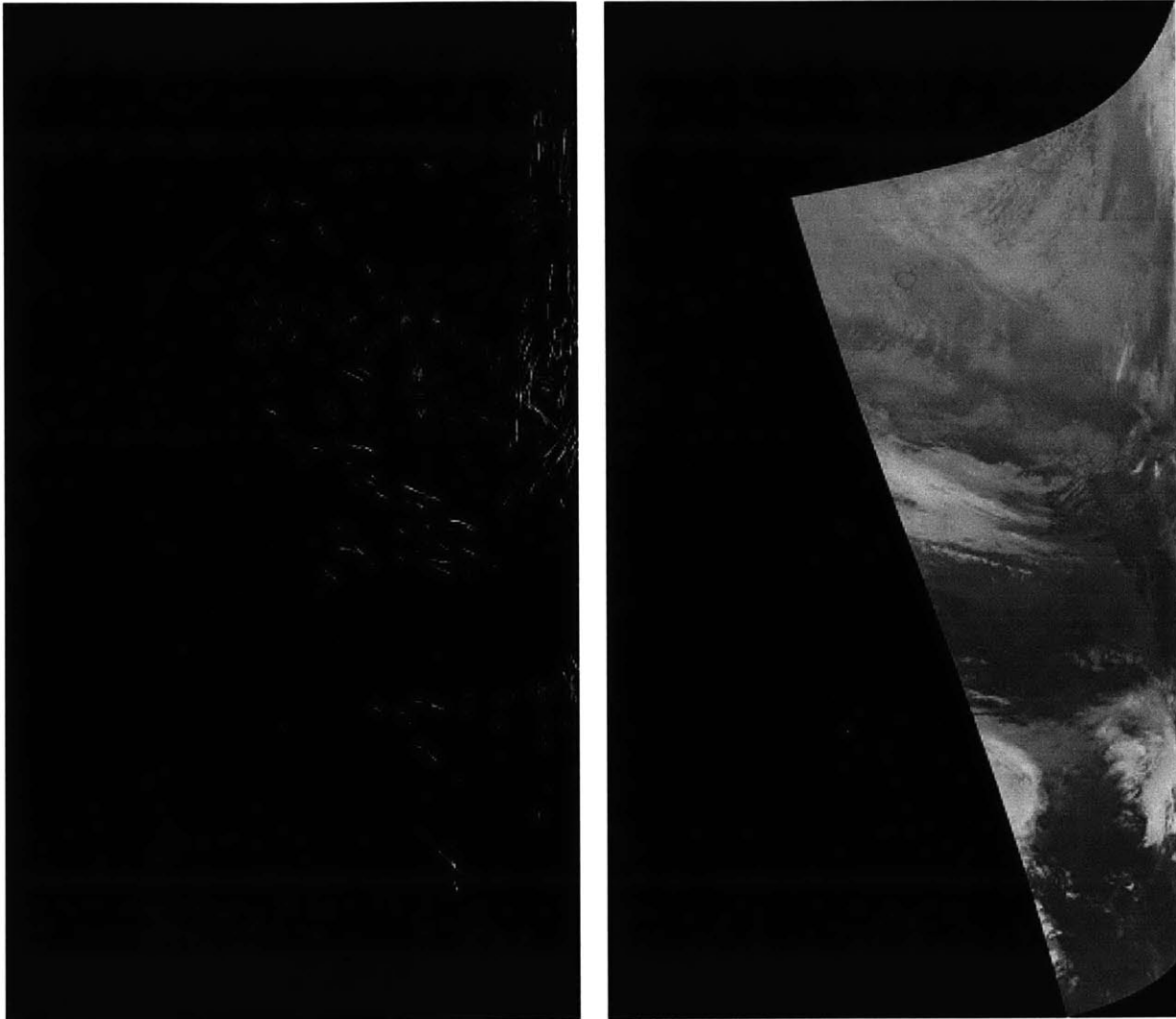


Figure F.14 - NOAA-16 satellite image and matching contrail mask (white pixel indicates contrail formation), November 16, 2001 1755 UTC.

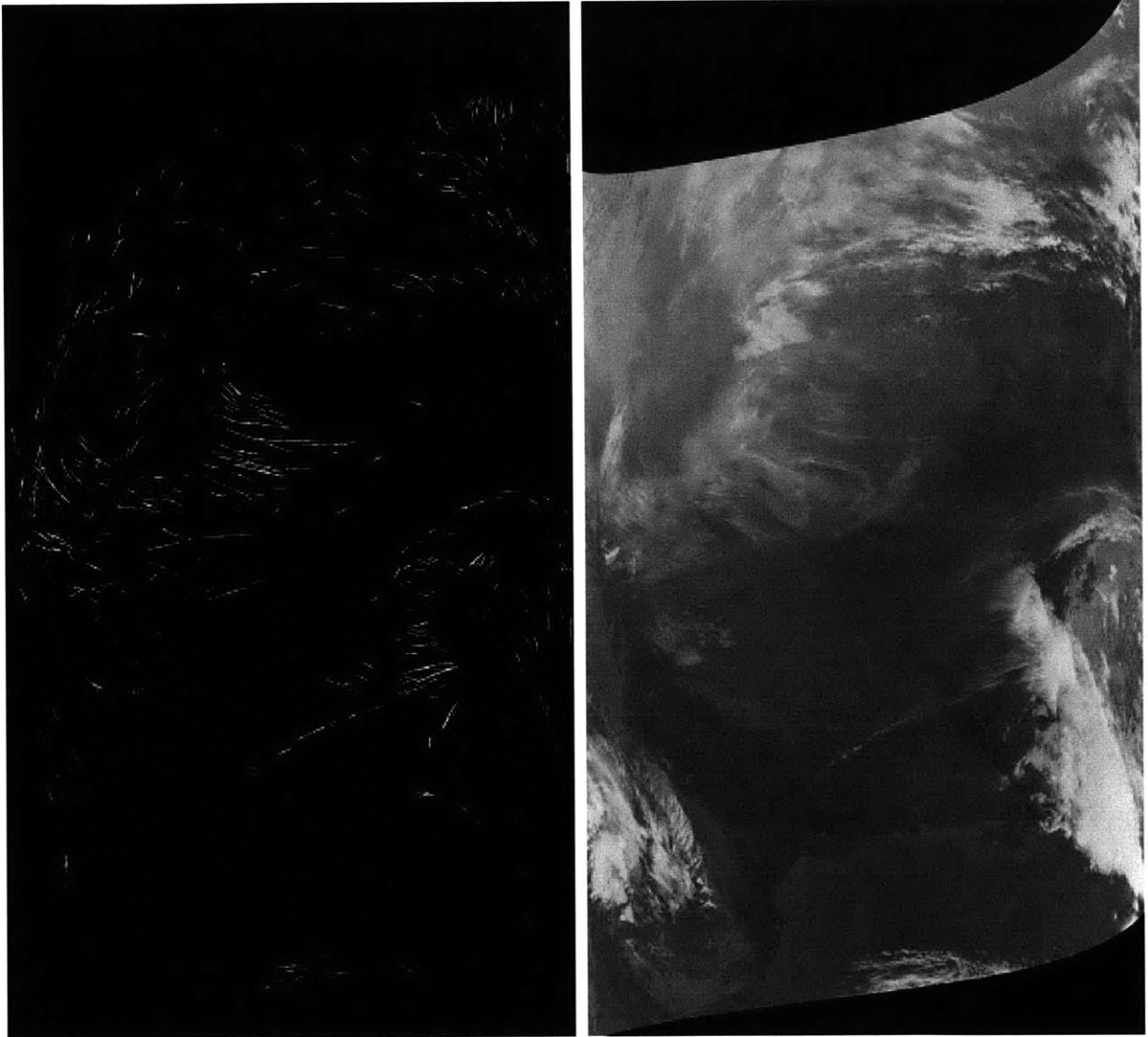


Figure F.15 - NOAA-16 satellite image and matching contrail mask (white pixel indicates contrail formation), November 16, 2001 1924 UTC.

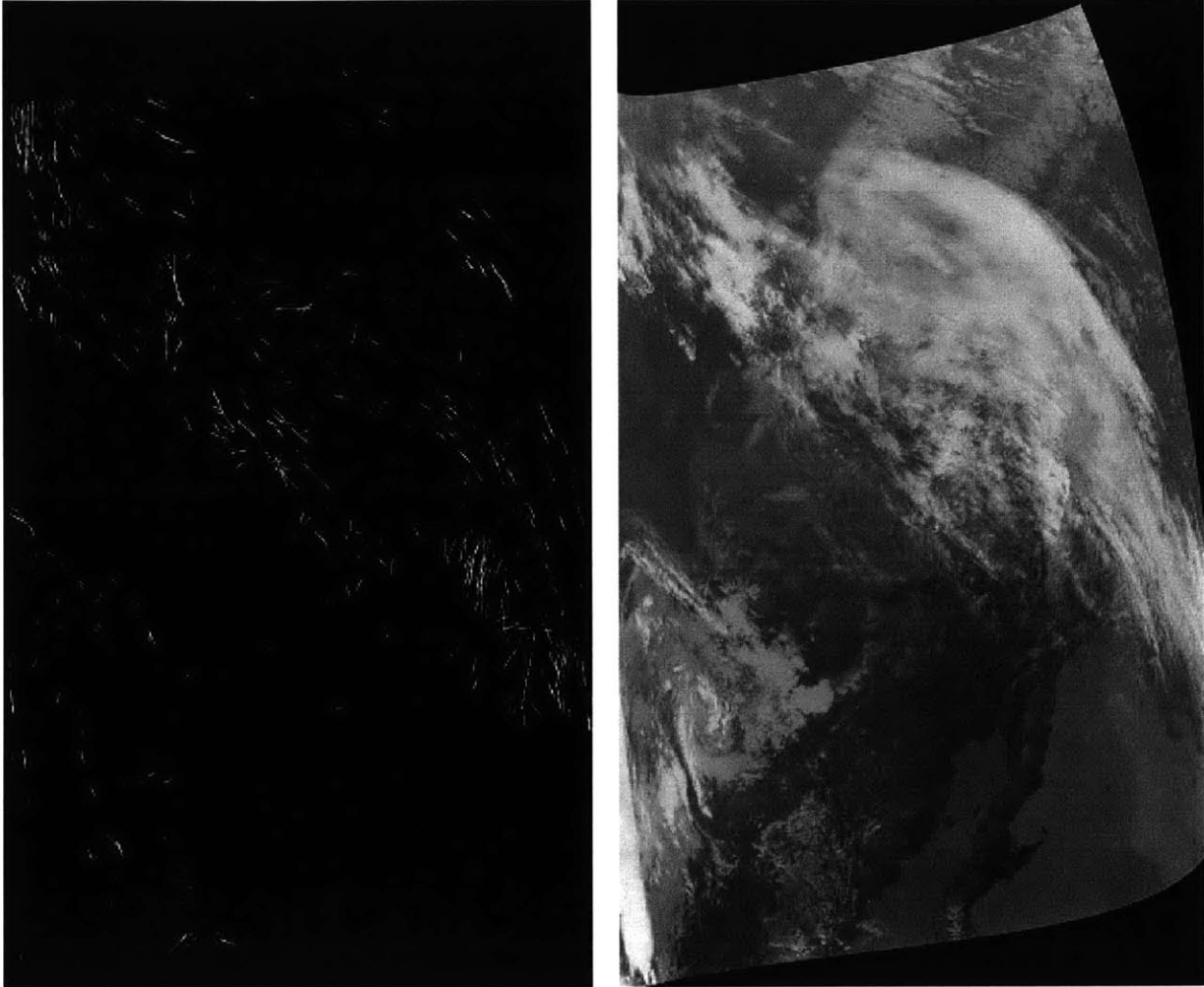


Figure F.16 - NOAA-16 satellite image and matching contrail mask (white pixel indicates contrail formation), November 16, 2001 2095 UTC.

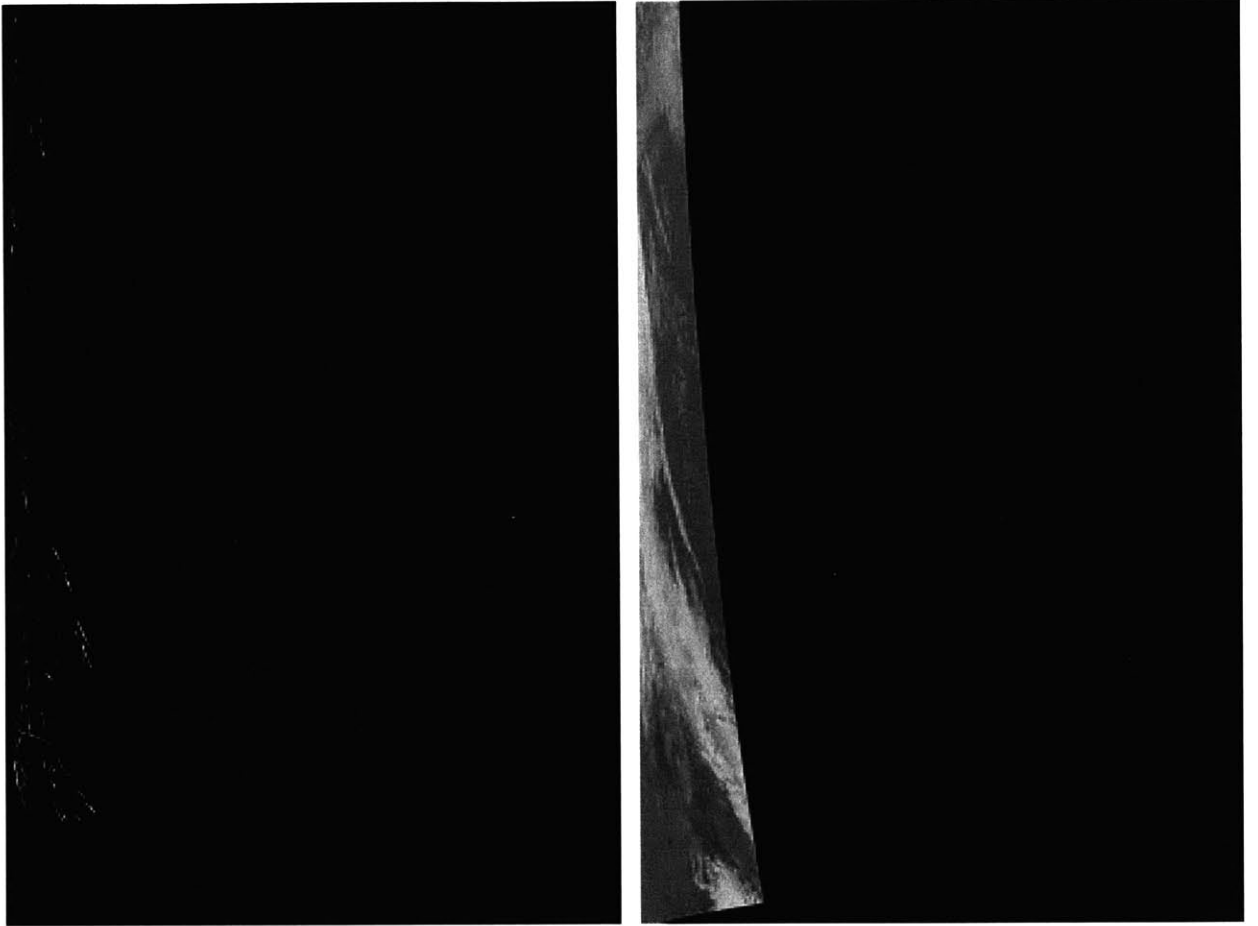


Figure F.17 - NOAA-16 satellite image and matching contrail mask (white pixel indicates contrail formation), November 16, 2001 2265 UTC.



Figure F.18 - NOAA-16 satellite image and matching contrail mask (white pixel indicates contrail formation), November 17, 2001 1738 UTC.

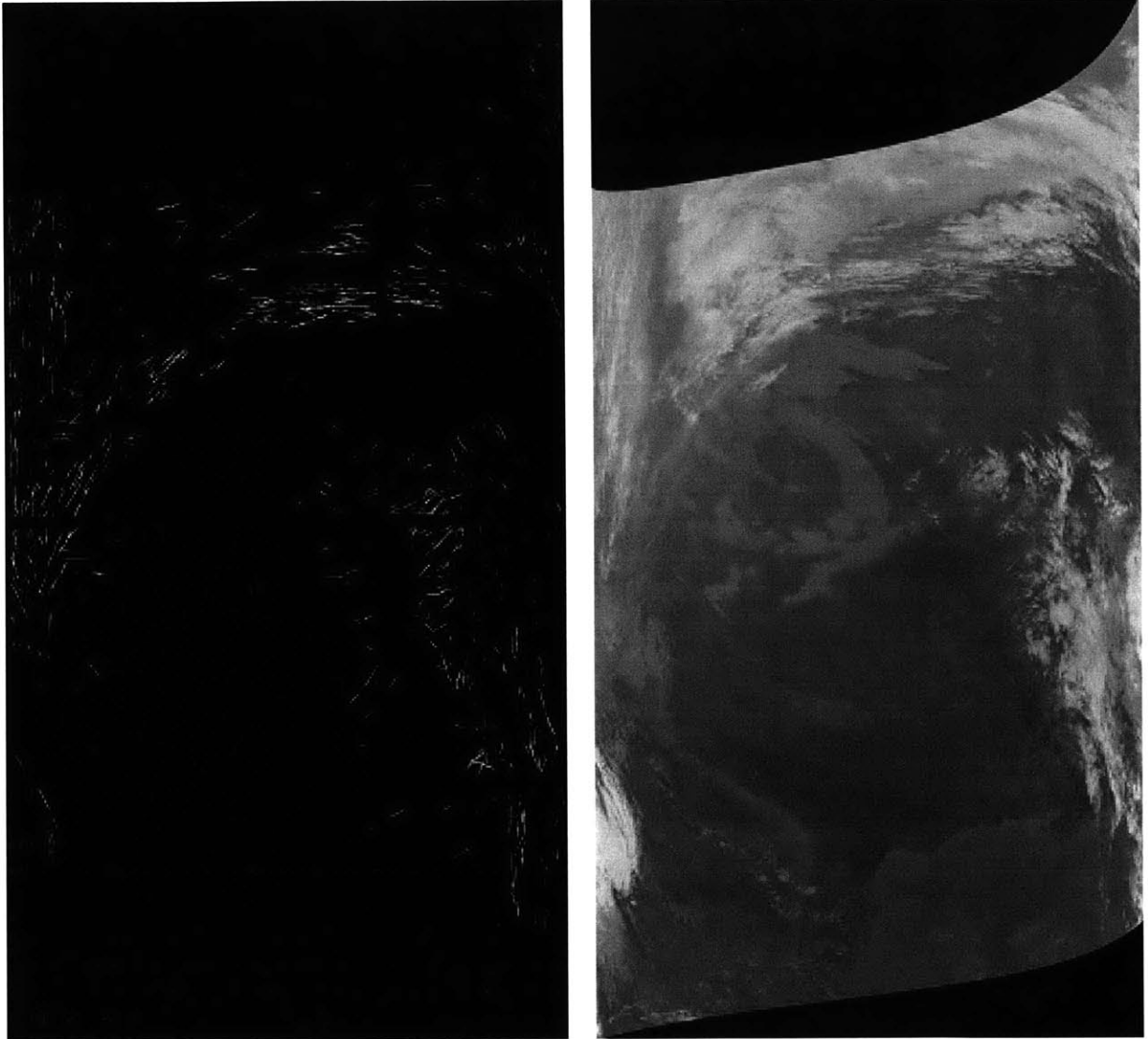


Figure F.19 - NOAA-16 satellite image and matching contrail mask (white pixel indicates contrail formation), November 17, 2001 1906 UTC.

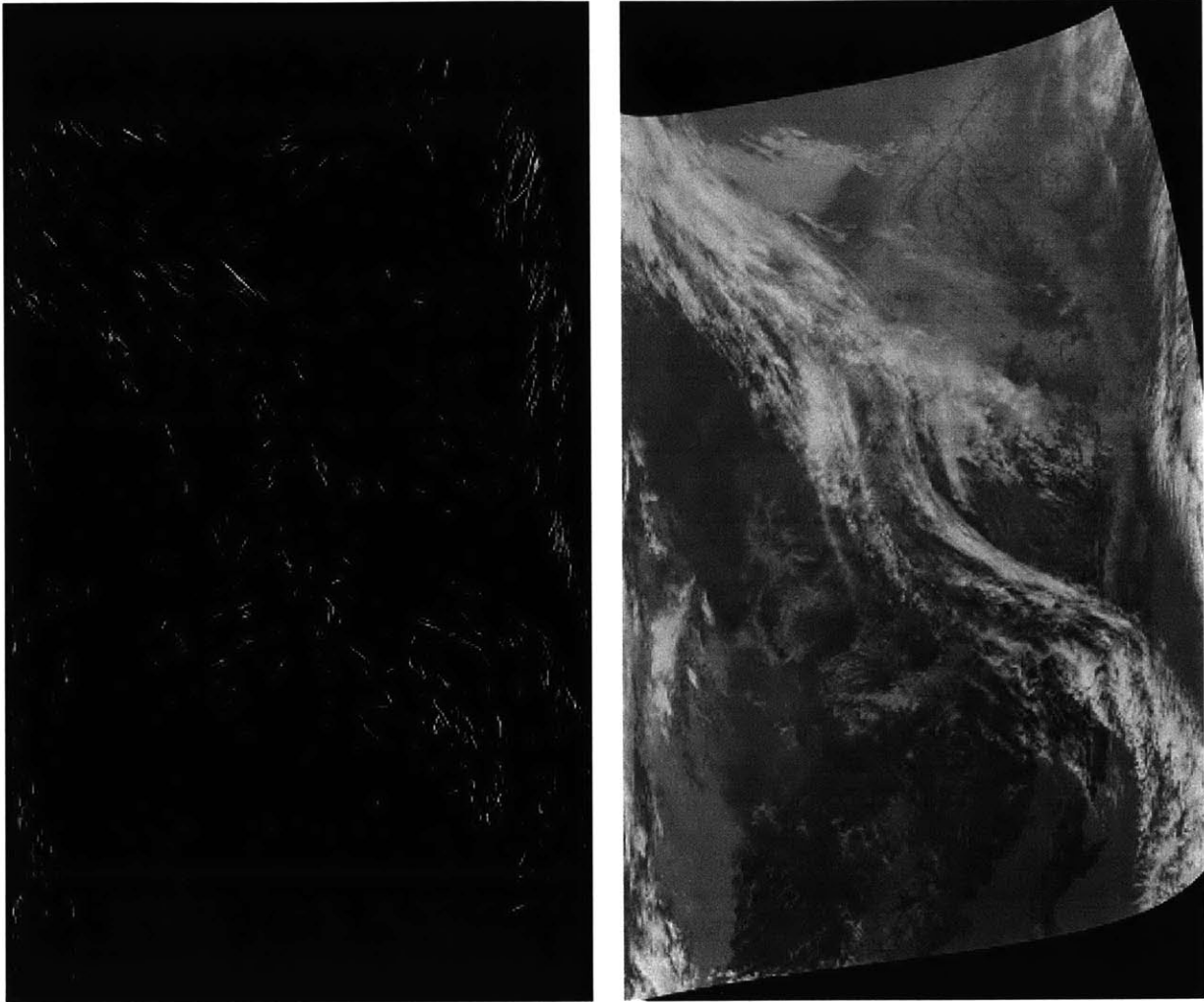


Figure F.20 - NOAA-16 satellite image and matching contrail mask (white pixel indicates contrail formation), November 17, 2001 2077 UTC.

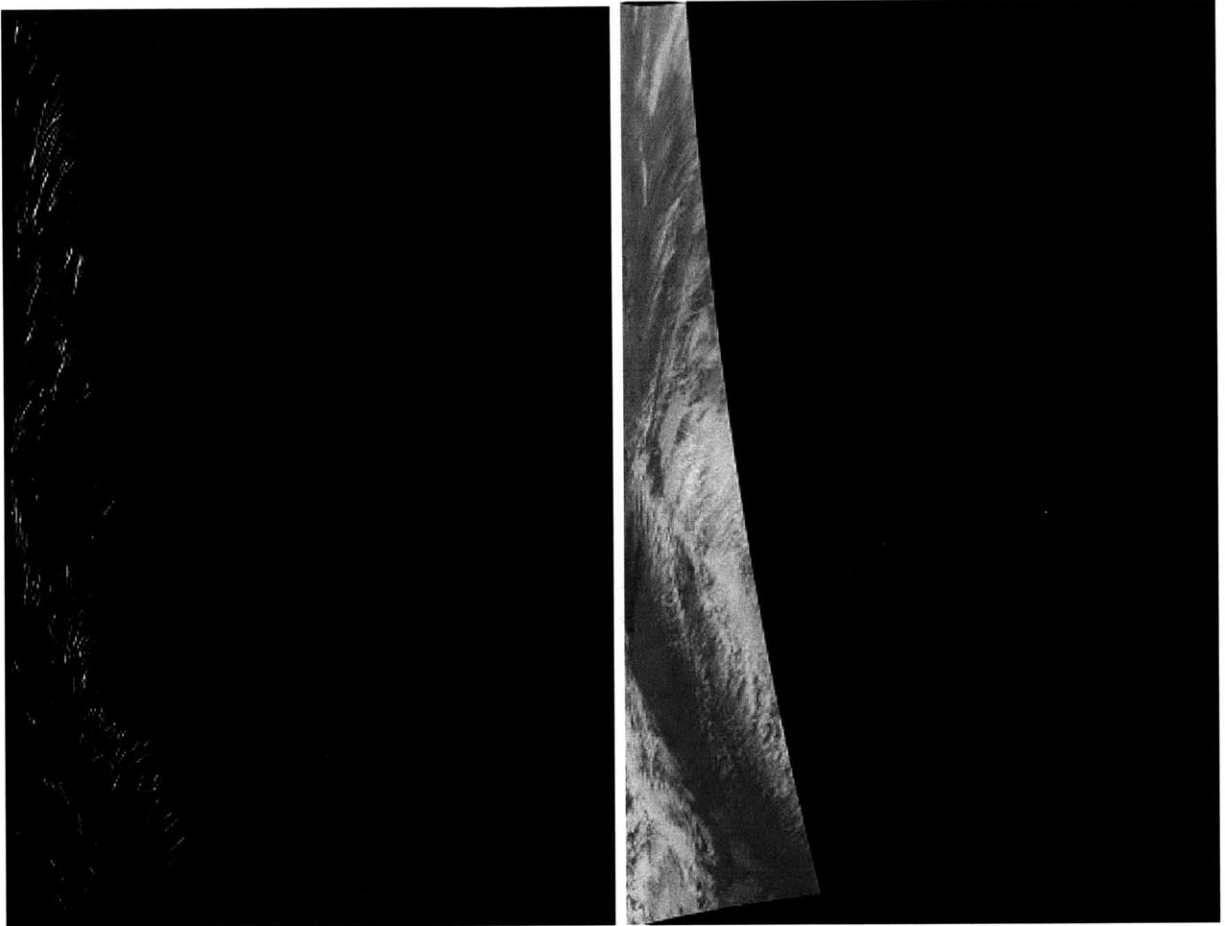


Figure F.21 - NOAA-16 satellite image and matching contrail mask (white pixel indicates contrail formation), November 17, 2001 2247 UTC.



Figure F.22 - NOAA-16 satellite image and matching contrail mask (white pixel indicates contrail formation), November 18, 2001 1720 UTC.

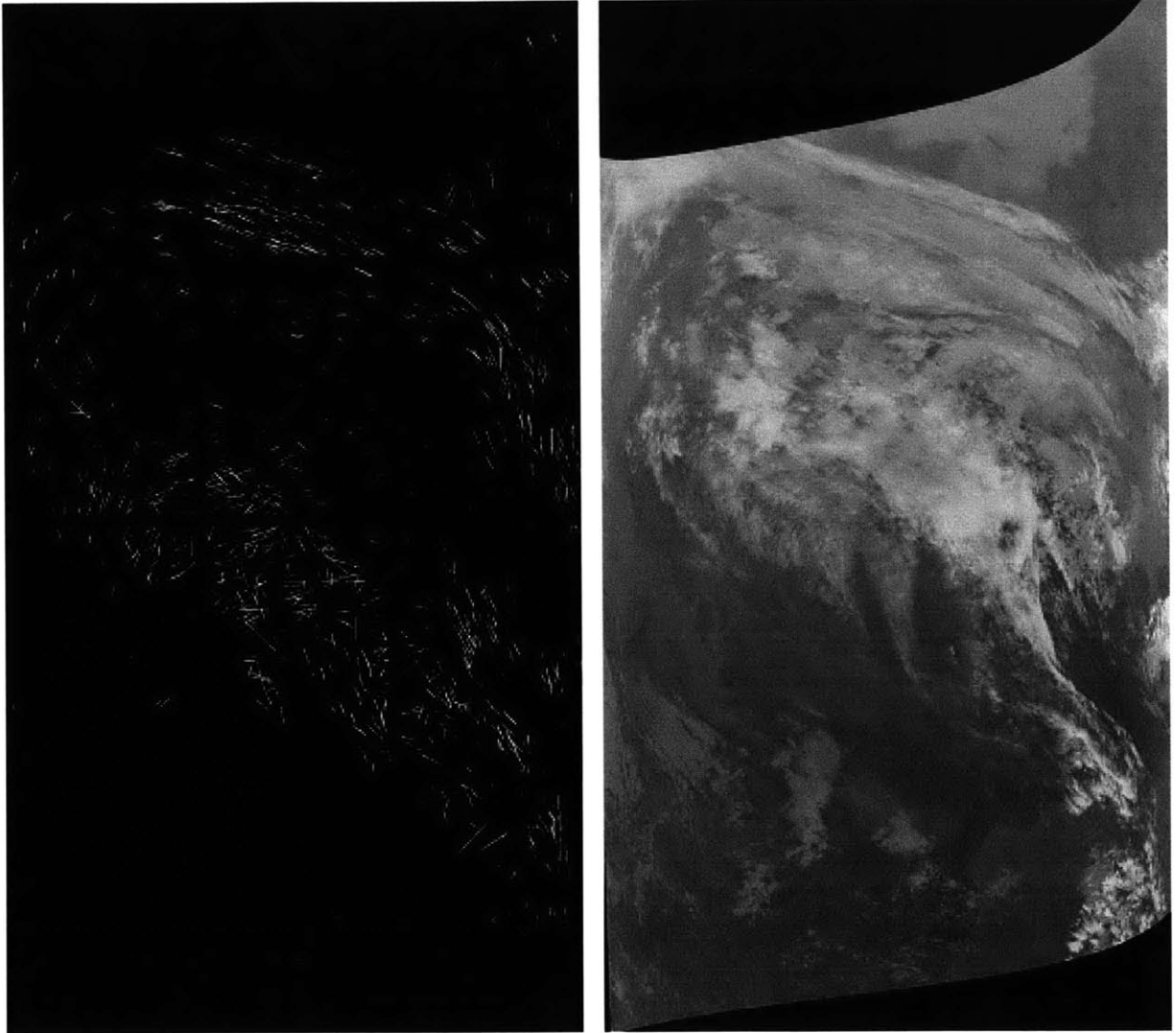


Figure F.23 - NOAA-16 satellite image and matching contrail mask (white pixel indicates contrail formation), November 18, 2001 1888 UTC.

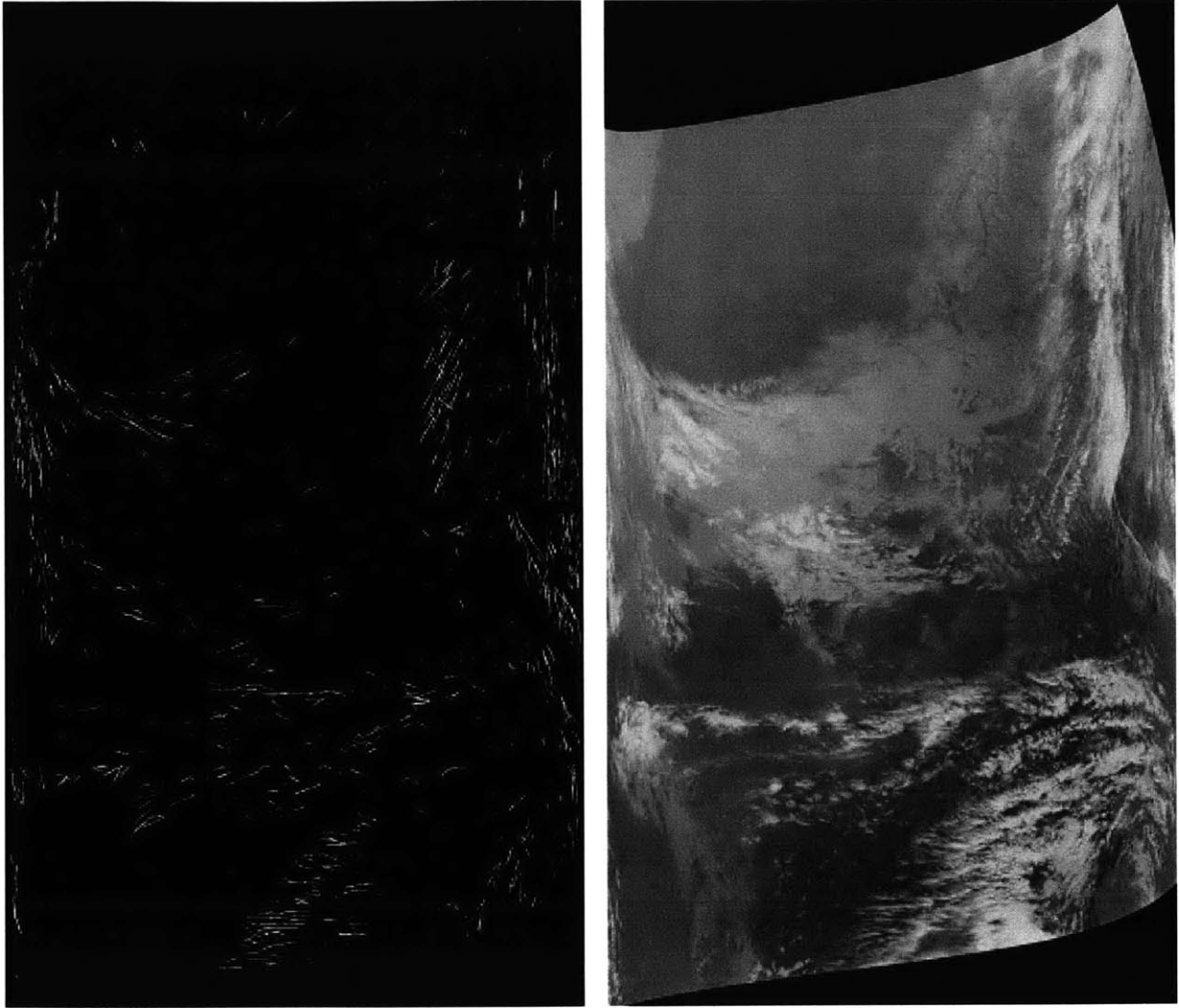


Figure F.24 - NOAA-16 satellite image and matching contrail mask (white pixel indicates contrail formation), November 18, 2001 2059 UTC.

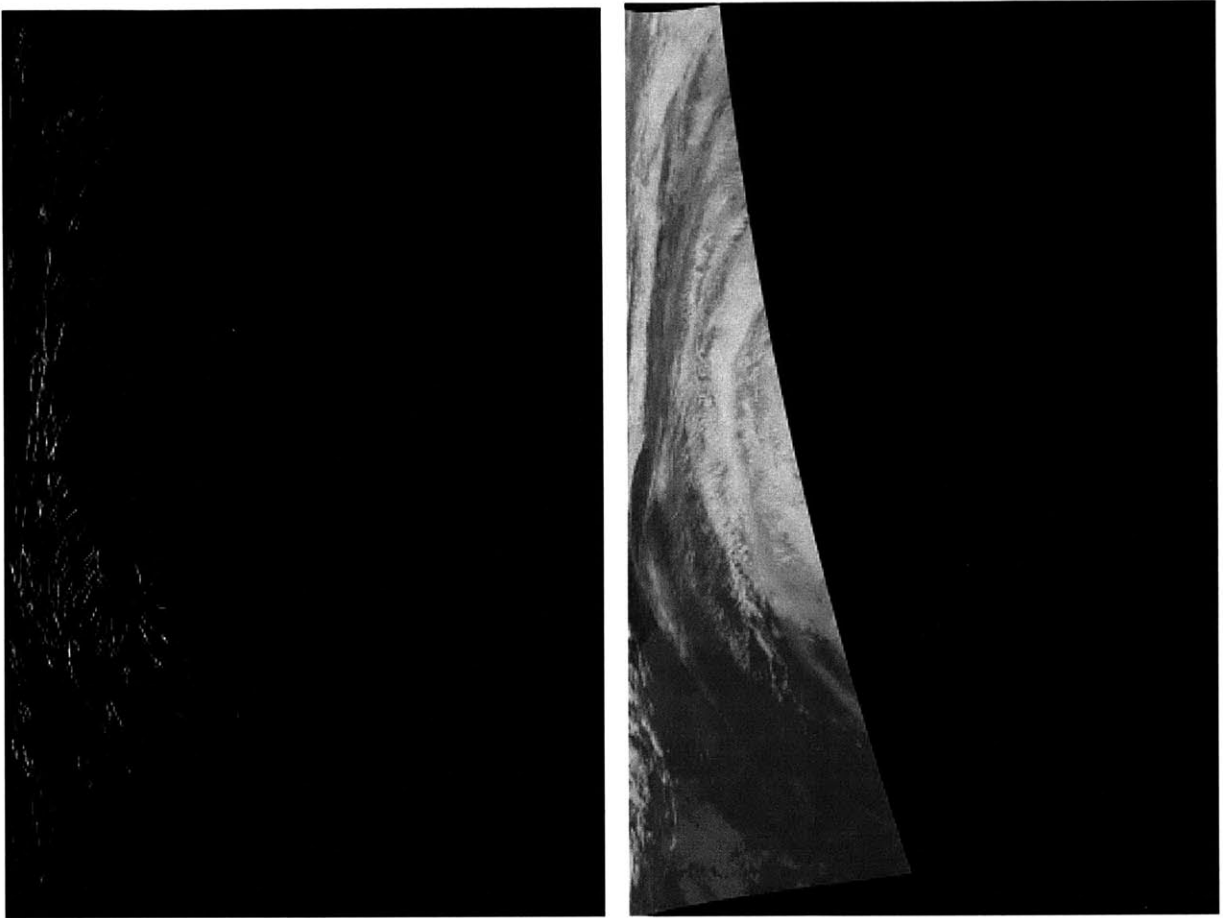


Figure F.25 - NOAA-16 satellite image and matching contrail mask (white pixel indicates contrail formation), November 18, 2001 2229 UTC.

APPENDIX G: ETMS METRICS FOR REROUTE ANALYSIS

For each of the reroute scenarios, ETMS flights with matching origin-destination pair, time period, and aircraft type were chosen. Metrics reported include:

- Average ETMS flight time
- Average ETMS fuel burn
- Average ETMS flight distance
- Average contrails formed (percent of flight distance)
- Average contrails formed (total length formed)
- Average contrail length per unit time
- Average contrail length per unit fuel burn

All contrail metrics were reported in both clear skies and in total. The numbers listed in the following tables are averages over all the flights.

Table G.1 – Average custom reroute contrails compared to current practice outputs for transatlantic flights. Note that the flight distance of both flights are the same, so both comparison metrics (% of flight by distance and overall distance of formation) yield the same relative change.

Departure Airport	Arrival Airport	ETMS Flight % of Flight as Contrails	ETMS Flight % of Flight as Contrails (clear skies)	Custom Flight % of Flight as Contrails	Custom Flight % of Flight as Contrails (clear skies)
BOS	EGLL	11.89	9.95	7.30	6.46
BOS	LFPG	18.56	17.99	6.84	6.67
EDDF	JFK	0.00	0.00	0.00	0.00
EDDF	ORD	5.36	5.36	0.00	0.00
EGLL	BOS	6.40	5.38	0.20	0.20
EGLL	JFK	0.83	0.00	7.55	7.32
EGLL	ORD	0.50	0.50	0.00	0.00
JFK	EDDF	0.00	0.00	0.04	0.00
JFK	EGLL	0.59	0.42	0.00	0.00
JFK	LFPG	0.00	0.00	0.00	0.00
LFPG	ORD	0.97	0.00	0.91	0.57
ORD	EDDF	11.22	6.35	4.81	4.81
ORD	EGLL	0.31	0.22	7.40	7.06
ORD	LFPG	33.28	33.11	29.43	28.92

Table G.2 – Current practice (ETMS) best and worst case estimations for continental flights, over 11/12/2001 & 11/15-18/2001. Results may be from different flights.

O-D Pair	Min. Fuel Burn (kg)	Max. Fuel Burn (kg)	Min. Time (sec)	Max. Time (sec)	Min Cost (05 USD)	Max. Cost (05 USD)
ATL-DFW	3981.44	5140.61	5940	7320	3159.86	3765.50
ATL-LAX	19181.11	21193.79	13860	14040	13438.53	14116.25
ATL-LGA	5101.62	5971.57	5940	6420	3478.53	3808.99
ATL-ORD	4830.32	6408.44	4920	9900	3133.59	5012.26
BOS-LAX	22400.26	25605.38	19020	20640	17322.60	19030.23
DFW-LAX	8205.82	10783.81	8940	10200	5549.37	6453.41
DFW-LGA	8433.02	10913.04	9960	11160	5920.70	6648.75
JFK-LAX	20339.87	23241.00	17940	19620	16251.95	17807.94
LAX-BOS	15374.81	19629.82	17700	19200	10562.87	11853.51
LAX-DFW	8187.46	10677.03	8460	10080	5217.20	6417.32
LAX-JFK	20959.16	29356.43	16620	18840	15566.57	18031.50
LGA-ORD	4598.36	5193.47	6420	6960	3540.58	3754.00
MIA-SEA	24683.14	26371.96	19860	21180	18899.44	19215.37
SEA-MIA	24407.88	28293.40	18780	19260	17757.50	18900.62

O-D Pair	Best Contrail Persistence (nm)	Worst Contrail Persistence (nm)	Best Contrail Persistence (nm in clear skies)	Worst Contrail Persistence (nm in clear skies)
ATL-DFW	0	265	0	265
ATL-LAX	0	24	0	24
ATL-LGA	0	7	0	7
ATL-ORD	0	68	0	68
BOS-LAX	0	532	0	422
DFW-LAX	0	244	0	142
DFW-LGA	0	251	0	251
JFK-LAX	0	387	0	387
LAX-BOS	0	301	0	301
LAX-DFW	0	115	0	115
LAX-JFK	0	261	0	261
LGA-ORD	0	171	0	171
MIA-SEA	0	584	0	489
SEA-MIA	0	192	0	192

Table G.3 – Current practice (ETMS) best and worst case estimations for transatlantic flights, over 11/12-18/2003. Results may be from different flights.

O-D Pair	Min. Fuel Burn (kg)	Max. Fuel Burn (kg)	Min. Time (sec)	Max. Time (sec)	Min Cost (05 USD)	Max. Cost (05 USD)
BOS-EGLL	77403.20	99427.74	19860	22020	46065.79	55252.87
BOS-LFPG	49680.32	58994.47	21300	22140	39846.21	42975.08
EDDF-JFK	80951.63	91187.44	26520	29760	54634.67	58582.49
EDDF-ORD	37081.30	38590.79	30660	33000	29147.68	30532.96
EGLL-BOS	62261.80	71349.99	23700	25980	46515.63	50811.09
EGLL-JFK	62305.67	73632.09	23640	27060	46917.71	50951.58
EGLL-ORD	44404.44	57452.56	27540	31140	29828.21	34021.77
JFK-EDDF	36818.79	51214.48	23880	25260	25475.60	29791.46
JFK-EGLL	74197.68	108031.66	20640	22620	47035.85	57300.09
JFK-LFPG	35411.96	49085.96	22980	23880	24595.44	28689.75
LFPG-JFK	29908.66	29908.66	28260	28260	25423.27	25423.27
LFPG-ORD	57756.70	60107.74	30120	30840	52278.83	52365.69
ORD-EDDF	53870.49	59310.00	27540	29460	32606.86	34834.16
ORD-EGLL	105808.67	141365.64	24840	25920	61591.66	71563.88
ORD-LFPG	49673.59	56400.80	26340	28140	30559.83	33142.26

O-D Pair	Best Contrail Persistence (nm)	Worst Contrail Persistence (nm)	Best Contrail Persistence (nm in clear skies)	Worst Contrail Persistence (nm in clear skies)
BOS-EGLL	0	1390.3211	0	1383
BOS-LFPG	0	1111.6519	0	1101
EDDF-JFK	0	20.9349	0	0
EDDF-ORD	51.5614	470.3134	0	367
EGLL-BOS	0	742	0	20
EGLL-JFK	0	1211	0	19
EGLL-ORD	0	1190.9649	0	1127
JFK-EDDF	0	1306.9245	0	1270
JFK-EGLL	0	1783.6109	0	1774
JFK-LFPG	0	1423	0	1423
LFPG-JFK	9	9	0	0
LFPG-ORD	6.2807	36.2879	0	0
ORD-EDDF	9.4211	915.214	0	892
ORD-EGLL	11.0927	849	8	807
ORD-LFPG	4.0266	1228.2807	0	1222

Table G.4 - Custom reroute best case scenario for contrail persistence for each origin-destination pair. These numbers are calculated from the average over all times examined (10 for continental, 14 for transatlantic). Cost was used as a tiebreaker.

O-D Pair	Time (sec)	Fuel Burn (kg)	Contrail Formation (nm)	Contrail Formation (nm, clear skies)	Cost (USD05)
ATL-DFW	6385.9	3651.28	0.00	0.00	3216.56
ATL-LAX	no custom reroute was improved				
ATL-LGA	6039.9	5302.28	0.00	0.00	3569.80
ATL-ORD	5218.7	4811.42	1.88	0.00	3150.08
BOS-LAX	18238.9	19917.07	50.40	25.82	16165.17
DFW-LAX	9168.0	8582.40	0.00	0.00	5571.00
DFW-LGA	11112.2	10980.88	0.00	0.00	6917.46
JFK-LAX	20995.5	22612.19	51.58	27.30	18518.43
LAX-BOS	16871.1	15776.13	0.63	0.00	10246.89
LAX-DFW	no custom reroute was improved				
LAX-JFK	18962.1	22921.95	14.03	14.03	17438.18
LGA-ORD	7532.2	4639.02	2.51	0.00	3888.77
MIA-SEA	19001.1	20602.42	191.29	180.61	16798.77
SEA-MIA	18305.0	22772.36	90.00	90.00	17017.85
BOS-EGLL	25150.4	68017.89	132.73	118.66	49125.97
BOS-LFPG	28940.7	48185.67	209.44	188.47	47294.48
EDDF-JFK	no custom reroute was improved				
EDDF-ORD	33042.4	37778.04	76.65	63.05	30587.65
EGLL-BOS	22142.4	60080.46	39.79	35.89	43311.20
EGLL-JFK	22559.9	61061.64	106.28	101.48	44081.20
EGLL-ORD	27434.6	46056.33	58.10	45.31	29906.03
JFK-EDDF	30690.0	33882.14	143.08	127.78	28039.66
JFK-EGLL	26678.6	71705.52	124.65	112.10	51974.38
JFK-LFPG	29167.6	32131.81	198.65	187.30	26627.35
LFPG-JFK	no custom reroute was improved				
LFPG-ORD	no custom reroute was improved				
ORD-EDDF	36490.8	41818.94	113.02	96.74	33810.01
ORD-EGLL	30342.5	87094.33	112.37	100.28	60813.29
ORD-LFPG	32891.1	38014.10	127.49	111.77	30573.17

Table G.5 - Custom reroute best case scenario for contrail persistence (in clear skies) for each origin-destination pair. These numbers are calculated from the average over all times examined (10 for continental, 14 for transatlantic). Cost was used as a tiebreaker.

O-D Pair	Time (sec)	Fuel Burn (kg)	Contrail Formation (nm)	Contrail Formation (nm, clear skies)	Cost (USD05)
ATL-DFW	6385.9	3651.28	0.00	0.00	3216.56
ATL-LAX	13458.5	17936.98	37.49	0.00	12852.79
ATL-LGA	6039.9	5302.28	0.00	0.00	3569.80
ATL-ORD	5218.7	4811.42	1.88	0.00	3150.08
BOS-LAX	18238.9	19917.07	50.40	25.82	16165.17
DFW-LAX	9168.0	8582.40	0.00	0.00	5571.00
DFW-LGA	11112.2	10980.88	0.00	0.00	6917.46
JFK-LAX	20995.5	22612.19	51.58	27.30	18518.44
LAX-BOS	16871.1	15776.13	0.63	0.00	10246.89
LAX-DFW			no custom reroute was improved		
LAX-JFK	18962.1	22921.95	14.03	14.03	17438.18
LGA-ORD	7532.2	4639.02	2.51	0.00	3888.77
MIA-SEA			no custom reroute was improved		
SEA-MIA	18305.0	22772.36	90.00	90.00	17017.85
BOS-EGLL	25150.4	68017.89	132.73	118.66	49125.97
BOS-LFPG	28940.7	48185.67	209.44	188.47	47294.48
EDDF-JFK			no custom reroute was improved		
EDDF-ORD	33042.4	37778.04	76.65	63.05	30587.65
EGLL-BOS	22142.4	60080.46	39.79	35.89	43311.20
EGLL-JFK	22559.9	61061.64	106.28	101.48	44081.20
EGLL-ORD	27434.6	46056.33	58.10	45.31	29906.03
JFK-EDDF	30690.0	33882.14	143.08	127.78	28039.66
JFK-EGLL	26678.6	71705.52	124.65	112.10	51974.38
JFK-LFPG	29167.6	32131.81	198.65	187.30	26627.35
LFPG-JFK			no custom reroute was improved		
LFPG-ORD			no custom reroute was improved		
ORD-EDDF	36490.8	41818.94	113.02	96.74	33810.01
ORD-EGLL	30342.5	87094.33	112.37	100.28	60813.29
ORD-LFPG	32891.1	38014.10	127.49	111.77	30573.17

Table G.6 - Custom reroute scenario for contrail persistence (in clear skies) for each origin-destination pair. This average is calculated using all the custom reroutes with decreased contrail persistence.

O-D Pair	Time (sec)	Fuel Burn (kg)	Contrail Formation (nm)	Contrail Formation (nm, clear skies)	Cost (USD05)
ATL-DFW	7618.05	4333.29	20.09	12.12	3830.77
ATL-LAX	no custom reroute was improved				
ATL-LGA	5970.75	5486.65	0.00	0.00	3598.60
ATL-ORD	6202.97	6084.20	2.27	0.00	3848.44
BOS-LAX	20749.77	22970.09	108.34	97.18	18479.33
DFW-LAX	10171.15	9232.32	16.50	15.10	6098.07
DFW-LGA	11276.49	10870.84	12.18	9.87	6942.01
JFK-LAX	20021.60	21615.75	68.21	53.68	17674.40
LAX-BOS	18885.83	16868.81	45.14	43.32	11244.79
LAX-DFW	no custom reroute was improved				
LAX-JFK	18995.95	22965.34	15.80	15.43	17470.01
LGA-ORD	8008.55	4684.09	27.50	19.15	4063.85
MIA-SEA	18941.00	21161.00	202.64	191.96	16923.61
SEA-MIA	19355.23	23275.87	97.15	97.15	17765.10
BOS-EGLL	25524.13	71173.89	321.89	284.61	50514.59
BOS-LFPG	28373.55	49058.49	341.36	308.66	46925.47
EDDF-JFK	no custom reroute was improved				
EDDF-ORD	30350.26	35876.26	165.88	142.21	28456.58
EGLL-BOS	21877.44	60829.49	167.23	156.63	43243.54
EGLL-JFK	22844.40	62813.32	196.23	181.61	44938.51
EGLL-ORD	26838.33	46131.56	113.77	100.02	29586.45
JFK-EDDF	31161.90	34508.40	207.49	187.06	28503.13
JFK-EGLL	27007.86	72784.08	201.13	177.99	52675.21
JFK-LFPG	29407.07	34558.14	395.92	358.94	27509.85
LFPG-JFK	no custom reroute was improved				
LFPG-ORD	no custom reroute was improved				
ORD-EDDF	35742.16	40829.05	146.75	130.47	33075.87
ORD-EGLL	30985.85	88408.45	184.80	172.32	61939.23
ORD-LFPG	33510.80	40298.18	266.60	241.07	31630.49

Table G.7 - Custom reroute scenario for contrail persistence (in clear skies) for each origin-destination pair. This average is calculated using only the step climb custom reroutes with decreased contrail persistence.

O-D Pair	Time (sec)	Fuel Burn (kg)	Contrail Formation (nm)	Contrail Formation (nm, clear skies)	Cost (USD05)
ATL-DFW	6721.05	3532.5	50.26	42.10	3296.80
ATL-LAX			no custom reroute was improved		
ATL-LGA			no custom reroute was improved		
ATL-ORD			no custom reroute was improved		
BOS-LAX	20864.1	22750.3	103.56	93.79	18482.34
DFW-LAX	10347.4	8710.9	17.34	16.10	6009.31
DFW-LGA	11325.2	9586.7	17.24	13.67	6592.21
JFK-LAX	19939.3	21552.5	67.50	50.96	17609.04
LAX-BOS	18520.2	15912.2	46.32	46.00	10847.33
LAX-DFW			no custom reroute was improved		
LAX-JFK			no custom reroute was improved		
LGA-ORD	8401.0	4733.0	38.84	27.92	4211.47
MIA-SEA	18993.0	21029.7	193.13	182.46	16916.04
SEA-MIA			no custom reroute was improved		
BOS-EGLL	25646.9	69422.7	176.84	154.99	50114.84
BOS-LFPG	28394.8	47454.7	247.58	224.70	46456.97
EDDF-JFK			no custom reroute was improved		
EDDF-ORD	30153.5	34873.4	137.03	122.18	28035.64
EGLL-BOS	22128.5	60089.3	72.93	65.62	43298.30
EGLL-JFK	22918.5	62123.6	169.48	155.68	44810.03
EGLL-ORD	26774.9	44423.2	79.15	66.90	29025.53
JFK-EDDF	31161.9	34508.4	207.49	187.06	28503.13
JFK-EGLL	27053.7	72792.1	173.34	148.43	52729.15
JFK-LFPG	29540.8	32744.5	246.55	227.10	27029.95
LFPG-JFK			no custom reroute was improved		
LFPG-ORD			no custom reroute was improved		
ORD-EDDF	35742.2	40829.1	146.75	130.47	33075.87
ORD-EGLL	30854.0	87075.4	138.69	128.25	61381.95
ORD-LFPG	33565.2	38617.8	182.18	166.77	31145.88

REFERENCES

- [1] Intergovernmental Panel on Climate Change. Aviation and the Global Atmosphere. Cambridge University Press: USA, 1999. [<http://www.grida.no/climate/ipcc/aviation/>].
- [2] Minnis, Patrick, et.al. “Contrails, Cirrus Trends, and Climate”. *Journal of Climate*, Vol 17. 15 April 2004. p.1671-1685.
- [3] Williams, Noland, Toumi. “Reducing the Climate Change Impacts of aviation by Restricting Cruise Altitudes”. *Transportation Research Part D* 7 (2002) pp.451-464.
- [4] Garrison, DuBois, Baughcum. “The Effect of Constrained Cruise Altitudes on Fuel Usage, NOx Production, and Flight Time for Commercial Aircraft”. *Boeing Commercial Airplanes: Seattle, Washington, October 2004*. NASA/CR—2004-213305.
- [5] Minnis, et.al. “Contrails, Cirrus Trends, and Climate”. *Journal of Climate*. Volume 17, 15 April 2004. pp.1671 – 1685.
- [6] “Aerosol Crimes and Coverup” , courtesy of Clifford E Carnicom. [<http://www.carnicom.com/abq.htm>] .
- [7] Intergovernmental Panel on Climate Change. *Climate Change - The IPCC Scientific Assessment*. Cambridge University Press: USA, 2001. [http://www.grida.no/climate/ipcc_tar/].
- [8] Environmental Protection Agency. “Aircraft Contrails Factsheet”. *Air and Radiation (6205J)*, EPA430-F-00-005, September 2000.
- [9] Appleman. “The Formation of Exhaust Condensation Trails by Jet Aircraft”. *Bulletin American Meteorological Society*, Vol.34, No. 1, January, 1953. pp.14-20.
- [10] Schumann, Ulrich. “Influence of Propulsion Efficiency on Contrail Formation”. *Aersp. Sci. Technol. Vole 4*. 2000. p.391-401.
- [11] Lee, Joosung Joseph. “Modeling Aviation’s Global Emissions, Uncertainty Analysis, and Applications to Policy”. *Massachusetts Institute of Technology*, September 2004.
- [12] Spichtinger, Peter, et al. “The global distribution of ice-supersaturated regions as seen by the Microwave Limb Sounder”. *Q.J.R. Meteorological Society* (2003), 129, pp.3391-3410.
- [13] From correspondence with Ilan Kroo, Stanford.
- [14] Sausen et.al. “A Diagnostic Study of the Global Distribution of Contrails Part I: Present Day Climate”. *Theoretical and Applied Climatology*. Springer-Verlag: Austria, 1998. v. 61, pp. 127-141.

- [15] Williams and Noland. "Variability of Contrail Formation Conditions and the Implications for Policies to Reduce the Climate Impacts of Aviation". Galley proof provided by the authors, To appear in Transportation Research Part D (2005).
- [16] "World Atlas of Maps Flags and Geography Facts".
[<http://worldatlas.com/webimage/countrys/na.htm>].
- [17] "ARM – Instruments: Rapid Update Cycle (RUC) Model Data".
[<http://www.arm.gov/xds/static/ruc.stm>].
- [18] "UM Support – UM FAQ".
[<http://www.met.rdg.ac.uk/~sws00cw2/FAQ/#What%20is%20the%20Unified%20Model>].
- [19] "Archived Weather Data Links on Everythingweather.com".
[<http://www.everythingweather.com/links/archived-data.shtml>].
- [20] "North Atlantic Jet Stream Map Archive: The California Regional Weather Server".
[http://squall.sfsu.edu/crws/archive/jet_atl_arch.html].
- [21] Minnis et.al. "Simulation of Contrail Coverage over the USA missed during the air traffic shutdown". European Conference on Aviation, Atmosphere, and Climate. June 30-July 3, 2003.
- [22] Padilla, Carlos E. Optimizing Jet Transport Efficiency: Performance, Operations, and Economics. McGraw-Hill" New York, 1996.
- [23] "Bureau of Transportation Statistics (BTS) – United States Department of Transportation (USDOT)". [<http://products.bts.gov/xml/fuel/report/src/index.xml>].
- [24] "Federal Reserve Bank of Minneapolis – Consumer Price Index Calculator".
[<http://minneapolisfed.org/Research/data/us/calc/index.cfm>].
- [24.5] Pratt & Whitney. Aeronautical Vestpocket Handbook. Pratt & Whitney: Pratt & Whitney Canada, May 1990.
- [25] FAA. "Economic Values for FAA Investment and Regulatory Decisions, A Guide". Contract No, DTFA 01-02-C00200. May 28, 2004. pp. ES-3-5.
- [26] "NOAA AVHRR Viewer from NASA LaRC: Images & predicts".
[<http://angler.larc.nasa.gov/avhrr/>].
- [27] Duda et.al. "CONUS Contrail Frequency Estimated from RUC and Flight Track Data". European Conference on Aviation, Atmosphere, and Limate. June 30-July 3, 2003.
- [28] Mannstein et al. "Operational detection of contrails from NOAA-AVHRR-data". International Journal of Remote Sensing, 1999, 1641-1660.

- [29] From correspondence with Minnis, Duda, Palikonda of NASA Langley.
- [30] "UTC Time Conversion". [<http://setiathome.ssl.berkeley.edu/utc.html>].
- [31] Busen & Schumann. "Visible contrail formation from fuels with different sulfur contents". *Geophysical Research Letters*. Vol. 22, No 11, June 1995.
- [32] Shevell. Fundamentals of Flight. Prentice Hall: Upper Saddle River, NJ, 1989.
- [33] Babikian, Lukachko, & Waitz. "The Historical Fuel Efficiency Characteristics of Regional Aircraft from Technological, Operational, and Cost Perspectives".
- [34] Jane's All the World's Aircraft. Various Editions.
- [35] "The-Eggs: Newsletter & Information Service of the E.G.U." [<http://the-eggs.org/articles.php?id=66>].
- Cumpsty, Nicholas. Jet Propulsion: A Simple Guide to the Aerodynamic and Thermodynamic Design and Performance of Jet Engines, Second Edition. Cambridge University Press: Cambridge, 2003.
- Detwiler. "Contrail Formation and Propulsion Efficiency". *Journal of Aircraft*. Vol.39, No4., July-August 2002.
- "Early Flying Myths and Legends". [http://www.pilotfriend.com/century-of-flight/new%20site/frames/myths_frame1.htm].
- "First Flight Centennial | Wright Brothers, Aviation Heritage, Outer Banks, Kitty Hawk North Carolina". [<http://www.firstflightcentennial.org/>].
- Hartman. Global Physical Climatology Change. Academic Press: San Diego, 1994.
- List, Robert. Smithsonian Meteorological Tables. Smithsonian Institute Press: City of Washington, 1951.
- "Maryland Maps – Perry-Castaneda Map Collection – UT Library Online". [<http://www.lib.utexas.edu/maps/maryland.html>]
- Moran & Shapiro. Fundamentals of Engineering Thermodynamics. John Wiley & Sons, Inc: New York, 1988.
- Rogers & Yau. A Short Course on Cloud Physics. Butterworth-Heinemann: USA, 1989.
- Schroeder et al. "On the Transition of Contrails Into Cirrus Clouds." *Journal of the Atmospheric Sciences*. Vol 57. 15 February 200. p.464-480.

Travis, Carleton, and Lauritsen. "Contrail Reduce Daily Temperature Range". Nature. Vol 418. 8 August 2002. p.601.

United States Environmental Protection Agency. "Aircraft Contrails Factsheet". EPA430-F-00-005, September 2000.

"United States Maps States Landforms Rivers and Information pages by World Atlas". [<http://worldatlas.com/webimage/country/usanewd.htm>].

Volpe National Transportation Systems Center, Environmental Measurements and Modeling Division. "System for assessing Aviation's Global Emissions (SAGE): Fuel Burn and Emissions". Version 1, September 2003.

Waitz. "Contrail Formation". Microsoft Powerpoint Presentation.